Evaluating New Malaria Vaccine Candidates



Andrés Noé

Green Templeton College

University of Oxford

A thesis submitted for the degree of

Doctor of Philosophy

Hilary Term 2021

50,000 words (exclusive of references, figures and tables)

Evaluating New Malaria Vaccine Candidates

Andrés Noé, Green Templeton College, University of Oxford

Thesis submitted for the degree of Doctor of Philosophy, Hilary Term 2021

Abstract

A highly effective malaria vaccine remains gravely needed. Vaccine-induced protection from liver-stage malaria requires high numbers of CD8+ T cells to find and kill *Plasmodium*-infected liver cells. A new strategy, prime-target vaccination, involves sequential viral-vectored vaccination by intramuscular and intravenous routes to target cellular immunity to the liver. Liver-resident memory CD8+ T cells (TRM) are necessary for protection against rodent malaria by this vaccine regimen. Ultimately, to most faithfully assess immunological responses by these local, specialised, hepatic T cells, periodic liver sampling is necessary. This, however, is not feasible at scale in human trials. This thesis explores the early response, kinetics and transcriptomics of CD8+ T cells in mice vaccinated with prime-target. Adoptively transferred liver TRM preferentially homed to the liver and *Plasmodium*-specific CD8+ T cells peaked shortly after intravenous boost. These T cells were present in the liver and blood, and expressed several molecules suggestive of tissue residency and liver-homing. In a human efficacy study of prime-target vaccination, multi-omic analyses were performed on hepatic fine needle aspirates and peripheral blood samples to study liver TRM and their circulating counterparts. While these peripheral 'TRM-like cells' differed to *bona fide* TRM in certain features, such as leucocyte adhesion and T cell differentiation, they were phenotypically similar and indistinguishable in terms of T cell residency transcriptional signatures. Single cell analyses identified several subpopulations, mutual clonality, and indicated a potential developmental trajectory shared between TRM and TRM-like cells. This thesis demonstrates the potential for using TRM-like cells as a correlate of prime-target induced protection against liver-stage malaria. A simple and reproducible correlate of protection would be particularly valuable in trials of liver-stage malaria vaccines as they progress to phase III, large-scale testing in African infants. This work provides a blueprint for understanding and monitoring liver TRM induced by a new liver-stage malaria vaccine approach.

Acknowledgements

This DPhil process has not occurred in a vacuum and I am fortunate to have benefited from the collaborative product of many talented people and an enriching environment. My many thanks to:

My supervisors. Dr Alex Spencer, who patiently taught a simple pretender how to hold a pipette and guided me through a maze of mice, flow cytometry, and an approach to science. I am grateful for your attention to detail, availability and laid-back demeanour to my (many) failed attempts. Prof. Adrian Hill whose drive, encouragement and ability to enable are admirable and were critical to the progress of this thesis. From you, I have been taught by and learnt from one of the greats of translational science, malaria and vaccine development. Prof. Sumi Biswas, I could hardly have wished for a more inclusive and approachable supervisor, your willingness to share knowledge on all matters vaccinology was particularly formative. My thesis committee, Prof. Paul Klenerman and Prof. Philip Bejon, whose insights were unique and influential, and whom I consider great role models for my future as a clinician lost in science.

The members of the Jenner Institute and NDM. The pre-erythrocytic malaria vaccine clinical team: Duncan Bellamy, Rebecca Makinson, A/Prof. Katie Ewer, Dr Amy Flaxman and Dr Mehreen Datoo. The VAC066 trial was a wonderful introduction into clinical vaccine evaluation. My fellow Jenner DPhil students: Dr Robert Ragotte, Dr Richard Morter, Danny Wright, and many more. You made the Jenner a place where I learnt, grew and cheerfully left the house for, every morning. Marta Ulaszewska, Andrew Worth, Dr Helen Ferry and Dr Neil Ashley, for your timely and unrivalled technical expertise. The various members of the PEM and TBV teams, and the wider Institute for helpful hallway hints. There are many other colleagues I have not named individually but have helped along the way, to whom I am also grateful.

The Rhodes Trust, particularly Mary Eaton, Dr Elizabeth Kiss and Charles Conn. I owe the great experiences and the unrivalled academic, professional and personal education I have had at Oxford to the Trust.

The many clinical trial volunteers without whom much of this work would not have been possible.

My friends, of whom there are too many to thank and too few who recognise the impact they have. Matthew Pierri for the enduring assistance and meticulous proof-reading. Dr Oscar Lyons for being a beacon of positivity and sharing your own DPhil journey. Other friends, far and near, I am indebted to you for the endless encouragement, chats, runs, pre-COVID travels, dinners, beers, debates, fights, laughs and dreams.

I am little more than an artefact of a lucky combination of genes, an engaging enabling environment and astonishing support. My family, Mum, Dad and Marco, without you I would not have made it to this point. My education has only been possible through the tremendous sacrifices, advocacy and backing by my parents. Marco, for giving me the opportunity to be better at each moment.

Finally and most emphatically: Lakshmi. My co-pilot, without whom, nothing.

Table of Contents

Abstract i

Acknowledgements ii

Table of Contents iv

Table of Figures viii

Table of Tables xii

List of Abbreviations xiii

Authorship statement xvi

1 Background 1

1.1 Malaria: an ancient disease presenting an ongoing challenge in global health 1
1.1.1 Human malaria-causing *Plasmodium* and related species 1
1.1.2 The Malaria Hypothesis 3
1.1.3 Recorded history 4
1.1.4 Modern era 5

1.2 The *Plasmodium falciparum* lifecycle 7
1.2.1 The pre-erythrocytic stage 7
1.2.2 The asexual blood-stage 9
1.2.3 The sexual-stage 12

1.3 Immunity against pre-erythrocytic *Plasmodium* species 14
1.3.1 Immunity to sporozoites 14
1.3.2 Immunity to liver-stage parasites 15
1.3.2.1 Human liver anatomy and immunology – a brief introduction 16
1.3.2.2 Innate immune responses 19
1.3.2.3 T cell activation by Plasmodium antigens 20
1.3.2.4 CD8+ T cell responses 21
1.3.2.5 Mechanisms of CD8+ T cell-mediated protection 23
1.3.3 Tissue-resident memory CD8+ T cells 24
1.3.3.1 Definition, differentiation, and durability 25
1.3.3.2 Functional and transcriptional adaptations 26
1.3.3.3 Plasmodium-specific liver TRM in mice and non-human primates 28
1.3.3.4 Human liver TRM: unique attributes and infectious disease protection 30

1.4 Malaria vaccine development 35
1.4.1 Pre-erythrocytic vaccines 36
1.4.1.1 CSP-based approaches 37
1.4.1.2 Whole sporozoite approaches 39
1.4.1.3 Viral vector approaches 40
1.4.1.4 TRM-targeted vaccine approaches 42
1.4.2 Asexual blood-stage and sexual-stage vaccines 44
1.4.3 The ideal malaria vaccine candidate 45
1.4.4 Difficulties in developing malaria vaccines 46

1.5 Thesis aims and outline 49
1.5.1 Rationale 49
1.5.2 Aims 49
1.5.3 Outline 50

2 Materials and methods 51

2.1 Materials 51

2.1.1 Reagents 51
2.1.2 Oligonucleotides 53
2.1.3 Buffers and media 53
2.1.4 Antibodies 54
2.1.5 Vaccines 56
2.1.5.1 Preclinical viral vector vaccines 56
2.1.5.2 Clinical trial viral vector vaccines 56
2.2 Animals and preclinical procedures 57
2.2.1 Injections 57
2.2.1.1 Intramuscular 57
2.2.1.2 Intraperitoneal 57
2.2.1.3 Intravenous 57
2.2.2 Blood sampling 58
2.2.3 Adoptive cell transfers 58
2.3 Clinical trials 59
2.3.1 Design 59
2.3.2 Procedures 60
2.3.2.1 Vaccinations 60
2.3.2.2 Fine needle aspirates of the liver 60
2.3.2.3 Controlled human malaria infection 62
2.4 Immunology 63
2.4.1 Isolating human PBMC 63
2.4.2 Freezing human PBMC 63
2.4.3 Thawing human PBMC 63
2.4.4 ELISpot 64
2.4.5 Flow cytometry 64
2.4.5.1 Human intracellular cytokine staining 64
2.4.5.2 Mouse intracellular cytokine staining 65
2.4.5.3 Fluorescence-assisted cell sorting 66
2.5 Molecular Biology 68
2.5.1 RNA isolation 68
2.5.2 *P. falciparum* quantitative polymerase chain reaction 68
2.5.3 Sequencing 69
2.5.3.1 Human mini-bulk RNA-seq 69
2.5.3.2 Human single-cell RNA-seq 69
2.5.3.3 Mouse bulk RNA-seq 69
2.6 Statistics and bioinformatics 70
2.6.1 Statistics, software, and versions 70
2.6.2 Flow cytometry 71
2.6.3 Human mini-bulk RNA-seq analyses 72
2.6.4 Human single-cell RNA-seq analyses 73
2.6.5 Mouse bulk RNA-seq analyses 75
3 Tissue-resident memory T cells and prime-target vaccination assessment in mice 77
3.1 Introduction 77
3.2 Results 80
3.2.1 Antigen-specific cell short-term time course 80
3.2.2 Liver TRM dynamics with and without IV boost 83
3.2.3 Investigating the dynamics of TRM-like cells shortly after IV viral vector vaccination 86
3.2.4 Investigating the dynamics of TRM-like cells in the presence and absence of antigen 88
3.2.5 Investigating the origin and expansion of AgSp TRM in the liver 92
3.2.6 Transcriptomic analysis of T cells following prime-target 96

3.3 Figures 102

3.4 Discussion 122
3.4.1 Novel findings 122
3.4.2 Limitations 128
3.4.3 Further questions 129
3.4.4 Conclusion 130

4 Assessing liver-resident memory T cells and their circulating counterparts 132

4.1 Introduction 132

4.2 Results 135
4.2.1 Liver fine needle aspirates faithfully represented hepatic immune cell populations 135
4.2.1.1 Fine needle aspirate yield and composition 135
4.2.1.2 Vaccination regimen and time after vaccination did not affect hepatic TRM 136
4.2.1.3 Liver FNA identified TRAP-specific T cells 136
4.2.1.4 Intracellular cytokine staining resulted in hepatic lymphocyte death 136
4.2.1.5 Hepatic lymphocytes correlated to matched peripheral blood lymphocytes 137
4.2.1.6 Hepatic TRM were phenotypically similar to peripheral blood TRM-like cells 137
4.2.2 RNA-seq delineated unique differences between liver TRM and TRM-like cells 139
4.2.2.1 FNA and PBMC memory T cells exhibited previously reported characteristics 139
4.2.2.2 Comparing liver TRM and TEM refined a tissue-resident T cell signature 140
4.2.2.3 TRM-like cells were not more activated than TRM 141
4.2.2.4 Distinctions between TRM and TRM-like cells were not dependent on cell location 142
4.2.3 Single-cell RNA-seq revealed subpopulations shared among TRM and TRM-like cells 143
4.2.3.1 All identified clusters contained TRM and TRM-like cells 143
4.2.3.2 Heterogeneity among TRM was present 144
4.2.3.3 There was a shared trajectory among T cells of varying identity 145
4.2.3.4 TCR analysis revealed clonal relationships between TRM and TRM-like cells 146

4.3 Figures 150

4.4 Discussion 167
4.4.1 Novel findings 167
4.4.2 Limitations 173
4.4.3 Further questions 174
4.4.4 Conclusion 175

5 Investigating TRM-like cells as correlates of vaccine-induced protection 177

5.1 Introduction 177

5.2 Results 181
5.2.1 TRM-like cells were induced in the short and medium-term after IV viral vector administration in humans 181
5.2.1.1 TRM-like cells were identified in the blood after IV boost 181
5.2.1.2 TRM-like cells were associated with within-assay AgSp T cells 182
5.2.1.3 TRM-like cells displayed heterogeneity that was preserved over time after IV boost 183
5.2.1.4 Clinical markers of inflammation were elevated after IV boost 185
5.2.2 IV viral vector induced a greater TRM-like cell response compared to IM viral vector 186
5.2.3 TRM-like cells correlated with established and validated markers of protection 188
5.2.3.1 TRM-like cells correlated with a range of TRAP-specific CD8+ T cell subsets 188
5.2.3.2 TRM-like cells correlated with IFNγ-secreting T cells more than a month post-CHMI 190
5.2.3.3 IV+3 TRM-like cell frequency was a correlate of vaccine-antigen immunity 191
5.2.4 TRM-like cells can be used to estimate protection following CHMI 192
5.2.4.1 A range of protection outcomes occurred as a result of CHMI 192
5.2.4.2 TRM-like cells independently correlated with vaccine-induced protection 193
5.2.4.3 TRM-like cell frequency could be used to model time-to-malaria diagnosis 195

5.3 Figures 199

5.4 Discussion 212
5.4.1 Novel findings 212
5.4.2 Limitations 217
5.4.3 Further questions 219
5.4.4 Conclusion 220

6 Discussion 222

6.1 Thesis overview 222

6.2 Chapter insights, implications, and inferences 223
6.2.1 Chapter 3: TRM and prime-target vaccination assessment in mice 223
6.2.2 Chapter 4: Assessing liver TRM and their circulating counterparts 228
6.2.3 Chapter 5: Investigating TRM-like cells as correlates of vaccine-induced protection 231

6.3 Final remarks 239

7 References 241

Table of Figures

Figure 1.1: Evolutionary relationships between *Plasmodium* species 3

Figure 1.2: Malaria mortality in the 20th and 21st century 6

Figure 1.3: The *P. falciparum* life cycle 7

Figure 1.4: Age distribution and outcome of *P. falciparum* infection 12

Figure 1.5: Liver anatomy and immunology 17

Figure 1.6: *P. falciparum* malaria vaccine candidates 37

Figure 2.1: VAC066 trial overview and timeline 59

Figure 3.1: Eleven-day time course experiment 102

Figure 3.2: Fourteen-day time course experiment 103

Figure 3.3: AgSp CD8+ T cell responses following IV Ad-OVA 103

Figure 3.4: Liver TRM and blood TRM-like cell correlations 104

Figure 3.5: TRM and TRM-like cell phenotyping 104

Figure 3.6: Transfer of liver and spleen CD69+ cells 105

Figure 3.7: AgSp cells following cell transfer from the spleen or liver 106

Figure 3.8: Transfer of liver CD69+ and CD69- cells 107

Figure 3.9: Transferring liver, spleen and blood cells after IV Ad-OVA 108

Figure 3.10: Transfer of prime-target liver and blood CD69+ CD8+ T cells (I) 109

Figure 3.11: Transfer of prime-target liver and blood CD69+ CD8+ T cells (II) 110

Figure 3.12: Transfer of prime-boost-target liver and blood CD69+ CD8+ T cells (I) 111

Figure 3.13: Transfer of prime-boost-target liver and blood CD69+ CD8+ T cells (II) 112

Figure 3.14: Transfer of prime-target bulk (non-sorted) liver and blood T cells (I) 113

Figure 3.15: Transfer of prime-target bulk (non-sorted) liver and blood T cells (II) 114

Figure 3.16: Prime-target with Ad-OVA or Ad-TIP, and FTY720 administration 115

Figure 3.17: Prime-target with and without a prime, and FTY720 administration 116

Figure 3.18: Transcriptomic analysis of T cells after prime-target 117

Figure 3.19: Transcriptomic comparison: day 28 post-IV boost TRM and TEM in tissues 118

Figure 3.20: Transcriptomic comparison: CD69+ early and late time point post-IV boost 119

Figure 3.21: Pathway analyses: CD69+ early and late time point post-IV boost 120

Figure 3.22: Transcriptomic comparison: OVA-pentamer+ early time point CD69+ Ad-OVA and Ad-TIP vaccinated groups 121

Figure 4.1: Liver and blood leucocyte populations 150

Figure 4.2: Liver TRM by group and time after vaccination 150

Figure 4.3: ELISpot assays from hepatic and blood samples 150

Figure 4.4: Quantitative correlations between liver (FNA) and blood (PBMC) samples 151

Figure 4.5: Expression of TRM markers on FNA TRM and PBMC TRM-like cells 151

Figure 4.6: Contour tSNE plot of FNA and PBMC CD8+ and CD8+ TRM 152

Figure 4.7: Contour tSNE plot of TRM/TRM-like cells compared to TEM 152

Figure 4.8: Contour tSNE plot of TRM and TRM-like cells 153

Figure 4.9: Phenotype characterisation of the three tSNE subsets 153

Figure 4.10: Metaparameter characterisation of the three tSNE subsets 154

Figure 4.11: Sequencing experiments overview and biplots comparing PCs 1, 2 and 3 154

Figure 4.12: Heatmap of sample distances 155

Figure 4.13: Heatmap of the 50 most variable genes between all samples 155

Figure 4.14: Volcano plot of differentially expressed genes: FNA CD69+ vs CD69- 156

Figure 4.15: Gene heatmap of FNA samples using the core TRM transcriptional signature 156

Figure 4.16: Volcano plot of differentially expressed genes: FNA CD69+ vs PBMC CD69+ 157

Figure 4.17: Heatmap and clustering of the FNA CD69+ vs PBMC CD69+ comparison 157

Figure 4.18: ORA and GSEA plots for GO categories of the FNA CD69+ vs PBMC CD69+ 158

Figure 4.19: GSEA plots for Szabo et al. gene sets in the FNA CD69+ vs PBMC CD69+ 158

Figure 4.20: FNA CD69- vs PBMC CD69-, and PBMC CD69+ vs CD69- comparisons 159

Figure 4.21: Bi-plots comparing PCs 1, 2 and 3 in scRNA-seq samples 159

Figure 4.22: Top 30 most variable genes in PC1-3 160

Figure 4.23: UMAP of 629 single cell gene expression 160

Figure 4.24: Venn diagram of genes differentiating FNA and PBMC cells 161

Figure 4.25: Heatmap of the C1 FNA vs C0 FNA cell comparison 161

Figure 4.26: Venn diagram of genes differentiating TRM clusters 161

Figure 4.27: Gene expression in genes differentiating TRM clusters 162

Figure 4.28: Violin plots of genes downregulated in Kumar et al. core TRM signature 162

Figure 4.29: UMAP plots with signature enrichment scores 163

Figure 4.30: Pseudotime trajectory superimposed on UMAP 163

Figure 4.31: Pseudotemporally associated genes 163

Figure 4.32: T cell clonality and clone size 164

Figure 4.33: MAIT clones and cells 164

Figure 4.34: TCR α chain usage of clonal T cells by sample and volunteer 165

Figure 4.35: TCR β chain usage of clonal T cells by sample and volunteer 165

Figure 4.36: TCR α and β chain usage of MAIT cells by sample 166

Figure 4.37: Clonal relationships between MAIT cells, and non-MAIT cells 166

Figure 5.1: VAC066 trial overview and timeline 199

Figure 5.2: TRM-like cells after IV boost 200

Figure 5.3: TRM-like cell phenotype after IV boost 201

Figure 5.4: Correlations between AgSp T cells and non-AgSp TRM-like cells 201

Figure 5.5: TRM-like cells after IV boost, by IV viral vector and by vaccination regimen 202

Figure 5.6: CD69+ CD11a hi subset composition 202

Figure 5.7: Clinical biochemistry and haematology 203

Figure 5.8: T cell subsets over prime, IM boost and IV boost vaccination 204

Figure 5.9: AgSp CD8+ T cell subsets 205

Figure 5.10: AgSp T cell response kinetic by IFNγ ELISpot 206

Figure 5.11: IV+3 TRM-like cells vs ELISpot and ICS responses 207

Figure 5.12: Kaplan-Meier log-rank comparisons of vaccinated compared to controls 208

Figure 5.13: IV+3 TRM-like cells vs indicators of vaccine-induced protection 208

Figure 5.14: Kaplan-Meier curves stratified by various correlates of protective efficacy 209

Figure 5.15: Univariate regression models for protection from malaria after CHMI 209

Figure 5.16: Multiple regression model for protection from malaria after CHMI 210

Figure 5.17: Other multiple regression models for protection from malaria after CHMI 211

Figure 6.1: Representation of the proposed relationship between TRM and TRM-like cells 224

Figure 6.2: Integrating and contextualising the findings of Chapter 3 (I) 226

Figure 6.3: Integrating and contextualising the findings of Chapter 3 (II) 226

Figure 6.4: TRM as correlates of vaccine-induced protection 233

Figure 6.5: TRM-like cells as correlates of vaccine-induced protection 234

Table of Tables

Table 2.1: Reagents and non-standard consumables used in this thesis 51

Table 2.2: Oligonucleotides used in this thesis 53

Table 2.3: Buffers used in this thesis 53

Table 2.4: Media used in this thesis 54

Table 2.5: Functional human antibodies 54

Table 2.6: Human antibodies for flow cytometry and intracellular cytokine staining 54

Table 2.7: Mouse antibodies for flow cytometry and intracellular cytokine staining 55

Table 3.1: Day three blood AgSp TRM-like cell and liver TRM frequency correlations 81

Table 4.1: Populations of CD8+ and CD4+ T cells expressing TRM markers 135

Table 4.2: Pan-tissue core TRM signature 140

Table 4.3: Differential gene expression between FNA and PBMC clusters 144

Table 4.4: Frequency of α and β TCR recombinants in 690 single T cells 147

Table 5.1: Cox proportional hazards models using statistically significant TRM-like cells 197

Table 5.2: Multiple regression Cox proportional hazards models using TRM-like cells 197

Table 6.1: Evidence relating to scenarios represented in Figure 6.5 237

List of Abbreviations

ACT	Artemisinin-combination therapies
Ad	Adenovirus
AgSp	Antigen-specific
AIC	Akaike information criterion
ALT	Alanine transaminase
AMA1	Apical membrane antigen 1
APC	Antigen-presenting cell
apeglm	Approximate posterior estimation for generalised linear models
B	Intramuscular boost
B+n	n days after intramuscular boost vaccination
BP	Biological process
BSA	Bovine serum albumin
CC	Cellular component
CD	Cluster of differentiation
CDR	Complementarity-determining region
CelTOS	Cell traversal protein for ookinetes and sporozoites
ChAd63	Chimpanzee adenovirus serotype 63
CHMI	Controlled human malaria infection (also referred to as challenge)
CoP	Correlate of protection
CSP	Circumsporozoite protein
CyRPA	Cysteine-rich protective antigen
DC	Dendritic cell
DDT	Dichlorodiphenyltrichloroethane
DGE	Differential gene expression
dLN	Draining lymph node
DMSO	Dimethyl sulphoxide
DNA	Deoxyribonucleic acid
dsRNA	Double-stranded ribonucleic acid
EDTA	Ethylenediaminetetraacetic acid
ELISpot	Enzyme-linked immune absorbent spot
FACS	Fluorescence-assisted cell sorting
FC	Fold change
FCS	Fetal calf serum
fcs	Functional class scoring
FDR	False discovery rate
FNA	Fine needle aspirate
GAP	Genetically attenuated parasites
GFP	Green fluorescent protein
GMFI	Geometric mean fluorescence intensity
GO	Gene ontology
GRCh38.p13	Genome Reference Consortium human genome build 38 patch release 13
GSEA	Gene set enrichment analysis
HLA	Human leukocyte antigen
HR	Hazard ratio
HSPGs	Heparan sulphate proteoglycans
ICAM	Intercellular adhesion molecules
ICS	Intracellular cytokine staining
IFN	Interferon
IL	Interleukin

IM	Intramuscular
IP	Intraperitoneal
iRBC	Infected red blood cell
IRF	Interferon regulatory factor
IU	Infectious units
IV	Intravenous
IV+n	n days after intravenous boost vaccination
IVC	Intravenous cannula
KC	Kupffer cell
KEGG	Kyoto encyclopaedia of genes and genomes
KW	Kruskal-Wallis test
L-glut	L-glutamine
LBI	Liver-to-blood inoculum
LLIN	Long-lasting insecticidal-treated bed nets
$\log_2$(FC)	Binary logarithm of the fold change value
LSA-1	Liver-stage antigen 1
LSEC	Liver sinusoidal endothelial cell
MAIT cell	Mucosal-associated invariant T cell
mCoP	Mechanistic correlate of protection
ME-TRAP	Multiple epitope string fused to thrombospondin-related adhesion protein
MEM	Minimum essential medium
MF	Molecular function
MHC	Major histocompatibility complex
MSigDB	Molecular signatures database
MSP1	Merozoite surface protein
MVA	Modified Vaccinia Ankara
MW	Mann-Whitney test
NA	Not applicable
NAI	Naturally-acquired immunity
nCoP	Non-mechanistic, statistical correlate of protection
ND	Not detected
NHP	Non-human primate
NK	Natural killer
NKT cells	Natural killer T cells
NO	Nitric oxide
ORA	Over-representation analysis
OVA	Ovalbumin
P	Intramuscular prime
P. falciparum	*Plasmodium falciparum*
P+n	n days after intramuscular prime vaccination.
PBMC	Peripheral blood mononuclear cells
PBS	Phosphate-buffered saline
PC	Principal component
PCA	Principal component analysis
Pen/strep	Penicillin & streptomycin
PFA	Paraformaldehyde
PfEMP1	*P. falciparum* erythrocyte membrane protein 1
PfRh	*P. falciparum* reticulocyte-binding protein homologs
PfRipr	*P. falciparum* reticulocyte-binding protein homolog interacting protein
pfu	Plaque forming units
PL	Phospholipase

PLGA	Poly-(lactic-co-glycolic acid)
PV	Parasitophorous vacuole
PVM	Parasitophorous vacuole membrane
QC	Quality control
qPCR	Quantitative-polymerase chain reaction
RAS	Radiation-attenuated sporozoites
RBC	Red blood cell
rlog	Regularised logarithm
RNA	Ribonucleic acid
RNA-seq	RNA-sequencing
scRNA-seq	Single-cell RNA-sequencing
SEB	Staphylococcal enterotoxin B
SFC	Spot-forming colonies
SPECT	Sporozoite microneme protein essential for traversal
Tcirc	Circulating *Plasmodium* parasite-specific CD8+ T cells
TCM	Central memory T cells
TCR	T cell receptor
TCRA	T cell receptor α locus
TCRB	T cell receptor β locus
TEM	Effector memory T cells
TGF	Transforming growth factor
TIP	Tuberculosis, immunodeficiency virus and *Plasmodium* antigens
TNF	Tumour necrosis factor
TRAJ	T cell receptor α chain joining region
TRAP	Thrombospondin-related adhesion protein
TRAV	T cell receptor α chain variable region
TRBJ	T cell receptor β chain joining region
TRBV	T cell receptor β chain variable region
TRM	Tissue-resident memory T cell
UMAP	Uniform manifold approximation and projection
VAC066	A phase I/IIa sporozoite challenge study to assess the safety, immunogenicity and protective efficacy of intravenous boosting with malaria vaccine candidates ChAd63 and MVA encoding ME-TRAP
vp	Viral particles
WHO	World Health Organisation
α-MEM	Minimum essential medium eagle α-modification
γ/α/2	IFNγ+, TNFα+ or IL-2+ cells

These are in addition to abbreviations for Système International d'Unités (SI) units of measurement, other common units (e.g., bp, kb, and Da), and chemical symbols for the elements.

Authorship statement

For Chapter 3, I conceived all experiments in conjunction with my supervisors. I performed all animal handling with essential assistance from research technicians and my supervisors. Dr Alexandra Spencer and Marta Ulaszewska provided essential training in procedures and support for most experiments. I completed all laboratory work and analyses, with input from my supervisors.

For Chapter 4, all experiments were conceived in conjunction with my supervisors and external advisors. The samples were collected as a part of the VAC066 clinical trial (see Materials and Methods). I performed the lymphocyte isolation from the hepatic fine needle aspirates, flow cytometry staining, and ELISpot set up together with Dr Alexandra Spencer. Sample acquisition and cell sorting were performed by Dr Helen Ferry at the Experimental Medicine Division Flow Cytometry Facility whilst I was in attendance. Smart-Seq2 protocol RNA-sequencing was performed at the MRC Weatherall Institute of Molecular Medicine Single Cell Facility. I completed the analysis of this data.

For the controlled human malaria infection study presented in Chapter 5, design and conduct of clinical procedures and primary laboratory assays (including only: intracellular cytokine staining and IFNγ ELISpots) were coordinated at the Jenner Institute laboratories by Professor Adrian Hill (principal investigator), Associate Professor Katie Ewer (lead immunologist), Dr Amy Flaxman (senior immunologist responsible for quality control) and Dr Mehreen Datoo (clinical coordinator). Laboratory assays were performed by the Jenner Institute pre-erythrocytic malaria lab group members. I contributed to the team of laboratory members performing the qPCR assays and processing PBMC samples for usage and storage during the study.

I presented some of the work outlined in Chapters 4 and 5 at the 2019 American Society of Tropical Medicine and Hygiene Annual Meeting (oral presentation), 2019 International Conference on Malaria Vaccines for the World (poster presentation), 2019 and 2020 Oxford Immunology Symposium (poster presentation, 2020 – cancelled). Chapters 4 and 5 form the basis of a manuscript that is in preparation for submission to the *Journal of Experimental Medicine*. All figures labelled with 'Figure created in BioRender.com' were created by me, Andrés Noé.

Chapter 1

1 Background

1.1 Malaria: an ancient disease presenting an ongoing challenge in global health

If cancer is described as 'The Empress of all Maladies' (1), malaria is justly 'The Queen of Diseases' (2). Malaria has shaped our history and genome like no other illness. The disease is caused by infection with the *Plasmodium* species. Here, I outline the context of present-day malaria and *Plasmodium* species, not least out of curiosity but to glean insights into how the disease can be controlled, eliminated, and eventually eradicated through vaccination.

1.1.1 Human malaria-causing *Plasmodium* and related species

Ancestors of *Plasmodium* species originated around half a billion years ago, likely around the time that compatible hosts became available. These 'pre-malaria' parasite ancestors were probably free-living, chloroplast-containing protozoa with obligate sexual reproduction (3). They were potentially adapted to parasitise the gastrointestinal tracts of aquatic invertebrates (3). Around two hundred million years ago, the parasites acquired an intracellular, asexual reproductive cycle and adapted to the aquatic larvae of the fly order, Dipterans, which includes mosquitoes (4). Since that time, which coincided with the appearance of biting invertebrates, pre-malaria parasites continued to evolve, propagate, and infect members of most land vertebrates. *Plasmodium* species infect humans through bites of female *Anopheles* species mosquitoes.

1.1.1 Human malaria-causing Plasmodium and related species

More than 250 *Plasmodium* species have been recognised, which can infect birds, snakes, mammals, and lizards. Six species are of clinical and public health importance in humans: *Plasmodium falciparum*, *Plasmodium vivax*, *Plasmodium ovale curtisi*, *Plasmodium ovale wallikeri*, *Plasmodium knowlesi and Plasmodium malariae* (5). Parasite morphology and biology, geographical distribution, and host relatedness have traditionally driven the field of *Plasmodium* evolutionary biology. However, in the last ten years, there has been an increasing understanding of several *Plasmodium* species' evolutionary interrelatedness, particularly those within the *Laverania* subgenus, through molecular genetics (6,7).

The *Laverania* subgenus of parasites contains the deadliest malaria-causing parasite *P. falciparum* (Figure 1.1). There have been various estimates concerning the speciation event resulting in *P. falciparum*, anywhere between 10,000 and 5.5 million years ago (8,9); however, the most recent estimates suggest that *P. falciparum* and *P. praefalciparum* began to diverge 40,000-60,000 years ago (9). *Laverania* species infect great apes, and *P. reichenowi* was, until 2009, believed to be the only other species in the subgenus (10). It is now known that there are at least seven great ape-associated species, all belonging to the same clade, that can infect gorillas, chimpanzees or humans (Figure 1.1) (6). Of these, *P. falciparum* is the only one to have transferred from non-human primates (NHP), adapted successfully, and spread globally. The other human malaria species fall within a single clade that encompasses all other known mammalian *Plasmodium* parasites (Figure 1.1). This clade and the lineages containing other human malaria parasites diverged over a hundred million years ago (11), long before the emergence of the lines leading to the *Laverania* subgenus.

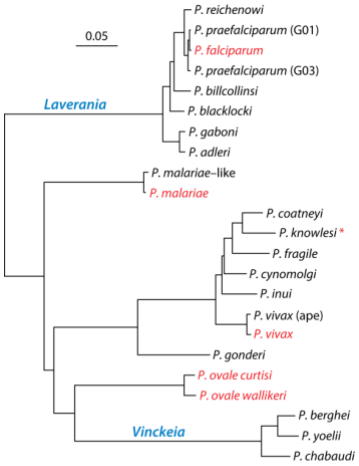


Figure 1.1: Evolutionary relationships between Plasmodium species. Whole-genome sequences were used to deduce protein sequences from 1,693 orthologous genes; from this, a maximum-likelihood tree was constructed. Human-malaria causing Plasmodium *species are highlighted in red. The scale bar indicates amino acid substitutions per site. * indicates* P. knowlesi *to be a zoonosis, capable of infecting humans. Figure taken from Sharp* et al. *(12).*

1.1.2 The Malaria Hypothesis

Plasmodium parasites have had a profound effect on the history and geography of human genetics (13). The malaria hypothesis posits that many human genetic polymorphisms, particularly those affecting erythrocytes, have been selected because they protect against malaria – by preventing infection or reducing disease severity. Haldane first suggested this in 1949 (14) and evidence for a large number of identified human genetic polymorphisms meets at least some of the hypothesis' principles – more than can be attributed to selection by any other agent (13,15). Regardless of the evolution and history of the disease, the hypothesis highlights the public health reality that humankind's previous contacts with malaria have left an immense burden of genetic disorders among us. Malaria is the selective pressure that has resulted in stable frequencies of sickle-cell disease (16), Duffy blood group-negativity (17), ovalocytosis (18), thalassaemia, and other red blood cell (RBC) disorders. These comprise the most common Mendelian diseases of humans. While the protective potential of these variants provides inroads for vaccine strategies (for example Duffy-binding protein-targeted vaccines against *P. vivax* (19)), this genetic burden is of equivalent magnitude as the current burden of malaria itself. Three to four hundred thousand babies are born with severe forms of these disorders each year (20). For humans to co-evolve with such a cunning parasite emphasises how influential this disease has been throughout history (21).

1.1.3 Recorded history

Malaria is an ancient disease. Intimations to what was almost certainly the condition are made in the Chinese *Nei Ching* ('The Canon of Medicine') from *circa* 2700 BC, Mesopotamian clay tablets from 2000 BC and Egyptian papyri from 1570 BC (15). While these early reports were mostly speculative, Homer and other early Greeks keenly noted the poor wellbeing, fevers and enlarged spleens in people living in marshy places as early as 750 BC (22).

Malaria entered Europe through Italy in roughly 200 BC (23), likely propelled by Roman soldiers and merchants (22). Before and in early stages of the Roman Empire, Sicily and Sardinia were infamous for summer and autumnal fevers. Potentially a result of infrastructural development, drainage and animal husbandry, malaria became increasingly rare in the Roman Campagna (23). In the 1,500 years after the fall of the Empire, prolonged eras of high malaria incidence interspersed with periods of no apparent malaria occurred in the area corresponding to modern-day Campania, Italy. This waxing and waning of malaria correlated with fluctuations in economic and agricultural fortune, and reflect the dependence of malaria on human lifestyle and activities (22).

Throughout the twentieth century, global malaria-related deaths never fell below half a million per year. Still, critical discoveries paved the way for first-generation antimalarial therapies, vector control and diagnostics (Figure 1.2). Scientific studies only became possible after the discovery of the parasites themselves by Charles Laveran in 1880 and the incrimination of mosquitoes as the vectors towards the late 1800s. Quinine's therapeutic effects "against all sorts of Agues" [William Slamon, Synopsis medicinae (1671)] or febrile illnesses had been known for centuries. However, it was only in the early 1900s that it became mass-produced and a favoured therapy for intermittent fevers. The restriction on supply lines caused by the World Wars led German scientists to synthesise chloroquine. In 1955, the newly formed World Health Organisation (WHO) set out the goal of malaria eradication. Emboldened by the combination of chloroquine and DDT – the highly

efficacious vector control agent and the subject of Paul Hermann Müller's 1948 Nobel prize in medicine – the WHO was armed with adequate means of vector control, diagnosis and treatment.

This goal was not achieved and no country eliminated malaria. The economic and political costs of eradication campaigns were exorbitant and unsustainable. Parasite and vector resistance emerged in several areas and malaria returned across the globe. While labelled a failure by many, these campaigns propelled malaria control efforts and provided promising outcomes, resulting in a remarkable decline of the malarious world. At the start of the 20th century, malaria accounted for around one in ten deaths. By the end of the century, this had dropped to one in a thousand – except in Africa (Figure 1.2), where there was little change to the high transmission belt covering large parts of West and Central Africa (24). The immense reduction of malaria mortality from the Western Pacific to the Mediterranean in the first 75 years of the 20th century was a truly exceptional (Figure 1.2), even if precarious, success in improving human health.

1.1.4 Modern era

Malaria was again a disaster in the late 1990s: malaria mortality had doubled in the preceding 10-20 years, and there was a stall in the financial and political capital to control the disease (5,24). In the first 15 years of this century, however, tremendous reductions in the malaria burden occurred. These gains were won by the widespread rollout of artemisinin-combination therapies (ACT) and long-lasting insecticidal-treated bed nets (LLIN) (Figure 1.2). Malaria spending rose by an order of magnitude between 2000 and 2008, and malaria deaths fell by 60% between 2000 and 2015 (25). Currently, malaria is the most problematic parasitic disease of humans, causing hundreds of thousands of deaths and hundreds of millions of clinical cases each year (25). *P. falciparum* causes 99% of malaria cases in Sub-Saharan Africa, where 94% of the malaria deaths occur (25). The most significant burden is found amongst infants, young children, and pregnant women.

1.1.4 Modern era

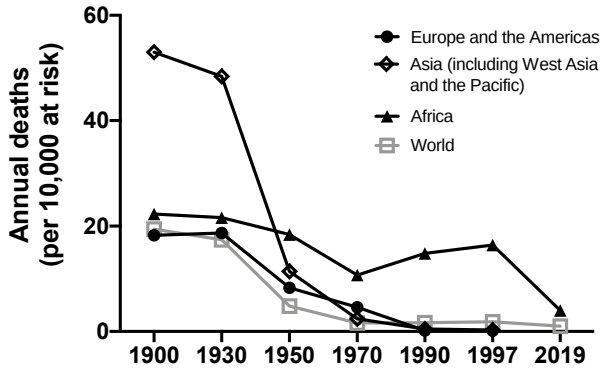


Figure 1.2: Malaria mortality in the 20th and 21st century. Tremendous results were achieved across Asia in the first half of the century. Critical to the success between 1930 and 1970 was DDT and other larval control, environmental management and treatment measures (e.g. therapeutic chloroquine). The emergence of multidrug-resistant P. falciparum*, insecticide-resistant* Anopheles *spp and the inaction of national health agencies to prioritise malaria due to lack of donor assistance were all associated with the resurgence of malaria in Africa (1970-1997). Although recent interventions, such as ACT and LLIN, have contributed to historically unprecedented declines in malaria across Africa since 2000, reductions have not occurred uniformly throughout the continent. There is ongoing high transmission in a belt covering large parts of West and Central Africa (24). Data from Carter and Mendis (15) and the 2020 World Malaria Report (25). Margin of error: 1.5-2.5-fold (26).*

Worryingly, however, progress has stalled, and malaria cases and deaths have begun to increase over the past five years (25). We are at another crossroads. The current challenges faced in the prevention of malaria are numerous. The ability of *P. falciparum* to develop resistance to artemisinin and chloroquine, and combination therapies (27,28), has endangered their ongoing efficacy. Insecticide resistance is also increasing in prevalence in *Anopheles* species mosquitoes throughout Sub-Saharan Africa and India. Resistance is especially worrying in the pyrethroid class of insecticides, used in most LLIN. Pyrethroids are becoming less effective at killing mosquitoes and models predict this could lead to increased malaria incidence (29). In some areas of Africa and India, there are increasing levels of *HRP-2* deletion (30,31). This gene deletion enables parasites to escape detection by a commonly used rapid diagnostic test. Despite this, there have been increasing calls for the elimination and subsequent eradication of malaria. In 2015, the World Health Assembly adopted the *Global Technical Strategy for Malaria 2016-2030*, including its "bold vision of a world free of malaria" (32). Even if the currently available means are used to their best ability, control and elimination pose daunting challenges, and many agree that eradication is not possible (24,33,34). Every 120 seconds, a child dies of malaria. New tools are urgently needed lest history repeats itself and malaria becomes even more disastrous once again (5,25,33,35).

1.2 The *Plasmodium falciparum* lifecycle

The *P. falciparum* life cycle progresses through female *Anopheles* mosquitoes and humans. The parasites develop through several stages to infect different cell types. Briefly, sporozoites are injected into humans, infect hepatocytes, and thereafter develop via the asexual blood-stage. Some parasites develop sexually and are ingested by a mosquito, which restarts the cycle upon human biting. Here, I discuss the *P. falciparum* lifecycle and mention the roles of several molecules that are the basis for vaccine candidate development.

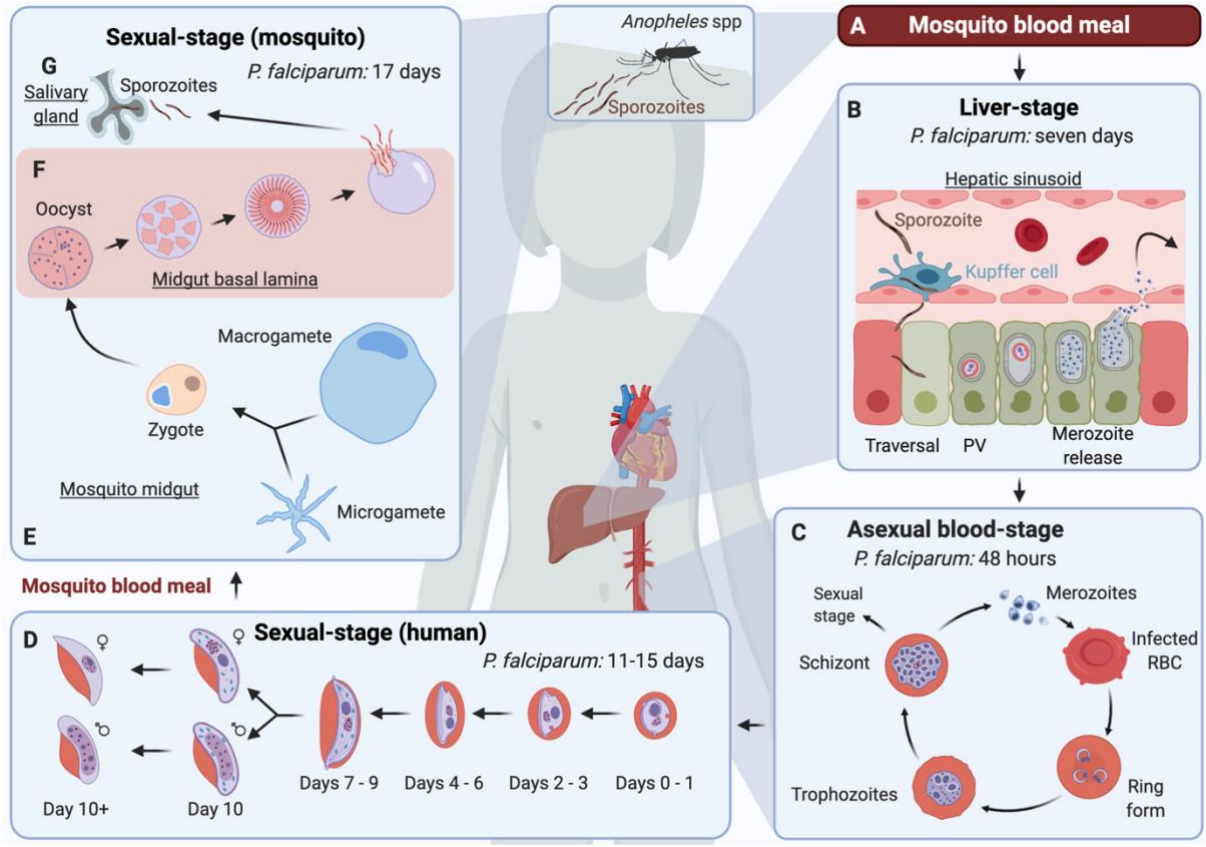


Figure 1.3: The P. falciparum *life cycle.* ***A****: Infected mosquitoes inject sporozoites into the skin which migrate to the liver.* ***B****: Sporozoites traverse through Kupffer cells or hepatocytes and invade hepatocytes. They develop inside parasitophorous vacuoles and undergo maturation, emerging as merozoites.* ***C****: Merozoites infect red blood cells and undergo asexual development to form progeny merozoites.* ***D****: A proportion of parasites undergo a developmental switch and form gametocytes.* ***E****: Gametocytes are taken up in a mosquito blood meal and reproduce in the midgut.* ***F****: Ookinetes (not shown) lodge themselves in the midgut basal lamina.* ***G****: Sporozoites are released and migrate to mosquito salivary glands, ready for onward transmission. Figure created in BioRender.com.*

1.2.1 The pre-erythrocytic stage

Sporozoites are injected into the human dermis during a mosquito blood feed. After an infected mosquito bite, approximately 100 sporozoites are introduced into the skin (36) (Figure 1.3A).

1.2.1 The pre-erythrocytic stage

Sporozoites move in the dermis via gliding, randomly reaching and penetrating blood vessels to access the bloodstream. About half of the injected sporozoites will leave the skin by two hours (37), travelling to the liver by the circulation within minutes (38). The number of sporozoites that reach the liver is unclear. Remaining sporozoites generate a host immune response after lysis and draining to lymph nodes.

Once in the circulation, a proportion of sporozoites travel to hepatic sinusoids (Figure 1.3B). Sporozoites cross the hepatic sinusoidal barrier by cell traversal through Kupffer cells (KC) or fenestrated endothelial cells (39). There is some contention about the necessity of KC invasion to allow *Plasmodium* species liver-stage infection (40,41). Traversal-essential molecules include cell traversal protein for ookinetes and sporozoites (CelTOS) (42), sporozoite microneme protein essential for traversal (SPECT) (43), SPECT2 (44), and phospholipase (PL) (45). SPECT and CelTOS are implicated in the traversal of sporozoites across the liver sinusoidal endothelial layer via KCs, while SPECT2 creates holes through membranes via a membrane attack complex-like domain (44). PL is highly conserved among *Plasmodium* species and disrupts cell membranes permitting the passage of sporozoites through cells (45).

Contact with hepatocytes converts sporozoites into an invasive phenotype. Several signals are associated with this phenotype, including activation of calcium-dependent protein kinase 6 (46), and parasite recognition of cluster of differentiation (CD)81 and scavenger receptor B1 (47). Circumsporozoite protein (CSP) is a 412 amino acid protein expressed on the sporozoite surface and liver parasites, and is exported into the hepatocyte cytoplasm (48). This protein contains a repetitive region and a type I thrombospondin repeat (5). CSP is the most abundant molecule on the sporozoite surface, is indispensable for sporozoite development and facilitates attachment to liver cells (5). Hepatocyte invasion necessitates CSP binding to heparan sulphate proteoglycans (HSPG), which activates removal of the N-terminal domain and reveals the

thrombospondin repeat (49,50). Thrombospondin-related adhesion protein (TRAP) is expressed by sporozoites and is found on the cell membrane and in micronemes (51). TRAP is involved in parasite binding to and invasion of hepatocytes (52), also mediated by HSPGs. The molecule has a short transmembrane and cytoplasmic tail that connects with the actomyosin system and provides the necessary traction to power movement, enabling the parasite to glide (53).

Initially, sporozoites traverse multiple cells inside transient vacuoles. Formation of these vacuoles does not require membrane remodelling or secretion of parasite organelles (44). Over several minutes, sporozoites can migrate through many hepatocytes before infecting a final hepatocyte (54). Once inside the terminal hepatocyte, the sporozoite exits the transient vacuole, forms a parasitophorous vacuole (PV) and proceeds through asexual replication (exo-erythrocytic schizogony) (Figure 1.3B). Replication of *P. falciparum* DNA commences within two days of hepatocyte invasion and parasites remain in the PV late into liver-stage development (55). It has been estimated that around 1 in 10^6 hepatocytes in mice, and 1 in 10^9 hepatocytes in humans are infected (56,57). Development takes approximately two days in rodent malaria and seven days in *P. falciparum*, after which 10,000-40,000 merozoites per infected hepatocyte enter into the blood by budding of membrane vesicles called merosomes (5,58). Clinically, the sporozoite and liver-stages of *P. falciparum* infection do not cause symptoms (59).

1.2.2 The asexual blood-stage

After release into the hepatic sinusoid, free merozoites begin invading erythrocytes through a process that is complete within two minutes (Figure 1.3C). There are three steps in merozoite invasion of erythrocytes: pre-invasion, active invasion and echinocytosis (60).

Pre-invasion involves initial contact between the merozoite and RBC. Merozoite surface protein 1 (MSP1) is the most abundant protein on the merozoite surface and is involved in the

initial recognition of RBC (61). It acts as a platform on the merozoite surface for several complexes that bind RBCs (62). The merozoite eventually reorientates itself such that its apex is in contact with the RBC membrane. At the apex, ligand binding involves two protein families on the merozoite: the erythrocyte binding-like proteins and *P. falciparum* reticulocyte-binding protein homologs (PfRh) (63). PfRh5 differs from other PfRh as it is smaller, lacks a transmembrane domain, and it forms a complex with PfRh5-interacting protein (PfRipr) (64) and cysteine-rich protective antigen (CyRPA) (65). PfRh5 binding to the RBC receptor basigin is an essential step for merozoite invasion (66). After the PfRh5-CyRPA-Ripr complex-basigin interaction, there is host cell influx of calcium ions (67). Following this, merozoite apical membrane antigen-1 (AMA1) binds to the erythrocyte membrane and forms a moving tight junction.

At this stage, active invasion begins. Merozoites are propelled into the RBC by the merozoite actomyosin motor complex (68). The parasite is enclosed by a parasitophorous vacuole membrane (PVM) as it invades and surface ligands are shed (69). Once the PVM is sealed at the posterior end of the merozoite and the RBC membrane is reconstituted, echinocytosis occurs and results in the RBC shrinking and forming spiky knobs (Figure 1.3C) (60). There is then recovery of the erythrocyte.

Cell division occurs once the merozoite has infected the erythrocyte. Within the infected RBC (iRBC), the merozoite develops from the growing stage trophozoite to a mature multi-nucleated schizont (Figure 1.3C). Throughout this process, the parasite exports proteins from the PVM, into the iRBC cytosol and the plasma membrane (70). Among the exported proteins is *P. falciparum* erythrocyte membrane protein 1 (PfEMP1), which induces iRBC adherence to vascular endothelium and prevents transport to and clearance in the spleen (71). Endothelial adherence leads to a phenomenon named sequestration, a major contributor to organ dysfunction in severe malaria. The parasite develops over 48h and produces between 16 and 32 daughter

merozoites that erupt from the iRBC once developed. The lifecycle continues when progeny merozoites meet another RBC. MSP1 also functions to permit merozoite exit from the RBC (72). The trophozoite and schizont developmental stages can be identified in the microscopic diagnosis of malaria (Figure 1.3C).

Asexual blood-stage parasites and immune responses to these cause the clinical symptoms and sequelae of malaria. Synchronization of parasite rupture from RBCs causes the classic fever periodicity of malaria. The release of parasite material triggers systemic cytokine release (73) and is responsible for fever, chills, headache, muscle pains and sweats. If treatment is commenced with suitable drugs, symptoms remit over a few days and complete treatment results in the eradication of infection. Incompletely treated, the illness abates, parasite densities are regulated to a low level and symptoms recur over subsequent weeks concurrent with rises in parasitaemia. In a fraction of those who are incompletely treated, the infection is not controlled and progresses to severe malaria and potentially death. The pathogenic features of severe malaria include exponential parasite growth, dysregulated host inflammatory responses, and microvascular obstruction due to endothelial activation and parasite adhesion to blood vessels (5,73). These result in at least one of the three overlapping syndromes of cerebral malaria, severe anaemia, or respiratory distress (74).

Most evidence points towards naturally-acquired immunity (NAI) being predominantly antibody-mediated and against blood-stages (5,75,76). Antibodies can prevent merozoite entry into RBC and direct killing of iRBC. The ability to protect from symptomatic disease depends on immunity against proteins displayed on the surface of iRBC, such as PfEMP1 (77,78). However, merozoite and iRBC surface antigens are highly variable, hindering the ability of NAI to induce complete protection (77,79). *Plasmodium* infection also modulates the host immune response and impedes immunity (5). The greater the transmission intensity the faster NAI is acquired, though the relationship between transmission and severe malaria is not linear (80) (Figure 1.4).

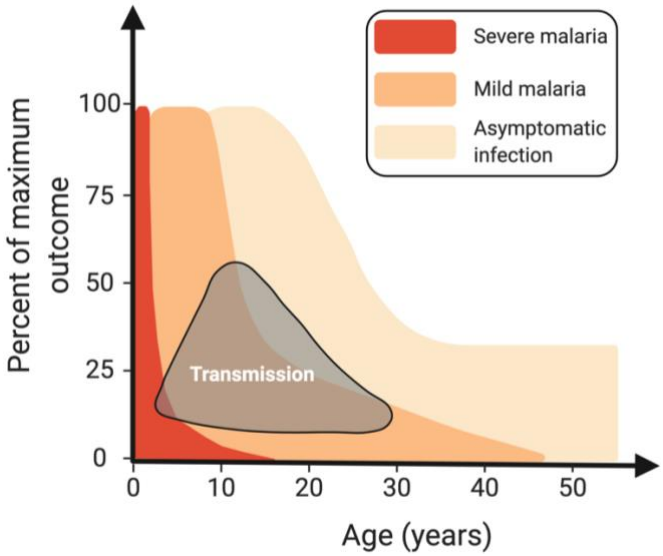


Figure 1.4: Age distribution and outcome of P. falciparum *infection. The age distribution of severe, mild, and asymptomatic infections are normalised and shown as a percentage of the maximum period prevalence achieved. Risk of severe disease and death is highest in young children and declines rapidly. Susceptibility to non-life-threatening clinical episodes of malaria continues but falls steadily such that by early adulthood, febrile episodes are few and mild. Risk of infection continues throughout life. Both asymptomatic and symptomatic* P. falciparum *infection contribute to transmission (grey shaded area), though this changes with age (more specifically, body surface area) and the frequency of exposure to mosquito biting (81). These are hypothetical percentages, and the relative contribution at each age will vary according to environmental, epidemiological, and ecological factors (81,82). Figure created in BioRender.com and partially adapted from Marsh and Kinyanjui (83) and McCann et al. (84).*

1.2.3 The sexual-stage

Some parasites undergoing asexual blood-stage development experience a switch that commits them to sexual development (Figure 1.3D). This developmental switch is crucial to the onward transmission to mosquitoes but remains poorly understood. Apicomplexa-specific transcription factor is necessary for gametocyte production in multiple *Plasmodium* species (85), and is an epigenetically regulated master switch involved in initiating gametocytogenesis (86). This switch occurs at a point in the previous schizogony cycle so when a merozoite invades an RBC its fate is pre-determined to either continue with asexual replication or to differentiate into sexual-stages. Sexual differentiation rates of *P. falciparum* can vary between 0 and 20% (87). While there is a stochastic element to this (88), environmental stimuli can also influence parasite sexual development; exposure to antimalarials and high parasitaemia are associated with increased gametocyte production (89). The first of five gametocyte stages is a round compact form enclosing hemozoin (Figure 1.3D). This and other forms are mostly absent from the vasculature (and not readily seen by diagnostic microscopy of the blood) as they sequester in the bone marrow, avoiding

splenic clearance (90). It takes approximately 11-15 days for gametocytes to mature through to an infectious stage and be taken up in a mosquito blood meal (90,91) (Figure 1.3D).

Within seconds of entering the *Anopheles* species mosquito, gametogenesis is initiated by three factors: a drop in temperature, the mosquito waste product xanthurenic acid and an increase in pH (92-94). Diploid zygotes are formed by the fusion of microgametes and macrogametes (Figure 1.3E). Attachment of the microgamete to the macrogamete is mediated by several proteins, including Pfs48/45 (95) and Pfs230 (96). Zygotes develop into ookinetes, which express the surface protein Pfs25. This is an essential molecule for ookinete survival, parasite traversal and further development (97,98). Ookinetes eventually embed themselves as oocysts beneath the mosquito midgut epithelium, in the basal lamina (98) (Figure 1.3F). Oocysts complete 10 to 11 rounds of mitosis to create a syncytial cell (sporoblast) with thousands of nuclei (99). Thousands of haploid daughter sporozoites disperse from the surface of the sporoblast (98). These sporozoites migrate to the mosquito salivary glands and are therefore ready to re-start the transmission cycle with the next mosquito bite (Figure 1.3G).

There are no clinical symptoms associated with sexual-stage development of *P. falciparum* (5). While humans in endemic areas can mount antibody responses to sexual-stage antigens such as Pfs48/45, Pfs230 and Pfs25 (100,101), and approaches aimed at inducing such antibodies are promising, it is not clear what effect, if any, naturally occurring responses have on transmission intensity. Drawing insights from natural immunity against *P. falciparum*, if present, could assist in developing 'unnatural' immunity through vaccination.

1.3 Immunity against pre-erythrocytic *Plasmodium* species

The human immune system can target any stage of the *P. falciparum* parasite to which it is exposed. However, NAI engenders responses against asexual blood-stage infection and individuals remain susceptible to repeated infections, suggesting that there is minimal natural immunity against the pre-erythrocytic stages (76,102,103). Protective humoral and cellular immune responses can be artificially maintained against both the sporozoite and developing intrahepatic stages in animal malaria models and humans by numerous approaches (104,105). Contemporary vaccine technology permits the induction of immune responses that are 'better than nature' (106). Still, an enduring challenge has been identifying the essential responses and maintaining levels sufficient to provide durability of protection. Here, I review the mechanisms by which naturally and 'unnaturally' induced immunity directed towards pre-erythrocytic *Plasmodium* stages can mediate partial and complete protection against malaria. Given the focus of this thesis on a malaria vaccine strategy targeted towards the induction of liver-resident memory CD8+ T cells, an emphasis is placed on exploring this literature.

1.3.1 Immunity to sporozoites

Sporozoites are extracellular pathogens from the moment the mosquito injects them until they invade hepatocytes. An antibody response with robust B cell and Th2-type T cell induction would be the most apt response to neutralise the sporozoite and prevent it from binding to ligands on the hepatocyte surface. Unfortunately, the speed (minutes to hours) and low number (less than a hundred) of sporozoites that migrate from the skin and enter hepatocytes make it almost impossible to mount an effective adaptive response under natural conditions. Serological surveys show that antibodies against CSP are lowly detected except in the most highly exposed individuals living in hyperendemic settings (107,108). Given the likelihood of repeated exposures throughout life in an endemic area, there is a characteristic age-related gradient where anti-CSP antibody titres increase with age (107,109). Indeed, this is indirect evidence that natural neutralising anti-

sporozoite immunity is difficult to develop. Naturally acquired anti-CSP antibodies do not correlate with the degree of anti-sporozoite protection. Hoffman *et al.* showed no difference in antibody levels between 60 individuals who did and 23 who did not develop parasitaemia and, equally, no relation between time-to-parasitaemia and anti-CSP antibody levels (110). Studies have since replicated these findings (107). Nonetheless, numerous vaccine candidates are based on the CSP antigen, with significant efficacy produced by inducing higher antibody levels than those which would naturally occur (111). Given that higher magnitude of antibodies, alone, are often insufficient to be protective, recent work has shown qualitative and functional features of vaccine-induced antibodies predict protection from infection across anti-sporozoite vaccine regimens (112).

Sporozoite-specific T cell responses can differ significantly between naturally exposed individuals and populations (113,114). Quantification of T cell immunity is hindered by low immunological responsiveness in malarious contexts. This hyporesponsiveness relates to several factors, such as i) low sporozoite inoculums leading to low T cell frequencies, ii) rapid contraction of effector T cells following exposure, iii) Major histocompatibility complex (MHC)-allele diversity, even within geographical regions, and iv) chronic co-infections with bacteria, helminths, and viruses, modulating the development of effective cellular anti-sporozoite immunity (5,107).

1.3.2 Immunity to liver-stage parasites

The liver is a unique immunological microenvironment given the need to balance the clearance of pathogens and danger signals entering from the portal circulation with maintaining tolerance to non-pathogenic antigens. The mechanisms behind the dampened and nonresponsive immune environment include low levels of MHC expression, direct cell-to-cell contact (e.g. between liver sinusoid endothelial cells (LSEC) and dendritic cells (DC)) and the expression of anti-inflammatory cytokines (115,116). Given suitable stimulation, however, the liver can generate a robust immune

response despite this tolerant milieu. As liver-stage parasites are intracellular an effective immune response would most likely be CD8+ T cell and Th1-type CD4+ T cell dominated.

1.3.2.1 Human liver anatomy and immunology – a brief introduction

The hepatic lobule is the basic structural unit of the liver. Lobules are composed of plates of hepatocytes one or two cells thick surrounding a central vein. Hepatocytes form a hexagon around the central vein with portal tracts (a branch of the hepatic artery, portal vein and bile duct) at each corner of the hexagon. Twenty per cent of hepatic blood volume is sourced from the hepatic artery, while the portal vein feeds the remaining 80% (Figure 1.5). Blood from these sources mix in the hepatic sinusoids, the hepatic capillary bed, allowing a large volume of blood through the liver (1.5L/minute). Adult total blood volume passes through about 25 times per hour. Sinusoids have an approximate diameter of 5–7µm and, as a result, the velocity of the blood is slowed down to 25–250µm/min (117). This is relatively slow when compared to other solid organs (118). After progressing through the sinusoids, blood collects in the central vein of each lobule and makes its way back to the heart (Figure 1.5).

1.3.2 Immunity to liver-stage parasites

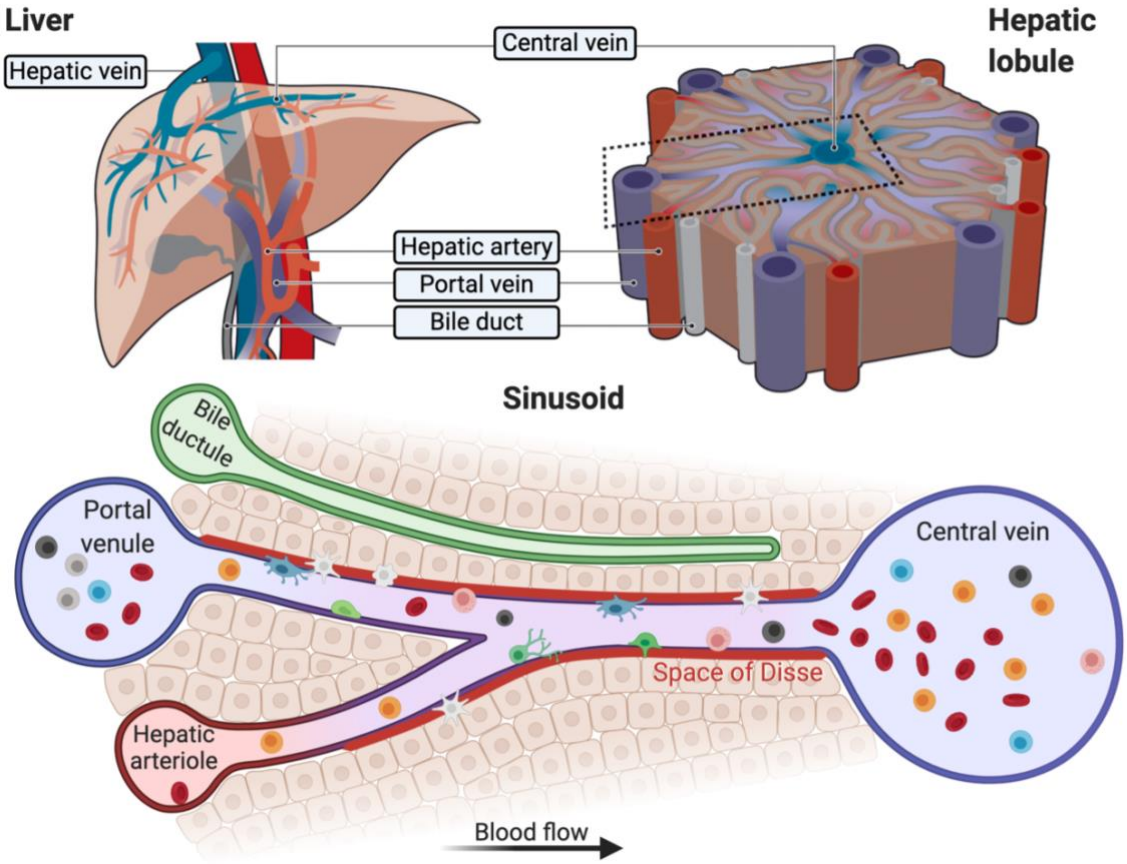


Figure 1.5: Liver anatomy and immunology. ***Liver****: Human liver macro-anatomy. The organ receives a dual blood supply, with afferent nutrient-rich blood from the portal vein and venules, and oxygenated blood from the hepatic artery and arterioles. Efferent blood flows via the hepatic vein (fed by lobular central veins). Bile is produced by hepatocytes and collects in the gall bladder via the bile ductules.* ***Hepatic lobule****: The functional unit of the liver. Each hexagonal lobule is bounded by portal tracts, which contain bile ductules, hepatic artery branches, and portal vein branches. The blood flows to the centre of each lobule and exits via central veins.* ***Sinusoid****: Representation of liver cell subsets (dashed box of the* ***hepatic lobule****). Hepatocytes are arranged in cords and surround the sinusoids. Fenestrated LSECs line the sinusoid (represented as solid purple lines here). Stellate cells are located within the space of Disse (represented by red lines between hepatocytes and LSECs) and are in close contact with KCs. Cells contained within the liver sinusoid include CD8+ TRM (green, adhered), αβ and γδ T cells (yellow, circulating), stellate cells (white, space of Disse), KCs (blue, adhered), RBCs (red, circulating), MAIT cells (dark grey, circulating), NK and NKT cells (peach, adhered) and B cells (light blue, in vessels). Not shown here are lymphatic vessels which are in the portal tract, and zonation of hepatocytes. Figure created with BioRender.com and partially adapted from Ficht and Iannacone (119). MAIT cell, mucosal-associated invariant T cell.*

Hepatocytes are the parenchymal cells of the liver. They make up 70-80% of all liver cells (120). These cells can induce an adaptive immune response, as they express MHC I molecules and inflammation can stimulate expression of MHC II (120). These cells also produce numerous acute-phase proteins and other soluble substances (including complement proteins 3 and 9). LSEC make up approximately 45% of non-parenchymal hepatic cells (120). LSECs express CD40, CD80 and CD86, MHC I and II and adhesion molecules (e.g. intercellular adhesion molecules (ICAM)), all involved in lymphocyte interaction and adaptive immunity. As might be expected, LSECs also have numerous pattern recognition receptors and play a role in the innate immune system. LSECs are

unlike those of other organs; they do not form tight junctions and have fenestrations grouped in clusters known as 'sieve plates' (121). Dissimilar to other organs, there is no basement membrane underlying the LSECs. They line the space of Disse, wherein the hepatic stellate cells reside (Figure 1.5). These features make the hepatic endothelial layer more porous than that of other organs. The liver's unique mix of characteristics permits direct cognate interactions between T cells and hepatocytes (122), without T cell extravasation (123).

KCs are localised in the sinusoidal lumen and adhere to LSECs (Figure 1.5). These cells comprise 30% of non-parenchymal hepatic cells (124). They are tissue-resident macrophages and form a large proportion of the human reticuloendothelial system. KCs, once activated, can produce several cytokines, including tumour necrosis factor (TNF) α, interleukin (IL)-1β, IL-6, IL-12, and IL-18 (125). Additionally, KCs can present antigen on their surface – they express MHC I and II and the co-stimulatory molecules necessary for the activation of T cells. Hepatic stellate cells are mostly found in the space of Disse and have dendritic-like protrusions that project around the sinusoids (120). Apart from being capable of lipid storage (such as vitamin A derivatives), stellate cells can present lipid antigens to natural killer T (NKT) cells and, possibly, to CD8+ T cells. DC are present around the portal triad and the central veins. Hepatic DCs differ to those found in lymphoid tissue by being less immunogenic, producing more cytokines and having a higher endocytotic activity (126).

Tissue-resident lymphocytes in the liver include natural killer (NK), NKT, T and B cells and make up a quarter of non-parenchymal cells (Figure 1.5). NK cells comprise 35-50% of hepatic lymphocytes and make up proportionally more of the lymphocyte population than other tissues (and at least three times greater than in blood) (127). NK cells can secrete effector molecules and modulate MHC expression by hepatocytes and stellate cells (127). NKT cells express characteristic NK markers and are mainly CD4+. They make up at least 30% of hepatic lymphocytes (compared to 0.5% of blood lymphocytes) and patrol the hepatic vasculature to detect pathogens (120). T cells form 25%

of liver-resident lymphocytes (127). Hepatic CD8+ T cells are more abundant than their CD4+ counterparts (128). Durability and turnover of memory CD4+ and CD8+ T cells are maintained by a combination of IL-7 and IL-15 (129). IL-7 supports cell viability, whereas IL-15 maintains basal homeostatic proliferation (129). Numerically, B cells contribute less than 10% of hepatic tissue-resident lymphocytes.

1.3.2.2 Innate immune responses

Sporozoites can enter CD11b+ phagocytes and conventional CD11c+ DCs (130), but knowledge of their capacity to activate these cells in the skin and the roles of different innate pattern recognition receptors in initiating innate and subsequent adaptive responses to sporozoites remains limited. A proportion of sporozoites do not enter the circulation and are processed by CD11c+ antigen-presenting cells (APC) within the skin draining lymph nodes (dLN) (131), allowing antigen presentation to adaptive counterparts. Sporozoite traversal through hepatocytes results in neighbouring cell MyD88 activation (132), which activates NF-κB and, in turn, triggers production of nitric oxide (NO). NO is detrimental to liver-stage *Plasmodium* development (133). KCs can phagocytose sporozoites (39), and hepatic inflammation and neutrophils can mediate sterile protection against sporozoites (134). Therefore, there is significant potential for innate immunity against sporozoites.

There is evidence for innate cellular immunity to infected hepatocytes. NK and NKT cells are plentiful in the livers of mice and humans and can reduce the burden of *Plasmodium* liver-stage parasites (135). NK cells proliferate in the liver after infection with *P. yoelii,* and inhibit parasite development in hepatocytes, *in vitro* and *in vivo* (136). Similarly, NKT cells can mediate liver-stage-specific protection against *P. yoelii* and *P. berghei* in mice (137). Merosomes and debris from burst hepatocytes can be cleared by infiltrating phagocytes (such as KCs, neutrophils and monocytes) (138). LSECs, KCs, stellate cells and hepatocytes are capable of antigen presentation to

T cells (139,140). Therefore the liver can act as a site for naïve CD8+ T cell priming and does not require infiltrating APCs (140,141). The exact role, and relative contribution in innate-adaptive bridging, of each these cells in response to *Plasmodium* pre-erythrocytic stages remain to be fully elucidated.

Secreted factors act on liver-stage parasites. Studies of murine *Plasmodium* species reveal that the type I interferon (IFN) transcription programme can be triggered by parasite-infected hepatocytes (142,143) and, together with innate cell IFNγ, can contribute to liver-stage protection (144). This detection occurs through the melanoma differentiation-associated gene 5 protein with signalling by mitochondrial antiviral signalling protein, IFN regulatory factor (IRF) 3 and IRF7 (56,137,143).

1.3.2.3 T cell activation by Plasmodium antigens

The innate immune system does not usually control liver-stage infection. Accordingly, the adaptive immune system is triggered for longer lasting control of infection. Sporozoites can be detected in skin dLNs as early as six hours following inoculation (37), and the first sign of T cell activation in dLNs (in natural infection) is seen one to two days after blood meal (131,145). T cell activation at the skin dLN and spleen are the most significant contributors to initial effector expansion and the pool of effector CSP-specific T cells in the liver, following administration of sporozoites (131,146,147). In contrast, activation of naïve hepatic CD8+ T cells tends to result in a tolerant immune response (122), but is still capable of inducing protective CSP-specific T cell responses (147).

While lymphoid tissues outside the liver can activate naïve T cells with sporozoite antigens (131), complete liver-stage development can induce superior anti-malarial CD8+ T cells responses (148,149). Reactivation of liver-stage parasite-specific memory CD8+ T cells is thought

to occur by hepatocytes and can induce rapid effector function (e.g. 4 hours for IFNγ) (131). The interactions that prime CD8+ T cell responses against *Plasmodium* liver-stage antigens (expressed after hepatocyte infection) are unknown. This is somewhat of an enigma since expression of these antigens is mostly constrained to parasites within hepatocytes, which are not professional APCs.

1.3.2.4 CD8+ T cell responses

Significant work has gone into identifying liver-stage T cell epitopes that are processed and presented from infected hepatocytes by MHC molecules, in the context of natural infection (150). Several studies have shown CD8+ T cell responses against CSP in the context of natural infection (113,151,152), but these are rarely associated with the absence of parasitaemia (153,154). Other antigens with naturally occurring T cell responses include liver-stage antigen 1 (LSA-1) (155,156) and TRAP (157). Data on the protective effect of these responses are mixed (107). One report showed that T cell IFNγ production following LSA-1 stimulation was associated with a reduced parasite prevalence on blood film (158) and an increased time-to-reinfection (156). Another showed that CD8+ T cell proliferation following LSA-1 exposure, but not IFNγ production, was associated with protection from malaria (159). Similarly, regarding TRAP responses, some studies show natural responses are very low and do not correlate with protection (157). However, TRAP reactivity measured with different assays shows a protective effect (160,161).

There is considerable evidence in studies of vaccine-induced 'unnatural immunity' to demonstrate that CD8+ T cells are central to protection against liver-stage malaria. Seminal reports showed that radiation-attenuated sporozoite (RAS)-induced protection was abrogated by CD8+ T cell depletion in mice (162,163). Over the past 33 years, data have accumulated supporting a major role for CD8+ T cells in immunity against liver-stage parasites. These data come from experiments involving RAS (164-168), liver-stage arresting genetically-attenuated parasites (GAP) (148,149,169,170), *Plasmodium*-specific CD8+ T cell transfer (171,172), liver-stage infection intravital

microscopy (173,174), and other studies (175). Recent work using viral vector vaccines in humans showed that liver-stage malaria protection is correlated with the frequency of peripheral *Plasmodium*-antigen-specific CD8+ T cells (176). Vast numbers of circulating *Plasmodium*-specific CD8+ T cells are required for sterile immunity. The quantity may be more than 100-fold higher than the amount necessary for "meaningful immunity" to bacterial and viral pathogens (177) with higher anti-*Plasmodium* requirements in mice compared to humans (176,178). Several reports have suggested that a threshold of antigen-specific CD8+ T cells of approximately 1% of total peripheral blood leucocytes is required to induce almost 100% reproducible and enduring protection against liver-stage malaria in mice (57,59,178). Strikingly, diversification of CD8+ T cell targets by whole sporozoite vaccination only minimally, if at all, reduces these numerical necessities (178). Despite numerous reports of the characteristics that affect CD8+ T cell priming and the induction of a protective response (131,145,146,179,180), the precise reasons why these exceptionally high levels of T cells are necessary remain unclear. Thus, while 'unnaturally-induced' T cells can eliminate the parasite from the liver, quantitative prerequisites must be met.

T cells are obligated to localise to sites of infection to mediate pathogen control. It therefore follows that peripherally activated CD8+ T cells must travel to the liver to clear liver-stage parasites. The exact marker that is specific for migration to the liver is yet to be identified. CXCR6 is expressed on many CD8+ T cells in the liver and this receptor's ligand, CXCL16, is plentifully expressed on liver endothelium (181). In seminal work, Geissman *et al.* showed that CXCR6 is vital for intrahepatic NKT cell retention (181). In the context of *Plasmodium* species infection, Tse *et al.* found that rather than CXCR6-deficient CD8+ T cells not being able to home to the liver, CXCR6 was a crucial factor for maintaining memory CD8+ T cells within the liver (182). This is altogether unsurprising, as CD8+ T cells may not need to home specifically to the liver due to the high flow rate of blood (and hence circulating cells) through the organ. Indeed, CSP-specific CD8+ effector T cells are found in several peripheral organs following vaccination (183), thus suggesting that homing may not be

strict. What may be central to CD8+ T cell hepatic recruitment may be those interactions facilitating residence through survival and retention, rather than homing-specific mechanisms.

1.3.2.5 Mechanisms of CD8+ T cell-mediated protection

Given the astronomical quantitative requirements for T cell-mediated protection in the hepatic stages of infection, what of the qualitative characteristics and requirements?

Elimination of liver-stage parasites is mediated by recognition and lysis of infected hepatocytes by *Plasmodium*-specific CD8+ T cells. Intravital imaging of CD8+ T cells has shown that they kill infected hepatocytes directly, with the formation of cellular clusters around infected hepatocytes (174). Perforin and granzymes mediate this cytolytic process (184,185). The absolute requirement for direct contact between CD8+ T cells and infected hepatocytes for parasite elimination remains an area of contention (131,186,187). Bystander killing, however, is minimal during the CD8+ T cell responses to liver parasites (188). Therefore, the high quantitative T cell requirements may relate to the spatial and temporal limitations of liver-stage infection: every single *Plasmodium*-infected hepatocyte must be found and eliminated in a relatively short period of time to achieve sterile immunity.

Liver-stage malaria protection is facilitated by several cytokines. Endemic setting studies provide a basis for the importance of cytokine-mediated protection. IFNγ responses directed against pre-erythrocytic antigens correlate with higher haemoglobin levels and reduced prevalence of severe malarial anaemia (161) and are associated with resistance to re-infection (156,189). Additionally, cumulative age-related exposure to *P. falciparum* increases the frequency of IFNγ responses (190,191). IFNγ is well known to play a part in impeding liver parasite development in experimental models (162,163,192). Butler *et al.* showed that antigen-specific T cells mediate immunity against rodent malaria species in an IFNγ-dependent manner (185). TNFα is also involved

in protection by T cells (193). High levels of TNFα production are associated with faster malaria resolution and improved prognosis in humans (194). Knockout of TNFα reduces memory CD8+ T cell-mediated protection against several murine malaria species in vaccinated mice (185) and TNFα knockout mice with nonlethal *Plasmodium* infection have significantly higher levels of initial parasitaemia than controls (195), potentially indicating a higher burden liver infection. Notably, the effector pathways T cells use to eradicate liver-stage infection may be species-specific (185). So, while it is likely that each *Plasmodium*-infected hepatocyte must be found by CD8+ T cells for the elimination of infection, cytokines can assist in the cytolytic process. Importantly, however, there is ongoing debate for many of these findings. The liver remains a black box regarding the mechanisms facilitating discovery, recognition, and eradication of *Plasmodium*-infected hepatocytes.

1.3.3 Tissue-resident memory CD8+ T cells

Memory CD8+ T cells are heterogeneous. Many subsets have been described depending on surface marker expression, proliferative, effector and migratory capabilities, localisation and maintenance (196). Classically, memory CD8+ T cells have been categorised into two subsets. Central memory T cells (TCM) reside in lymphoid tissues, including the spleen and lymph nodes, and express high levels of CD62L, CCR7 and IL-7Rα (197). In contrast, effector memory T cells (TEM) reside in peripheral organs and the blood and express low levels of CD62L and CCR7 (197). In 2009 another memory T cell population was identified, named tissue-resident memory T cells (TRM) (198). TRM are present in almost every tissue studied (199), including the reproductive tract, lung, thymus, salivary glands, pancreas, nervous tissue, heart, kidney and liver (200-202). CD8+ TRM have been pathogenically implicated in a number of diseases and, in other contexts, are essential for protection to lethal infectious challenges (203).

1.3.3 Tissue-resident memory CD8+ T cells

1.3.3.1 Definition, differentiation, and durability

The hallmark characteristics of tissue-resident T cells include i) long-term maintenance and self-renewal, ii) abundance at barrier sites, iii) sensing of microbial products, cytokines, alarmins and stress ligands, and iv) rapid provision of antimicrobial and tissue-protective factors (200). Memory T cells are thought to be derived from populations of cells that previously expressed genes associated with effector T cells, and have since turned off expression of these genes, but retain epigenetic markers of their developmental path (204,205). This is central to TRM hallmark iv): the ability to rapidly re-establish effector cell function upon pathogen re-exposure.

The generation and maintenance of tissue-resident lymphocytes are contingent upon various processes including tissue infiltration, retention, and suppression of exit. The early transcriptional identity of TRM precursor cells and the signals controlling their fate are yet to be fully understood, however, nonlymphoid TRM precursors are transcriptionally different from circulating memory and effector cells (206). These precursors exhibit chromatin accessibility at sites near genes usually expressed by mature TRM. TRM enter tissues early in the immune response and are distinct from recirculating memory cells in the peripheral circulation and lymphoid organs (202). At these early stages, memory CD8+ T cells acquire the intrinsic genetic and epigenetic signatures allowing tissue residence (206). The interplay between microenvironment and intrinsic transcriptional regulators is also prescriptive in maintaining tissue residency (202). Upon tissue infiltration, lymphocytes tend to adapt to their microenvironment and go through local differentiation (196). Therefore, while the gene expression profile of different populations of CD8+ TRM share characteristics, it is also influenced by the tissue environment (207,208).

The primary signal for TRM reactivation is cognate antigen, but tissue-wide inflammation and damage in tissue parenchyma can result in non-cognate pathogen protection mediated by TRM (209). Similarly, TRM can be maintained in the absence of antigen, albeit at lower levels than

with antigen (210). TRM therefore can react with the speed and frontline surveillance features of innate lymphocytes. Simultaneously, TRM maintain the specificity, diversity and amplifying functions characteristic of circulating T cells (200).

The precise longevity of TRM remains unclear. In mice, the cells are quantitatively stable in tissues for months and can persist without a source of local antigen presentation (196). In humans, their frequency is maintained over decades (211,212). There is evidence from parabiosis experiments that circulating cells do not replenish TRM at 'rest' (199), suggesting autonomous proliferation and renewal. The expansion of pre-existing TRM dominates local responses in the female reproductive tract of mice, and self-sustaining expansion is the most significant contributor to boosted secondary TRM populations (213). Similar results are also observed in the skin (213). *In situ* homeostatic proliferation has been shown to occur in both IL-15-dependent and -independent manners (214,215). Other signals that have been linked with increased survival of TRM include 4-1BB, aryl hydrocarbon receptors, and autophagy and mitochondrial fitness (207,216,217). By contrast, inflammatory states allow the recruitment of circulatory cells into tissues, which then adopt a TRM signature (218). TEM have been suggested as crucial for the maintenance of TRM-like CD8+ T cells and protective immunity in the lung post-influenza infection. Circulating TEM, and not TCM, are the precursors to lung TRM induced by influenza A virus (218). Thus, the maintenance of TRM is likely affected by tissue localisation, inflammatory state, presence of antigen, and other factors.

1.3.3.2 Functional and transcriptional adaptations

TRM differ significantly from circulating memory T cells in terms of function and transcriptional regulation (202,208). The most widely recognised markers of TRM include surface expression of CD69, CD103, CD49a and CD44 molecules (219,220). TRM express genes associated with adhesion (*Itga1*, *Itgae*, *Chd1*), immunoregulation (*Cd244*, *Icos*) and tissue retention (*Rgs1* and *Rgs2*) (220). At

the same time, they downregulate tissue egress genes, including *S1pr1*, *S1pr4* and *S1pr5*, and those required for homing to lymph nodes (*Ccr7*) (202). TRM express high levels of IFNγ, granzyme B, and TNF mRNA (221). Remarkably TRM also express various inhibitory receptors such as CTLA-4, 2B4 and PD-1 (196). The simultaneous effector and inhibitory phenotype of these cells likely reflects a cellular state where rapid cytotoxic functions are kept under tight regulation by inhibitory signals (200). Thus, these cells are poised for reactivation in peripheral tissues.

The transcriptional regulation of TRM in mice is well established. In seminal work, Mackay *et al.* described 35 genes that orchestrate T cell residency in mice, regardless of lineage or tissue origin (208). Two of these transcription factors, Hobit and Blimp1, were shown to be fundamental regulators of the universal transcriptional program. Recent work by Milner *et al.* additionally identified Runx3 as a necessary transcription factor for the differentiation and homeostasis of murine TRM in multiple tissues (206). Two T-box transcription factors, T-bet and Eomes, need to be downregulated for T cells to receive signals from transforming growth factor (TGF)-β and allow TRM formation (222). Similarly, T-bet expression must be downregulated to preserve expression of the β-chain of the IL-15 receptor (214). Therefore, these transcription factors at least partly control IL-15 and TGF-β signalling, which are required for correct formation and function of TRM (207). Downregulation of KLF2, another transcription factor, regulates the expression of CD62L and S1P and, thus, prevents recirculation of TRM from the liver (223,224).

Among the characteristics that are common to TRM from different organs, the relative importance of these characteristics differs according to tissue. For example, while skin CD8+ TRM showed partial defects in development without Hobit, these cells were not affected by a lack of Blimp1 (225). Contrastingly, CD8+ T cells lacking only Blimp1 showed a critical defect in homing to the lung following influenza infection (226). Similarly, Sowell *et al.* showed that the effect of mTOR (a regulator of proliferation, differentiation and survival) on CD8+ T cell differentiation and TRM

formation varies in a tissue-dependent fashion (upregulating TRM proliferation in some, while downregulating TRM proliferation in others) (227). Even among some of the most widely recognised markers of TRM, CD69 and CD103, heterogeneity is present across tissue (199). CD103, for example, is selectively upregulated in TRM of the small intestine and skin but not necessarily in the liver (198,201,208,228).

The discovery of TRM is in large part due to experiments allowing discrimination of tissue-resident populations from those that are circulating (200). Parabiosis experiments provide direct evidence that tissue-resident cells do not recirculate (199), and it has been suggested that these are one of the only ways that cells can be conclusively defined as "resident" (220). Two assumptions that underlie many studies of TRM are that i) single-cell suspension-derived T cell isolation is efficient and produces an unbiased representation of all cell subsets, and ii) that cell surface markers identify TRM faithfully. Steinert *et al.* challenged these assumptions by demonstrating that the number of TRM found in tissue sections can be far greater (as much as 60 times greater) than the number of TRM recovered from single-cell suspensions of the same tissues (199). Furthermore, the relative proportions of memory T cell subsets can be skewed by sample preparation techniques. Due to the relatively recent discovery of TRM, some of the information regarding T cell-mediated liver-stage malaria protection should be re-examined. For example, a previously established means to distinguish between TCM and TEM (as both are CD44+ cells) was by CD62L expression (197). Like TEM, TRM also express low levels of CD62L and would classify as TEM with this criterion (56,229). A potential means to differentiate TRM and TEM would be that TRM are, by and large, CD69+. Thus, TRM may generally be identified by being CD44+, CD62L- and CD69+ in mice (208).

1.3.3.3 Plasmodium-*specific liver TRM in mice and non-human primates*

Liver TRM have recently emerged as a promising target for protection against liver-stage malaria, although the importance of memory phenotype CD8+ T cells that persist within the liver long

precedes the 'discovery' of *bona fide* TRM (230,231). CD4+ TRM have been identified by surface marker expression in the mouse liver (232) and can protect against reinfection in other tissues (233), but liver CD4+ TRM have not yet been comprehensively characterised, nor has their residency been unequivocally demonstrated; therefore, they are not discussed here. To date, all data on *Plasmodium*-specific TRM have been generated in murine and NHP models, mostly examining CD8+ T cells.

Several mouse studies demonstrate that while hepatic TRM are localized within the hepatic sinusoids (181,201,234-236) they do not recirculate (201,234,237). The sinusoids provide TRM with an optimal niche for direct interaction with APCs, such as KCs and DCs. This allows for the rapid detection of antigen. Unlike circulating TEM, TRM patrol the sinusoids; they 'crawl', have an amoeboid shape and move slowly at approximately 10μm/min, independent of vascular flow and antigen recognition (123,201). The proximity of each hepatocyte to a sinusoid allows easy access by liver TRM to surface antigen presentation (201,235,236). Instead of needing CD103-αE integrin interactions to maintain themselves in the liver, hepatic TRM use the adhesion molecule LFA-1 and its interaction with ICAM-1 to patrol the sinusoids (236). Similarly, CXCR6 is required for liver TRM maintenance (182). Survival of hepatic CD8+ TRM is contingent on IL-15 following vaccination with *P. berghei* sporozoites (238).

CD8+ TRM are potent mediators of protection against liver-stage malaria in mice. CD8+ T cells recognise *P. berghei*-infected hepatocytes via antigen-dependent MHC I presentation (188,201) and there is direct evidence of liver-stage malaria parasite killing by CD8+ T cells bearing a transgenic T cell receptor (TCR) specific for a parasite epitope (174). Given that TRM are the only known conventional CD8+ T cell that can effectively patrol liver sinusoids (239), it is likely that these are the cells that identify infected hepatocytes and directly kill or recruit other immune actors to kill parasitised cells. Evidence in support of this comes from studies showing that depletion of TRM,

induced by different vaccine regimens (237), abrogates protective efficacy against subsequent *P. berghei* infection. Indeed, mice with fewer liver CD8+ T cells are less protected against sporozoite challenge, even though they have normal numbers of memory CD8+ T cells in the spleen (182). Conversely, TRM are stably maintained in the liver and are sufficient at mediating protection against *P. berghei* (237). In rhesus macaque *P. knowlesi* infection, the depletion of TRM (when induced by sporozoite and chemoprophylaxis administration), results in loss of sterile protection (235). *Plasmodium*-induced liver TRM have a unique transcriptional profile, different from that which is described for TRM induced by other microbes (223). Significant differences were found in immune function genes as well as those regulating cell trafficking, cell cycle, and intracellular signalling. The frequency of *Plasmodium*-antigen-specific hepatic CD8+ T cells also correlates with protection against challenge with *P. berghei* in mice (240,241) and *P. knowlesi* in NHPs (235). Further indirect and correlative evidence for liver-resident CD8+ T cells as being necessary for durable sterile protection is abundant (168,242,243). The contribution of hepatic CD8+ TRM to naturally induced immune responses is plausible through activation-induced liver seeding and liver-autonomous proliferation but is likely minimal if present. This is a line of inquiry that has not been investigated, as opposed to naturally-acquired circulating *Plasmodium*-specific T cell responses, which have been thoroughly investigated (107).

1.3.3.4 Human liver TRM: unique attributes and infectious disease protection

Direct isolation and visualisation of human liver TRM are difficult and, until 2017, human liver TRM remained unidentified. Stelma *et al.* were the first to characterise the CD69+ CD8+ T cell compartment of the liver, finding that only a subset co-expressed CD103 (244). They discovered that TRM expressed low levels of *S1pr1* and *Klf2*, and >90% were CXCR6+. Since this initial study, the Maini group at University College London has produced many new insights in the field of human liver TRM (211,217,245-248), particularly in the context of viral hepatitides.

1.3.3 Tissue-resident memory CD8+ T cells

The human liver contains populations of both CD69+ CD103- and CD69+ CD103+ CD8+ T cells, that can be distinguished from infiltrating but not resident CD69- CD103- T cells by expression of common residency molecules (CD49a, CXCR6, S1PR1 and KLF2) (244,246,249). In contrast to TRM in other organs, CD69+ CD103- CD8+ TRM numerically dominate (211,246,247,250) and they express chemokine receptors supporting liver retention (CXCR6, CXCR3, and a lack of CX3CR1) (244,246,247,249). CD27+ has also been used to identify hepatic TRM (244,246). CD69+ CD103+ cells make up just over 10% of the intrahepatic memory T cell pool, whereas these cells are virtually undetectable (<1%) in the periphery (251). Despite CD69+ CD103- CD8+ T cells being weaker effectors than their CD103+ counterparts, the CD103- population is the dominant effector population in the liver (250). CXCR3+ CD69+ CD103± CD8+ T cells, including global and hepatitis virus-specific T cells, have the potential for longevity and self-renewal of more than a decade within the liver (211). However, in the context of liver transplantation, hepatic leucocytes are mostly replenished from the blood, and these liver-seeding T cells can acquire characteristics of long-lived, donor-derived cells, such as CD69 and CD103 expression (211). Therefore, the human liver is a flexible niche for TRM.

Functional characterisation of human liver TRM has relied on *in vitro* and histological methods. By repeatedly stimulating with IL-15 (which is constitutively expressed in the liver and induces T cell differentiation (252,253)), or antigen exposure followed by TGF-β (known to induce CD103 (222)), peripheral blood mononuclear cells (PBMC) can be induced to differentiate into cells bearing a strong resemblance to liver TRM (246). 'Induced TRM' express high levels of exhaustion markers such as PD-1 and CD39 (246). These inhibitory molecules, along with paradoxically vigorous, prompt and autonomous IL-2 and IFNγ expression, are hypothesised to allow hepatic CD8+ TRM to maintain themselves while simultaneously performing noncytolytic immunosurveillance (246). Supporting this, non-stimulated CD69+ and CD69- CD8+ T cells isolated from the liver express equivalent levels of cytokine mRNA expression (i.e. IFNγ, TNFα and MIP-1β) (244).

1.3.3 Tissue-resident memory CD8+ T cells

Immunohistochemistry of liver sections shows TRM to be compartmentalised within the vasculature of the human liver (246), like mice. Contrasting mice, human liver CD45RA- CD69+ CD103+ T cells express lower levels of granzyme B when compared to CD69- counterparts and circulating memory CD8+ T cells (246). It has been hypothesised that exposure to signals within the hepatic microenvironment (246) and cognate antigen recognition (250) within the liver may be needed for CD69+ CD103- TRM to further differentiate (e.g. into CD69 CD103 double-positive cells) and slide further toward the non-recirculating end of a 'tissue-residency spectrum' (247,254). In contrast to mice, the prevalence of Ki67+ cells is four-fold higher in intrahepatic CD69- CD8+ T cells than CD69+ CD8+ T cells (244). This, along with the finding that there is no differential expression of Nur77 between hepatic CD69+ and CD69- CD8+ T cells (244), suggests that persistent T cell activation (as observed, for example, in *Plasmodium*-antigen-specific hepatic TRM of mice (223)) may not be necessary for TRM maintenance in humans.

The transcriptional regulation and profile of tissue-residing T cells may provide insights into how vaccines should ideally modulate T cell immunity to induce TRM phenotypes. Influential work by Kumar *et al.* demonstrated that CD69+ memory T cells found in tissues (therein defined as TRM) were phenotypically and transcriptionally different from CD69- tissue and blood memory T cells (therein defined as TEM) and exhibited a core transcriptional and functional signature (219). This signature involved upregulation of genes encoding molecules for tissue retention (CD49a, CRTAM, CXCR6), inhibition (PD-1) but rapid response once activated (IFNγ, IL-2, IL-17), and simultaneous downregulation of molecules associated with tissue egress (CD62L, S1PR1, CX3CR1) and cell turnover (Ki67) (219). Hobit is expressed in resident and circulating CD8+ T cells in humans, and when expressed, is associated with cells lacking residency markers. Indeed, Stelma *et al.* found less hepatic CD69+ CD8+ T cells expressed T-bet and Hobit when compared to blood CD8+ and hepatic CD69- CD8+ T cells (244). A key regulator of the TRM phenotype in human liver CD8+ TRM

is the prototypic hepatic cytokine IL-15, which upregulates autophagy, driving acquisition of tissue-retention markers and preventing mitochondrial depolarisation (217). Since the work of Kumar *et al.*, several reports have emerged characterising human liver lymphocyte (255) or human liver CD8+ T cell transcriptional regulation (256) in healthy and diseased livers (257). These studies have helped to parse the heterogeneity within and among human TRM populations. There are likely different transcriptional regulators involved in human and mouse liver TRM development and within human liver TRM subpopulations.

The evidence for human CD8+ TRM as critical mediators of protection against hepatotropic infections is evolving, most notably in the context of chronic viral infections. In people with hepatitis B and hepatitis C virus infection, there is a negative correlation between virus-specific TRM in the liver and control of viral load (245,246), suggesting that TRM can effectively perform immunosurveillance and viral suppression. It is worth noting, however, that hepatitis virus-specific hepatic CD8+ T cells are not always beneficial for the liver and host (258,259). The innate-like ability of TRM to generate a state of tissue-wide alarm and contribute to heterologous protection has been demonstrated in mice (209,260) and, recently, in humans (250,261). However, in human acute hepatitis A, this bystander activation is deleterious and results in over-activation and liver damage. Kim and Shin hypothesised that the balance between T cell immunoprotection and immunopathology is influenced by the cytokines inducing reactivation, among other factors (262). Analogous to findings in mice wherein TRM pathogen-specificity drives intrinsic characteristics (223), liver TRM specific for hepatitis virus antigens exhibit a unique phenotype compared to non-virus-specific liver TRM (244).

Human evidence for the role of TRM in *Plasmodium* liver-stage infection clearance is scant. Attenuated *P. falciparum* sporozoite vaccination regimens that are protective against homologous rechallenge in humans induce higher frequencies of hepatic TRM in NHPs, when compared to non-

protective regimens (166,168,242). Despite considerable evidence in mice, more work is needed to elucidate the protective function of human liver TRM in response to hepatotropic pathogens.

1.4 Malaria vaccine development

Vaccines have saved more lives and benefited society more than any other class of medicine (263). Two infections, smallpox and rinderpest, have been eradicated and polio will follow. More than seventy vaccines have been licensed for use against more than thirty pathogens, and most health economists agree that immunisation is the most cost-effective means to save lives and preserve health. Vaccines likely represent the exit strategy out of a world mired in the social, economic and health consequences of a catastrophic COVID-19 pandemic. For almost all successfully licensed vaccines, natural immunity against infection has been demonstrated, and the vaccines mimic the protective immune response (263). By contrast, for malaria (as well as HIV, tuberculosis, and other infectious diseases), preventive or sterile immunity is not found in natural settings and development of effective 'traditional' vaccines has been difficult. In 1899 Robert Koch, after publishing the first description of naturally acquired malarial immunity, postulated on the prospects of malaria vaccines:

> "*One may assume an anti-malarial immunity, which under ordinary conditions is acquired only in 4–6 years and after repeated attacks, to be conferred artificially and in a short time. Seeing, however, that as yet we have no idea how to obtain the toxins necessary for the immunizing process, chances of progress in this direction are small.*" (264)

Sadly, Koch's doubtful forecast has proved correct. More than 120 years on there is still no highly effective vaccine. Meaningful progress has been made towards this goal, and there are numerous candidates being trialled in humans within endemic settings or 'challenge' controlled human malaria infection (CHMI) studies. So far, malaria vaccine strategies have mostly targeted distinct life-cycle stages of the *P. falciparum* parasite and the focus has been on the pre-erythrocytic stage (Figure 1.6). A large proportion of the malaria vaccines being developed are based on *P. falciparum* subunit proteins, which have demonstrated partial immunogenicity in humans. Therefore, efforts have also focused on delivery and adjuvant platforms to induce favourable

immune responses and maximise protective immunity while minimising adverse reactions. This section dwells on the most promising pre-erythrocytic malaria vaccine candidates. The prospects for asexual blood-stage and sexual-stage vaccines, the ideal candidate, and difficulties inherent to malaria vaccinology are discussed in brief.

1.4.1 Pre-erythrocytic vaccines

A vaccine promoting an immune response that stops *P. falciparum* early on in human development is highly desirable. The number of *P. falciparum* parasites involved in infection undergoes immense numerical fluctuations throughout the transmission cycle. This forms the basis of the 'bottleneck hypothesis' (5) suggesting that attacking a numerical bottleneck in parasite growth at the liver-stage, when there is also relative spatial and immunological quiescence, could achieve protection more easily than at other stages (Figure 1.6, grey encircled numbers). In contrast to, for example, vaccines targeting asexual blood-stage parasites that are present in far greater quantities and have evolved numerous immune evasion mechanisms. Pre-erythrocytic vaccines have the potential to prevent death and disability, as well as onward transmission if they are of high enough efficacy and can prevent or substantially reduce blood-stage infection (33,38,265).

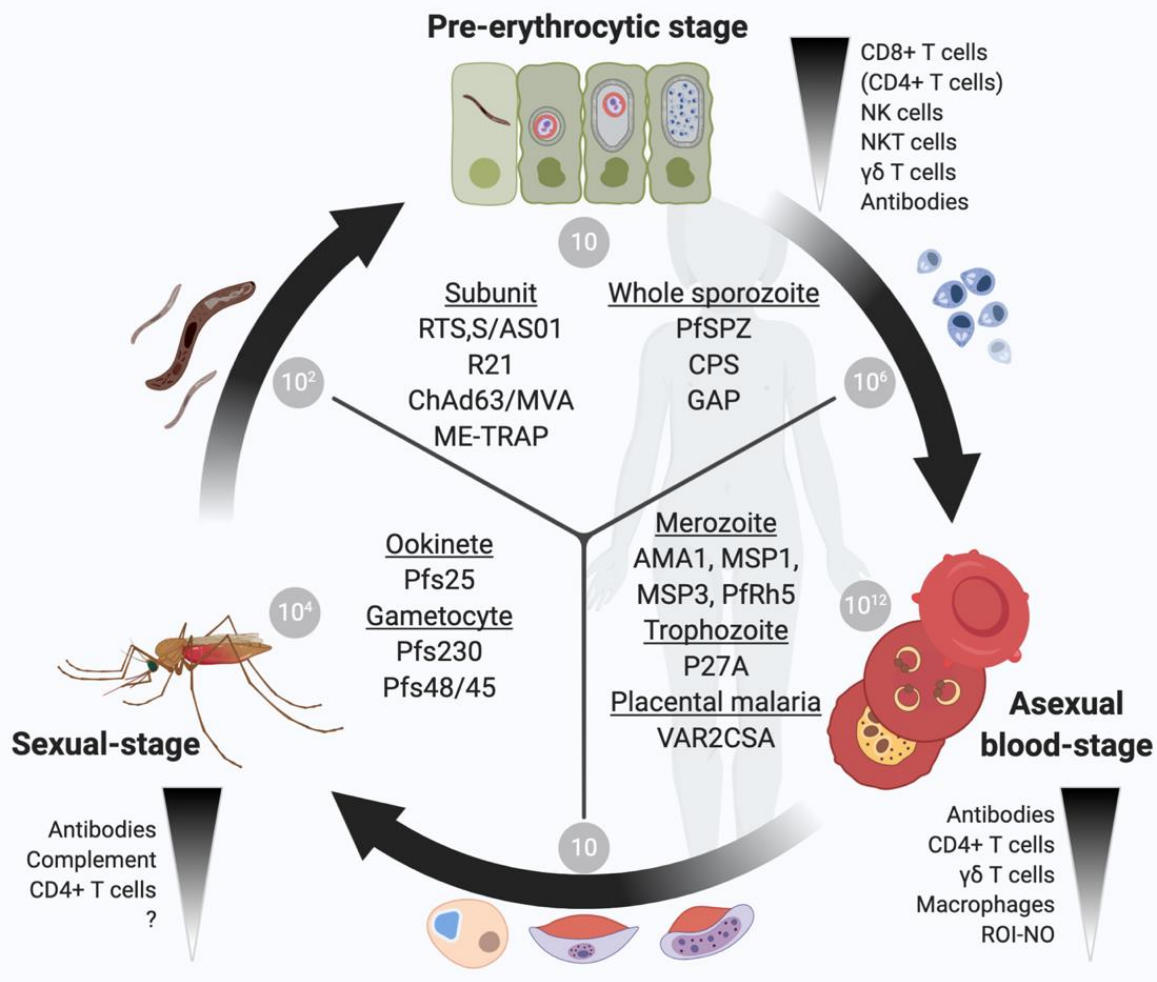


Figure 1.6: P. falciparum *malaria vaccine candidates. A per-stage summary of selected vaccine candidates against* P. falciparum*. Encircled numbers represent the maximum parasite population in individual hosts at the indicated stage. The numerical bottlenecks that occur at sporozoite skin migration and hepatocyte invasion (top), and ookinete penetration of the midgut (bottom), are considered priority areas for vaccine development. Natural and vaccine-induced immune mechanisms are displayed at various stages on the outside of the cycle (76). Figure created with BioRender.com.*

1.4.1.1 CSP-based approaches

The most advanced *P. falciparum* vaccine candidate is RTS,S/AS01 (Figure 1.6). This pre-erythrocytic subunit vaccine targets CSP and uses the hepatitis B surface antigen (HBsAg) as the antigenic carrier matrix. The immunodominant B cell epitope from the central region of CSP (comprised of NANP repeats) and the C-terminal regions are fused to HBsAg and expressed with free HBsAg in yeast. Thus the vaccine is named RTS,S to denote the CSP repeat region (R), T cell epitopes (T) fused to HBsAg (S) and assembled with unfused copies of HBsAg (S). RTS,S spontaneously forms lipoprotein particles with the CSP fragment on their surface (266). The vaccine

is formulated in GlaxoSmithKline's proprietary adjuvant AS01E. RTS,S immunity is thought to be mediated mainly by high CSP-specific antibody titres, as well as more limited T cell responses (267).

The vaccine has undergone human clinical trials spanning across four decades (with trials ongoing). The vaccine is efficacious in non-endemic settings, protecting about half of subjects against CHMI two to three weeks after the last dose, and 22% at five months after the previous dose (268). RTS,S/AS01 induces low rates of protection of limited duration in malaria-endemic areas. The final RTS,S/AS01 phase III trial analyses included almost 9000 children between 5 and 17 months old in the modified intention-to-treat analysis, considering all participants who received at least one vaccine dose (269). This trial showed 36% and 32% efficacy against clinical and severe malaria, respectively, using a four-dose regimen at the median follow-up of four years. Anti-CSP antibody titres have been shown to wane rapidly (270). A 7-year follow-up analysis of a three-dose subgroup showed initial efficacy against febrile malaria (4.4%), but protection was offset by negative efficacy and rebound cases in later years in settings of higher-than-average exposure to *P. falciparum* (271). A recent study has not replicated the negative efficacy finding, however (272).

Despite the limitations inherent to the vaccine, RTS,S/AS01 has the potential for public health impact if correctly deployed. In July 2015, the European Medicines Agency (EMA) adopted a positive opinion of RTS,S/AS01 as a safe and efficacious preventative malaria vaccine (273). This was a watershed moment in malaria's long history. Following the decision by the EMA, the WHO gave support to begin large-scale implementation studies using a four-dose regimen in 5-to-17-month-old children residing in moderate-to-high transmission settings. Three countries were selected: Ghana, Kenya, and Malawi. So far more than 1.2 million RTS,S/AS01 doses have been administered. Safety and impact analyses, 24 months after beginning vaccination, are due to start in 2021 (274).

1.4.1 Pre-erythrocytic vaccines

There have been several attempts to develop second-generation CSP-based vaccines, using RTS,S or other technologies (275-277). One of these is the RTS,S-like vaccine called R21, formulated with increased CSP:HBsAg, which has shown promise in animal models (278) and early clinical trials (279).

1.4.1.2 Whole sporozoite approaches

Despite evidence from monkeys (in the 1940s (280)), mice (in the 1960s (281)) and humans (in the 1970s (282)) showing that sporozoite administration could induce sterile immunity, this approach was not pursued with vigour until the early 2000s (283). This work culminated in 2010 with a publication detailing the Good Manufacturing Practice (GMP) process required to harvest, purify, and cryopreserve sporozoites (284), rendering a clinically viable approach (285). *P. falciparum* sporozoites can be attenuated by several means: radiation (called the PfSPZ vaccine) (286); chemoprophylactically by simultaneous administration of antimalarial drugs (called chemoprophylaxis with sporozoites (CPS)) (287); or genetically (called GAP) (288) (Figure 1.6). These approaches have been described as the gold standard for pre-erythrocytic vaccination (201). Sporozoite-based vaccines express thousands of *Plasmodium* antigens and induce a broad immune response. PfSPZ are unable to progress further than early liver-stage development (285). CPS permits the full development of parasites in the liver while preventing blood-stage replication through pre-erythrocytic killing by chloroquine (289). GAPs have targeted removal of genes necessary for complete liver-stage development (290), thereby maximising parasite immunological exposure but preventing the pathogenic blood-stage infection. All sporozoite vaccines rely upon both T cells (including γδ T cells) (168,201,242,243,291) and antibodies for sterile protection (163,292,293), but many immunological questions remain unanswered and their resolution likely depends on the type of attenuation, sporozoite dose and route of administration.

1.4.1 Pre-erythrocytic vaccines

Sporozoite approaches have shown promise in clinical trials. The PfSPZ vaccine has afforded sterile protection in non-endemic (166,168,242,294) and endemic (293,295,296) settings against homologous (166,295) and heterologous (293,294,296) sporozoite challenge at time points of between six and twelve months. Notably, protection often requires more than four doses. Further endemic setting efficacy trials involving hundreds of people are either complete and being published or are ongoing, with results expected soon (297). A phase III trial of PfSPZ is scheduled to begin in 2021 on the island of Bioko. In malaria-naïve volunteers, CPS confers high rates of sterile protection against homologous sporozoite challenge (287) that can last up to 28 months (298) but induces only modest heterologous protection (299). GAPs are undergoing trials in non-endemic settings for safety, immunogenicity, and efficacy (NCT03163121; NCT03168854).

Several impediments exist for the whole sporozoite vaccine strategy to reach widespread use. These include the need for high numbers of parasites and intravenous (IV) administration to induce sterile protection, the need for a low temperature cold chain to maintain viability, long-lived chemoprophylactic agents (for CPS) and the need to produce large numbers of sterile sporozoites at scale and under approved GMP conditions. As a result of these challenges, several other subunit approaches have been pursued.

1.4.1.3 Viral vector approaches

Viral vectors in heterologous prime-boost strategies have been used with the aim of inducing T cells that target infected hepatocytes (251). Using several platforms and antigens, these strategies have generated some protection in CHMI trials (176,275,300,301).

TRAP has been extensively investigated as a vaccine antigen in non-endemic CHMI studies, due to the protein's indispensable role in gliding motility and infection of hepatocytes (302). Full-length TRAP from the T9/96 *P. falciparum* Thailand strain is often fused to a multiple epitope (ME) string

which contains approximately 14 CD8+ T cell epitopes as well as three CD4+ T cell epitopes from tetanus toxin, Bacille Calmette-Guerin (BCG) and CSP, and two B cell epitopes (303). The individual components of the ME string induce immunity, and some have been trialled, without much success. Heterologous prime-boost vaccination with chimpanzee adenovirus serotype 63 (ChAd63) and modified Vaccinia Ankara (MVA) expressing ME-TRAP is a potent inducer of CD8+ T cells in humans (Figure 1.6). ChAd63 can infect human cells but does not naturally circulate in humans, meaning anti-vector immunity is minimised. It is rendered replication-deficient by deletion of the E1 genomic region and manufactured in HEK293T cells (304). MVA was rendered replication-deficient by serial passage through chick embryo fibroblasts. Iterative development (106,302,305) and recent optimisation has suggested that three doses of viral vector are optimal at inducing ME-TRAP-directed IFNγ secreting T cells: ChAd63 at time point zero, ChAd63 at four weeks, and MVA at eight weeks (306). An Oxford-based phase IIa trial used ChAd63-MVA expressing ME-TRAP, which protected 3 of 14 volunteers and delayed time-to-parasitaemia in five additional volunteers against heterologous *P. falciparum* CHMI (176). Whereas another study using the same regimen, showed sterile immunity in 13% and a delay to malaria diagnosis in a further 33% of individuals (300).

Endemic-setting studies of ME-TRAP vaccines have shown variable efficacy. In a low transmission area of Kenya, vaccination reduced the risk of natural infection by 67% in adults (307). Another study showed 10% efficacy in The Gambia (308), while no significant difference between control and vaccinated groups was observed in Kenyan children (309). The ChAd63-MVA vaccine showed promise in Gambian and Burkinabe children (310,311), but when trialled in a high transmission area of Burkina Faso, there was no significant protective efficacy in children with previous malaria (312). Some of these studies have indicated that protection correlates with CD8+ T cell response.

1.4.1.4 TRM-targeted vaccine approaches

Inducing liver CD8+ TRM for *P. falciparum* liver-stage protection is the focus of some vaccine efforts. While previous vaccine strategies may have induced liver CD8+ TRM, it is only recently that investigators have sought to produce these liver-resident T cells specifically, and it is these strategies that I name 'TRM-targeted vaccines'.

TRM-targeted vaccines have been trialled against several pathogens. Recent work has shown that IV BCG can provide up to 90% protection from *Mycobacterium tuberculosis* challenge and that protection is in part mediated by TRM (313). Intratracheal and intranasal BCG vaccination in mice produces TRM that, once adoptively transferred to naïve mice, are protective against *M. tuberculosis* challenge (314). Moreover, intranasal live-attenuated influenza virus vaccination generates TRM in the lung that provide heterosubtypic protection in mice (315). Generation of TRM and efficacy in these examples necessitated the administration of vaccine by non-intramuscular (IM) routes. Other examples of tissue targeting in vaccination – so-called 'prime-and-pull' approaches – include the attraction of T cells to tissues by administering inactivated microbes (316), mAbs fused to pathogen epitopes (317), chemokines (318), and inflammatory agents (210). A rapidly evolving body of literature indicates that TRM also play a crucial part in neoplasm immunosurveillance, tumour infiltration, and cancer vaccine-induced tumour regression (319-321). These studies provide evidence to suggest that TRM-targeted strategies may be an attractive option to induce tissue-restricted anti-*Plasmodium* immunity.

By variation in routes of immunisation, it is possible to induce TRM and confer sterile protection to sporozoites by liver-resident CD8+ T cells. The approach developed by Gola *et al.* capitalises on this (237). The strategy attempts to prime endogenous CD8+ T cells in the periphery and target them to the liver through antigen presentation on hepatocytes (hence the name 'prime-target'). The authors first demonstrated prime-target using nanoparticles. IV administration of the

nanoparticle poly-(lactic-co-glycolic acid) (PLGA) presenting OVA (PLGA-OVA) results in KCs taking up PLGA and accumulation of PLGA in hepatic parenchyma (322). One hundred per cent of mice demonstrated sterile protection to sporozoite challenge after Ad-OVA IM/PLGA-OVA IV, but not Ad-OVA IM or Ad-OVA IM/PLGA-OVA IM, vaccination (237). Ad-OVA IM/PLGA-OVA IV produced a ten-fold increase in total hepatic OVA-specific CD8+ T cells compared to Ad-OVA IM alone. Additionally, the approach induced a greater frequency of antigen-specific TRM when compared to Ad-OVA IM vaccination only. Further, IV administration of recombinant viral vectors such as a ChAd63 and MVA encoding OVA, induced high level protection two months after IV boost. By replacing OVA for liver-stage malaria antigens in prime-target vaccination, 100% sterile protection against transgenic sporozoites was demonstrated (237). The prime-target strategy has now undergone further pre-clinical and clinical trials here in Oxford and forms the basis of much of this thesis.

Several other studies have reported TRM-targeted vaccines against liver-stage malaria. Fernandez-Ruiz *et al.* used an adjuvanted peptide-mAb complex (directed towards splenic CD8α+ DCs) followed by an IV recombinant adeno-associated virus vector (directed towards hepatocytes, which allowed antigenic expression through the hepatocyte-specific α1 antitrypsin promoter region (323)), to generate high frequencies of liver TRM (201). These liver TRM were shown to mediate sterile protection against liver-stage malaria (201). While this three-component approach is complicated and "impractical for use in the field," the study demonstrated that i) strategies maximising TRM may be of highest efficacy, ii) adjuvants can encourage TRM formation, and iii) hepatic antigen engenders liver TRM formation. In other work, IM priming with DNA and IV boosting with RAS induced proliferating antigen-specific liver CD8+ T cells and 100% sterile protection in mice (241). However, the necessity of TRM to this approach was suggested but not demonstrated. In very recent work, IV vaccination with a glycolipid-peptide conjugate vaccine designed to induce simultaneous stimulation of NKT and liver peptide-specific T cells showed the

generation of intrahepatic *Plasmodium*-specific CD8+ T cells expressing canonical markers of liver TRM (324). The half-life of these liver TRM was approximately 14 months and protection against sporozoite challenge lasted more than 200 days (324). Therefore, the work by Gola *et al.*, Fernandez-Ruiz *et al.*, and others, suggest that high numbers of enduring hepatic TRM can be induced by vaccination and may be necessary and sufficient for vaccine-induced protection against liver-stage malaria (168,182,201,237,324).

1.4.2 Asexual blood-stage and sexual-stage vaccines

Blood-stage parasites are an appealing malaria vaccine target because this is the symptomatic and pathogenic stage of the life cycle. Candidates have mostly focused on the generation of antibodies that block merozoite invasion of RBCs. This approach is informed by 60 years' worth of evidence towards antibody-mediated protection from parasitaemia: in 1961, the transfer of purified IgG from immune Nigerian and Gambian adults cleared parasitaemia in children (75,325). These vaccines candidates have not had much success, with antigens including MSP1, AMA1 and MSP3 failing to reliably protect against CHMI or natural infection (326,327). There are now, however, numerous encouraging blood-stage vaccine candidates in clinical development. The target antigens include the most clinically advanced PfRh5 (328), P27A (329), and VAR2CSA (330) in placental malaria vaccine candidates. A viral vectored PfRh5 regimen induced cross-strain anti-PfRh5 neutralising antibodies (331), and efficacy studies using a virus-like particle candidate are underway. The difficulties in developing vaccines against merozoites involve i) the brief time (less than one minute) that merozoites are accessible to antibodies between subsequent RBC infections, ii) dispensable invasion pathways, iii) antigenic polymorphism, and iv) the large number of parasites (10^6-10^{12}) that need to be eliminated (297) (Figure 1.6).

Vaccine candidates can also target sexual-stage antigens to interrupt malaria transmission; these are often termed transmission-blocking vaccines. They intend to prevent *Plasmodium* infection in

a vaccinated community through antibody-mediated inhibition of parasite development mainly in the *Anopheles* vector after a blood meal is taken from a gametocyte carrier (33). Only delayed and indirect benefit is elicited by these vaccines as they are designed to prevent further infection (and hence transmission) (332). Immunisation of chickens with sexual-stages of *P. gallinaceum* was shown to block parasite infectivity in 1958 (333) and, 30 years later, the major transmission-blocking vaccine antigen candidates, Pfs25, Pfs48/45 and Pfs230, were identified (334-336) (Figure 1.6). Since then and despite several additional targets being identified and tested pre-clinically, the lead candidates have not changed (297). Clinical investigation of transmission-blocking candidates is in its infancy and much of the focus is on formulating vaccines with technologies to enhance immunogenicity (337,338). The key hurdles that need to be surmounted include raising antibodies at sufficiently high titres against these relatively non-immunogenic antigens and identifying essential antibody characteristics required for transmission-blockade (e.g. ability to recruit human/mosquito complement or mediate opsonization) (33,339). There will also be a need to consider new policy, regulatory and clinical trial approaches (especially for phase III studies) given the indirect benefit of these vaccine candidates (340).

1.4.3 The ideal malaria vaccine candidate

The ideal candidate vaccine against *P. falciparum* would target a conserved antigen or multiple antigens and induce permanent sterile protection after one dose in early life. A promising approach, at least in principle, could be the combination of candidates that target antigens expressed in multiple life-cycle stages (278,327,341,342). The advent of -omics technologies applied to the field of malaria vaccines allows the opportunity to explore many other additional antigens as well (343,344). The multi-stage multi-antigen approach is more likely to emulate natural immunity which probably involves the induction of protection to a wide range of antigens. Additionally, it may be that stage-specific protective efficacy is synergistic when applied in combination (345).

The development of multi-antigen vaccines has proven challenging as multiple vaccine components can cause immunological interference, especially when activating similar elements of the immune system, and only modest efficacy has been achieved (327,342,346-350). It has been shown that by using diverse vaccine platforms resulting in distinct humoral and cellular responses there may be more success (278,351), but this is not always the case (352,353). Currently, assertions as to which antigens would be used in such multi-antigen multi-stage vaccines are speculative as most individual candidates have not been tested in combination (nor achieve remarkable efficacy individually, without optimisation). It is likely, however, that candidates from throughout the lifecycle (sporozoite and liver components of the pre-erythrocytic stage, asexual blood-stage and sexual-stage) are required to induce broadly-acting long-lasting immunity and protection. Such vaccines may be capable of preventing symptoms and pathology, and interrupting transmission. These two goals, however, will require discrete clinical and biological endpoints, target populations, target product profiles, regulatory approval processes, and implementation approaches (332).

1.4.4 Difficulties in developing malaria vaccines

The complexity of *P. falciparum* and its infection of humans brings about many of the difficulties associated with developing a vaccine against it. The first of these difficulties is that the parasite life cycle is complex and leads to the expression of a diverse protein population. *P. falciparum* proteins are mostly expressed in a stage-specific manner (354), and those antigens that are expressed across stages are poorly immunogenic (5). The *P. falciparum* 23Mb nuclear genome encodes about 5,300 genes across 14 chromosomes (355). As a result, the parasite has plenty of genome space to alter surface antigen expression (56) and there is extreme antigenic variability across most of the *P. falciparum* lifecycle (104). For example, *Plasmodium* species carry approximately 60 different copies of the *var* (*P. falciparum*) or *vir* (*P. vivax*) family of surface genes (356,357). Switches between these throughout a single infection may assist the parasite in evading host immune

responses (358). There are several important polymorphisms between strains and species (104); for example, TRAP and LSA-1 show a high degree of variation when compared across more than 600 *P. falciparum* genomes collected around the world (359). The parasite has evolved remarkable strategies to evade host immunity (5,360) and malarial immunosuppression can negatively impact vaccine immunogenicity (361). Prior or ongoing malaria produces immune dysregulation that can adversely affect the priming of adaptive immunity. Lastly, age strongly influences both antibody and T cell responses – different vaccine formulations may be required, over the course of life in malaria-endemic areas, to ensure optimal protection.

There are several difficulties associated specifically with generating liver-stage malaria T cell vaccines. Principally, a significant problem with targeting liver-stage malaria is that if even one single parasite survives, the parasite life cycle can continue and cause death and disability (362). While reductions in parasite liver burden signify partial liver-stage efficacy, transmission-blockade would require complete parasite killing before the blood-stage. The likelihood of CD8+ T cells encountering and killing all infected hepatocyte is rare and has been likened to finding a proverbial needle in a haystack. The duration of liver-stage infection is relatively short (363). Thus, inducing a robust CD8+ T cell response in the restricted time required to clear the infection, whether that is from within tissues or from circulating lymphocyte populations, necessitates rapid effector functions (364). Sporozoites and immature hepatic stages induce little, if any, inflammation (104,365) indicating that their pattern recognition receptor ligands may be sequestered away. Human liver-stage malaria is also difficult to model. *P. falciparum* hepatocyte infection is problematic to reproduce *in vitro*, although this has been achieved with hepatoma cell lines. There is a limited number of hepatoma cell lines with different human leukocyte antigens (HLA) and only recently has an *in vitro* system recapitulated the entire liver-stage of *P. falciparum* (366). The throughput of these assays is low. Even if robust high throughput assays

to model *P. falciparum* hepatocyte infection are generated, there is no guarantee that these insights translate to natural infection.

1.5 Thesis aims and outline

1.5.1 Rationale

While knowledge regarding TRM has progressed substantially in the past ten years, little is known about how they are affected by vaccination and are re-populated in tissues. TRM have an exquisite capacity for tissue surveillance and protection against liver-stage malaria, but their contribution to systemic recall responses remains to be determined. Furthermore, TRM pose a significant translational challenge as they are inaccessible and difficult to measure in humans. Therefore, a circulating counterpart to tissue-residing T cells would be invaluable to the study of TRM-targeted vaccine strategies.

This thesis makes use of mouse models and a large CHMI study to explore a circulating counterpart to TRM, in the context of a vaccine strategy that is known to induce and mediate protection through TRM. By building a case for TRM recirculation potential in mice, the mouse work provides a mechanistic basis on which to explore hypotheses in the human work. Further to this, the clinical trial uses liver fine needle aspirates (FNA) to survey human liver TRM effectively, compare them to circulating cells, and establish a relationship between the two. Finally, the thesis culminates by integrating insights and demonstrates an association between vaccine-induced liver-stage malaria protection and the TRM circulating counterpart.

1.5.2 Aims

The aims of the work in this thesis were to:

1) Identify and investigate a TRM-based correlate of protection (CoP) for prime target vaccination, in mice,
2) Explore, in-depth, the quantitative and qualitative relationship between liver TRM and peripheral blood counterparts in humans, and

3) Investigate a circulating TRM-based cell subset as a correlate of vaccine-induced immunity and protection against *P. falciparum* CHMI.

1.5.3 Outline

The outline of subsequent chapters is as follows:

Chapter 2: Materials and methods used in the thesis,

Chapter 3: Results I – Tissue-resident memory T cells and prime-target vaccination assessment in mice,

Chapter 4: Results II – Assessing liver-resident memory T cells and their circulating counterparts,

Chapter 5: Results III – Investigating TRM-like cells as correlates of vaccine-induced protection, and

Chapter 6: Summary and discussion of findings from the thesis, including implications, recommendations, and future directions.

Chapter 2

2 Materials and methods

2.1 Materials

2.1.1 Reagents

A list of all commercially available reagents and non-standard consumables used in these experiments is shown in Table 2.1.

Table 2.1: Reagents and non-standard consumables used in this thesis.

Reagent/consumable	**Supplier**	**Catalogue number (cat. no.)**
0.2µm syringe filter	Sartorius	16534
0.5mL insulin syringe with needle	Nu-Care Products	M4892
12-well tissue culture plates	Appleton Woods	BC011
15mL Falcon Conical Centrifuge Tubes	Thermo Fisher (Fisher scientific)	FB55950
1mL insulin syringe with needle	Nu-Care Products	M4891
1mL syringe, BD Plastipak	Nu-Care Products	M0013
2% chlorhexidine, 70% isopropyl alcohol applicator (ChloraPrep)	CareFusion	260800
20-gauge Surflo IV catheter with wings	VWR International	TERUSR-DM2225WX
20mL syringe, BD Plastipak	Nu-Care Products	M0862
2mL syringe, BD Emerald	Nu-Care Products	M7727
50mL Falcon Conical Centrifuge Tubes	Thermo Fisher (Fisher scientific)	352070
50mL syringe, BD Plastipak	Nu-Care Products	M3086
5mL round bottom polystyrene tube	Corning	352003
5mL syringe, BD Emerald	Nu-Care Products	M7731
6-well tissue culture plates	Thermo Fisher (Fisher scientific)	TKT-520-030T
60mm petri dishes	Thermo Fisher (Fisher scientific)	430166
70µm cell strainers	Thermo Fisher (Fisher scientific)	352350
96-well U bottom plates	VWR International	734-0057
Agincourt Ampure XP beads	Beckman Coulter	A63882
ArC Amine reactive compensation bead kit	Thermo Fisher (Invitrogen)	A10346
Benzonase nuclease	Merck Millipore	70664
β-*mercaptoethanol (50 mM)*	Thermo Fisher (Gibco)	31350010
Bioanalyzer high sensitivity DNA kit	Agilent	5067-4626

Bovine Serum Albumin (BSA), lyophilised	Sigma-Aldrich	A9418-100G
Brefeldin A (1000x)	Thermo Fisher (eBioscience)	00-4506-51
Casyton fluid	OLS Omni Life Science	5651808
Cluster tubes	Corning	4401
Cryogenic vials	STARLAB	E3110-6122
Cytofix/Cytoperm fixation/permeabilization kit	BD Biosciences	555028
Dimethyl Sulphoxide (DMSO)	Sigma-Aldrich	D2650
dNTP mix	Thermo Fisher (Thermo Scientific)	R0192
ERCC spike in	Thermo Fisher (Invitrogen)	4456740
Ethanol 99.5%	VWR International	20821.330
Ethylenediaminetetraacetic acid (EDTA)	Sigma-Aldrich	E7889
Fetal calf serum (FCS)	Sigma-Aldrich	F2442
FTY720 (fingolimod hydrochloride)	Sigma-Aldrich	SML0700-5MG
Golgi Plug	BD Biosciences	555028
Golgi-Stop	BD Biosciences	554724
Heparin	Sigma-Aldrich	H3149
HEPES buffer (1M)	Thermo Fisher (Gibco)	15630056
HM70A with plus ultrasound system with CA1-7AD S-Vue transducer	Samsung	HM70A
Isofluorane	Oxford University Veterinary Services	n/a
L-glutamine (L-glut) 200mM	Sigma-Aldrich	G7513-100ML
Leucosep tubes	Sigma-Aldrich	Z642843-300EA
Low EDTA Tris-EDTA buffer	Thermo Fisher (Invitrogen)	12090015
Lymphoprep	STEMCELL Technologies	07851
Minimum Essential Medium (MEM) Eagle α-modification (α-MEM)	Sigma-Aldrich	M4526
Monensin (1000x)	Thermo Fisher (eBioscience)	00-4505-01
Neutral buffered formalin	Sigma-Aldrich	HT501128
Nextera XT 96-index kit	Illumina	FC-131-1002
Nextera XT DNA sample preparation kit	Illumina	FC-131-1096
Nuclease-free water	New England Biolabs	B1500S
OneComp eBeads compensation beads	Thermo Fisher (Invitrogen)	01-1111-42
Paraformaldehyde (PFA) (16% w/v)	Alfa Aesar	43368
PBS powder	Thermo Fisher (Gibco)	21600-069
PBS tablets	Sigma-Aldrich	P4417-100TAB
PBS, 10x	Thermo Fisher (Gibco)	70011044
Penicillin-Streptomycin (pen/strep) (100x)	Sigma-Aldrich	P0781-100ML
Peptide: SIINFEKL	ProImmune	n/a
Percoll	Sigma-Aldrich	P1644-500ML
Perm/Wash Buffer	BD Biosciences	554723
Phosphate-buffered saline (PBS), Dulbecco's	Sigma-Aldrich	D8537-500ML
QuantiFluor dsDNA system	Promega	E2670
Recombinant RNase Inhibitor	Takara Bio	2313B
RBC Lysis Buffer	Thermo Fisher (eBioscience)	00-4333-57
RNAlater stabilization solution	Thermo Fisher (Invitrogen)	AM7020
RNase AWAY	Sigma-Aldrich	83931-250ML
RNase-free DNase set	Qiagen	79256

RNaseZap	Sigma-Aldrich	R2020-250ML
RNaseZap RNase Decontamination Wipes	Thermo Fisher (Invitrogen)	AM9786
RNeasy mini kit	Qiagen	74106
RPMI-1640 cell culture medium	Sigma-Aldrich	R0883-500ML
SeqAmp DNA Polymerase	Takara Bio	638509
SMARTScribe reverse transcriptase	Takara Bio	639537
Sodium Azide (NaN3)	Sigma-Aldrich	S2002
Spinal Needles, BD Quincke	Nu-Care Products (Becton Dickinson)	BT405256
Staphylococcal enterotoxin B (SEB)	Sigma-Aldrich	S4881
SUPERase-In RNase-Inhibitor	Thermo Fisher (Invitrogen)	AM2694
Transfer pipettes	Thermo Fisher (Fisherbrand)	FB55348
Triton X-100	Sigma-Aldrich	T9284
Water RT-PCR grade	Thermo Fisher (Invitrogen)	AM9935

2.1.2 Oligonucleotides

Table 2.2 provides details of the oligonucleotides used in this thesis.

Table 2.2: Oligonucleotides used in this thesis.

Oligonucleotide	**Sequence**	**Supplier**
ISPCR oligonucleotide	5'-AAGCAGTGGTATCAACGCAGAGT-3' Dissolved at 100µM Custom oligo, RNase-free HPLC purification	QIAGEN
Lock nucleic acid-modified template-switching oligonucleotide	5'-AAGCAGTGGTATCAACGCAGAGTACATrGrG+G-3' Dissolved at 100µM in TE Custom 250 nmol RNA oligo, RNase-Free HPLC Purification	QIAGEN
Oligo-dT$_{30}$VN	5'–AAGCAGTGGTATCAACGCAGAGTACT30VN-3' Dissolved at 100µM in lysis buffer Custom oligo, RNase-free HPLC purification	QIAGEN

2.1.3 Buffers and media

Outlines of all commercially available and non-standard buffers and media used in these experiments are shown in Table 2.3 & Table 2.4.

Table 2.3: Buffers used in this thesis.

Name	**Components**	**Use**
33% isotonic Percoll	33% Percoll 10% 10x PBS 57% sterile water	Mouse liver lymphocyte separation
ACK Lysis buffer	8.29g NH_4Cl (0.15M) 1g $KHCO_3$ (1mM) 37.2mg Na_2EDTA 800mL deionised H_2O pH adjusted to 7.2-7.4 with HCl (1M) before making a final solution up to 1L with deionised H_2O	Mouse cell RBC lysis
Fine Needle Aspirate (FNA) buffer	0.5% Bovine Serum Albumin Dulbecco's PBS 12.5mL HEPES (final concentration of 25mM)	Fluorescence-assisted cell sorting (FACS) buffer

		for use with FNA samples
Lysis buffer	48.8% 0.4% TritonX-100+SUPERase-In RNase-Inhibitor 40 U/µL 25% dNTP Mix (dATP, dCTP, dGTP, and dTTP, each at 10mM) 25% Oligo-dT$_{30}$VN 0.2% ERCC spike in	Human cell lysis prior to single-cell and mini-bulk RNA-sequencing (RNA-seq)
PBS-BSA	0.5% Bovine Serum Albumin 0.05% Sodium azide Dulbecco's PBS	Flow cytometry buffer
Perm-Wash	10% 10x Perm-Wash 90% deionised H_2O	Cell washes while performing intracellular staining
RLT Buffer	Proprietary blend of detergents (QIAGEN cat. no. 1053393) 1% 2-Mercaptoethanol	RNA extraction with QIAGEN RNeasy Plus kits
Sort buffer	0.5% Bovine Serum Albumin Dulbecco's PBS	Flow cytometry/FACS buffer

Table 2.4: Media used in this thesis.

Name	Components	Use
Complete α-MEM	500mL α-MEM, 5mL L-glut, 5mL pen/strep (100U penicillin, 100µg streptomycin), 500µL 2-mercaptoethanol (50µm), 50mL of heat-inactivated FCS	Mouse cell resuspension and general tissue culture usages
R0	500mL RPMI-1640 medium with sodium bicarbonate, without L-glut 5mL L-glut, 5mL of pen/strep	Human cell washes after collection and thawing
R10	500mL RPMI-1640 medium with sodium bicarbonate, without L-glut 50mL heat-inactivated FCS, 5mL L-glut, 5mL of Pen/Strep	General tissue culture cell media
Supplemented RPMI	500mL RPMI-1640 medium with sodium bicarbonate, without L-glut 50mL heat-inactivated FCS, 5mL L-glut, 5mL of pen/strep, 14mL HEPES, 12,500 IU Heparin (final concentration 15 IU/mL)	FNA sample catch collection media

2.1.4 Antibodies

The antibodies used in these experiments are displayed in Table 2.5, Table 2.6 and Table 2.7.

Table 2.5: Functional human antibodies

Target	Clone	Isotype	Supplier	Cat. no.
CD28	CD28.2	Mouse IgG1 κ	ThermoFisher	16-0289-81
CD49d	9F10	Mouse IgG1 κ	ThermoFisher	16-0499-81

Table 2.6: Human antibodies for flow cytometry and intracellular cytokine staining

Target	Fluorochrome	Clone	Isotype	Supplier	Cat. no.
CD103	BV711	Ber-ACT8	Mouse IgG1 κ	BioLegend	350222

CD103	BV605	Ber-ACT8	Mouse IgG1 κ	BioLegend	350218
CD107a	BV605	H4A3	Mouse IgG1 κ	BioLegend	328634
CD11a	A700	HI111	Mouse IgG1 κ	BioLegend	301228
CD11a	PE/Cy5	HI111	Mouse IgG1 κ	BioLegend	301210
CD11b	A700	ICRF44	Mouse IgG1 κ	BioLegend	301356
CD11c	BV650	3.9	Mouse IgG1 κ	BioLegend	301638
CD14	PE	M5E2	Mouse IgG2a κ	BioLegend	301806
CD16	BV650	3G8	Mouse IgG1 κ	BioLegend	302042
CD16	FITC	3G8	Mouse IgG1 κ	BioLegend	302006
CD161	BV605	HP-3G10	Mouse IgG1 κ	BioLegend	339916
CD186 (CXCR6)	PerCP-Cy5.5	K041E5	Mouse IgG2a κ	BioLegend	356010
CD20	BV570	2H7	Mouse IgG2b κ	BioLegend	302332
CD20	BV510	2H7	Mouse IgG2b κ	BioLegend	302340
CD279 (PD-1)	BV711	NAT-103	Mouse IgG1 κ	BioLegend	367428
CD279	BV650	EH12.2H7	Mouse IgG1 κ	BioLegend	329950
CD3	Pacific Blue	UCHT1	Mouse IgG1 κ	BioLegend	300431
CD3	Pacific Blue	OKT3	Mouse IgG2a κ	BioLegend	317314
CD4	BV570	RPA-T4	Mouse IgG1 κ	BioLegend	300534
CD4	PE/Cy7	OKT4	Mouse IgG2b κ	BioLegend	317414
CD4	BUV496	Sk3	Mouse IgG1 κ	BD Biosciences	612936
CD45	BV780	2D1	Mouse IgG1 κ	BioLegend	368528
CD45RA	APC/Fire750	HI100	Mouse IgG2b κ	BioLegend	304152
CD56	BV570	5.1H11	Mouse IgG1 κ	BioLegend	362540
CD56	PE	39D5	Mouse IgG1 κ	BioLegend	355504
CD69	AF488	FN50	Mouse IgG1 κ	BioLegend	310916
CD69	FITC	FN50	Mouse IgG1 κ	BioLegend	310904
CD69	AF647	FN50	Mouse IgG1 κ	BioLegend	310918
CD8	APC	RPA-T4	Mouse IgG1 κ	BioLegend	344721
CD8	BUV395	RPA-T8	-	BD Biosciences	563795
CD8α	APC	SK1	Mouse IgG1 κ	BioLegend	344722
IFNγ	PE	4S.B3	Mouse IgG1 κ	BioLegend	502509
Ki67	PE/Cy7	Ki-67	Mouse IgG1 κ	BioLegend	350526
Live-Dead Aqua	AmCyan	-	-	ThermoFisher	L34957
TCR α/β	PEDazzle594	IP26	Mouse IgG1 κ	BioLegend	306726
TCR Vα7.2	AF700	3C10	Mouse IgG1 κ	BioLegend	351728
TCR γ/δ	PE/Cy7	B1	Mouse IgG1 κ	BioLegend	331222

Table 2.7: Mouse antibodies for flow cytometry and intracellular cytokine staining

Marker	**Fluorochrome**	**Clone**	**Isotype**	**Supplier**	**Cat. no.**
CD103	BV711	2E7	Armenian Hamster IgG	BioLegend	121435
CD11a	PE/Cy7	I21/7	Rat IgG2a κ	BioLegend	153108
CD183	APC/Fire 750	CXCR3-173	Armenian Hamster IgG	BioLegend	126540
CD186	FITC	SA051D1	Rat IgG2b κ	BioLegend	151108
CD279	BV605	29F.1A12	Rat IgG2a κ	BioLegend	135219
CD3ε	APC	145-2C11	Armenian Hamster IgG	eBioscience	17-0031
CD4	eFluor 450	RM4-5	Rat IgG2a κ	eBioscience	48-0042-80
CD4	FITC	RM4-4	Rat IgG2b κ	eBioscience	11-0043-81
CD44	APC/Cy7	IM7	Rat IgG2b κ	BioLegend	103027
CD45.1 (Ly5.1)	BV421	A20	Rat IgG2a κ	BioLegend	110731

CD62L	PE/Cy7	MEL-14	Rat IgG2a κ	eBioscience	25-0621-81
CD69	PE/Cy7	H1.2F3	Armenian Hamster IgG	BioLegend	104512
CD69	BV421	H1.2F3	Armenian Hamster IgG	BioLegend	104528
CD69	Pacific Blue	H1.2F3	Armenian Hamster IgG	BioLegend	104524
CD8	PerCP/Cy5.5	53-6.7	Rat IgG2a κ	BioLegend	100734
CD8α	FITC	53-6.7	Rat IgG2a κ	eBioscience	11-0081
IFNγ	APC	XMG1.2	Rat IgG1 κ	eBioscience	17-7311
IFNγ	eFluor 450	XMG1.2	Rat IgG1 κ	eBioscience	48-7311
IFNγ	PE	XMG1.2	Rat IgG1 κ	BioLegend	505807
Ki67	AF647	B56	Rat IgG2b κ	BioLegend	151206
Live-Dead Aqua	AmCyan	-	-	ThermoFisher	L34957
SIINFEKL	PE	-	MHC I Pentamer H-2Kb SIINFEKL (referred to as "OVA-pentamer")	Proimmune	F093-2B-G

2.1.5 Vaccines

2.1.5.1 Preclinical viral vector vaccines

Human Adenovirus (Ad) Type 5 encoding ovalbumin (OVA – together referred to as Ad-OVA), Ad-green fluorescent protein (GFP), Ad-TIP and MVA-OVA were all produced by the Jenner Institute Viral Vector Core Facility. "TIP" (for Tuberculosis, Immunodeficiency virus and *Plasmodium*), in these experiments, is used as an irrelevant antigen. It contains epitopes from various pathogens, including the protective H-2K^{d}-restricted Pb9 epitope from *P. berghei* CSP (367). The Ad-GFP and Ad-TIP vectors were used in experiments as irrelevant antigen comparators, to control for non-OVA-antigen-specific effects of the viral vectors.

2.1.5.2 Clinical trial viral vector vaccines

ChAd63 ME-TRAP was manufactured under GMP conditions by the Clinical Biomanufacturing Facility (CBF), University of Oxford. MVA ME-TRAP was manufactured under GMP conditions by IDT Biologika GmbH, Germany.

2.2 Animals and preclinical procedures

All animal work was performed in accordance with the UK Animals (Scientific Procedures) Act, approved by the University of Oxford Animal Care and Ethical Review Committee and conducted under license P9804B4F1. Animals were group-housed in individually vented cages under specific pathogen-free conditions, with constant temperature and humidity and with lighting on a 12:12 light/dark cycle (8am to 8pm). For induction of short-term anaesthesia, animals were anaesthetised using vaporised isofluorane in all instances. All animals were humanely sacrificed at the end of each experiment by an approved schedule 1 method with confirmation of death by a second schedule 1 method. Female mice of at least six weeks of age were used in the following strains: C57BL/6JOlaHsd (Envigo, UK) and B6.SJL-Ptprc^{a} (Ly5.1) Pepc^{b}/BoyJ (Biomedical Services, Oxford UK).

2.2.1 Injections

2.2.1.1 Intramuscular

Mice were anaesthetised prior to injection. IM injections were performed into the tibial muscle with 50µL viral vector in sterile PBS. Mice received 1x10^{8} infectious units (IU) of Ad or 1x10^{6} plaque-forming units (pfu) of MVA vaccines.

2.2.1.2 Intraperitoneal

Intraperitoneal (IP) injections were performed in the lower right quadrant at a 45° angle to the surface of the skin. If injection was required over multiple days, the side of injection was alternated. FTY720 (or PBS) was administered IP at 1mg/kg or 5mg/kg in a volume of 100µL.

2.2.1.3 Intravenous

Mice were placed in a 30°C warmer to stimulate dilation of the tail veins and placed in a restrainer for injection. IV injections were performed into tail veins with 100µL viral vector in sterile PBS, at a dose of 1x10^{9} IU Ad vector.

2.2.2 Blood sampling

Mice were placed in a 30°C warmer to stimulate dilation of the tail veins. A small cut of the tail was made, and blood flow was encouraged by gently stroking the tail. Blood samples for cellular immunology were immediately collected into microcentrifuge tubes containing EDTA (final concentration approximately 3µg/µL). For blood sampling by cardiac puncture, syringes were prepared by lining the inside of the syringe chamber with pre-diluted heparin. Mice were placed under terminal anaesthesia. Blood samples were taken from the heart, accessed either via the left side of the chest through the diaphragm or by performing a thoracotomy. The blood sample was immediately transferred into microcentrifuge tubes.

2.2.3 Adoptive cell transfers

Spleens, livers, and blood were harvested at the relevant time point after immunisation. Single-cell suspensions were prepared by grinding the tissue through a 70µm cell strainer. Liver homogenates were passed over a 33% isotonic Percoll gradient to separate lymphocytes from hepatocytes. Following RBC lysis with ACK, cells were resuspended in complete α-MEM. Cells were counted, resuspended to 10^8cells/mL, and stained with the appropriate fluorochrome-conjugated antibodies. After fluorescent staining, cells were washed with Sort Buffer and resuspended to approximately 10^7cells/mL, ready for FACS. Cells were sorted, according to experiment-specific criteria, into a 15mL Falcon tube with 1mL FCS. Cells were resuspended in sterile PBS to a total volume whereby each animal would receive 100µL. These cells were then taken back to the animal facility on ice and injected into the tail vein of recipient mice (as indicated in 2.2.1.3). In the various cell transfer experiments, between $9x10^3$ and $4.6x10^6$cells were transferred (see experimental designs for specifics).

2.3 Clinical trials

2.3.1 Design

The human samples were taken as part of a phase I/IIa sporozoite challenge study to assess the safety, immunogenicity, and protective efficacy of IV boosting (prime-target) with malaria vaccine candidates ChAd63 and MVA encoding ME-TRAP (hereafter this study is referred to as VAC066 – Figure 2.1). All recruited volunteers were healthy, malaria-naïve adults aged between 18 and 45 years. Written informed consent was given by all participants for enrolment in the trial and use of their samples in laboratory analyses. Volunteers were recruited at either the Centre for Clinical Vaccinology and Tropical Medicine, University of Oxford; National Institutes for Health Research (NIHR) Southampton Clinical Research Facility, University Hospital Southampton or NIHR Imperial Clinical Research Facility, Hammersmith Hospital.

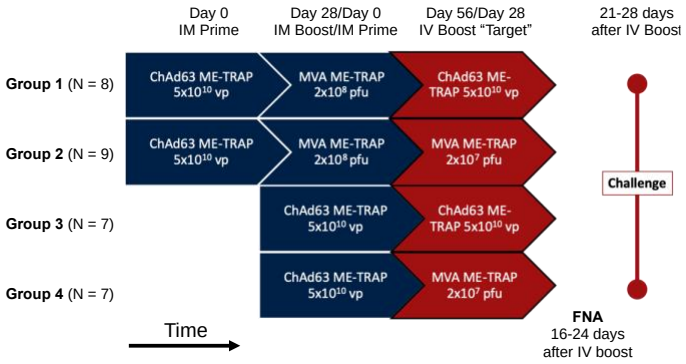


Figure 2.1: VAC066 trial overview and timeline. Detailed schematic of the trial. The final study cohort included 35 volunteers, across five groups, with group sizes as indicated. Not shown in this figure is the infectivity control group (N=5) that did not receive any vaccinations. All intervention group volunteers received either two or three injections of viral vectors encoding ME-TRAP. Doses were as indicated. FNA occurred between 16 and 24 days after IV vaccination/boost. Volunteers underwent CHMI on two separate days (4/2/2019 and 5/2/2019) and participants were equally and randomly divided across these days. Volunteers were treated with 20mg artemether/120mg lumefantrine (Riamet) upon malaria diagnosis or 21 days after challenge.

The study protocol and associated documents were reviewed and approved by the UK National Research Ethics Service, Committee South Central–Oxford REC A (18/SC/0384), the Medicines and Healthcare Products Regulatory Agency (EudraCT: 2017-001075-23), and the Oxford University Clinical Trials and Research Governance team, who independently and externally monitored compliance with Good Clinical Practice guidelines. The study was registered on the clinicaltrials.gov

registry (registration number: NCT03707353). The study was conducted according to the principles of the Declaration of Helsinki (2008) and the International Conference on Harmonization Good Clinical Practice guidelines.

There were four vaccine (intervention) and one infectivity control group. All vaccinations encoded ME-TRAP, and the interval between vaccinations was approximately 28 days. Group 1 received IM ChAd63, followed by IM MVA and IV ChAd63; group 2, IM ChAd63, IM MVA and IV MVA; group 3, IM ChAd63 and IV ChAd63; and group 4, IM ChAd63 and IV MVA. The infectivity control group did not receive any vaccinations. Vaccine doses given IM and IV are shown in Figure 2.1.

Prior to VAC066, a phase I study to assess the safety and immunogenicity of IV and subcutaneous administration ChAd63 and MVA encoding ME-TRAP (hereafter referred to as VAC064), in healthy adults, was performed (237). Several doses of ChAd63, ranging from $5x10^8$ to $5x10^{10}$ viral particles (vp), and MVA, from $2x10^6$ to $5x10^7$pfu were assessed. Samples from this trial were used to compare the immunogenicity of IV (from VAC064) and IM prime (from VAC066) vaccination using viral vectors.

2.3.2 Procedures

2.3.2.1 Vaccinations

All volunteers in vaccination groups of VAC066 were administered either ChAd63 ME-TRAP or MVA ME-TRAP IV (Figure 2.1). Vaccines were administered into an indwelling IV cannula (IVC). Following vaccination, volunteers underwent stringent observation throughout the first 30 minutes, and at 60 minutes and 8 hours after vaccination.

2.3.2.2 Fine needle aspirates of the liver

Fifteen participants of VAC066 were asked to participate in FNA sampling, equally across the four vaccination groups. Thirteen of these volunteers underwent FNA sampling. The two that were not

sampled dropped out due to logistical reasons. Prior to the FNA, an IVC was inserted for access in case of an adverse event. At the time of insertion, a 25mL sample of blood was collected for paired immunology.

For the FNA, a 22-gauge spinal needle with an internal trocar was used to gain access, along an anaesthetised tract, to the edge of the liver capsule. After asking the volunteer to breathe out, the needle was inserted a further 2–3 cm into the parenchyma and the internal trocar was removed. Liver cells were collected into a 20mL syringe containing 3mL of ice-cold, sterile saline. Aspiration was performed as the needle was withdrawn 1–2 cm but still while remaining in the liver parenchyma using a fanning technique (245,368). The syringe was detached and 3mL of cold supplemented RPMI was used to flush the contents of the syringe and needle into a 50mL Falcon tube with 30mL supplemented RPMI solution. One more aspirate pass was performed before placing the entire sample in an icebox and immediately transported for processing (along with the matched blood sample). Any aspirate with frank blood was discarded. After the procedure, the volunteer was observed for 60 minutes with vital signs taken every 15 minutes. The FNA procedure was performed by an interventional radiologist, with assistance.

All samples were received in the laboratory within 3 hours of collection. Best practice for working with RNA was followed throughout FNA sample processing (described in 2.5.1). The tube containing the FNA sample was spun at 500g for 10 minutes with the supernatant carefully poured off and resuspended in RBC Lysis Solution at room temperature for 5 minutes. Thereafter, 20mL of sterile, FNA buffer was added, the sample was spun again and one more round of lysis was performed. Subsequently, the cells were resuspended in 500µL of ice-cold FNA buffer. Any clumps were removed with a sterile P200 pipette tip. Cells were counted with a haemocytometer.

Cells were transferred from the 50mL tube to a 1.5mL RNA-free Eppendorf tube and centrifuged in a benchtop centrifuge at 4000rpm for 4 minutes. The supernatant was carefully removed with a pipette. A volume of 50µL surface stain fluorochrome-antibody mix was added and incubated on ice for between 30 and 40 minutes. Thereafter, cells were washed with 250µL FNA buffer and resuspended in 500µL PBS-HEPES (final concentration 25mM). Samples were then transferred to the flow cytometry suite and underwent FACS within 4.5 hours of collection.

2.3.2.3 Controlled human malaria infection

CHMI of volunteers by infected mosquitoes was carried out at Imperial College London. Each volunteer was exposed to five *P. falciparum*-infected mosquitoes for 5-10 minutes. The TRAP antigen in the infecting strain (3D7) differed by 37 amino acids (~6.5%) from the vaccine strain (T9/96), thereby constituting a heterologous strain challenge (176). Previous experience with CHMI trials at the Jenner Institute has shown that >99% of naïve individuals bitten by five infected mosquitoes develop patent parasitaemia (A/Prof. Katie Ewer, Jenner Institute, unpublished data). Volunteers were followed up twice per day from five days after challenge. Volunteers were treated with Riamet upon malaria diagnosis or 21 days after challenge. None of the volunteers in the infectivity control group achieved sterile protection. The primary efficacy endpoint was time-to-malaria diagnosis, diagnosed given the following criteria:

1) Malaria symptoms and a quantitative-polymerase chain reaction (qPCR) result indicating ≥1,000parasites/mL, or
2) A qPCR result indicating ≥10,000parasites/mL regardless of symptoms.

2.4 Immunology

2.4.1 Isolating human PBMC

Heparinised blood was drawn and processed within four hours. The blood was poured into a 50mL Leucosep tube with 15mL Lymphoprep pre-poured below a polyethylene barrier. The blood was then centrifugated at 1000g for 13min at room temperature with no brake. Two 1mL samples of plasma were then taken off the top fraction with the rest being taken off with a Pasteur pipette and discarded. The remaining PBMC fraction was transferred to a new 50mL Falcon tube, which was topped up to 40mL with R0 and spun at 1800rpm for 5min at room temperature. The supernatant was poured off quickly, the pellet resuspended, and the tube topped up to 30mL with R0. The tube was spun at 1400rpm for 7 mins at room temperature. The supernatant was poured off quickly, the pellet resuspended, and the tube topped up to 10mL exactly with R10 for counting. A CASY TT (OLS OMNI Life Science Inc., cat. no. 2501126) was used to count the cells as per the manufacturer's protocol. Counted cells were 5.7-15µm in diameter. Cells were separated, suspended in R10, and used within 4 hours.

2.4.2 Freezing human PBMC

Cells were resuspended in ice-cold FCS, to a maximum volume of 5mL. The cells were then placed in the fridge for 30 minutes. Thereafter, an equal volume of ice-cold 20% DMSO in FCS was added to the cells and mixed by pipetting gently up and down. One millilitre aliquots were then distributed into labelled cryovials, immediately placed in a CoolCell container, and transferred to a –80°C freezer. Each cryovial had a final concentration between five and twelve million cells. After overnight incubation at –80°C, the frozen cells were transferred to liquid nitrogen for long term storage.

2.4.3 Thawing human PBMC

Cryovials were removed from liquid nitrogen storage and placed immediately on dry ice. Samples were thawed until approximately 60% remained frozen, at which point 0.5mL R10 (at 37°C) was pipetted into the cryovial to encourage thawing. As thawing progressed, this was repeated, and the

sample was pipetted into a 15mL Falcon tube with 10mL R10. This was repeated for all samples. Cells were spun at 1800rpm for 5 minutes, the supernatant discarded and resuspended in 2mL R10. At this point, 2µL of Benzonase nuclease was added, and cells were incubated at 37°C 5% CO_2 for between one and four hours. After this, the cells were topped up and washed with R10 before counting and use.

2.4.4 ELISpot

ELISpot assays were performed as previously described (306). *Ex vivo* (18 to 20-hour stimulation) ELISpot assays were performed using Multiscreen IP ELISpot plates (Millipore), human IFNγ SA-ALP antibody kits (Mabtech) and BCIP NBT-plus chromogenic substrate (Moss Inc.), using freshly collected cells. The coating antibody was monoclonal anti-human IFNγ 1-D1K (mouse IgG1), and the detection antibody was biotinylated monoclonal 7-B6-1 (mouse IgG1). Cells were cultured in R10, with FCS previously screened for low reactivity. All samples were stimulated with a pool of TRAP peptides from two species of *P. falciparum* or with R10 medium (as a negative/unstimulated control). PBMC ELISpots were plated with 100,000 lymphocytes per well, in triplicate. FNA ELISpots were plated with 50,000 lymphocytes per well, in duplicate. Spots were counted using an ELISpot counter (Autoimmun Diagnostika, Germany). Results are expressed as the mean of the replicate IFNγ spot-forming colonies (SFC) per million PBMC. Background responses in un-stimulated control wells were less than 15 spots and were subtracted from those measured in peptide-stimulated wells.

2.4.5 Flow cytometry

2.4.5.1 Human intracellular cytokine staining

Intracellular cytokine staining (ICS) was performed similarly to previously described protocols (306). One to two million cells in 100µL R10 from each volunteer were placed in three separate wells of a 96 well U-bottom plate. Stimulation mix was added to each well, with each volunteer's sample having three different stimulation conditions: TRAP-stimulated, SEB-stimulated and media (unstimulated). The 50µL stimulation mix was made up of 0.4% (v/v final concentration) CD28

functional antibody, 0.4% CD49d functional antibody, 2% CD107a-BV605 antibody, stimulator (TRAP peptide pool at 5µg/mL, SEB at 5µg/mL or R10 media) and 46.6µL R10. The plate was incubated at 37°C 5% CO_2 for 2h. Fifty microlitres of protein transport inhibitor mix was then added to each well (0.2µL Golgi-Plug and 0.125µL Golgi-Stop in R10 per well). The plate was incubated at 37°C 5% CO_2 overnight for 16-20h.

The plate was washed in PBS-BSA before the addition of pre-mixed surface antibodies (diluted in PBS-BSA) for flow cytometry. These antibodies included CD69, CXCR6, CD3, Live/Dead, CD4, CD20, PD-1, CD103, CD8a, CD11a and CD45RA. The cells were then washed with PBS-BSA. Thereafter, the cells were fixed and permeabilised with Cytofix/Cytoperm on ice for a maximum of 5 minutes. After washing with Perm-Wash, intracellular staining antibodies (IFNγ and Ki67) were added (diluted in Perm-Wash), and the plate was incubated for a minimum of 30 minutes at 4°C. The cells were then washed twice with Perm-Wash and twice with PBS-BSA and acquired on an LSRII or LSRFortessa SORP X-20 flow cytometer. Antigen-specific (AgSp) cells were identified using IFNγ. When identifying AgSp cells using IFNγ, the response in the stimulated wells was adjusted for background by subtracting the IFNγ proportion of paired media-stimulated wells from TRAP-stimulated wells.

When performing only surface staining of human PBMC, no overnight stimulation was performed, and no intracellular markers staining was performed.

2.4.5.2 Mouse intracellular cytokine staining

Spleens, lymph nodes, livers and blood were harvested at the relevant time point after immunisation. Single-cell suspensions were prepared and counted as outlined in **Error! Reference source not found.**. All samples were centrifuged at 500g for 5 minutes and resuspended in 100µL complete α-MEM and transferred to 96-well U-bottom plates. A 50µL stimulation mix was then added to each well, made up with complete α-MEM, and 0.1% (v/v final concentration) Golgi Plug

and 1µg/mL stimulator (OVA peptide SIINFEKL or media). Plates with cells and stimulatory mix were incubated at 37°C 5% CO_2 for 5-6hrs. After this, plates were stored at 4°C overnight.

The following day, cells were washed in PBS-BSA. Surface staining for the antibodies listed in Table 2.7 was performed in a dark fridge for at least 30 minutes. Subsequently, cells were fixed with 10% neutral buffered formalin solution (containing 4% PFA) for 5min on ice, prior to ICS (for IFNγ and Ki67) with antibodies diluted in Perm-Wash. Cells were acquired on an LSRII or LSRFortessa SORP X-20 flow cytometer. Murine T cells were determined by gating on live, size, singlet, single cells (FSC-W), CD3+ and either CD4+CD8− or CD4−CD8+. AgSp cells were identified using either IFNγ or phycoerythrin-conjugated MHC I pentamer for H-2K^b SIINFEKL (OVA-pentamer). When identifying AgSp cells using the IFNγ method, antigen specificity was defined by intracellular production of IFNγ after ex-vivo restimulation and background subtraction of the response in unstimulated wells (media) from that in paired stimulated wells (SIINFEKL peptide). When identifying AgSp cells by OVA-pentamer, no 6hr stimulation, overnight rest or ICS was performed, and flow cytometry was done on the same day as staining.

2.4.5.3 Fluorescence-assisted cell sorting

FACS was performed using the above surface staining flow cytometry methods for cell preparation. Human cell sorting was conducted using a FACSAriaIII using a 70µm nozzle and single-cell purity. All mini-bulk samples consisted of 100 cells and were attained using a two-way sort based on CD69 status (positive or negative), pre-gated on single live CD20- CD45+ CD3+ CD4- CD8+ CD45RA- cells. All single sorted cells were CD69+. Mini-bulk samples were collected into 0.2mL PCR tubes and single cells were collected directly into RNase free 96-well PCR plates with 4.01µL lysis buffer. Upon collection, samples were vortexed, spun and placed on dry ice within 10 minutes and thereafter stored at -80°C. Single-cell fluorochrome fluorescence intensity was linked to cell position in 96-well PCR plates (index sorting was performed), to allow for single-cell paired surface protein and

transcriptome analysis. Cell sorting was performed at the University of Oxford Experimental Medicine Flow Cytometry Facility.

Mouse cell sorting was conducted using a MoFlo XDP Cell Sorter (Beckman Coulter) using a 70μm nozzle and recovery mode. Liver, blood, and spleen samples for the transcriptomics experiment contained a numeric range of cells, from $3.2x10^3$ to $9.1x10^5$cells, and were gated on permutations of CD69+/- CD8+ Live+ and H-$2K^b$ SIINFEKL Pentamer+/- (see Chapter 3 for experimental details). Samples were collected into 5mL polypropylene FACS tubes with 3mL RNAlater Stabilization Solution. Upon collection, samples were vortexed, spun and placed on dry ice within 20 minutes and thereafter stored at -80°C. Cell sorting was performed at the Jenner Institute Flow Cytometry Facility.

2.5 Molecular Biology

2.5.1 RNA isolation

Aseptic technique was always used when working with RNA. Gloves were changed frequently, and tubes were closed whenever possible. Purified RNA was kept on ice when aliquots were used for downstream applications. RNaseZap RNase Decontamination Solution (Invitrogen) was used to remove RNase contamination from bench surfaces, non-disposable plasticware, and laboratory equipment. Sterile, disposable RNase-free polypropylene tubes were used throughout.

RNA isolation from mouse lymphocytes occurred using the RNeasy Plus Mini Kit protocol. In brief, cells stored in RNAlater Stabilization Solution were centrifuged at 3000g for 10 minutes. The cell pellet was then washed with RNase-free PBS. Cells were lysed and homogenised in the denaturing guanidineisothiocyanate–containing RLT buffer. The lysate was then passed through a genomic DNA eliminator spin column. Ethanol was added to the flow-through to provide appropriate binding conditions for RNA, and the sample was then applied to a RNeasy spin column, where total RNA binds to the membrane and contaminants were washed away. RNA was then eluted in 30µL, or more, of RNase free water. RNA was immediately converted to cDNA for qPCR or taken to the sequencing facility for RNA-seq.

A preliminary check of RNA purity in water was conducted using the ratio of the spectrophotometric readings at 260nm and 280nm by using a NanoDrop. The integrity and size distribution of total purified RNA was checked using an Agilent 2100 Bioanalyzer. RNA Integrity Number (RIN) was used as a measure of RNA integrity, and samples mostly had RIN values over six, with rare exceptions.

2.5.2 *P. falciparum* quantitative polymerase chain reaction

The primary diagnostic tool during CHMI was qPCR. Blood was collected in EDTA vacutainers twice daily, and total DNA was extracted on a QIAsymphony automated DNA extraction robot. The qPCR

assay was set up exactly as previously described (176,327). Mean parasite equivalent values of <20 or with only one positive replicate were classed as negative.

2.5.3 Sequencing

2.5.3.1 Human mini-bulk RNA-seq

Smart-Seq2 libraries were generated following the established protocol (369), with a few alterations. The first-strand buffer included SMARTScribe Reverse Transcriptase. No DTT was added for reverse transcription. SeqAmp DNA Polymerase was used for cDNA amplification. cDNA underwent pre-amplification by PCR for 24 cycles. Post-PCR clean-up was performed using a Biomek 4000 Automated Liquid Handler (Beckman Coulter). Nextera library preparation was performed using a Mosquito LV genomics instrument (SPT Labtech). Libraries were sequenced on an Illumina NextSeq with 75bp paired-end reads. Library preparation and sequencing were performed at the Weatherall Institute of Molecular Medicine (WIMM) Single Cell Facility.

2.5.3.2 Human single-cell RNA-seq

Smart-Seq2 libraries were generated following the established protocol (369), with the same alterations as above in 2.5.3.1. cDNA underwent pre-amplification by PCR for 24 cycles. Post-PCR clean-up and Nextera library preparation were performed manually. Libraries were sequenced on an Illumina NextSeq with 75bp paired-end reads. Library preparation and sequencing were performed at the WIMM Single Cell Facility.

2.5.3.3 Mouse bulk RNA-seq

Smart-Seq2 libraries were generated following the established protocol (369), with no alterations. cDNA underwent pre-amplification by PCR for 22 cycles. Post-PCR clean-up and Nextera library preparation were performed manually. Libraries were sequenced on an Illumina NovaSeq6000 with 75bp paired-end reads. Library preparation and sequencing were performed at The Wellcome Centre for Human Genetics.

2.6 Statistics and bioinformatics

2.6.1 Statistics, software, and versions

Prism version 8 (GraphPad Software Inc.) and RStudio (base R version 3.6.2) were used for analyses. Median values with interquartile ranges are shown in all figures unless otherwise stated. Significance testing of differences between group means (for normally distributed data) used the two-tailed Student's t-test, or medians used the two-tailed Mann-Whitney (MW) test. Correlations were analysed using Spearman's rank correlation coefficient (r) for non-parametric data. An α (probability of type I error) of 0.05 was used, and p values below this were considered statistically significant. In the event of multiple comparisons, two multiple comparison correction methods were used. If there were between five and fifteen tested comparisons, a Kruskal–Wallis (KW) test with Dunn's correction for comparisons between multiple groups was applied. If there were more than fifteen tested comparisons, a two-stage linear step-up, Benjamini, Krieger and Yekutieli approach was used to control the false discovery rate (FDR). The FDR was in most cases was set at 5%, if not lower. This approach determines a p value threshold below which comparisons can be deemed true discoveries. Unadjusted p values were presented and those representing true discoveries were highlighted.

Chapter 5 involved the analysis of T cell subsets as correlates of vaccine-induced protection. Immunological correlations with time-to-malaria diagnosis or other variables were pre-specified and prioritised analysis of T cell subsets based on observations from preclinical studies using prime-target vaccination. For log-transformed PCR data, an arbitrary value of 1 was added to each PCR value to allow log transformation of 0.0 values ($y=\log_{10}(1+\text{PCR value})$). The mean number of parasites per replication cycle (area under the curve) was calculated using the trapezoid rule (176), included all parasite count values and was compared between groups. Replication cycles were defined by the date of CHMI: days 6.5-8 (first cycle post-hepatocyte release), days 8.5-10 (second cycle) and days 10.5-12 (third cycle) post-CHMI. Analyses compared median time-to-malaria

diagnosis between strata dichotomised by median T cell frequency. Univariate and multiple regression Cox proportional hazards models were fitted using flow cytometry, ELISpot response and ICS data with T cell response as the independent variable and time-to-malaria diagnosis as the dependent variable. T cell populations which were associated with statistically significant reductions in hazard ratio were considered in the multiple regression analysis and, in addition, predictors with biologically relevant relationships to protection from malaria were considered in multiple regression. Models were fit using log-transformed data. Multiple regression model development was carried out in a forward stepwise manner: covariates were added one at a time, at each stage including the covariate which resulted in the model with the lowest Akaike Information Criterion (AIC) value. AIC was used as an aid for choosing between competing (nested) models. Lower AIC values indicated a preferred model. Specifically, the Δ_i method was used, where $\Delta_i = AIC_i - AIC_{min}$ (370). AIC_i was the AIC of the ith model, and AIC_{min} was the lowest AIC obtained among the set of models examined (i.e. the preferred model). As suggested by Burnham and Anderson (370), models with $\Delta_i > 10$ were considered not descriptive of the dependent variable. Collinearity occurs when two or more independent variables are highly correlated with one another in a regression model. The variance inflation factor measures how well an independent variable is explained by other independent variables (48). It was used to assess collinearity.

2.6.2 Flow cytometry

Flow cytometry data were analysed using FlowJo v10.5 (Beckton Dickinson). T-distributed Stochastic Neighbour Embedding (tSNE) is a machine learning algorithm for nonlinear dimensionality reduction and visualisation. When run using FlowJo, the settings used were: 1000 iterations, perplexity 50, eta 200 and theta 0.5. tSNE was run several times to ensure the stability of inferences. In these iterations, the clusters were indifferent to varying perplexity.

2.6.3 Human mini-bulk RNA-seq analyses

Trim Galore v0.6.4 was used to trim adapters ("Trim Galore" 2016. The Babraham Institute, GitHub Repository). Primary quality control (QC) was performed on fastq files using fastQC v0.11.9 (via Trim Galore) and multiQC v1.6 (371). Trimmed reads were aligned to the human genome (the Genome Reference Consortium Human genome build 38 patch release 13 (GRCh38.p13)) plus added ERCC "spike-in" sequences using STAR v2.5.3a (372). Unstranded read counting was carried out and Ensembl gene counts were generated using featureCounts v2.0.0 (373).

Secondary QC was performed on samples by considering absolute read counts, uniquely mapped reads and reads assigned to transcripts. Two samples were removed due to low total read counts, and another four were removed due to low library complexity. Genes with more than ten counts across all samples were kept for further analyses.

DESeq2 v3.10 (374) was used for normalisation and feature selection. For visualisation and clustering, the regularised logarithm (rlog) transformation was applied to count data. This was done to transform the data to the binary logarithm scale in a way which minimised differences between samples for genes with small counts and normalised with respect to sample library size (374). Principal component analysis (PCA) was performed on the 500 most variable gene rlog transformed count values. Non-normalised counts were input to DESeq2 and samples were paired according to volunteer and sample type. Differential expression analyses used a generalised linear model where counts were modelled using a negative binomial distribution. The Wald test was the default used for hypothesis testing when comparing gene expression between two sets of paired variables. Multiple test correction was applied by using the Benjamini and Hochberg/FDR method (375). The binary logarithm of fold change ($\log_2$(FC)) values were shrunk using the Approximate Posterior Estimation for generalised linear models (apeglm) to generate more accurate $\log_2$(FC) estimates and aid in downstream analyses (376).

Functional analyses were performed on each contrast's list of differentially expressed genes. The differential gene expression (DGE) list was taken after apeglm shrinkage. A mix of over-representation analyses (ORA) and functional class scoring (fcs) were used. For ORA, the DGE list was composed of genes with an FDR<0.05 and the hypergeometric test was used to determine whether the input gene list was over-represented in gene categories. Multiple test correction was applied by using the Benjamini and Hochberg/FDR method. Gene categories included Gene Ontology (GO) project (377) molecular function (MF), cellular component (CC) and biological process (BP) classes, and Molecular Signatures Database (MSigDB) v7.0 gene sets (378). The fcs performed was Gene Set Enrichment Analysis (GSEA). GSEA is a computational method that determines whether an a priori defined set of genes shows statistically significant, concordant differences between two biological states (379). Multiple test correction was applied by using the Benjamini and Hochberg/FDR method. GSEA analyses used the $\log_2$(FC) values from the entire DGE list. The R packages clusterProfiler v3.14.3 (380), fgsea v1.12 (381), enrichplot v1.6 and pathview 1.26 (382) were used to perform these analyses.

2.6.4 Human single-cell RNA-seq analyses

For adapter trimming, Trim Galore v0.6.4 was used to remove contaminating adapter and oligo-dT primers. Primary QC, alignment and feature counting were performed as per 2.6.3.

Secondary QC was performed on cells by considering total counts, total features, the proportion of mitochondrial DNA, cell cycle state and mapping rate. Initial secondary cell QC (383) included the total number of counts per cell (median ±3 median absolute deviations), the total number of features per cell (number of detected genes per cell – median ±3 median absolute deviations) and the percentage of mitochondrial DNA (cells must have had less than 6% mitochondrial DNA). Cell cycle was assigned using the cyclone function from the scran package version 1.14.6 (384). Cells in G1 and S phase of the cell cycle and with a minimum of 50% uniquely mapped reads were kept for

downstream analysis. Of the 736 cells commencing secondary QC, 629 remained for further analysis. Genes appearing in nine or fewer cells were removed prior to differential expression analysis. There were no apparent batch, plate or volunteer effects causing the removal of cells, nor was there a noticeable batch effect in the remaining cells.

Seurat v3.1.4 (385) was used for normalisation, variance stabilisation and feature selection. sctransform (via Seurat) was used to perform normalisation and variance stabilisation for PCA and initial clustering (386). PCA was performed using Seurat and used the 2000 most variable features. Clusters of cells were identified using a graph-based shared nearest neighbour modularity optimisation-based clustering algorithm (387), implemented by the Seurat FindClusters function. Uniform manifold approximation and projection (UMAP) (388), a dimension reduction technique, used the first 12 principal components (PC). Seurat was used for DGE analyses including only genes that were detected in at least 25% of cells in both populations (min.pct argument). Differential expression was based on the non-parametric Wilcoxon rank-sum test using normalised data. P values were adjusted using Bonferroni correction based on the total number of genes in the dataset, and only adjusted p values (padj) were used. DGE was designated as genes with an absolute value of the natural logarithm of the fold change (ln(FC)) greater than 0.5 and padj less than 0.05 unless otherwise indicated.

Further analyses of single-cell RNA-seq (scRNA-seq) data were performed. Pseudotime analysis was performed with slingshot v1.4.0 (389). Slingshot uses clusters of cells to uncover global structure by interpreting Euclidean distances. The slingshot package then converts this structure into smooth lineages represented by a one-dimensional variable called "pseudotime." Single Cell Signature Explorer was used to assign single-cell scores according to multi-gene features (390). Both pseudotime and signature analyses were projected onto the UMAP. TraCeR was used to reconstruct single-cell α and β TCRs and complementarity-determining regions (CDR) (391). Prior

to running TraCeR, 46 cells were removed due to low read counts (identified by small file size (<2Mb), incompatible with adequate sequencing). Therefore, TraCeR was run on 690 cells in two batches. TraCeR Assemble and Summarise functions were implemented using Bowtie2 v2.4.2 (392), Trinity v2.11.0 (393), IgBLAST v1.15.0 (394) and Kallisto v0.46.1 (395). Mucosal-associated invariant T (MAIT) cells were identified by TCR as cells expressing *TRAV1-2* paired with i) *TRAJ33*, ii) *TRAJ12* or iii) *TRAJ20*, as previously described (396).

2.6.5 Mouse bulk RNA-seq analyses

Skewer v0.2.2 was used to trim sequence adapters of Illumina paired-end sequencing. Trimmed reads were aligned to the *Mus musculus* genome (GRCm38.ERCC assembly) using HISAT2 v2.1.0 (397) and the matching feature definition file accession NCBI: GCA_000001635.4. Samtools (v1.9) was used to sort BAM files (398). Picard v2.18.4 ("Picard Toolkit." 2019. Broad Institute, GitHub Repository) markDuplicates was used to identify and remove duplicated reads. Ensembl gene counts were generated using featureCounts v1.6.4 (373). Secondary QC was performed on samples by considering absolute and proportional read counts, library complexity, uniquely mapped reads and reads assigned to transcripts. Three samples were removed due to low total read counts and another three were removed due to low library complexity (24 samples remained).

DESeq2 v3.10 (374) was used for normalisation and feature selection. For visualisation and clustering, the rlog transformation was applied to count data. PCA was performed on rlog-transformed count values. Non-normalised counts were input to DESeq2. The Wald test was the default used for hypothesis testing when comparing gene expression between samples. Multiple test correction was applied by using the Benjamini and Hochberg/FDR method (375). The $\log_2$(FC) values were shrunk using apeglm (376).

Functional analyses were performed on each contrast's apeglm-shrunk DGE list. Both ORA and fcs were used. For ORA, the DGE list was composed of genes with an FDR<0.05 and the hypergeometric

test was used to determine whether the input gene list was over-represented in gene categories. Multiple test correction was applied by using the Benjamini and Hochberg/FDR method. Gene categories included GO project (377) MF, CC and BP classes and MSigDB v7.0 gene sets (378). The fcs performed was GSEA. GSEA analyses used the $\log_2$(FC) values from the entire DGE list. The R packages clusterProfiler v3.12.3 (380), fgsea v1.10 (381), enrichplot v1.5 and pathview 1.20 (382) were used to perform these analyses.

Chapter 3

3 Tissue-resident memory T cells and prime-target vaccination assessment in mice

3.1 Introduction

The initial discovery of memory T cell heterogeneity, whereby differential CCR7 expression demarcated TCM and TEM (197), indicated T cell migration outside blood as a crucial determinant of memory preservation and protective immunity. The identification of TRM has dramatically altered our understanding of adaptive immunity. TRM are widely distributed in the body and can be identified in almost all tissues in both mice and humans (212,399). CD69 and CD103 are two markers of tissue residency that show tissue-specific patterns of expression in a manner that is conserved between individuals (212,219). Crucially, TRM sit at portals of pathogen entry working as immune sentinels, ready to rapidly respond and compose local and systemic protective immunity to eliminate microorganisms (400-402).

The protective role of CD8+ T cells against liver-stage *Plasmodium* parasites, as discussed in Chapter 1, is highly relevant to vaccination. Vaccination strategies are required to generate very high frequencies of peripheral CD8+ T cells to protect from subsequent sporozoite challenge (176,178). Knowledge on whether and how these peripheral cells contribute directly to protection against liver-stage malaria is incomplete. TRM, however, have been shown to directly contribute to the killing of *Plasmodium*-infected hepatocytes (201,237), and can be induced through RAS vaccination (166,201,403), or prime-target-type subunit vaccination

strategies (201,237,241). Liver-resident T cells patrol the hepatic sinusoids, are often primed outside the liver, and are sufficient for protection against liver-stage malaria following vaccination (201,237,241,404). Understanding the generation, dynamics, and function of TRM following vaccination are crucial avenues of research. Enhanced knowledge of these processes would have implications in terms of basic science – as cell fate decisions are highly complex and redundantly regulated – and in terms of translational science, affecting vaccine design to better protect from liver-stage *Plasmodium* infections.

The prime-target vaccination approach developed by Gola *et al.* is a translatable and potentially deployable vaccine strategy capable of inducing liver TRM against liver-stage malaria (237). The strategy encompasses an IM 'prime' of T cells in the periphery, followed by an IV 'target' or boost. Targeting CD8+ T cells to the liver was achieved using either PLGA or recombinant viral vectors. Non-replicating Ad vectors generate a unique T cell response with a protracted contraction phase and can persist in several tissues for up to a year following administration (405,406). Gola and colleagues showed prime-target to generate durable AgSp CD8+ T cells in the liver for up to 6 months and to improve the efficacy of subunit immunisation in mice using clinically relevant antigens (237). This study presented findings from a phase I clinical trial indicating that IV ChAd63-ME-TRAP was well tolerated and peripherally immunogenic in healthy volunteers. Notably, however, the identification of human liver TRM was not performed.

Immunosurveillance by memory CD8+ T cells is a dynamic process wherein unique characteristics and plasticity can provide the optimal response to a pathogen. It is therefore no surprise that the definition of TRM as "permanently residing in tissues" is flexible. There are now several reports indicating TRM can become dislodged and re-establish residence within dLN and even distant tissues (400,401,407-409). These CD8+ and CD4+ 'ex-TRM' can egress via afferent lymphatics, can be identified in the circulation following TCR-dependent and TCR-independent

activation (400,409). These T cells become circulating TEM and preserve phenotypic and transcriptional features of *bona fide* TRM, as well as exhibiting a predilection to traffic back to the tissue of origin. Similarly, 'TRM precursors' arising from effector cells have been identified as early as four days after initial antigen exposure and share properties with ex-TRM (410-412). The complexity of TRM-lineage T cells remains to be fully understood.

Given the knowledge that TRM are likely necessary and sufficient for liver-stage malaria protection and that prime-target induces liver TRM, the focus of experiments described in this chapter was to gain an understanding of the early T cell responses, dynamics and transcriptomics following prime-target vaccination in order to identify a translatable CoP. This builds on other work by Spencer *et al.* (413) and Gola *et al.* (237) who investigated the relationships between vaccine-induced T cell-mediated protection, *Plasmodium* parasite killing and T cell tissue residency following prime-target vaccination in mouse models.

The aim of the work in this chapter was to identify and investigate a TRM-based CoP for prime-target vaccination. The specific objectives were to:

1) Quantify and qualify the TRM response after prime-target strategies known to induce sterile protection in rodent malaria challenge models,
2) Investigate the dynamics of memory T cells following prime-target vaccination, and
3) Identify a biomarker panel to detect TRM after prime-target vaccination.

3.2 Results

3.2.1 Antigen-specific cell short-term time course

To assess the presence of memory T cells in different organs at early time points post-IV Ad, mice were vaccinated in an offset manner to enable simultaneous analysis post-Ad-OVA administration (Figure 3.1A). The presence of OVA-specific (in this chapter, OVA-specific cells are termed "AgSp") T cells between one and eleven days after IV Ad-OVA administration was compared to the day of IV Ad-OVA administration. CD11a was used to identify liver-patrolling, tissue-resident T cells in the liver (236); memory T cells in the blood that expressed high levels of CD11a were designated TRM-like cells.

The data demonstrated an early peak in the frequency of AgSp cells. The frequency of CD11a hi T cells as a percentage of total AgSp CD8+ T cells showed a rapid increase in the blood (KW approximate p=0.007), but no individual significant differences compared to the day of IV boost (D0) were observed (Figure 3.1B). CD11a hi cells peaked one day (D1) after IV Ad-OVA in the liver. When AgSp CD11a hi cells were expressed as a proportion of total CD8+ T cells, the peak appeared at D3 in the liver, but there was no significant difference in the blood compared to the day of IV boost (KW exact p=0.0684, Figure 3.1C).

The frequency of *Plasmodium*-specific TRM in the liver are important, but ultimately, for protection against liver-stage malaria, absolute numerical thresholds must be met (59,413). The quantity of AgSp TRM and CD8+ T cells peaked in the liver at day 3 post-IV boost, at $7x10^5$ and $2x10^6$ cells, respectively (Figure 3.1D). The expansion of total TRM (CD11a hi CD44+ CD8+ T cells) was also observed following IV boost; total TRM numbers followed a similar kinetic, however, the number was approximately ten-fold higher than AgSp TRM (Figure 3.1E).

CD103 expression was examined on AgSp CD11a hi T cells following IV boost. The geometric mean fluorescence intensity (GMFI) of CD103 peaked on liver TRM at D1 after vaccination (Figure 3.1F), but no change in CD103 expression on blood TRM-like cells was observed. Cells expressed comparable levels of CD103 across blood and liver. A transient increase in the frequency of liver TRM that expressed CD103 was seen, though this did not reach statistical significance (p=0.0571, Figure 3.1G). A high proportion of CD11a hi cell populations had increased GMFI of CD103 or a greater frequency of CD103+ when compared to the within-mouse corresponding CD11a lo/med population (data not shown).

When delivered intravenously, Ad elicits a potent immune response in the liver (414,415) and, relatedly, CD103+ TRM can exit tissues after activation and exhibit an increased predilection for tissue re-entry (409). Therefore TRM-like cells in the periphery may be activated TRM that have left the liver, with an increased potential for tissue reseeding. The frequency of AgSp TRM-like cells sampled early after IV Ad-OVA correlated with liver AgSp populations. These associations did not reach significance but were most closely correlated when considering D3 and D11 liver compared to D3 blood populations (Table 3.1).

Table 3.1: Day three blood AgSp TRM-like cell and liver TRM frequency correlations. TRM and TRM-like cell frequencies were defined as the OVA-pentamer+ CD69+ CD11a hi CD44+ frequency of CD8+ T cells in the blood and liver, respectively.

	Blood D3 vs. Liver D0	**Blood D3 vs. Liver D1**	**Blood D3 vs. Liver D3**	**Blood D3 vs. Liver D7**	**Blood D3 vs. Liver D11**
Spearman r	0.0	0.8	0.9	0.6	0.99
Exact p value	>0.999	0.3333	0.0833	0.4167	0.0833

To determine the effect of the IV boost transgene, mice were primed as before and targeted with Ad-OVA or Ad-TIP (Figure 3.2). This allowed phenotyping of the early T cell response to prime-target, until 14 days after target. CD69 was used in addition to CD11a to identify liver TRM, and TRM-like cells in the blood.

A short-term increase in AgSp TRM-like cells after IV Ad-OVA was simultaneously observed in spleen, liver, and blood. AgSp liver TRM increased from 62% to 92% of total AgSp CD8+ T cells at D1, decreasing to 44% and 42% at D7 and D14, respectively (Figure 3.3A). Blood TRM-like cells increased from 62% to 74% of all AgSp CD8+ T cells at D1, decreased to 52% (11% below baseline (D0) levels) on D7 and returned to baseline by D14. AgSp spleen TRM increased from 56% to 74% of total AgSp CD8+ T cells and returned to baseline levels by D3. Similar to the trend as a proportion of total AgSp CD8+ T cells, AgSp liver TRM increased to 0.58% of CD8+ T cells at D1, decreased to approximately 0.1% of CD8+ T cells on D3 and D7 and returned to baseline by D14 (Figure 3.3B). At all time points, there was a liver:spleen and liver:blood ratio of greater than one, when comparing AgSp CD69+ CD11a hi CD44+ cells as a proportion of total CD8+ T cells (Figure 3.3C). These ratios were elevated at D7 compared to D3 and D14, but not compared to D0.

TIP antigen delivery was not as effective in generating short-term AgSp TRM-like cell populations, compared to IV Ad-OVA. AgSp liver TRM increased to 88% of total AgSp CD8+ T cells at day one (D1) after IV Ad-TIP and returned to baseline by D3 (Figure 3.3D). There were no significant differences after IV Ad-TIP administration in blood and spleen TRM populations. There were no significant differences in the liver:blood and liver:spleen TRM ratio at any time point following IV Ad-TIP (data not shown).

The short-term increase in TRM-like cells in the blood was compared to the frequency of D14 liver TRM levels, but no association reached statistical significance. A strong positive correlation was observed between the frequency of TRM as a proportion of total AgSp CD8+ T cells observed on blood D1 and liver D14 TRM (Figure 3.4). Similarly, liver D0 and blood D1 TRM frequencies were strongly positively correlated ($p=0.233$). Blood D3 TRM-like cells had a weak negative correlation with liver D14 TRM.

TRM marker expression was compared on TRM-like cells in all organs at early time points following IV boost. A peak in the frequency of non-AgSp CD103+ TRM was observed in all organs at D1 after IV viral vector (Figure 3.5A). The magnitude of this increase, as a proportion of total CD8+ T cells, was most significant in the liver as up to 3% of CD8+ T cells were CD103+. In the liver, CD69+ cells had a greater proportion of CD103+ and CXCR6+ populations at all time points, compared to the within-mouse CD69- population (Figure 3.5B). Liver CD69+ cells had a higher proportion of PD-1+ cells at D7 and D14, but not at D1 and D3, compared to CD69- cells.

These data suggested AgSp blood TRM-like cells measured very early after IV boost may have been associated with the frequency of liver TRM at later time points. TRM-like cells and TRM expressed similar levels of TRM phenotypic and identification markers, especially early after IV boost, suggestive of a common origin. Therefore, mobilisation and homing of cells sampled just before and after IV boost was further examined.

3.2.2 Liver TRM dynamics with and without IV boost

To investigate the effect of IV boost and cell origin on cell destination, adoptive transfer experiments were performed. To discriminate between cells of donor and host origin, congenic mice expressing either CD45.1 (Ly5.1) or CD45.2 (Ly5.2) were used in these experiments. CD69+ CD8+ T cells isolated from the spleen or liver of Ad-OVA vaccinated Ly5.1+ mice were transferred into Ly5.1- naïve and were subsequently vaccinated IV with Ad-OVA or remained unvaccinated (Figure 3.6A).

On day 7 after IV Ad-OVA, the frequency of transferred cells in the liver was significantly higher when cells originated from the liver compared to the spleen $CD69^+$ cells (Figure 3.6B, left, two-way ANOVA p=0.0043). IV Ad-OVA did not significantly alter the frequency of Ly5.1+ cells. There were no significant differences between the four groups in the spleen Ly5.1+ frequency of CD69+

cells (Figure 3.6B, right). These data suggested liver TRM travel to and maintain themselves in the liver once adoptively transferred.

Cells that were transferred from the liver maintained a TRM phenotype. The proportion of transferred liver cells that maintained CD69 expression and expressed CD11a hi, in naïve mice (group 2), was greater than 75% and this was increased compared to cells transferred from the spleen (Figure 3.6C, left). IV Ad-OVA administration resulted in a decrease in the TRM frequency of Ly5.1+ transferred cells in the liver. In contrast, an increase in the CD69+ CD11a hi frequency of transferred spleen cells was seen in the IV Ad-OVA group, compared to no IV Ad-OVA administration (Figure 3.6C, left). In the liver, the absolute number of transferred cells maintaining a TRM phenotype was not significantly different between groups 1 and 2 (Figure 3.6C, right). Groups 3 and 4 had very low or an undetectable number of Ly5.1+ TRM in the liver (data not shown). In contrast, only a very small proportion of transferred cells established residency in the spleen (Figure 3.6D).

Transferred AgSp cells followed similar kinetics as total transferred cells. Transferred cells made up the majority of AgSp TRM in the livers of mice that did not receive IV Ad-OVA (Figure 3.7A, left). Spleen-derived (groups 3 and 4) AgSp TRM were undetectable in the liver and spleen. In IV vaccinated groups, there were up to 100-fold increase in the number of AgSp TRM compared to non-IV vaccinated groups, in both the liver (Figure 3.7A, middle) and spleen (spleen data not shown), irrespective of the origin of transferred cells. Taken together, these data suggested that the decreased Ly5.1+ frequency of AgSp TRM was due to an expansion of the Ly5.1- AgSp TRM population. OVA specificity was not part of the cell transfer criteria, though in the absence of IV Ad-OVA, AgSp cells formed a higher proportion of the liver transferred cell fraction, compared to spleen transferred cells (Figure 3.7A, right). When mice were administered IV Ad-OVA, OVA-specific cells decreased as a proportion of transferred cells (not significant, MW p=0.0952).

IV vaccination with Ad resulted in increased frequencies of CD8+ T cells in the liver compared to the spleen. In IV vaccinated groups, Ad-OVA induced similar numbers of total AgSp CD8+ T cells per tissue, irrespective of the origin of the transferred cells (KW exact p=0.172, Figure 3.7B, left). In groups that received no Ad-OVA, the numbers of AgSp CD8+ T cells were either very low or undetectable (data not shown). As a proportion of total CD8+ T cells, the liver had higher frequencies of AgSp CD8+ T cells; there was a significant difference between liver group 3 compared to spleen group 3 (Figure 3.7B, right). There was no difference between responses in the liver and spleen in group 1 (MW p=0.222). There was a higher liver:spleen ratio in the spleen cell transferred IV Ad-OVA group, compared to the liver cell transferred IV Ad-OVA group (Figure 3.7C).

This experiment provided information regarding the effect of IV Ad-OVA and cell origin on cell destination following adoptive transfer. The data suggested that if dislodged or mobilised (by physical removal and transfer), liver TRM returned to the liver in preference to other organs. In addition, IV Ad-OVA resulted in downregulation of CD69 and proliferation in liver TRM, signifying that TRM may have secondary memory or effector potential.

Having observed homing of liver cells back to the liver, the homing ability of liver T cells differentiated by CD69 status was examined. CD8+ T cells expressing either high levels of CD69 or no CD69 were transferred from livers of mice that had received IM Ad-OVA, into naïve recipient mice that were subsequently vaccinated with IV Ad-OVA or remained unvaccinated (Figure 3.8A).

Irrespective of IV Ad-OVA, transferring CD69+ cells led to a higher TRM frequency of Ly5.1+ cells, compared to CD69- cell transfer (Figure 3.8B, left). Comparing the two CD69+ transferred groups, a five-fold reduction in the frequency of TRM was observed in the liver in IV Ad-OVA mice. The spleen frequency of TRM as a proportion of Ly5.1+ cells was higher in CD69+ compared to CD69-

groups (Figure 3.8B, right). Similar trends were seen in the liver and spleen when comparing Ly5.1+ TRM as a frequency of CD8+ T cells (Figure 3.8C). Of note, the frequency of Ly5.1+ TRM of CD8+ T cells was approximately ten-fold higher in the liver compared to the spleen, when comparing individual mice (Figure 3.8C, left y-axis compared to right y-axis). The total number of Ly5.1+ TRM in the liver was not significantly different between CD69+ IV Ad-OVA and no IV Ad-OVA groups (Figure 3.8D, left).

CD69- tissue-residing T cells have previously been referred to as TEM, particularly when compared to tissue-residing CD69+ T cells. Group 1 had a significantly lower frequency of CD69+ of Ly5.1+, compared to group 2 (Figure 3.8E, left). IV Ad-OVA did not significantly affect the CD69+ Ly5.1+ population of CD8+ cells (Figure 3.8E, middle). Groups receiving IV Ad-OVA had higher CD69- Ly5.1+ frequencies of CD8+ T cells (Figure 3.8E, right).

Taken together, these data suggest that liver TRM return to and maintain residency characteristics in the liver. This effect appears to be partially dependent on the expression of CD69, as CD69- liver cells did not demonstrate similar homing back to the liver. Lastly, these data would suggest that CD69+ cells downregulated CD69 in response to IV Ad-OVA, to expand the CD69- frequency of CD8+ T cells, whereas CD69- transferred cells were not able to increase expression of the molecule.

3.2.3 Investigating the dynamics of TRM-like cells shortly after IV viral vector vaccination

Having shown that liver TRM home back to the liver prior to IV Ad-OVA and TRM isolated post-IV boost primarily originate from CD69+ T cells, it was important to determine whether TRM-like cells observed early after IV Ad-OVA would home to the liver and form *bona fide* liver TRM (Figure 3.9A).

The highest frequency of liver TRM was observed in mice that received blood-derived cells (Figure 3.9B). Stratifying these same data by IV Ad-OVA administration, there was a lower TRM frequency of Ly5.1+ cells in the liver (not significant, p=0.099) and spleen in the IV Ad-OVA animals compared to mice that did not receive IV Ad-OVA (Figure 3.9C), like previous experiments. There was no difference in the CD69+ CD11a hi frequency (% Ly5.1+) between IV Ad-OVA and no IV Ad-OVA blood cell transferred groups. These data suggested that day one post-IV Ad-OVA blood TRM-like cells can retain their CD69+ status and home to the liver.

The phenotype of CD8+ CD69+ T cells derived from different locations was also examined following adoptive transfer. Within the liver, Ly5.1+ cells originating from donor livers demonstrated similar levels of PD-1 expression to host cells (Figure 3.9D & E). PD-1 expression between donor and host cells was comparable when mice received liver-, spleen- or blood-derived cells (Figure 3.9F, left). Ly5.1+ CD69+ cells had significantly higher CD44 GMFI compared to Ly5.1- populations in the liver, irrespective of transferred cell origin (Figure 3.9F, middle). Blood-derived and liver-derived Ly5.1+ cells had equivalent CD11a GMFI compared to host cells (Ly5.1-) cells (Figure 3.9D, E & F right). Notably, there were no significant differences in GMFI of PD-1, CD11a or CD44 according to transferred cell origin. These data suggest that the phenotypes of host-derived and donor-derived cells in the liver were similar when transferring liver and blood CD8+ CD69+ cells post-IV Ad-OVA.

The total number of AgSp CD8+ induced by IV Ad-OVA was consistent with previous transfer experiments. IV Ad-OVA generated approximately $5x10^5$ and $1x10^5$ AgSp CD8+ cells in the liver and the spleen, respectively (Figure 3.9G). IV Ad-OVA had no differential effect on AgSp cell induction when comparing liver, blood and spleen transferred cell groups (data not shown). In addition, IV vaccination with Ad-OVA resulted in similar frequencies of AgSp CD8+ T cells in the liver and spleen (Figure 3.9H).

Overall, these data suggested that blood-derived CD69+ T cells found shortly after IV Ad-OVA had a high capacity to home to the liver and maintain themselves as liver TRM. Although not directly compared, this capacity was at least as high as that of 'steady-state' liver TRM, sampled and transferred before IV Ad-OVA administration. In contrast to liver- and spleen-derived CD69+ T cells, blood-derived CD69+ T cells in the liver did not downregulate CD69 in response to IV Ad-OVA.

3.2.4 Investigating the dynamics of TRM-like cells in the presence and absence of antigen

Ad-based vaccines have inherent inflammatory effects, inducing a sizeable innate immune response in addition to a large proportion of the adaptive response directed to non-transgene antigens (416). The inflammation in the liver and ongoing Ad-specific response could impact OVA-specific T cell homing to the liver. To control for this, the same experiment as above (Figure 3.9) was repeated, but cells were transferred into Ad-OVA or Ad-TIP vaccinated mice (Figure 3.10A).

In agreement with previous experiments, transferred blood-derived cells had a high propensity to maintain their CD69 expression. Considering Ly5.1+ cells in the liver, the frequency of CD69+ Ly5.1+ cells was higher in mice receiving blood-derived cells compared to liver-derived cells (two-way ANOVA proportion of variation: 88%, $p<0.0001$) (Figure 3.10B, C, D, left)). There was a small increase in the frequency of CD69+ cells due to OVA (two-way ANOVA proportion of variation: 3.9%, $p=0.0291$) (Figure 3.10D, left). A higher frequency of CD69+ cells was observed in Ly5.1+ cells compared to Ly5.1- populations (Figure 3.10D, left). In the spleen, the frequency of CD69+ Ly5.1- cells was always less than 0.5% or undetectable (data not shown). An antigen effect was more apparent in the spleen (two-way ANOVA proportion of variation: 34%, $p=0.0096$) (Figure 3.10D, right). There were, however, no significant differences in the frequency of CD69+ Ly5.1+ between the liver- and blood-cell-transferred mice.

Both liver- and blood-derived CD8+ CD69+ transferred T cells that were exposed to prime-target, had a phenotype that was more 'TRM-like' when compared to recipient-derived cells that had been exposed to Ad-OVA or Ad-TIP alone (Figure 3.10B & C). Transferred cells had higher levels of expression of the TRM markers CD11a, PD-1 and CD44, compared to host-derived (Ly5.1-) cells (Figure 3.11A). The Ad antigen significantly affected the expression of CD11a and CD44 (two-way ANOVA proportions of variation: 15%, p=0.0021 and 3%, p=0.0105, respectively). However, there was no apparent difference in the expression of these markers when comparing between blood- and liver-derived Ly5.1+ cells (data not shown).

The total TRM proportion of CD8+ T cells was higher in Ad-OVA groups, compared to Ad-TIP groups (Figure 3.11B). The frequency of OVA-specific transferred cells was low and was not different between group 1 and group 2 (Figure 3.11C). The IFNγ+ fraction of Ly5.1+ cells in groups 3 and 4 were either very low or undetectable (data not shown). Overall, transferred cells constituted a very low proportion of the overall CD8+ T cell pool (Figure 3.11D), likely a result of the low number of cells that were initially transferred.

To further assess the homing ability of liver and blood cells where a higher proportion of these cells were OVA-specific, donor mice were primed with Ad-OVA followed by an IM MVA-OVA boost vaccination (Figure 3.12A). Group sizes were reduced to three mice to maximise the number of transferred cells per animal.

Blood-derived TRM-like cells once again had a high propensity to maintain their CD69 expression (Figure 3.12B, C, middle panel). In the liver, there were no significant differences between Ad-OVA and Ad-TIP groups in terms of the frequency of CD69+ Ly5.1+ cells (data not shown). The frequency of CD69+ Ly5.1+ was higher in blood-derived T cell transferred groups, compared to liver transferred groups (Figure 3.12B, C & D, left). In the spleen, all groups had a reduced frequency of

CD69+ Ly5.1+ cells compared to the liver (differences not tested). Blood-derived cell transfer groups had a higher frequency of CD69+ Ly5.1+ than liver-derived cell transfer groups (Figure 3.12D, right).

Expression of liver homing molecules, including CXCR6 and CD11a, was also examined. In the liver, Ly5.1+ blood cell transferred groups (3 and 4) had higher levels of CD11a expression compared to groups 1 and 2 and when compared to Ly5.1- groups 3 and 4 (Figure 3.13A, left). Overall GMFI of CXCR6 in groups 1-4 of Ly5.1+ cells was higher than that of all Ly5.1- groups (analysis not shown). The medians of Ly5.1+ groups 1 and 2, and groups 3 and 4, were higher than the corresponding Ly5.1- groups, but this was not statistically significant (Figure 3.13A, middle left). Ly5.1+ groups 3 and 4 had higher CD44 GMFI compared to groups 1 and 2 (Figure 3.13A, middle right). Similar to CD11a GMFI, Ly5.1+ groups 3 and 4 had higher PD-1 GMFI compared to Ly5.1+ groups 1 and 2, and Ly5.1- groups 3 and 4 (Figure 3.13A, right).

To further assess the importance of CD69 in the establishment of residency characteristics, Ly5.1+ TRM were compared to Ly5.1+ TEM. In this instance, TEM were identified as liver CD69- CD11a- (lo/med) CD44+ CD8+ T cells. Median CXCR6 GMFI was higher in Ly5.1+ TRM compared to TEM, with the group 3 and 4 comparison reaching significance (Figure 3.13B, left). Both groups 1 and 2, and groups 3 and 4 Ly5.1+ TRM had higher PD-1 GMFI (Figure 3.13B, right). The GMFI of CXCR6 and PD-1 were higher in blood transferred groups (analyses not shown).

The data also showed that transferred cells had a higher propensity to differentiate into *bona fide* TRM in the presence of homologous antigen, that is in IV Ad-OVA groups. IV Ad-OVA groups had a higher frequency of TRM Ly5.1+ cells when compared to Ad-TIP groups (Figure 3.13C, left). As a proportion of total CD8+ T cells, IV Ad-OVA groups had an increased TRM proportion compared to

Ad-TIP groups (Figure 3.13C, right). Groups that received IV Ad-OVA had an increased frequency of AgSp TRM within the population of AgSp CD8+ T cells (Figure 3.13D).

This experiment confirmed much of what had been seen previously and provided two new insights. First, cells isolated and transferred from the blood had robust expression of liver homing molecules either equal to or greater than transferred liver cells or corresponding host (Ly5.1-) cells. Secondly, transferred cells that retained their CD69+ status had higher expression of TRM homing and functional molecules, compared to transferred cells that did not.

Having performed the previous experiments with FACS sorted cells, in which cells are stained and manipulated prior to transfer, it was important to determine whether the cell-sorting procedure introduced a bias through differential effects on cells of different origins. Therefore, an experiment was performed to explore the liver homing ability, phenotype, and antigen-specificity of transferred cells that were not FACS sorted. Total liver and blood cells were transferred from mice, who had previously received IM Ad-OVA, one day after IV Ad-OVA, into mice administered Ad-OVA or Ad-TIP (Figure 3.14A).

In the absence of FACS sorting, there were no substantial differences between liver-derived and blood-derived cell transfer groups, in contrast to previous experiments. Liver-derived transferred cells had similar phenotypes as blood-derived transferred cells (Figure 3.14B & C). Liver-derived cell transfer groups had higher frequencies of CD69+ Ly5.1+ cells in the liver, compared to blood-derived cell transfer groups, although these differences did not reach statistical significance (Figure 3.14D, left). This trend may be accounted for by the relative enrichment of CD69+ cells in the liver, compared to the blood. The total number of CD69+ Ly5.1+ CD8+ cells isolated from the liver increased 10-15-fold when transferring non-sorted cells, compared to previous experiments where sorted cells were transferred. There were no differences observed in the frequency of CD69+

in the spleen when comparing the groups (Figure 3.14D, right). There were also no significant differences between any of the four groups when considering CD11a, CD44 or PD-1 GMFI, in Ly5.1+ or Ly5.1- populations (Figure 3.14E).

Ad-OVA was associated with increased TRM in the liver, irrespective of TRM antigen specificity. Compared to Ad-TIP, Ad-OVA resulted in higher OVA-Pentamer specific TRM frequencies of transferred Ly5.1+ cells (Figure 3.15A, left). Ad-OVA groups had higher median TRM frequencies of Ly5.1+ cells, compared to Ad-TIP groups (Figure 3.15A, right). These differences did not reach statistical significance, nor were there differences between Ad-OVA groups. The same trends were seen in the AgSp TRM and TRM frequencies of total CD8+ T cells (Figure 3.15B). One of these comparisons was significantly different; the group 1 median AgSp TRM frequency was greater than that of group 2 (Figure 3.15B, left). These trends occurred in the context of very low Ly5.1+ frequencies of CD8+ T cells (all values below 5%; Figure 3.15C).

Taken together, these previous three experiments provided valuable insight into the effects of Ad transgene antigen expression and transferred cell origin on the generation and phenotype of liver TRM. The three experiments involved the transfer of cells one day after IV Ad-OVA to identify the kinetics of these cells. Groups with transferred blood cells were associated with high CD69+ and TRM frequencies of Ly5.1+ cells (Figure 3.15D, left & middle), although this depended on isolating and transferring CD69+ CD8+ T cells by FACS. IV Ad-OVA was associated with higher frequencies of TRM as proportions of total CD8+ T cells, compared to IV Ad-TIP (Figure 3.15D, right).

3.2.5 Investigating the origin and expansion of AgSp TRM in the liver

The next experiment was performed to compare the effects of homologous or heterologous transgene antigen delivery by IV Ad after an IM prime, and to assess the impact of blocking egress of T cells from lymph nodes, through FTY720 administration, on hepatic T cell populations (Figure

3.16A). FTY720 is a sphingosine-1-phosphate receptor modulator that results in T cell accumulation in lymph nodes (417) and sequesters recirculating naïve T cells from peripheral organs and the circulation to lymph nodes (418). This immunomodulator was given before, and after IV Ad until tissue harvest.

Animals that received IV Ad-OVA had an overall higher AgSp response in the liver (Figure 3.16B, left & middle). Animals from groups 1 & 3 combined (Ad-OVA) had increased frequency of AgSp TRM ($p=0.0001$) and AgSp CD8+ T cells ($p=0.0015$), when compared to groups 2 & 4 combined (Ad-TIP). When comparing animals administered FTY720 (groups 1 & 2) or saline (groups 3 & 4), there was no difference in AgSp TRM and AgSp CD8+ T cell frequency (analyses not shown). There were no statistically significant differences between groups 1 & 3 (Ad-OVA) and groups 2 & 4 (Ad-TIP) in terms of the frequency of AgSp TRM (% AgSp CD8+ T cells) (Figure 3.16B, right).

In IV Ad-OVA vaccinated mice, an increase in the level of expression and in the frequency of positive cells was observed when examining functional and homing TRM markers in TRM compared to TEM. Phenotypic comparisons between TRM and TEM were made between groups 3 and 4 as these groups underwent homologous (IM, IV Ad-OVA – group 3) and heterologous transgene antigen (IM Ad-OVA, IV Ad-TIP – group 4) vaccination. The AgSp TRM subset had uniformly higher GMFI values of CXCR6, PD-1 and CD103 when compared to the corresponding TEM subset (Figure 3.16C). The IV Ad-TIP group demonstrated higher CXCR6 GMFI compared to the Ad-OVA group (Figure 3.16C, left). Given that the absolute values of these differences were relatively small, proportions of TRM/TEM expressing these markers were assessed. The marker positive frequency of AgSp TRM was similarly higher than the corresponding TEM population in both groups 3 and 4 (Figure 3.16D). These results suggested that the antigen delivered in the IV viral vector was less critical in defining TRM phenotype than viral-vector induced inflammation or cell CD69 status.

The administration of FTY720 did not significantly affect the number of OVA-pentamer specific and total T cells in the spleen or liver. Differences between FTY720 and saline groups (groups 1 and 2 compared to groups 3 and 4, respectively) were not present in the liver or spleen when looking at the number of AgSp TRM and AgSp CD8+ (Figure 3.16E, F). IV Ad-OVA groups, compared to IV Ad-TIP groups, tended to have higher numbers of AgSp TRM and AgSp CD8+ T cells; these differences were most pronounced in the spleen (Figure 3.16E, F, right). Similar trends were seen when looking at the total number of CD8+ T cells (Figure 3.16G). No differences in the frequency of CD8+ of total live lymphocytes were observed (data not shown).

While this experiment did not show differences between FTY720 compared to saline groups, it provided insights into the phenotype of AgSp TRM, compared to TEM, building on what is already known from the literature. FTY720 was used in this experiment to determine if liver OVA-specific TRM and CD8+ T cells induced by IV Ad-OVA were recruited from the periphery or if they were internally generated. Administration of FTY720 had neither widespread nor consistent effects on liver or spleen lymphocyte numbers or frequencies; therefore, the dose of FTY720 was increased in the following experiment. Mice received an IM Ad-OVA prime, or not, and were further divided into FTY720 or saline groups (Figure 3.17A). There was a two-month period between prime and target vaccinations to minimise the contribution of OVA expression from the IM vaccination.

The data demonstrated that FTY720 administration was associated with both higher frequencies and numbers of OVA-specific TRM. In the liver, both groups of FTY720-treated mice had higher frequencies of CD8+ T cells within the population of total live lymphocytes, but this was not the case in the spleen (Figure 3.17B, left; spleen data not shown). Similarly, FTY720-treated mice had an increase in the frequency of AgSp CD8+ T cells in the liver, but not in the spleen (Figure 3.17B, middle left; spleen data not shown). Groups 1 and 3 (FTY720) had higher frequencies of AgSp TRM

compared to groups 2 and 4 (saline) in both the liver and the spleen (Figure 3.17B, middle right; spleen data not shown). The difference in the frequency of AgSp TRM was also reflected in the total number of AgSp TRM observed in the liver (Figure 3.17B, right).

IV Ad-OVA prime compared to Ad-OVA prime-target led to comparable frequencies of OVA-specific TRM in the liver seven days after IV boost. Groups 1 and 2 (Ad-OVA prime-target), compared to groups 3 and 4 (IV Ad-OVA prime), showed no differences in terms of liver AgSp TRM when expressed as proportions of total TRM, total CD8+ T cells or AgSp CD8+ T cells (data not shown). A similar trend was seen in the spleen (data not shown). In the liver, groups 1 and 2 had more than double the median frequency of AgSp as a proportion of CD8+ T cells, compared to groups 3 and 4 (difference not significant, p=0.0658; Figure 3.17C, left), this was also true in the spleen (Figure 3.17C, right). The liver:spleen AgSp TRM ratio was 3-4-fold higher in both IM Ad-OVA groups, compared to groups that did not have IM Ad-OVA (Figure 3.17D).

Once again, prime-target vaccination was associated with TRM expressing higher levels and higher frequencies of functional and homing TRM markers, when compared to TEM. Consistent with the previous experiment, higher levels of CD103 were observed on AgSp TRM compared to TEM; in addition, groups 1 and 2 (Ad-OVA prime-target) AgSp TRM expressed higher levels of CD103 compared to groups 3 and 4 (IV Ad-OVA prime) (Figure 3.17E). The PD-1+ population of AgSp TRM was composed of two cell subpopulations, according to group (Figure 3.17F, G). Groups 1 and 2 (IM Ad-OVA prior to IV Ad-OVA) had higher frequencies of PD-1 med AgSp TRM, compared to groups 3 and 4 (no IM Ad-OVA prior to IV Ad-OVA), and compared to the population of TEM (Figure 3.17F, left). In contrast, groups 1 and 2 had 5-fold lower frequency of PD-1 hi AgSp TRM compared to groups 3 and 4 (Figure 3.17F, right). There was no difference in the frequency of PD-1 hi cells between TRM and TEM in groups 3 and 4. Interestingly, Groups 3 and 4 TRM had a population of

CD44 hi cells that were present at much higher frequencies than observed in groups 1 and 2 (analyses not shown).

Together, the previous two experiments indicated the importance of adequate T cell priming prior to IV Ad-OVA. An IM Ad-OVA prime was associated with an increased number of OVA-specific CD8+ T cells, improved 'targeting' of OVA-specific TRM to the liver and a more 'TRM-like' phenotype. In the liver, FTY720 led to an increase in AgSp CD8+ and TRM frequencies, and a small but significant rise in total liver AgSp TRM number suggesting naïve T cells, but not memory T cells were depleted from this organ.

3.2.6 Transcriptomic analysis of T cells following prime-target

The following experiment was performed to examine the transcriptome of live CD8+ CD69+ cells by bulk Smart-seq2 RNA-seq, in the liver, blood and spleen, at early and late time points after IV Ad. All animals received an Ad-OVA prime and half received IV Ad-OVA, while the other half received IV Ad-TIP (Figure 3.18A). The experiment was designed to identify TRM transcriptionally at a memory time point and explore differences between early (day 1) and late (day 28) samples after IV Ad. Additionally, gene-based recognition of OVA-specific cells early after IV Ad-OVA was investigated.

Three cell populations were FACS isolated from each tissue pool, with each pool being the combination of five animals' tissues (Figure 3.18A). Each sample then underwent RNA-seq, resulting in a total of 30 sequenced samples (Figure 3.18A, right). Six samples were removed as part of the quality control process (see Chapter 2). These samples were mostly derived from population (P)1: OVA-Pentamer+ CD69+ CD8+ live cells.

PCA was performed on all samples that passed quality control. PC1 was almost entirely accounted for by the variability found between AgSp and non-AgSp cells and represented 26% of the variance amongst all samples (Figure 3.18B). PC2 was essentially dichotomised according to the time point sampled after vaccination, with a suggestion that there was more heterogeneity within the late timepoint samples, compared to the early time point samples, across PC2. Tissue type was a driver of differences within T cell OVA-pentamer± status. The antigen delivered as an IV boost (target vaccination) did not appear to differentiate samples. These clusters were corroborated by considering Euclidean distances between samples (Figure 3.18C). The main difference between samples was in antigen specificity and, within the AgSp subgroup, samples were most closely related according to the time point at which they were collected after IV boost. At the early time point after IV boost, CD69 status did not differentiate samples.

When analysing samples collected 28 days after IV boost, CD69+ compared to CD69- cells was effectively a comparison of TRM and TEM. Due to the finding that the antigen delivered in the IV boost did not appear to drive transcriptome variability (Figure 3.18B), Ad-OVA and Ad-TIP groups were merged for this comparison. The most variable genes among these samples included *Rap1gap2*, *Klrg1* and *Cx3cr1* (Figure 3.19A); genes proposed to play an important role in CD69+ T cell residence within tissues (208), suggesting residency signatures represented a significant source of variation between these samples. Forty-three genes were significantly differentially expressed ($|Log_2(FC)|>1$, FDR<0.001) across TRM and TEM samples. Downregulated genes in TRM included genes involved in T cell tissue retention and signalling such as *S1pr5*, *Ccl9* and *S1pr1*; whereas upregulated genes included *Aim2*, *Lag3* and *E2f3* (Figure 3.19B).

Mackay *et al.* described a universal transcriptional program of lymphocyte tissue residency (208). The genes in this transcriptional program separated late timepoint samples according to CD69 status (Figure 3.19C). CD69+ liver samples appeared to have a higher expression of genes that were

upregulated in the Mackay *et al.* signature, compared to the spleen (data not shown). When considering downregulated genes from the Mackay signature, there was a uniform downregulation of these genes in liver and spleen samples (Figure 3.19C, right). Despite these tissue-level differences, the Mackay *et al.* signature did allow transcriptomic identification of TRM, and differentiation from TEM.

Commitment to memory lineages occurs early after infection (419). If late and early timepoint CD69+ cells shared expression profiles of certain residency genes, then a gene signature could be used to identify T cells with a heightened residency profile, and potentially precursor TRM, early after IV boost. As several OVA-specific CD69+ samples did not pass QC, this contrast focused on comparing day 28 OVA-Pentamer negative CD69+ to day 1 OVA-Pentamer negative CD69+ samples. The most variable genes included several immunoglobulin component-encoding genes (*Igha*, *Ighg2c* and *Jchain*) and the mitochondrially-encoded genes *COX2*, *COX3*, *ATP6* and *ND4L* (Figure 3.20A). One hundred and twenty-seven genes were differentially expressed between day 28 CD69+ and day 1 CD69+ samples (|Log2(FC)|>1, FDR<0.001; Figure 3.20B). These included *Serpinb6a*, *Dusp6* and *Ccl5* which were upregulated in day 28 samples, as compared to genes encoding the Ly6 superfamily of GPI-linked cell-surface molecules (*Ly6k*, *Ly6a*, *Ly6c1* and *Ly6c2*) which were upregulated in day 1 samples.

Only 5 of the genes in the Mackay *et al.* signature of lymphocyte tissue residency were differentially expressed between the early and late timepoint samples that were CD69+. Closer inspection of the gene counts in these samples suggested that the lack of differential expression between late and early timepoint samples may have been due to organ-specific expression of the Mackay *et al.* signature. Expression of *Prdm1*, *Cxcr6*, *Klf2* and other genes showed that spleen and liver samples, particularly at the late time point, varied in their ability to produce these transcriptional factors

(Figure 3.20C). This implies that the Mackay *et al.* signature was not able to reliably differentiate samples derived from early TRM-like cells and late, *bona fide* TRM.

Including OVA-pentamer positive samples into the previous comparison allowed hypothesis regarding genes that may have been upregulated in *bona fide*, long-term AgSp TRM and in AgSp TRM-precursors, found in the effector phase of an immune response. Exclusively considering genes upregulated in the Mackay *et al.* signature, demonstrated that OVA-Pentamer positive liver samples express *Prdm1*, *Osgin1* and *Glrx* at comparably high levels when compared to day 28 OVA-Pentamer positive liver samples (Figure 3.20D). These results suggested that the *Prdm1*, *Osgin1* and *Glrx* are worth investigating further as potential gene markers of CD8+ T cells that have an increased propensity to form TRM at memory time points.

Functional analyses suggested that the differences between day 28 and day 1 CD69+ samples related to several biological processes. The putative differences occurred at the plasma membrane and were due to increased canonical Wnt signalling and a reduced inflammatory response in late timepoint CD69+ samples; there was enrichment of IFN-β and innate immune signalling in early timepoint samples (Figure 3.21A). The biological process differences related to T cell activation, viral response, and adaptive immunity (Figure 3.21B). Day 1 CD69+ samples did not uniformly upregulate genes associated with T cell activation; genes such as *Eomes* and *Itgad* were increased in expression in day 28 CD69+ samples. Day 1 samples showed molecular function over-representation of protein kinase and double-stranded RNA (dsRNA) binding genes, compared to day 28 CD69+ samples (Figure 3.21C). These likely represented an intracellular response to Ad infection in the acute phase, as viral associated RNA (a non-coding RNA found in Ad) mimics dsRNA and can build up to sufficiently high levels which then activates several protein kinases.

A limitation of this experiment was that the most degraded RNA came from cells in P1, and several samples from P1 did not pass quality control. P1 consisted of early and late timepoint samples that were CD69+ OVA-pentamer+, as opposed to P3, which were OVA-pentamer–. As a result, it was not possible to compare day 1 OVA-pentamer+ and day 28 OVA-pentamer+ CD69+ samples. Therefore, comparison of late and early timepoint samples was focussed on P3, as this allowed comparison of early TRM-like cells and late TRM, irrespective of antigen specificity. To assess the sensitivity of these analyses to the presence of OVA-pentamer+ cells, gene expression of day 1 vs day 28 CD69+ samples with and without OVA-pentamer+ samples were compared (Figure 3.21D). There was a substantial overlap between the gene lists created by comparing early vs late time point samples in the presence and absence of P1. Significantly (FDR<0.01) differentially expressed genes that were shared among the two comparisons (P3 with and without P1) included *Il18rap*, *Irf7* and several IFN-induced Ifit protein genes (Figure 3.21D). Indeed, PCA demonstrated that P1 samples followed the same pattern of variability as P3 samples and that P1 samples were not substantial outliers (Figure 3.21E). As such, despite the experiment being limited by a lack of vaccine-antigen specific sample comparisons, several genes were identified as antigen-specificity-agnostic differentiators of early TRM-like cells and memory time point, *bona fide* TRM.

Memory cell fate could be decided at as early a stage as the first cell division of proliferation (420). Comparing CD69+ early timepoint OVA-specific, Ad-OVA vaccinated group samples to Ad-TIP vaccinated group samples may allow identification of genes involved in target-antigen-specific T cell activation. Focussing on the most variable genes between day 1 OVA-pentamer+ CD69+ samples: 19 genes had increased expression in OVA-vaccinated samples and not TIP-vaccinated samples (Figure 3.22A, highlighted box). Of these 19 genes, eleven were significantly upregulated in OVA-vaccinated samples. The 11 genes included *Il2ra*, *Rgs16, Zbtb32* and TNF receptor superfamily stimulatory molecule genes (including *Tnfrsf9*) (Figure 3.22B & C). The same comparison in CD69- (i.e. CD69- early timepoint OVA-specific, Ad-OVA vaccinated group samples

compared to Ad-TIP vaccinated group) samples resulted in a uniform distribution of p values suggesting that most comparisons end up with insufficient evidence to reject the null hypothesis (data not shown). Less than ten genes were differentially expressed ($|Log_2(FC)|>2$, FDR<0.01) and none of these were the 11 genes discussed above (data not shown). A similar picture was seen in the CD69+ non-OVA-specific comparison (data not shown). These results suggested the 11 genes that were identified represented biomarkers of early CD69+ IV Ad transgene-specific AgSp T cell activation.

This RNA-seq experiment suggested that antigen specificity was the main driver of heterogeneity amongst the samples but also that there was sub-structure according to the time point sampled. TRM could be identified transcriptionally at day 28 and differentiated from tissue-residing TEM. The universal transcriptional program of tissue residency described by Mackay *et al.* was unable to differentiate TRM from early time point CD69+ TRM-like cells. Lastly, transcriptomic analyses allowed the identification of a panel of Ad transgene-specific TRM-like cell genes.

3.3 Figures

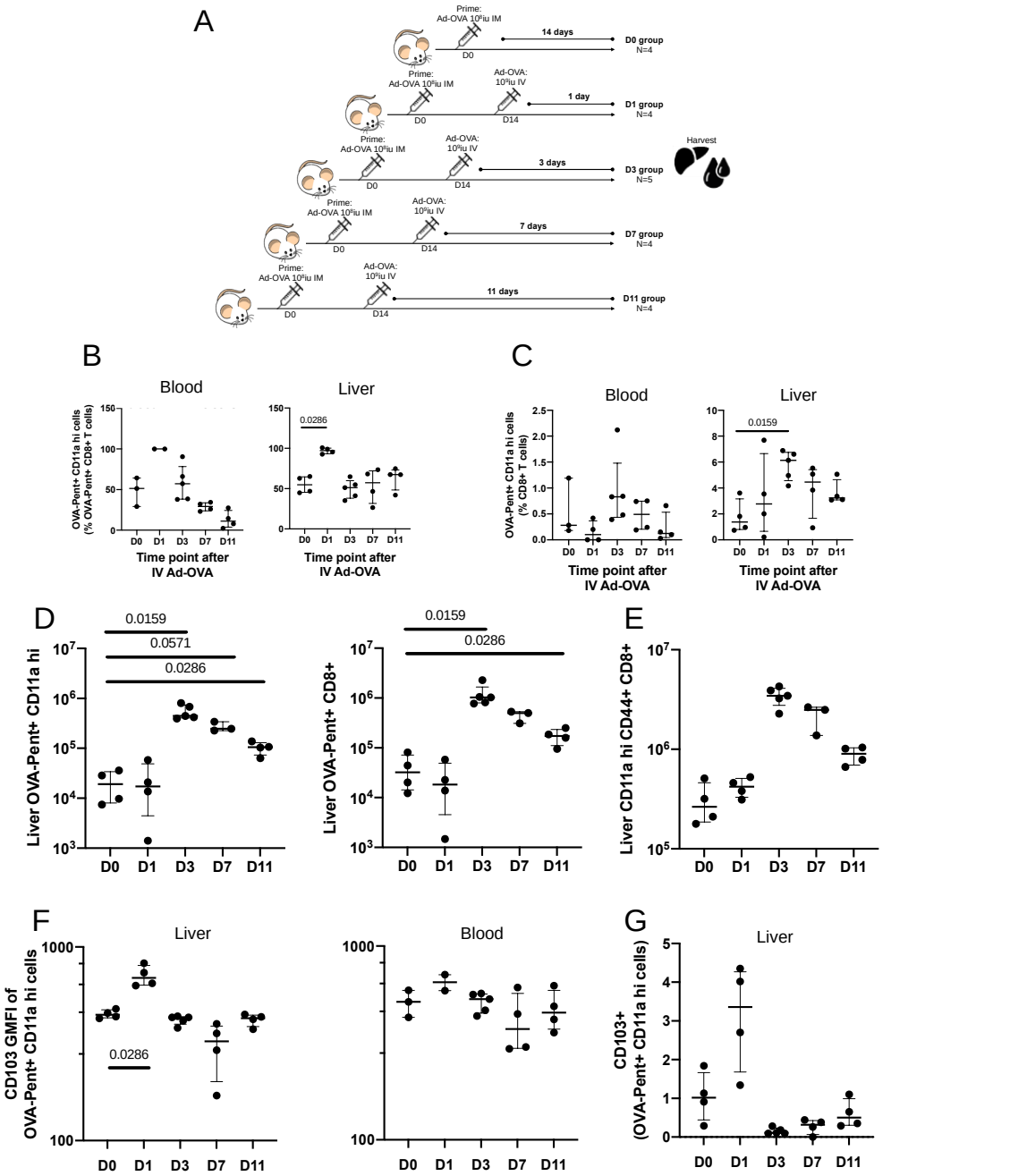


*Figure 3.1: Eleven-day time course experiment. **A**: Time course experimental design. All groups received IM Ad-OVA. Fourteen days later, four groups received IV Ad-OVA and these four groups were profiled for the AgSp cell response between one and eleven days after IV Ad-OVA. There were between four and five mice in each group. At the indicated time point liver and blood were harvested and analysed. **B & C**: AgSp responses in the blood and liver. **B**: The AgSp CD11a hi frequency of total AgSp CD8+ cells was examined in both blood and liver. OVA antigen specificity of T cells was identified using an SIINFEKL-H-2K^b-pentamer conjugated to phycoerythrin ("OVA-pentamer"). **C**: The AgSp CD11a hi frequency of total (OVA-specific and non-OVA-specific) CD8+ cells was examined in the blood and liver. **D**: Liver AgSp T cells. Liver AgSp TRM (OVA-pentamer+ CD11a hi CD44+ CD8+ T cells) and liver AgSp CD8+ T cell numbers. Each liver is resuspended in 0.5mL of media, as a single-cell suspension. OVA antigen specificity of T cells was identified using the OVA-pentamer. **E**: Total liver TRM. Liver TRM were identified as CD11a hi CD44+ CD8+ T cells. These are presented for illustrative purposes, and differences between groups were not tested. **F & G**: CD103 expression. Liver and blood AgSp TRM and TRM-like cell CD103 GMFI (**F**), and CD103+ frequency of liver TRM (**G**). Median values are presented by the line, and error bars represent the interquartile range. Significance testing of differences between individual groups was performed using the two-tailed MW test and the resultant exact p values of all tested comparisons are shown (unless specifically mentioned).*

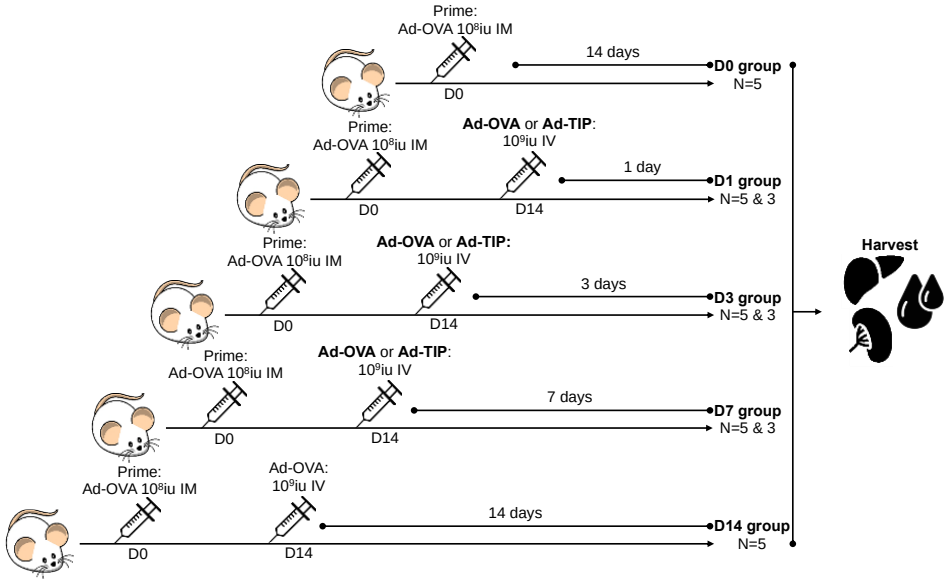


Figure 3.2: Fourteen-day time course experiment. Time course experimental design. All groups received IM Ad-OVA. Fourteen days later, four groups received IV Ad-OVA, another three groups received IV Ad-TIP and all groups were profiled for the AgSp cell response between one and fourteen days after IV boost. There were between five mice in each Ad-OVA group and three mice in each Ad-TIP groups. At the indicated time point liver, spleen and blood were harvested and analysed.

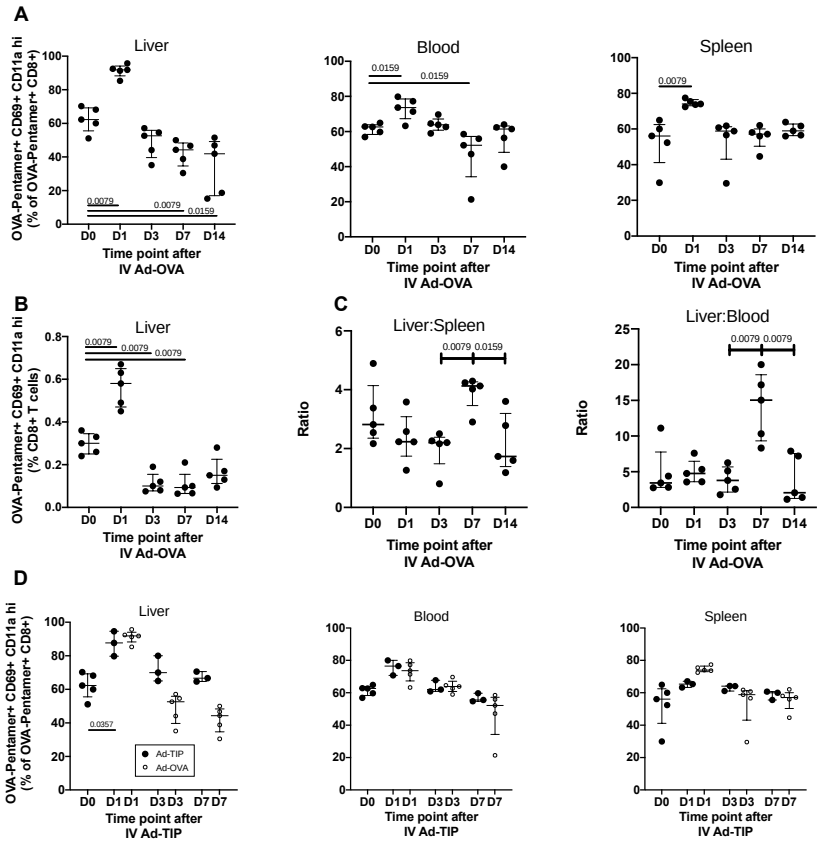
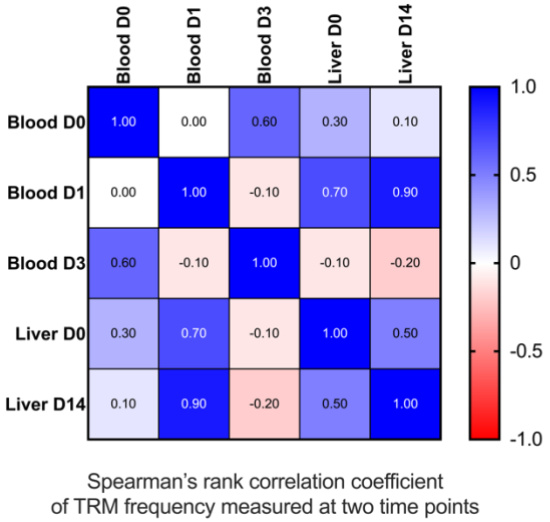


*Figure 3.3: AgSp CD8+ T cell responses following IV Ad-OVA. Experimental design as in Figure 3.2. Ad-OVA results from 5 mice per group all sacrificed on the same day. Ad-TIP results from 3 mice per group. **A**: AgSp TRM and TRM-like cells. OVA-Pentamer+ CD69+ CD11a hi CD44+ CD8+ CD4- CD3+ live single lymphocytes as frequencies of total OVA-Pentamer+ CD8+ T cells in the liver (left), blood (middle) and spleen (right). OVA antigen specificity of T cells was identified using an OVA-pentamer. **B**: Liver AgSp TRM. Liver OVA-Pentamer+ TRM frequency of total CD8+ cells. **C**: The fold difference of TRM between organs. Liver-to-spleen (left) and liver-to-blood (right) within-mouse ratios of OVA-Pentamer+ CD69+ CD11a hi CD44+ CD8+ frequencies of total CD8+ T cells. None of the ratios was less than one. **D**: OVA-Pentamer+ CD69+ CD11a hi CD44+ CD8+ as frequencies of total OVA-Pentamer+ CD8+ T cells in the liver (left), blood (middle) and spleen (right), following Ad-TIP vaccination. The same populations from Ad-OVA vaccinated mice are presented alongside (in open*

circles) for reference (as in A). Median values are presented by the line, and error bars represent the interquartile range. Significance testing of differences between individual groups was performed using the two-tailed MW test and the resultant exact p values of all tested comparisons are shown (unless specifically mentioned).



Exact p values

	Blood D0	Blood D1	Blood D3	Liver D0	Liver D14
Blood D0		1.000	0.350	0.683	0.950
Blood D1	1.000		0.950	0.233	0.083
Blood D3	0.350	0.950		0.950	0.783
Liver D0	0.683	0.233	0.950		0.450
Liver D14	0.950	0.083	0.783	0.450	

Figure 3.4: Liver TRM and blood TRM-like cell correlations. Correlation matrix of blood TRM-like cells and liver TRM at various early time points following IV Ad-OVA. Spearman's rank correlations were assessed between OVA-Pentamer+ CD69+ CD11a hi CD44+ CD8+ as frequencies of total OVA-Pentamer+ CD8+ T cells in the liver and blood. Exact p values for each association are presented to the right. No adjustment for multiple comparisons was made.

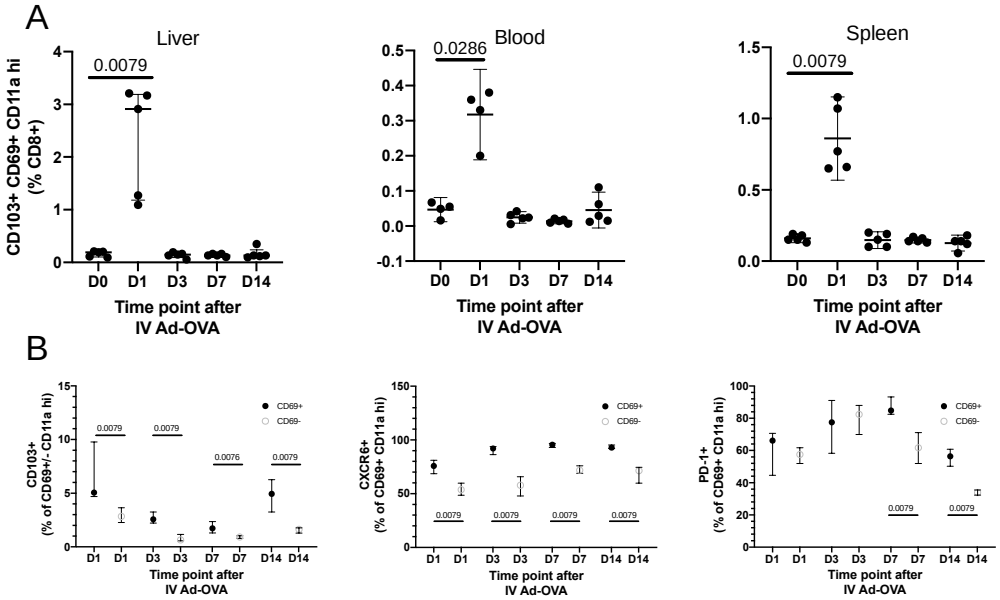
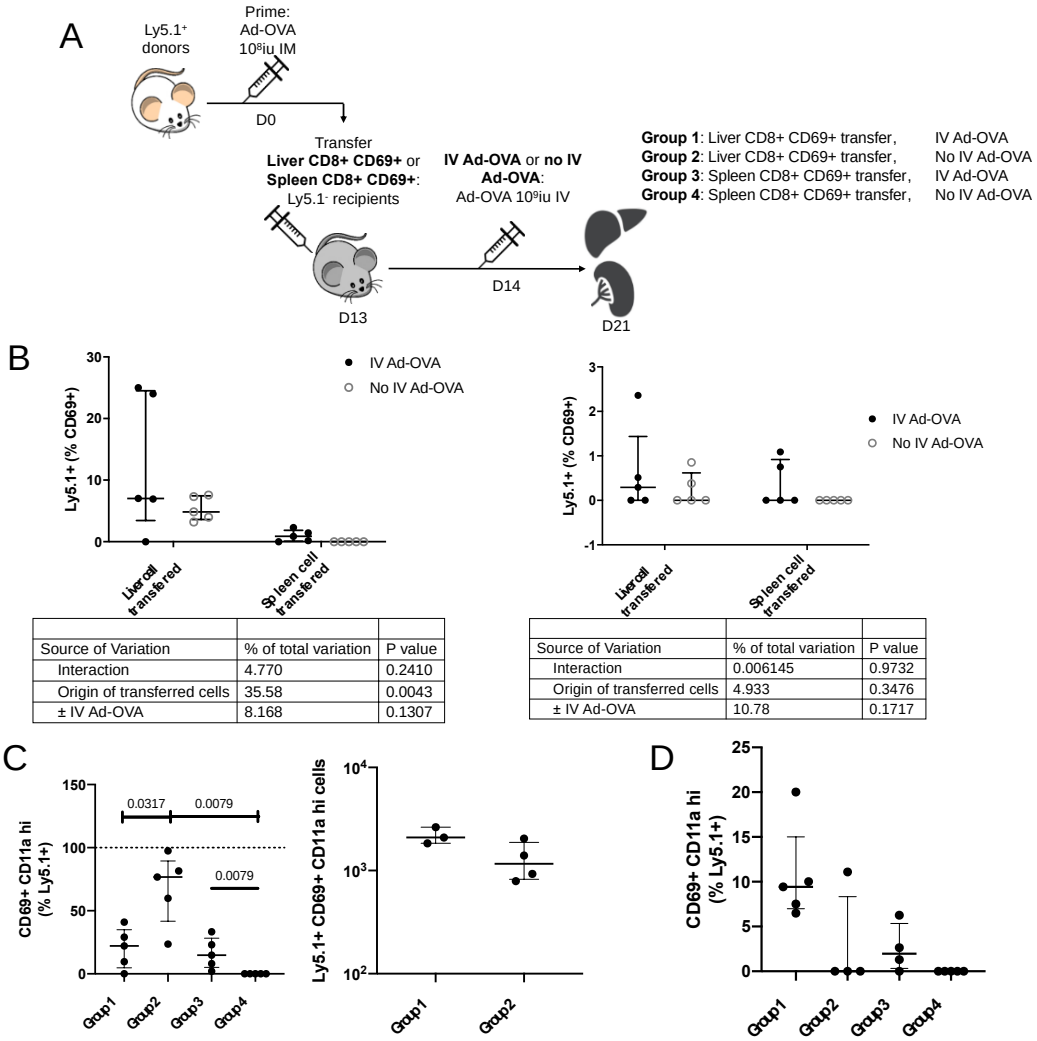


*Figure 3.5: TRM and TRM-like cell phenotyping. All groups received IM Ad-OVA. Fourteen days later, four groups received IV Ad-OVA and all groups were profiled for the AgSp cell response between one and fourteen days after IV boost. Results from 5 mice per group all sacrificed on the same day. Data are from AgSp and non-AgSp T cells. **A**: CD103+ CD69+ CD11a hi CD44+ CD8+ as frequencies of total CD8+ T cells in the liver (left), blood (middle) and spleen (right). **B**: Frequency of CD103, CXCR6 and PD-1 positive cells of liver TRM. Median values are presented by the line, and error bars represent the interquartile range. Significance testing of differences between individual groups was performed using the two-tailed MW test and the resultant exact p values of all tested comparisons are shown (unless specifically mentioned).*



Source of Variation	% of total variation	P value
Interaction	4.770	0.2410
Origin of transferred cells	35.58	0.0043
± IV Ad-OVA	8.168	0.1307

Source of Variation	% of total variation	P value
Interaction	0.006145	0.9732
Origin of transferred cells	4.933	0.3476
± IV Ad-OVA	10.78	0.1717

*Figure 3.6: Transfer of liver and spleen CD69+ cells. **A**: Experimental design. Ten Ly5.1+ donor mice received IM Ad-OVA. Fourteen days later, liver and spleen CD69+ CD8+ T cells were isolated and transferred to naïve Ly5.1- mice. Mice in groups 1 & 2 received 2.4x10^5 liver CD8+ CD69+ cells and groups 3 & 4 received 1.26x10^5 spleen CD8+ CD69+ cells each. Half of the mice received IV Ad-OVA one day after adoptive transfer. There were five mice in each group. At the indicated time point liver and spleen were harvested and analysed. **B**: Liver and spleen transferred cells. Ly5.1+ cells as frequencies of CD69+ CD44+ CD8+ T cells in the liver (left) and spleen (right). Results from two-way ANOVAs are presented. **C**: Liver TRM from transferred cells. Liver CD69+ CD11a hi CD44+ frequency of total Ly5.1+ CD8+ T cells (left) and total number of liver Ly5.1+ CD69+ CD11a hi CD44+ CD8+ T cells (right). **D**: Spleen TRM from transferred cells. Spleen CD69+ CD11a hi CD44+ frequency of total Ly5.1+ CD8+ T cells. Median values are presented by the line, and error bars represent the interquartile range. Significance testing of differences between individual groups was performed using the two-tailed MW test and the resultant exact p values of all tested comparisons are shown (unless specifically mentioned).*

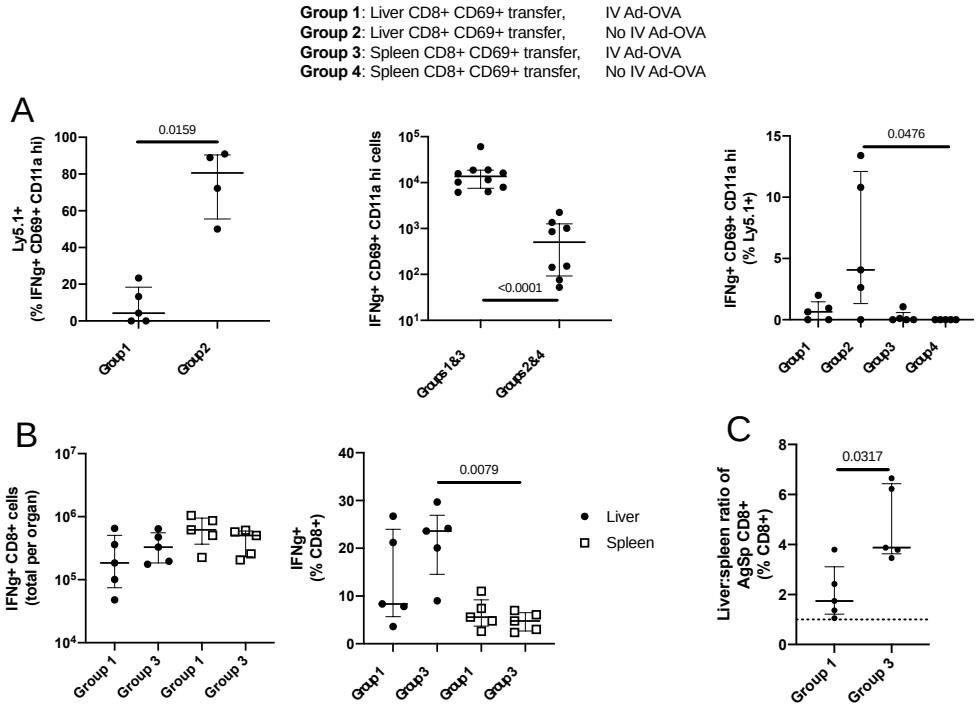


*Figure 3.7: AgSp cells following cell transfer from the spleen or liver. Experimental design as in Figure 3.6. Groups are summarised at the top of the figure. Antigen specificity was defined by intracellular production of IFNg following ex-vivo restimulation, following background subtraction of the response in unstimulated wells (media) from stimulated samples (SIINFEKL peptide) ("IFNg method"). **A**: Liver AgSp TRM. All graphs show the liver. Ly5.1+ The frequency of Ly5.1+ cells within the IFNg+ CD69+ CD11a hi CD8+ T cells (left), total number of liver IFNg+ CD69+ CD11a hi CD44+ CD8+ T cells (middle) and frequency of IFNg+ CD69+ CD11a hi of Ly5.1+ CD8+ T cells (right). **B**: Liver and spleen AgSp CD8+. Total IFNg+ CD8+ T cells per organ (left) and the IFNg+ frequency of total CD8+ T cells (right). Closed circles show values from the liver and open squares, from the spleen. For clarity, animals that did not receive Ad-OVA after transfer are not shown here. **C**: The ratio of AgSp CD8+ between liver and spleen. Within each animal, the frequency of IFNg+ CD8+ cells in the liver divided by the frequency of IFNg+ CD8+ T cells in the spleen. None of the ratios were less than one. The dotted line is at y=1. Median values are presented by the line, and error bars represent the interquartile range. Significance testing of differences between individual groups was performed using the two-tailed MW test and the resultant exact p values of all tested comparisons are shown (unless specifically mentioned).*

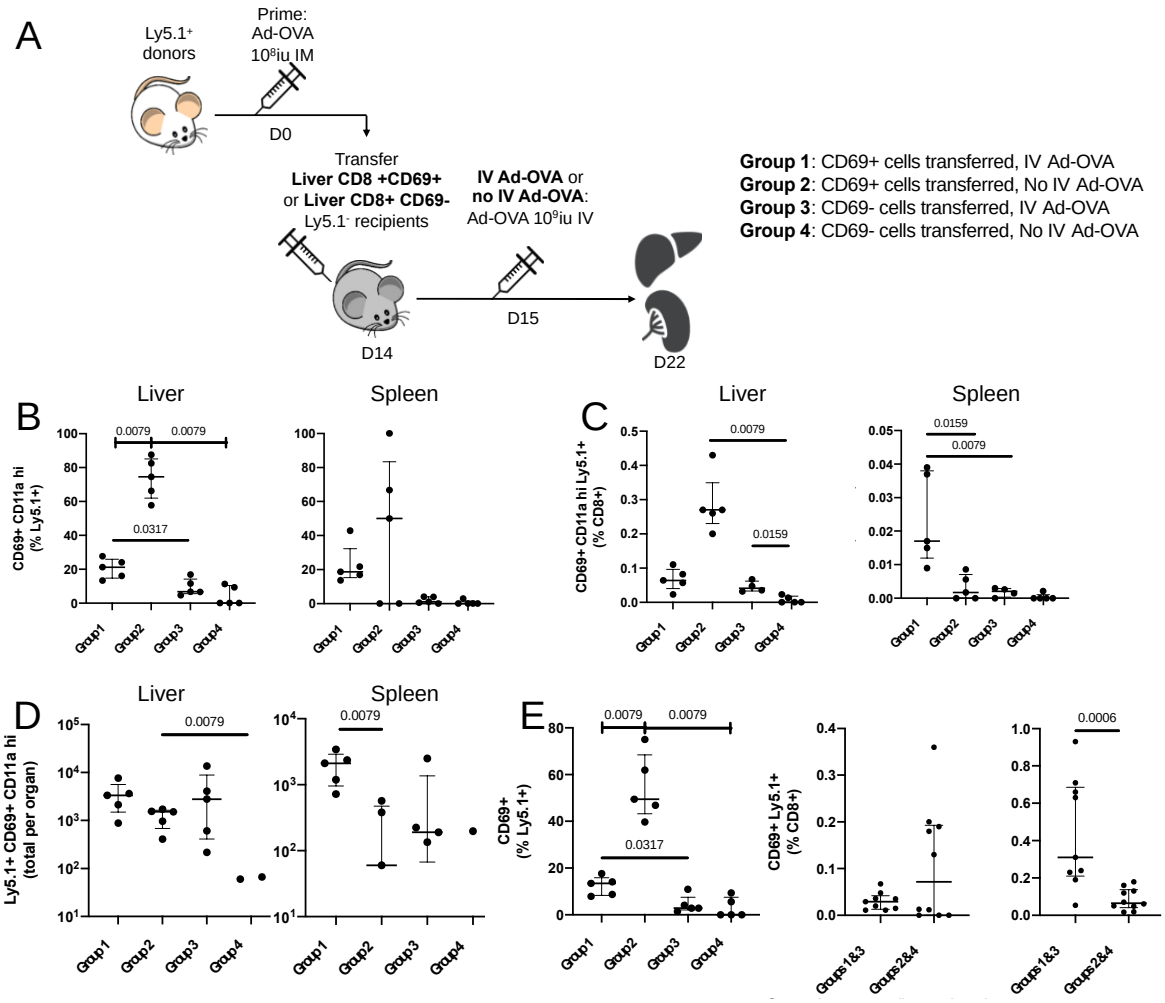


*Figure 3.8: Transfer of liver CD69+ and CD69- cells. **A**: Experimental design. Ten Ly5.1+ donor mice received IM Ad-OVA. Fourteen days later, liver CD69+ and CD69- CD8+ T cells were isolated and transferred to naïve Ly5.1- mice. Mice in groups 1 & 2 received 1.1x10^5 liver CD8+ CD69+ cells and groups 3 & 4 received 1.395x10^6 liver CD8+ CD69- cells, each. Half of the mice received IV Ad-OVA one day after adoptive transfer. There were five mice in each group. At the indicated time point liver and spleen were harvested and analysed. **B**: Transferred TRM. CD69+ CD11a hi CD44+ CD8+ as frequencies of total Ly5.1+ CD8+ T cells in the liver (left) and spleen (right). **C**: Transferred TRM as the frequency of total CD8+. Ly5.1+ CD69+ CD11a hi CD44+ CD8+ as frequencies of total CD8+ T cells. **D**: Transferred TRM numbers. Ly5.1+ CD69+ CD11a hi CD44+ CD8+ as total number of cells per organ. **E**: Liver CD69+ and CD69- transferred T cells. Liver CD69+ frequency of Ly5.1+ cells (left), liver CD69+ Ly5.1+ frequency of total CD8+ grouped by IV Ad-OVA vs no IV Ad-OVA (middle) and liver CD69– Ly5.1+ frequency of total CD8+ grouped by IV Ad-OVA vs no IV Ad-OVA (right). Median values are presented by the line, and error bars represent the interquartile range. Significance testing of differences between individual groups was performed using the two-tailed MW test and the resultant exact p values of all tested comparisons are shown (unless specifically mentioned).*

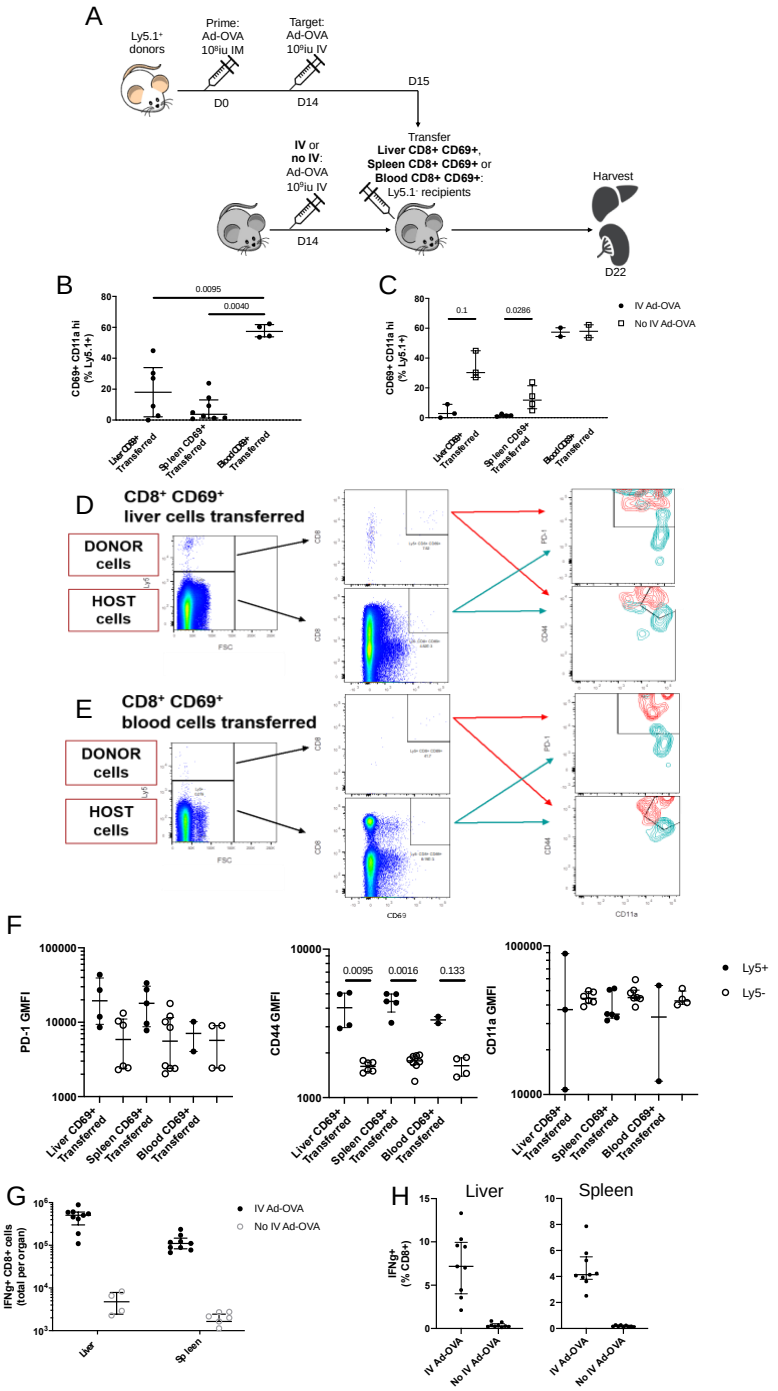


Figure 3.9: Transferring liver, spleen and blood cells after IV Ad-OVA. ***A****: Experimental design. Ten Ly5.1+ donor mice received IM Ad-OVA. Fourteen days later, these ten mice received IV Ad-OVA. Separately, 9 out of 18 naïve Ly5.1- recipient mice received IV Ad-OVA. Liver, spleen and blood CD69+ cells from the 10 Ly5.1+ mice were transferred into the Ly5.1- vaccinated and naïve recipients; there were six, eight and four mice per group, respectively. These groups received 5x10^5 liver, 3.63x10^5 spleen and 3.25x10^3 blood CD69+ CD8+ cells, each. Half of each group received IV Ad-OVA, one day prior to cell transfer. Seven days after transfer, the liver and spleen were harvested and analysed.* ***B****: Liver TRM from transferred cells. CD69+ CD11a hi CD44+ frequency of Ly5.1+ CD8+ T cells.* ***C****: Liver TRM from transferred cells by IV Ad-OVA. CD69+ CD11a hi CD44+ frequency of Ly5.1+ CD8+ T cells. B & C show the same data, but C is split by IV Ad-OVA.* ***D & E****: Donor and host cell phenotype comparison, by the origin of transferred cells. The left-most panes show the dichotomies of donor (Ly5.1+) and host (Ly5.1-) T cells. The middle panel identifies CD8+CD69+ cells. The right panel compares the expression of PD-1 (top y-axes), CD44 (bottom y-axes) and CD11a (x-axis). Gates on the plot indicate what would constitute a 'marker positive' population. Red contour plots represent donor-derived cells and blue contour plots represent host-derived cells.* ***D****: Stratification for a sample where liver CD8+CD69+ cells were transferred.* ***E****: Stratification for a sample where blood CD8+CD69+ cells were transferred. Plots are representative of samples.* ***F****: Liver donor and host-derived TRM phenotyping. GMFI of liver Ly5.1+ and Ly5.1- cells stratified by the origin of cells for PD-1 (left), CD44 (middle) and CD11a (right).* ***G****: Liver and spleen AgSp CD8+ T cells. Total organ IFNg+ CD8+ T cells in the liver and spleen, by IV Ad-OVA administration.*

*Closed black circles represent IV Ad-OVA mice; open grey circles represent naïve mice. **H**: Liver and spleen AgSp CD8+ T cell frequencies. Liver (left) and spleen (right) IFNg+ frequency of CD8+ T cells, by IV Ad-OVA administration. Median values are presented by the line, and error bars represent the interquartile range. Significance testing of differences between individual groups was performed using the two-tailed MW test and the resultant exact p values of all tested comparisons are shown (unless specifically mentioned).*

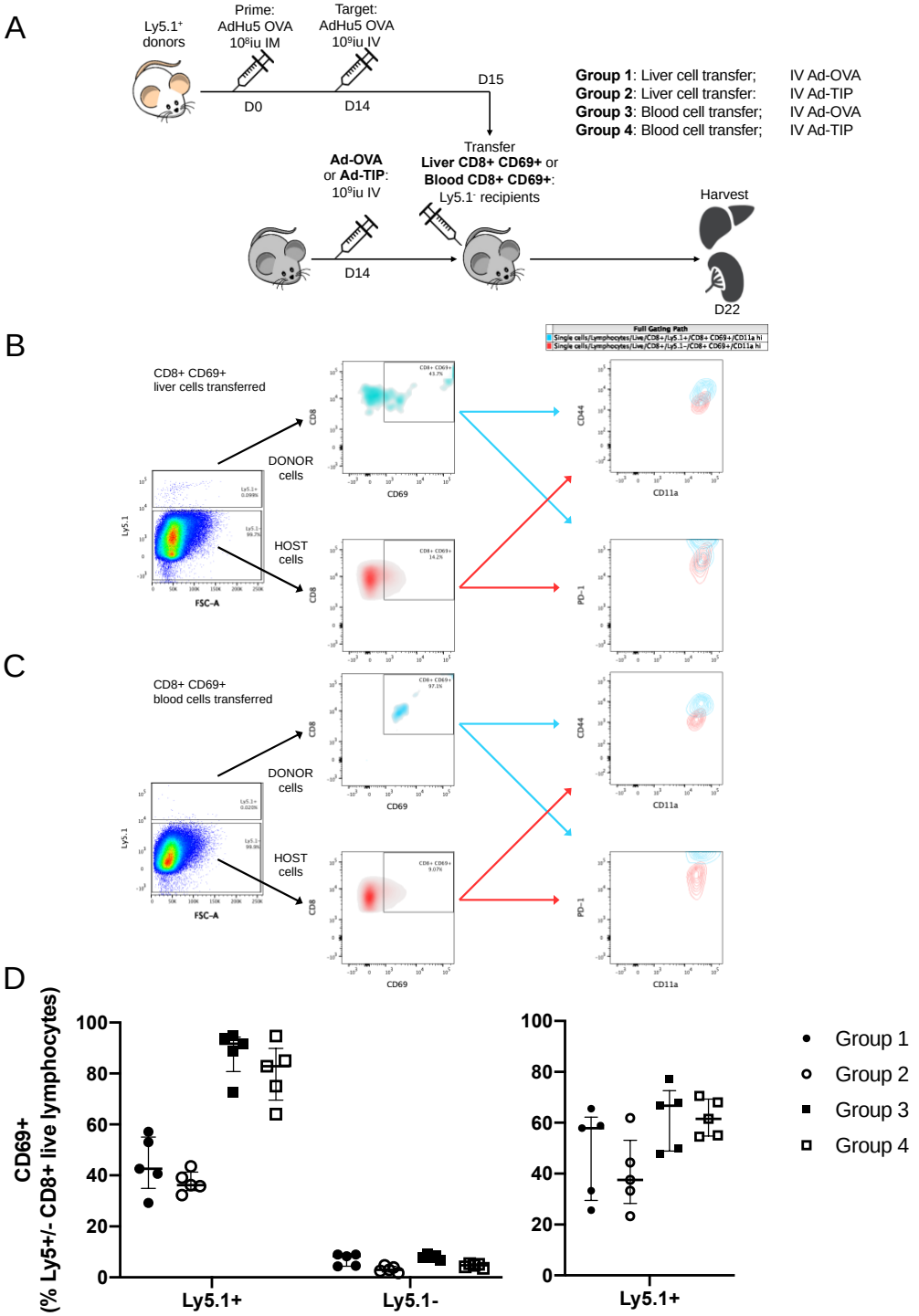
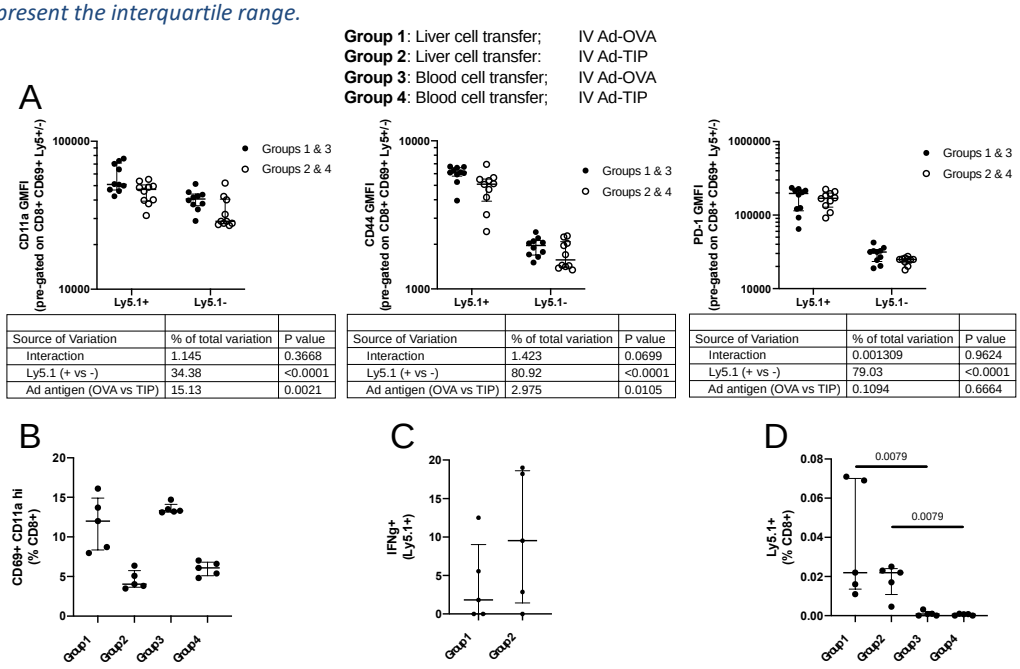


*Figure 3.10: Transfer of prime-target liver and blood CD69+ CD8+ T cells after IV Ad-OVA or Ad-TIP. **A**: Experimental design. Ten Ly5.1+ donor mice received IM Ad-OVA. Fourteen days later, these ten mice received IV Ad-OVA. Separately, ten mice received IV Ad-OVA and another ten received IV Ad-TIP (in this context, an irrelevant antigen). Liver and blood CD8+ CD69+ cells from the 10 Ly5.1+ mice were transferred into the Ly5.1- recipients. Mice in groups 1 & 2 received $5.5x10^5$ liver Ly5.1+ CD8+ CD69+ cells and groups 3 & 4 received $2x10^4$ blood Ly5.1+ CD8+ CD69+ cells each. There were five mice per group. Seven days after transfer, the liver and spleen were harvested and analysed. Groups are summarised to the right. **B & C**: Donor and host cell phenotype comparison in the liver, by the origin of transferred cells. The left-most panes show the dichotomies of donor (Ly5.1+) and host (Ly5.1-) T cells. The middle panel identifies CD8+CD69+ cells. The right panel compares the expression of CD44 (top y-axes), PD-1 (bottom y-axes) and CD11a (x-axis). Blue contour plots represent*

*donor-derived cells and red contour plots represent host-derived cells. **B**: Stratification for a sample where liver CD8+CD69+ cells were transferred. **C**: Stratification for a sample where blood CD8+CD69+ cells were transferred. Plots are representative of samples. **D**: Liver and spleen CD69+ frequency of donor- and host-derived cells. The left plot shows liver CD69+ frequency of Ly5.1+ (donor) and Ly5.1- (host) CD8+ T cells, by groups. Results of two-way ANOVA are presented in-text. Right plot shows spleen CD69+ frequency of Ly5.1+ (donor) CD8+ T cells. Spleen CD69+ frequencies of Ly5.1- (host) CD8+ T cells were all less than 0.5% and are not shown here. Median values are presented by the line, and error bars represent the interquartile range.*



Source of Variation	% of total variation	P value
Interaction	1.145	0.3668
Ly5.1 (+ vs -)	34.38	<0.0001
Ad antigen (OVA vs TIP)	15.13	0.0021

Source of Variation	% of total variation	P value
Interaction	1.423	0.0699
Ly5.1 (+ vs -)	80.92	<0.0001
Ad antigen (OVA vs TIP)	2.975	0.0105

Source of Variation	% of total variation	P value
Interaction	0.001309	0.9624
Ly5.1 (+ vs -)	79.03	<0.0001
Ad antigen (OVA vs TIP)	0.1094	0.6664

*Figure 3.11: Transfer of prime-target liver and blood CD69+ CD8+ T cells after IV Ad-OVA or Ad-TIP. Experimental design as in Figure 3.10. Groups are summarised at the top of the figure. **A**: Liver donor and host-derived CD69+ CD8+ T cell phenotyping. GMFI of liver Ly5.1+ and Ly5.1- cells, stratified by Ad-OVA or Ad-TIP administration, for CD11a (left), CD44 (middle) and PD-1 (right). Results from a two-way ANOVA, performed on non-transformed data, are presented below each plot. **B**: Liver TRM frequencies. Liver CD69+ CD11a hi frequency of CD8+ T cells. **C**: Liver AgSp transferred cells. Liver IFNg+ frequency of Ly5.1+ CD8+ T cells. No IFNg+ cells were detectable in groups 3 & 4. **D**: Transferred CD8+ T cells in the liver. Liver Ly5.1+ frequency of CD8+ T cells. Median values are presented by the line, and error bars represent the interquartile range.*

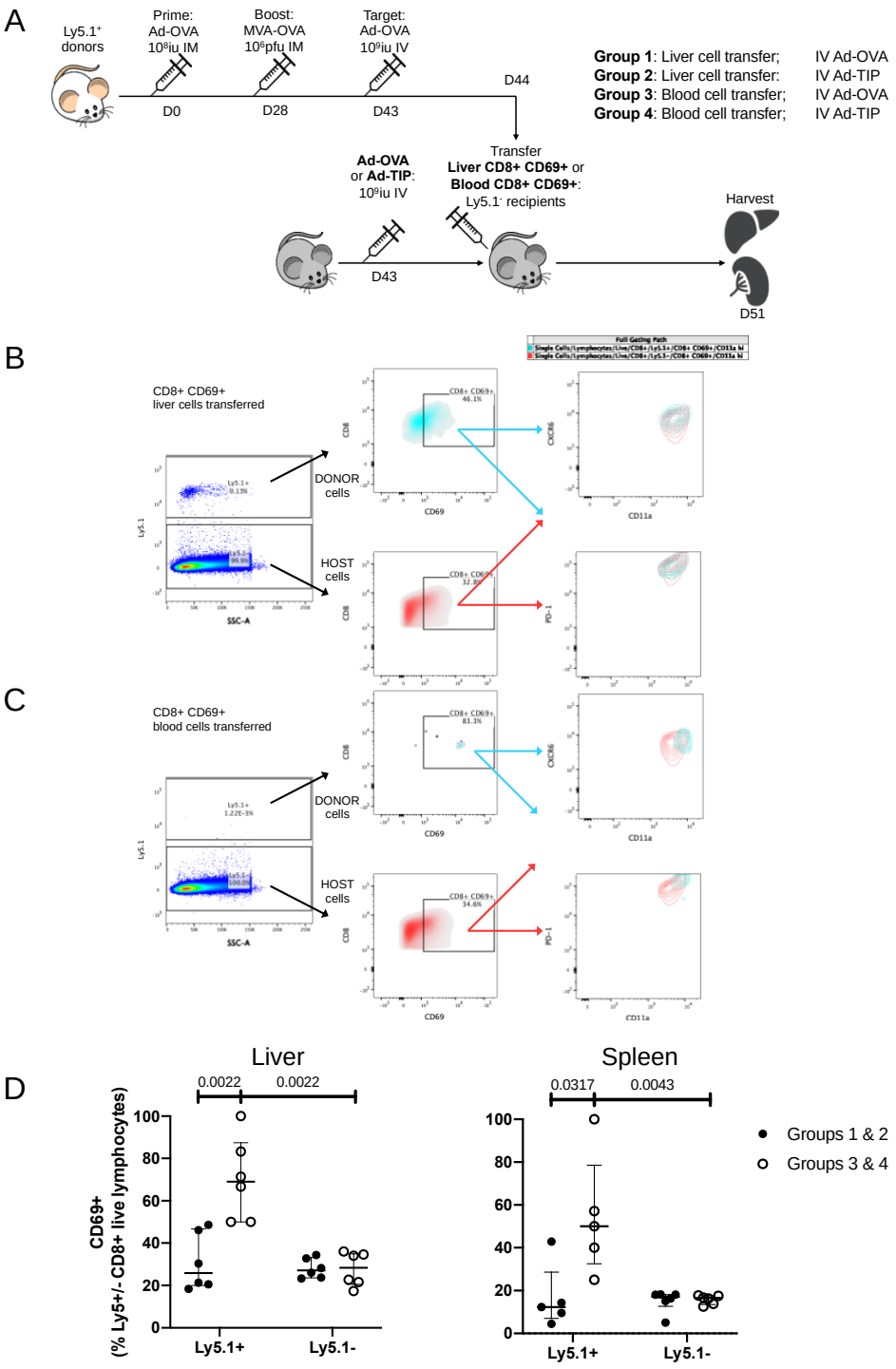


*Figure 3.12: Transfer of prime-boost-target liver and blood CD69+ CD8+ T cells, after IV Ad-OVA or Ad-TIP. **A**: Experimental design. Ten Ly5.1+ donor mice received IM Ad-OVA. Twenty-eight days later, the mice received IM MVA-OVA. Thirteen days later, the ten mice received IV Ad-OVA. Separately, six mice received IV Ad-OVA and another six received IV Ad-TIP (in this context, an irrelevant antigen). Liver and blood CD8+ CD69+ cells from the 10 Ly5.1+ mice were transferred into the Ly5.1- recipients. Mice in groups 1 & 2 received 8.5x10^5 liver Ly5.1+ CD8+ CD69+ cells and groups 3 & 4 received 1.5x10^4 blood Ly5.1+ CD8+ CD69+ cells each. There were three mice per group. Seven days after transfer, the liver and spleen were harvested and analysed. Groups are summarised to the right. **B & C**: Donor and host cell phenotype comparison in the liver, by the origin of transferred cells. The left-most panes show the dichotomies of donor (Ly5.1+) and host (Ly5.1-) T cells. The middle panel identifies CD8+CD69+ cells. The right panel compares the expression of CXCR6 (top y-axes), PD-1 (bottom y-axes) and CD11a (x-axis). Blue contour plots represent donor-derived cells and red contour plots represent host-derived cells. **B**: Stratification for a sample where liver CD8+CD69+ cells were transferred. **C**: Stratification for a sample where blood CD8+CD69+ cells were transferred. Plots are representative of samples. **D**: Liver and spleen CD69+ frequency of donor- and host-derived cells. The left plot shows liver CD69+ frequency of Ly5.1+ (donor) and Ly5.1- (host) CD8+ T cells, by the origin of transferred cells. The left plot shows spleen CD69+ frequency of Ly5.1+ (donor) and*

Ly5.1- (host) CD8+ T cells, by the origin of transferred cells. Significance testing of differences between individual groups was performed using the two-tailed MW test and the resultant exact p values of all tested comparisons are shown (unless specifically mentioned). Median values are presented by the line, and error bars represent the interquartile range.

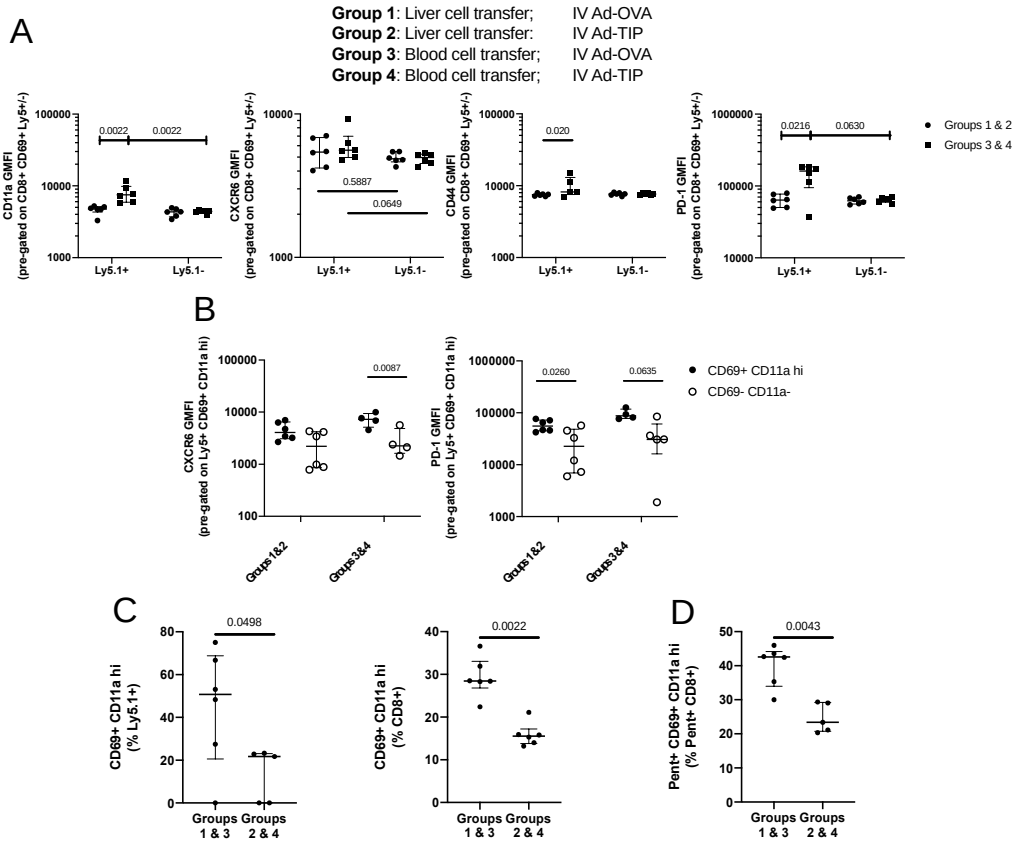


*Figure 3.13: Transfer of prime-boost-target liver and blood CD69+ CD8+ T cells, after IV Ad-OVA or Ad-TIP. Experimental design as in Figure 3.12. Groups are summarised at the top of the figure. **A**: Liver phenotype of liver and blood transferred cells. GMFI of Ly5.1+ and Ly5.1- CD69+ CD8+ T cells for CD11a (left), CXCR6 (middle left), CD44 (middle right) and PD-1 (right). Circles show values from groups 1 & 2 and squares show values from groups 3 & 4. **B**: Liver phenotype of TRM and TEM from liver and blood transferred cells. GMFI of Ly5.1+ CD69+ CD11a hi CD44+ CD8+ T cells for CXCR6 (left) and PD-1 (right). Closed circles show values for TRM and open circles show values for TEM. **C**: Liver total TRM frequencies. The liver CD69+ CD11a hi frequencies of Ly5.1+ cells (left) and of total CD8+ (right). **D**: Liver AgSp TRM frequencies. The OVA-pentamer+ CD69+ CD11a hi CD44+ frequency of total OVA-pentamer+ CD8+ T cells. Significance testing of differences between individual groups was performed using the two-tailed MW test and the resultant exact p values of all tested comparisons are shown (unless specifically mentioned). Median values are presented by the line, and error bars represent the interquartile range.*

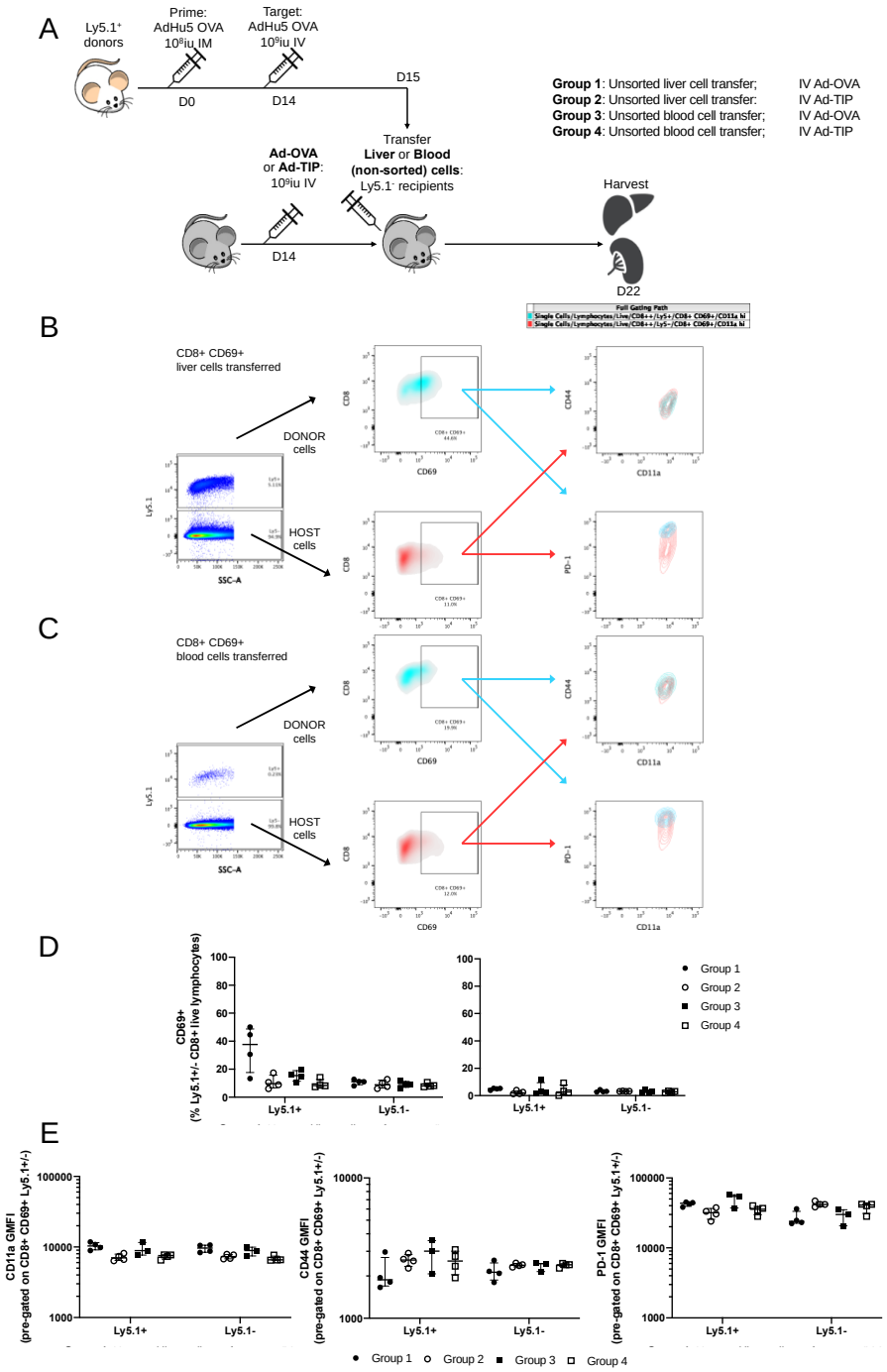


Figure 3.14: Transfer of prime-target bulk (non-sorted) liver and blood T cells, after IV Ad-OVA or Ad-TIP. ***A****: Experimental design. Ten Ly5.1+ donor mice received IM Ad-OVA. Fourteen days later, the ten mice received IV Ad-OVA. Separately, eight mice received IV Ad-OVA and another eight received IV Ad-TIP (in this context, an irrelevant antigen). Unsorted/bulk liver and blood cells from the 10 Ly5.1+ mice were transferred into the Ly5.1- recipients. Mice in groups 1 & 2 received 8.6x10⁶ unsorted liver lymphocytes and groups 3 & 4 received 1.1x10⁶ unsorted blood lymphocytes each. There were four mice per group. Seven days after transfer, the liver and spleen were harvested and analysed. Groups are summarised to the right.* ***B & C****: Donor and host cell phenotype comparison in the liver, by the origin of transferred cells. The left-most panes show the dichotomies of donor (Ly5.1+) and host (Ly5.1-) T cells. The middle panel identifies CD8+CD69+ cells. The right panel compares the expression of PD-1 (top y-axes), CD44 (bottom y-axes) and CD11a (x-axis). Blue contour plots represent donor-derived cells and red contour plots represent host-derived cells.* ***B****: Stratification for a sample where bulk liver cells were transferred.* ***C****: Stratification for a sample where bulk blood cells were transferred. Plots are representative of samples.* ***D****: Liver and spleen CD69+ frequency of donor- and host-derived cells. The left plot shows liver CD69+ frequency of Ly5.1+ (donor) and Ly5.1- (host) CD8+ T cells, by group. The left plot shows spleen CD69+ frequency of Ly5.1+ (donor) and Ly5.1- (host) CD8+ T cells, by group. Closed circles show values from group 1; open circles, group 2; closed squares, group 3; and open squares, group 4.* ***E****: Liver phenotype of liver and blood transferred cells. GMFI of Ly5.1+ and Ly5.1- CD69+ CD8+ T cells for CD11a (left), CD44 (middle) and PD-1 (right). Symbols represent groups, as in A. Significance testing*

of differences between individual groups was performed using the two-tailed MW test and the resultant exact p values of all tested comparisons are shown (unless specifically mentioned). Median values are presented by the line, and error bars represent the interquartile range.

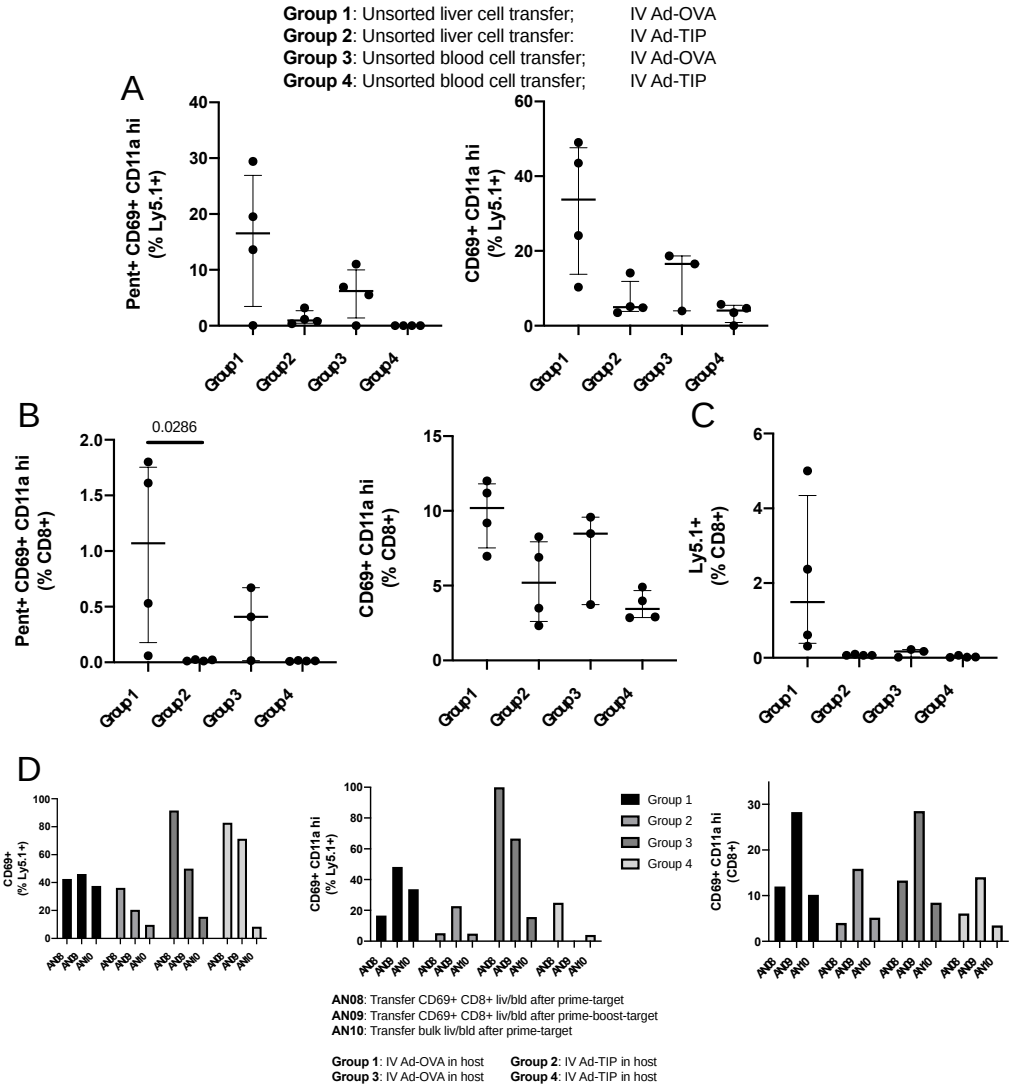


*Figure 3.15: Transfer of prime-target bulk (non-sorted) liver and blood T cells, after IV Ad-OVA or Ad-TIP. Experimental design as in Figure 3.14. Groups are summarised at the top of the figure. **A**: AgSp and total liver TRM from transferred cells. The OVA-pentamer+ CD69+ CD11a hi CD44+ frequency of Ly5.1+ CD8+ T cells (left) and the CD69+ CD11a hi CD44+ frequency of Ly5.1+ CD8+ T cells (right). **B**: AgSp and total liver TRM. The OVA-pentamer+ CD69+ CD11a hi CD44+ frequency of CD8+ T cells (left) and the CD69+ CD11a hi CD44+ frequency of CD8+ T cells (right). **C**: Transferred cells. Ly5.1+ frequency of CD8+ T cells. **D**: Cross-experiment comparisons of liver CD69+ and TRM. Comparisons of the previous three experiments: AN08, AN09 and AN10. Experiments and groups summarised at the bottom of the figure. CD69+ frequency of Ly5.1+ CD8+ T cells (left), CD69+ CD11a hi CD44+ frequency of Ly5.1+ CD8+ T cells (middle) and CD69+ CD11a hi CD44+ frequency of CD8+ T cells (right). No formal comparisons were made. Significance testing of differences between individual groups was performed using the two-tailed MW test and the resultant exact p values of all tested comparisons are shown (unless specifically mentioned). Median values are presented by the line, and error bars represent the interquartile range.*

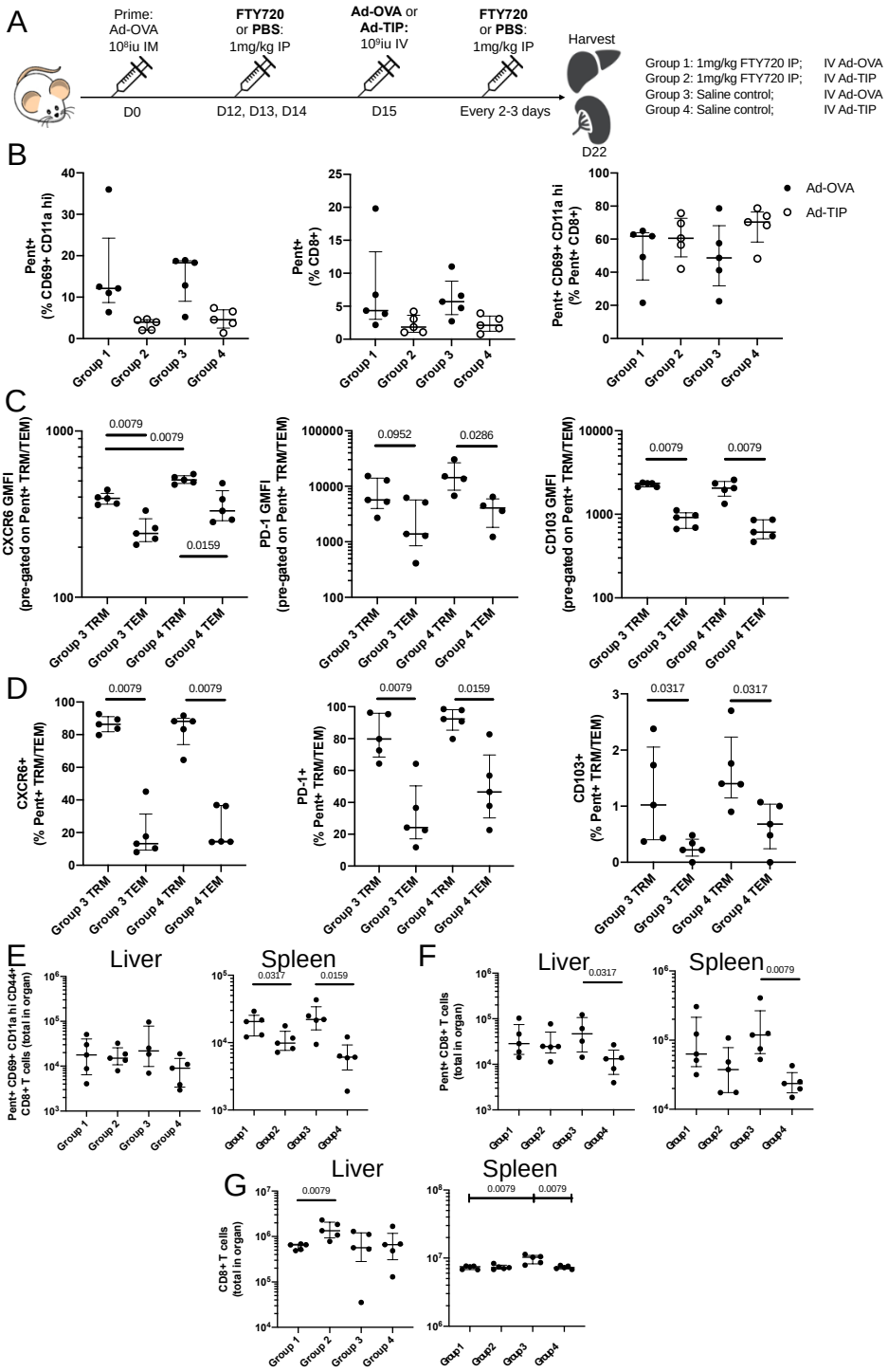


Figure 3.16: Prime-target with an Ad-OVA or Ad-TIP, and FTY720 administration. ***A****: Experimental design. Twenty mice received IM Ad-OVA. At day 12, 13 and 14, half of the mice received FTY720, and the other half received PBS (saline vehicle control). One day later, ten mice received IV Ad-OVA, and the other ten received IV Ad-TIP. There were five mice per group. Seven days after IV boost, liver and spleen were harvested and analysed. Groups are summarised to the right.* ***B****: Liver AgSp TRM and CD8+ T cells. Liver OVA-pentamer+ frequency of CD69+ CD11a hi CD44+ CD8+ T cells (left), liver OVA-pentamer+ frequency of CD8+ T cells (middle) and liver OVA-pentamer+ CD69+ CD11a hi CD44+ frequency of OVA-pentamer+ CD8+ T cells (right), all by IV Ad administration.* ***C****: Liver AgSp TRM and TEM expression of CXCR6, PD-1 and CD103. GMFI of liver AgSp TRM and TEM for CXCR6 (left), PD-1 (middle) and CD103 (right) focusing on Ad-OVA and Ad-TIP comparisons. TRM defined as CD69+ CD11a hi CD44+ CD8+ T cells and TEM defined as CD69- CD11a med/lo CD44+ CD8+ T cells.* ***D****: Liver AgSp TRM and TEM frequencies of CXCR6, PD-1 and CD103. Frequencies of liver AgSp TRM and TEM for CXCR6 (left), PD-1 (middle) and CD103 (right) focusing on Ad-OVA and Ad-TIP comparisons. For clarity, only animals that did not receive FTY720 are shown here.* ***E, F, G****: Liver and spleen AgSp TRM and CD8+, and CD8+ T cells. In each, liver values are presented on the left and spleen values are presented on the right.* ***E****: OVA-pentamer+ CD69+ CD11a hi CD44+ CD8+ T cell numbers.* ***F****: OVA-pentamer+ CD8+ T cell numbers.* ***G****: CD8+ T cell numbers. Significance testing of differences*

between individual groups was performed using the two-tailed MW test and the resultant exact p values of all tested comparisons are shown (unless specifically mentioned). Median values are presented by the line, and error bars represent the interquartile range.

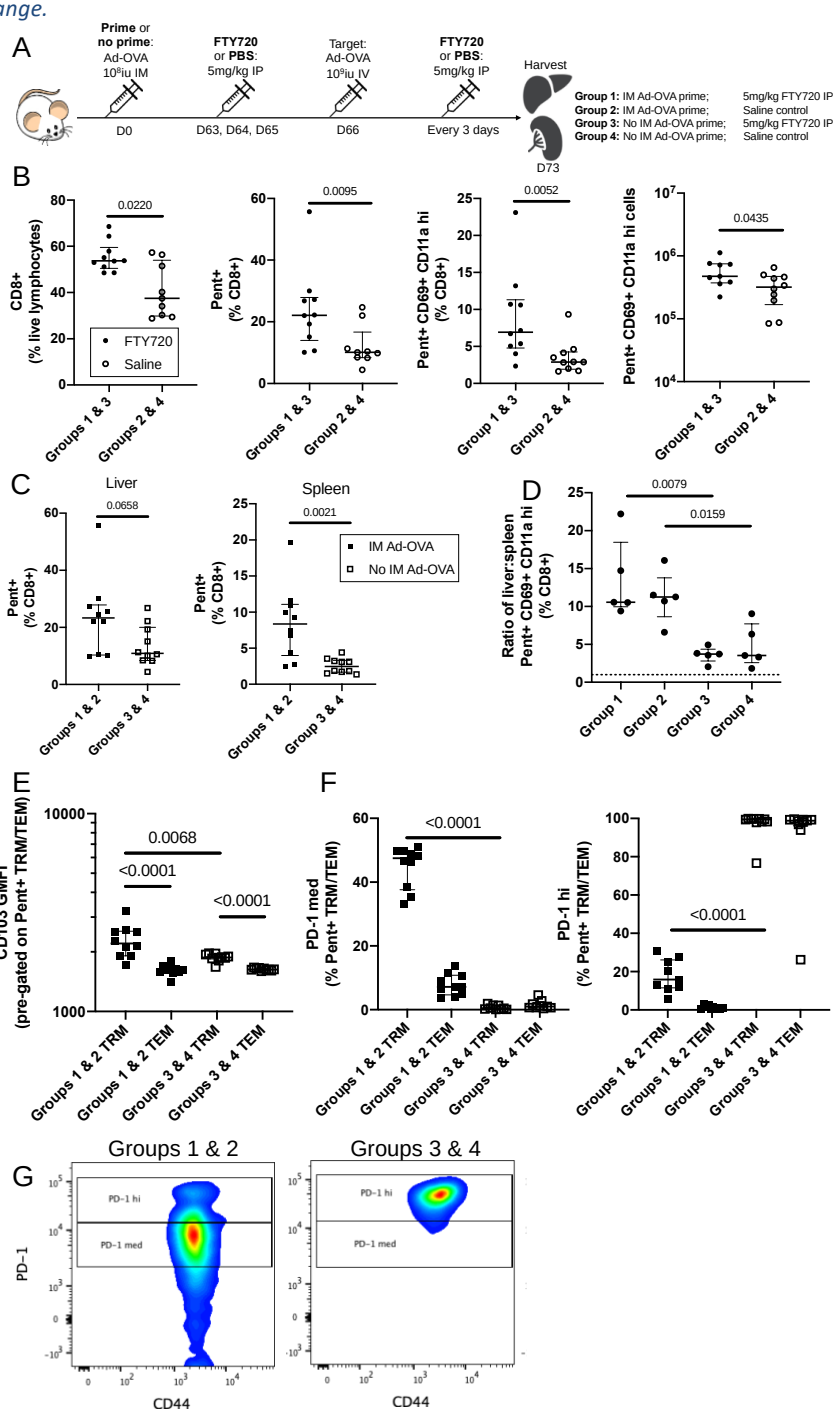
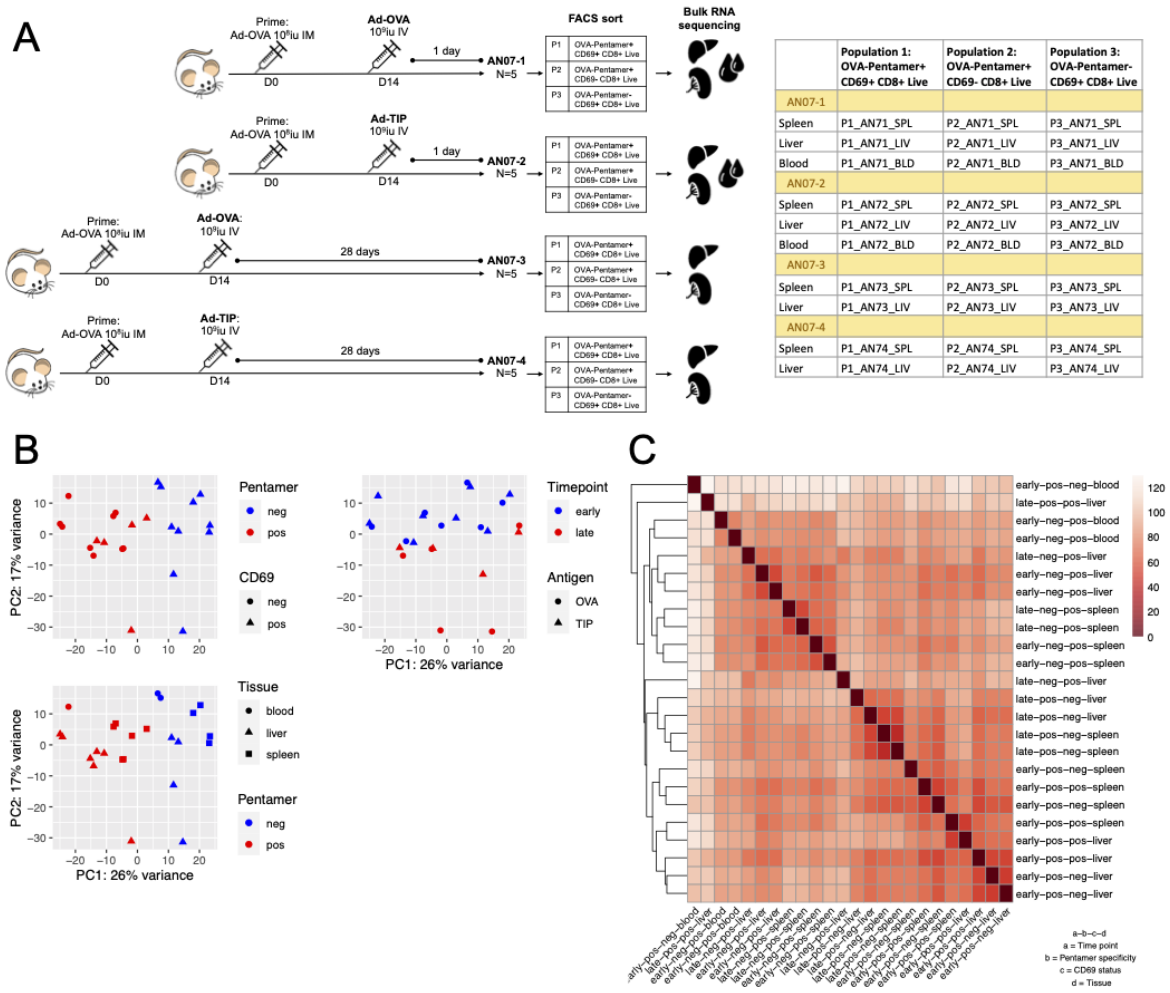


*Figure 3.17: Prime-target with and without a prime, and FTY720 administration. **A**: Experimental design. Ten mice received IM Ad-OVA. At day 63, 64 and 65, half of the mice received FTY720, and the other half received PBS (saline vehicle control). One day later, all 20 mice received IV Ad-OVA. There were five mice per group. Seven days after IV vaccination, liver and spleen were harvested and analysed. Groups are summarised to the right. **B**: Liver CD8+, AgSp CD8+ and AgSp TRM by FTY720 administration. CD8+ T cell frequencies of total lymphocytes (left), OVA-pentamer+ frequency of CD8+ T cells (middle left), OVA-pentamer+ CD69+ CD11a hi CD44+ frequency of CD8+ T cells (middle right) and total liver OVA-pentamer+ CD69+ CD11a hi CD44+ CD8+ T cell numbers; all by FTY720 administration. **C**: Liver and spleen AgSp CD8+ T cells by IM Ad-OVA administration. Liver (left) and spleen (right) OVA-pentamer+ frequency of CD8+ T cells. **D**: The ratio of AgSp TRM between liver and spleen. Liver-to-spleen within-mouse ratios of OVA-pentamer+ CD69+ CD11a hi CD44+ frequencies of total CD8+ T cells. None of the ratios were less than one. The dotted line is at y=1. **E**: CD103 expression by AgSp TRM and TEM. CD103 GMFI of OVA-pentamer+ TRM and TEM, by the administration of prime vaccination. TRM defined as CD69+ CD11a hi CD44+ CD8+ T cells and TEM defined as CD69- CD11a med/lo CD44+ CD8+ T cells. **F**: PD-1 med and hi frequencies of AgSp TRM and TEM. PD-1 med (left) and PD-1 hi (right) frequencies of OVA-pentamer TRM and TEM,*

*grouped by the administration of prime vaccination. **G**: Liver PD-1 med and hi populations groups by prime administration. Representative flow cytometry plot of PD-1 vs CD44 for OVA-pentamer+ CD69+ CD11a hi CD44+ CD8+ T cell populations. The left plot shows a liver sample representative of groups 1 & 2 and the right plot shows a liver sample representative of groups 3 & 4. Significance testing of differences between individual groups was performed using the two-tailed MW test and the resultant exact p values of all tested comparisons are shown (unless specifically mentioned). Median values are presented by the line, and error bars represent the interquartile range.*



	Population 1: OVA-Pentamer+ CD69+ CD8+ Live	Population 2: OVA-Pentamer+ CD69- CD8+ Live	Population 3: OVA-Pentamer- CD69+ CD8+ Live
AN07-1			
Spleen	P1_AN71_SPL	P2_AN71_SPL	P3_AN71_SPL
Liver	P1_AN71_LIV	P2_AN71_LIV	P3_AN71_LIV
Blood	P1_AN71_BLD	P2_AN71_BLD	P3_AN71_BLD
AN07-2			
Spleen	P1_AN72_SPL	P2_AN72_SPL	P3_AN72_SPL
Liver	P1_AN72_LIV	P2_AN72_LIV	P3_AN72_LIV
Blood	P1_AN72_BLD	P2_AN72_BLD	P3_AN72_BLD
AN07-3			
Spleen	P1_AN73_SPL	P2_AN73_SPL	P3_AN73_SPL
Liver	P1_AN73_LIV	P2_AN73_LIV	P3_AN73_LIV
AN07-4			
Spleen	P1_AN74_SPL	P2_AN74_SPL	P3_AN74_SPL
Liver	P1_AN74_LIV	P2_AN74_LIV	P3_AN74_LIV

*Figure 3.18: Transcriptomic analysis of T cells after prime-target. **A**: Experimental design. Twenty mice received IM Ad-OVA. Fourteen days later, ten mice received IV Ad-OVA, and the other ten received IV Ad-TIP. For half of the groups, liver, spleen and blood were harvested and analysed one day after IV boost. For the other half, twenty-eight days elapsed between IV boost and harvest, and liver and spleen were analysed. There were five mice per group, and these were staggered, so harvest occurred on the same day. Single-cell suspensions for each organ were pooled per group and sorted into three populations: OVA-pentamer+ CD69+ CD8+ live cells (P1), OVA-pentamer+ CD69- CD8+ live cells (P2) and OVA-pentamer- CD69+ CD8+ live cells (P3). Samples are summarised to the right. Samples were stored in RNALater stabilisation solution and stored at -20°C for ~20 days. Samples then underwent RNA extraction and were sequenced using the Smart-seq2 RNA-seq protocol. **B**: Principal component plots according to experimental variables. PCA shows 26% variance in samples accounted for by PC1 and 17% variance, by PC2. The three plots show the same data, but with different symbols and colours to illustrate the various experimental variables: OVA-pentamer + (pos) or – (neg), CD69 + (pos) or – (neg), early or late time point, antigen delivered in IV viral vector vaccine (OVA or TIP) and the tissue examined (blood, liver or spleen). **C**: Euclidean distances between samples. Distances between samples were calculated in Euclidean space and clustered according to distance similarity. Samples that are closest in Euclidean space are clustered together. Euclidean distance is represented by the dendrogram on the left of the plot: longer horizontal length corresponds to a greater Euclidean distance. Sample identity legend presented on the bottom right.*

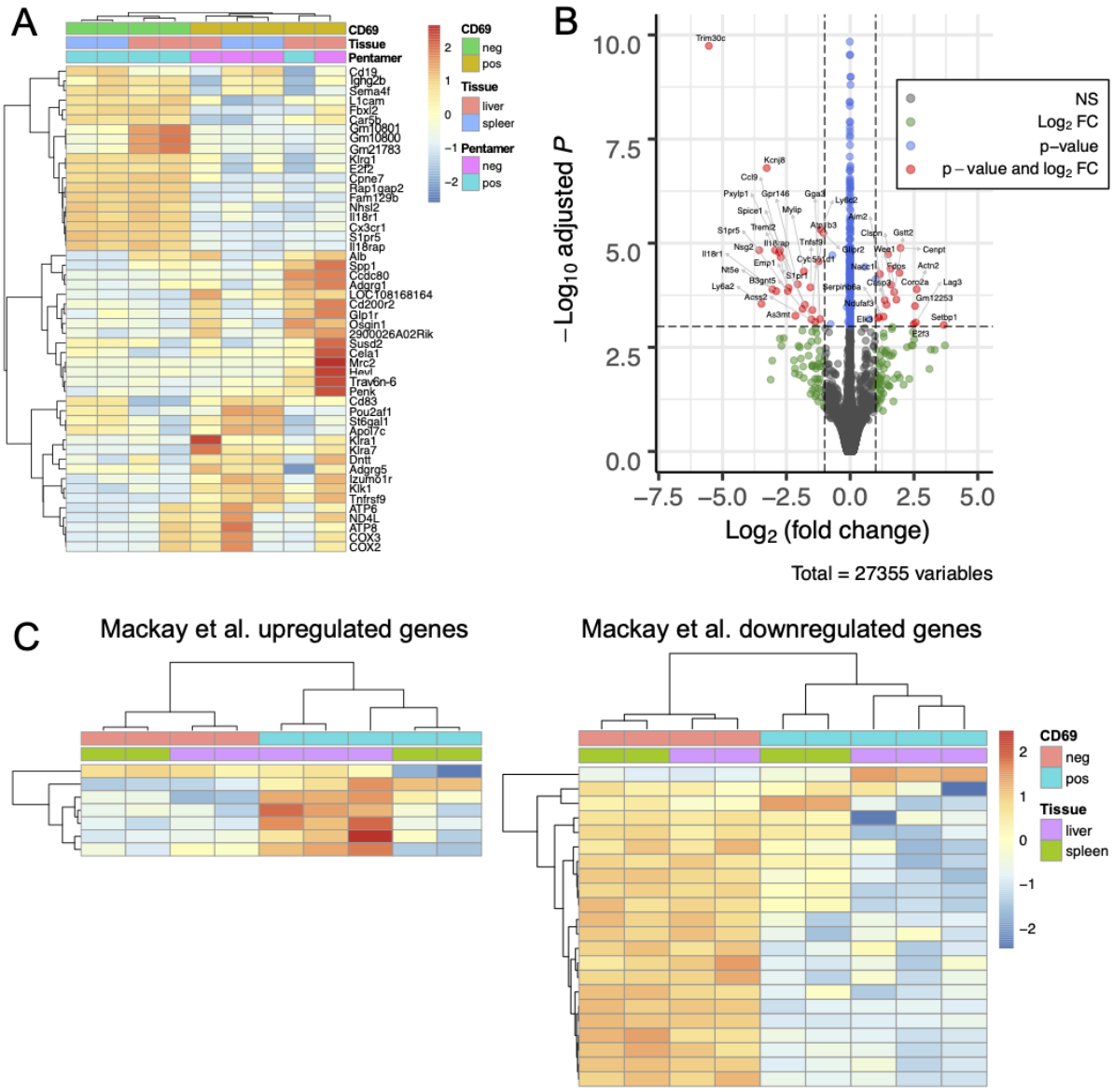


*Figure 3.19: Transcriptomic comparison of day 28 post-IV boost TRM and TEM in tissues. **A**: Heatmap of the most variable genes in day 28 post-IV boost CD69+ and CD69- samples. Fifty most variable genes in day 28 post-IV boost CD69+ and CD69- samples. Gene count values are centred and scaled across rows. Yellow/red corresponds to increased counts compared to other samples, and blue corresponds to decreased counts. Genes were selected according to those with the greatest variance across samples. Columns are clustered based on Spearman's correlation of rlog normalised count values. Rows are clustered according to Pearson correlation of the rlog normalised gene counts. **B**: Volcano plot of upregulated and downregulated genes between day 28 post-IV boost CD69+ and CD69- samples. The top 50 upregulated and downregulated genes have been annotated. Positive log2(FC) values indicate greater gene expression in CD69+ samples, compared to CD69- samples. Negative log2(FC) values indicate greater gene expression in CD69- samples. DGE of 27,355 genes was tested for significance using the Wald test. P values were adjusted using the Benjamini-Hochberg correction (FDR). **C**: Heatmap of the genes upregulated and downregulated in the Mackay et al. signature. Samples (columns) clustered according to Spearman's rank correlation of samples according to upregulated genes (left) and downregulated genes (right) in the Mackay et al. universal transcriptional program of lymphocyte tissue residency. Genes (rows) are clustered according to Pearson correlation of the rlog normalised gene counts. Gene count values are centred and scaled across rows.*

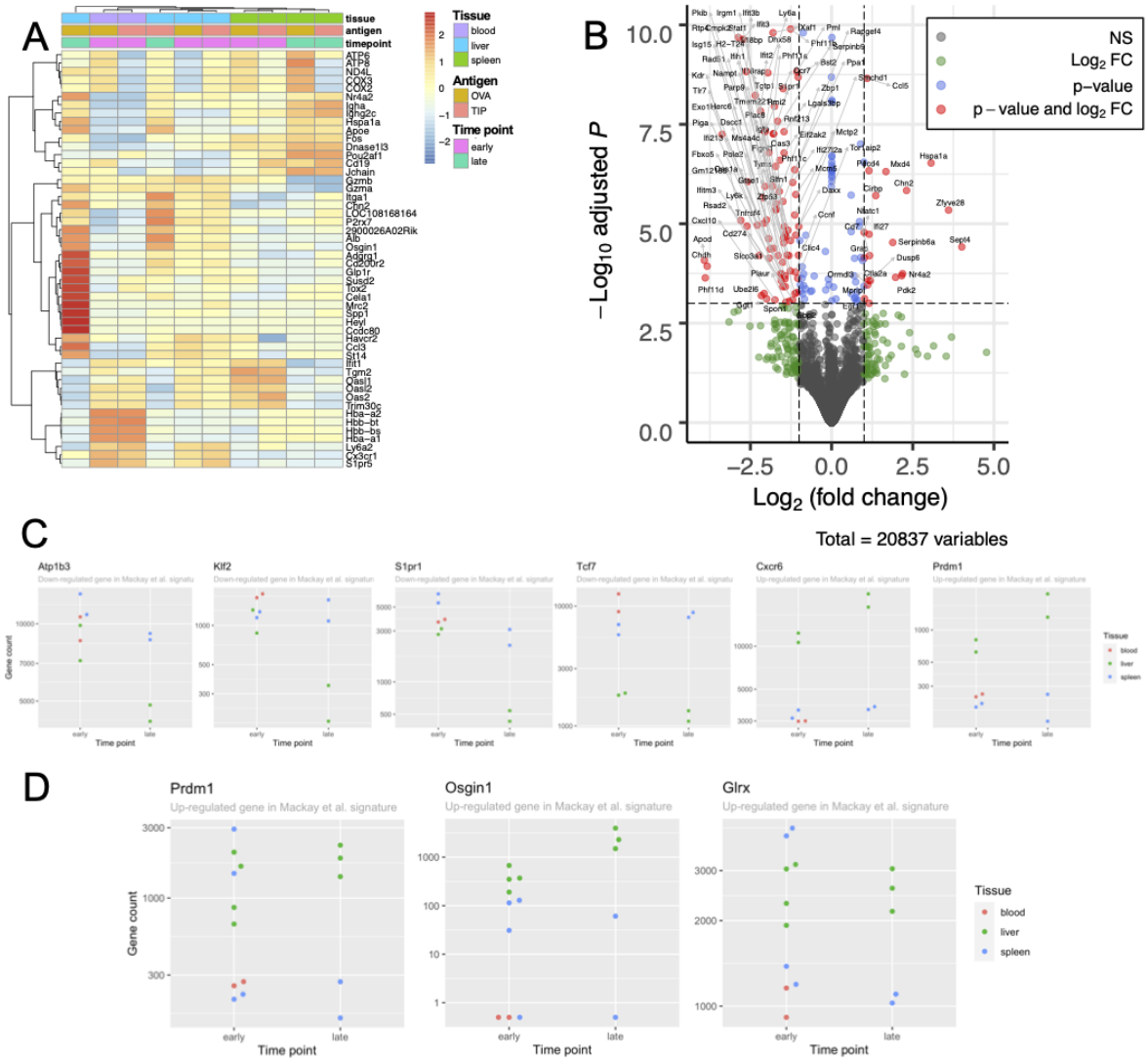


Figure 3.20: Transcriptomic comparison of CD69+ early and late time point post-IV boost samples. ***A****: Heatmap of the most variable genes in CD69+ early (day 1) and late time point (day 28) post-IV boost samples. Fifty most variable genes in CD69+ early and late time point OVA-pentamer- samples. Gene count values are centred and scaled across rows. Yellow/red corresponds to increased counts compared to other samples, and blue corresponds to decreased counts. Genes were selected according to those with the greatest variance across samples. Columns are clustered based on Spearman's correlation of rlog normalised count values. Rows are clustered according to Pearson correlation of the rlog normalised gene counts.* ***B****: Volcano plot of upregulated and downregulated genes between CD69+ early (day 1) and late time point (day 28) post-IV boost samples. The top 50 upregulated and downregulated genes have been annotated. Positive log2(FC) values indicate greater gene expression in late time point samples, compared to early time point samples. Negative log(FC) values indicate greater gene expression in early time point samples. DGE of 20,837 genes was tested for significance using the Wald test. P values were adjusted using the Benjamini-Hochberg correction (FDR).* ***C****: Counts for a selection of differentially expressed genes from the Mackay et al. signature. Presented counts underwent regularised logarithm normalisation and compared late and early time points.* Atp1b3, Klf2, S1pr1 *and* Tcf7 *are downregulated in the Mackay et al. signature, and* Cxcr6 *and* Prdm1 *are upregulated.* ***D****: Counts for a selection of differentially expressed genes from the Mackay et al. signature including population 1 (OVA-pentamer+) samples. Presented counts underwent regularised logarithm normalisation and compared late and early time points. All given genes are upregulated in the signature.*

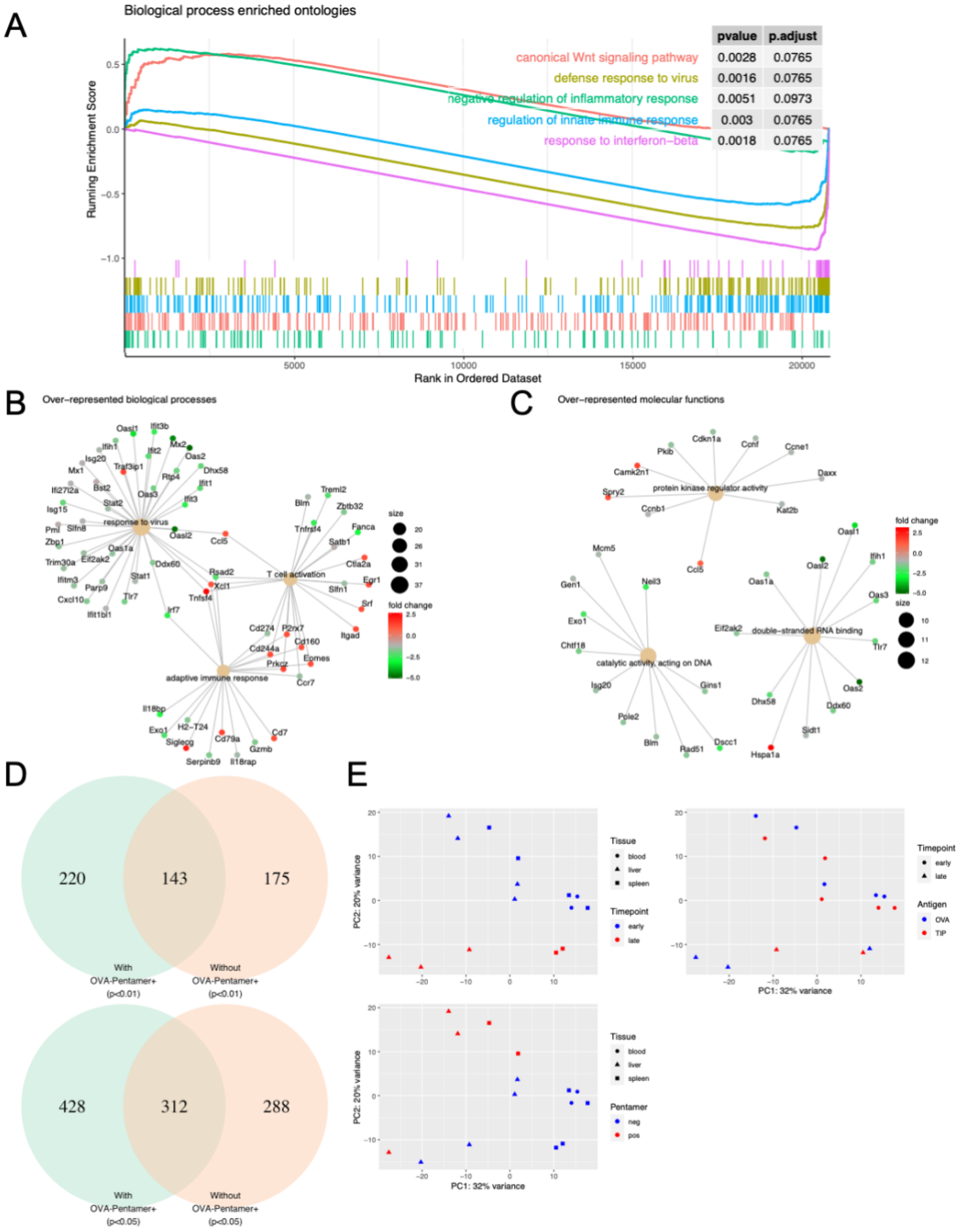


Figure 3.21: Transcriptomic pathway analyses of CD69+ early and late time point post-IV boost samples. ***A****: Enrichment plots for biological process gene ontology categories of the CD69+ early and late time point post-IV boost samples comparison. Gene set enrichment analyses visualised by category running enrichment score among the pre-ranked list of all 20,837 genes. A category's enrichment score is the maximum deviation from zero encountered in the running score. If the normalised enrichment score is positive, this suggests enrichment of the category in late time point CD69+ samples. A negative normalised enrichment score indicates enrichment of the category in early time point CD69+ samples. The ranked list metric is the binary logarithm of the fold change of gene expression between CD69+ early and late time point post-IV boost samples.* ***B & C****: Over-representation analysis plots for gene ontology categories of the CD69+ early and late time point post-IV boost samples comparison. A hypergeometric test was used to test for significance of gene category over-representation. Gene categories presented have an FDR < 0.05."Fold change" values in the legend refer to log(FC) values and size refers to the number of genes involved in the category.* ***B****: Over-representation analysis gene-concept network plot for Gene Ontology biological processes.* ***C****: Over-representation analysis gene-concept network plot for Gene Ontology molecular functions.* ***D****: Differential expression between CD69+ early and late time point post-IV boost samples*

*when including OVA-pentamer+ samples. Number of differentially expressed genes when including OVA-pentamer+ (blue) and when excluding OVA-pentamer+ (orange) samples. The overlap represents the number of genes that are differentially expressed in both comparisons at different alpha levels (p<0.01 top, p<0.05 bottom). **E**: PCA of CD69+ early and late time point post-IV boost samples, including OVA-pentamer+ samples. PCA shows 32% variance in samples accounted for by PC1 and 20% variance, by PC2. The three plots show the same data, but with different symbols and colours to illustrate the various experimental variables: OVA-pentamer + (pos) or – (neg), CD69 + (pos) or – (neg), early or late time point, antigen delivered in IV viral vector vaccine (OVA or TIP) and the tissue examined (blood, liver or spleen).*

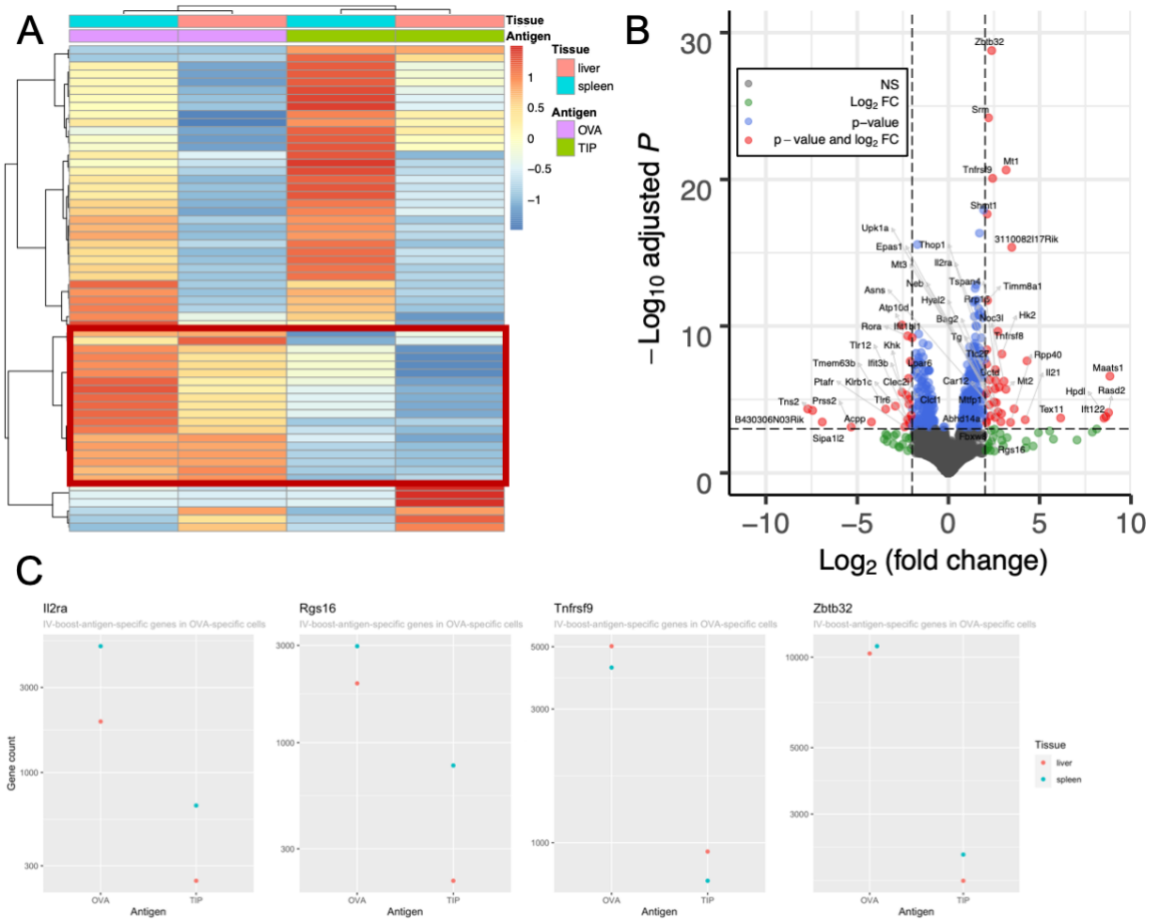


*Figure 3.22: Transcriptomic comparison of OVA-pentamer+ early time point CD69+ Ad-OVA and Ad-TIP vaccinated group samples. **A**: Heatmap of the most variable genes in OVA-pentamer+ early time point CD69+ Ad-OVA and Ad-TIP vaccinated group samples. Gene count values are centred and scaled across rows. Yellow/red corresponds to increased counts compared to other samples, and blue corresponds to decreased counts. Genes were selected according to those with the greatest variance across samples. Columns are clustered based on Spearman's correlation of rlog normalised count values. Rows are clustered according to Pearson correlation of the rlog normalised gene counts. **B**: Volcano plot of upregulated and downregulated genes between OVA-pentamer+ early time point CD69+ Ad-OVA and Ad-TIP vaccinated group samples. All differentially expressed genes have been annotated. Positive log2(FC) values indicate greater gene expression in Ad-OVA vaccinated group samples, compared to early time point samples. Negative log(FC) values indicate greater gene expression in Ad-TIP vaccinated group samples. DGE was tested for significance using the Wald test. P values were adjusted using the Benjamini-Hochberg correction (FDR). **C**: Gene counts for a selection of the differentially expressed CD69+ AgSp signature. Presented counts underwent regularised logarithm normalisation and compared late and early time points. All genes were upregulated in early time point OVA-pentamer+ CD69+ Ad-OVA vaccinated groups, compared to Ad-TIP vaccinated groups. None of the genes were differentially expressed when considering early time point OVA-pentamer+ CD69- or OVA-pentamer- CD69+ Ad-OVA vs Ad-TIP comparisons.*

3.4 Discussion

3.4.1 Novel findings

The data described in this chapter provide an indication of the early tissue-resident response, kinetics, and transcriptomics of CD8+ T cells in mice and in the context of the liver-stage malaria vaccination strategy, prime-target, encoding model antigens. Time course experiments showed that AgSp cells peak between day one and three post-IV boost. These AgSp cells were present in several sites, including the liver and blood, and expressed several molecules suggestive of tissue residency and liver-homing. Blood AgSp cells present one to three days after vaccination were associated with the eventual liver AgSp response (albeit the correlations were not significant). When sampled early after vaccination, these AgSp blood cells were termed "TRM-like cells." Liver CD69+ TRM, sampled just prior to IV boost, were shown to home preferentially to the liver. TRM-like cells showed a comparably heightened partiality for tracking to the liver when sampled early after IV boost. The CD69 molecule was shown to be important in the homing and maintenance of TRM-like cells in the liver. TRM-like cells could not be distinguished transcriptionally from TRM using a tissue-residency transcriptional signature. Finally, a panel of genes that could allow identification of prime-target AgSp TRM-like cells was identified.

Tissues are often exposed to pathogens, and TRM are critical in protecting against invading pathogens (421,422). This is particularly the case in *Plasmodium* liver-stage infection (201,237). TRM are the first T cell responders to infection and their activation can even precede innate responses (209,401). Contrary to the dogma that TRM are non-recirculating, several reports have demonstrated that TRM can egress from tissues in both steady-state conditions and as a result of reactivation (400,401,409). TRM-like cells identified very early after IV Ad may represent a population of temporarily or permanently recirculating TRM that egressed from the liver. This corresponds with findings by Fonseca *et al.*, that indicate the size of the initial memory T cell expansion correlates to initial 'TRM reserve' (400) and other work wherein systemic recall

responses can be shaped by liver TRM (401). Unlike these reports, however, TRM-like cells did not appear to be characterised by a uniformly effector phenotype.

Alternatively, or in combination, TRM-like cells may not have originated from TRM and, instead, from TEM or TCM. The ability of naïve T cells to form TRM is imprinted before tissue entry, potentially at activation, and can be identified in the effector phase (412). If the same is true in the case of antigen re-exposure, this suggests that early memory T cell responses could be used to predict the accumulation of TRM at later time points. Indeed, TRM-like cells at day 1 post-IV boost were associated with day 14 TRM in the liver. Behr *et al.* showed that circulating memory CD8+ T cells can contribute to forming TRM populations at non-mucosal sites (407), however secondary TRM development is largely dependent on *in situ* proliferation of pre-existing TRM (401,423). Therefore, it may be that the magnitude and characteristics of the TRM-like cell response after IV Ad-OVA is independent of the contemporaneous TRM population, but that a small fraction of the cells is composed of TRM precursors that can exit the vasculature and become non-recirculating.

TRM-like cells were shown to have a high capability to establish themselves in the liver. Work by Holz *et al.* showed that liver TRM form after TCR-dependent activation of naïve CD8+ T cells but that inflammatory and antigenic signals, in combination, preferentially tailor their development (404). In agreement with this observation, the data described above indicate that AgSp TRM can be found after both the IM prime and IV boost of a prime-target vaccination regimen. Previous work has shown that liver TRM can be re-introduced to the liver after IV administration into donor mice (237,424) and that the functional characteristics of these CD8+ T cells are comparable to host-derived TRM (201,404). TRM-like cells isolated one day after IV Ad-OVA had a similar phenotype and liver-homing ability to 'steady state' liver TRM, suggesting that these cells may have been able to re-seed the liver to shape local recall responses. This has

previously been postulated (201), and recently, Behr *et al.* showed that tissue-experienced ex-TRM return to tissues and local lymph nodes, and control infection (401). Thus, I propose a model whereby the IM prime vaccination of prime-target activates naïve CD8+ T cells, some of which form liver TRM due to antigen presentation and hepatic Ad-mediated inflammation. Early after the IV boost (target) vaccination, TRM are among the first responders to IV Ad and produce TRM-like cells as progeny. These TRM-like cells serve as a proxy of the size of the TRM response after prime, and through re-seeding of the liver, contribute to the post-IV boost TRM niche in the liver. This hypothesis supports the "outside-in" migration and transdifferentiation model of memory T cells that has very recently been described (400). In addition to previously established knowledge of mature TRM, precursor TRM and ex-TRM, the current data add to this field.

This model does not exclude the notion that ex-liver TRM may re-seed other organs, nor does it preclude the contribution of other T cell types to the early resident T cell response. The establishment and maintenance of liver TRM is likely to be unique as they are the only known TRM that 'reside' inside the vasculature (201,246,422). Because liver TRM are localised in the hepatic sinusoids at steady state, circulating precursors have direct access to the TRM niche without a need to egress from the blood and may have a lower threshold for the establishment of residency. Adoptively transferred mature liver TRM can travel to the skin and small intestine, albeit at markedly reduced frequencies compared to the liver (424). Thus, ex-liver TRM may be best suited to re-establish themselves in the liver after recirculation. On the other hand, and unlike other organs harbouring TRM, there may be a limited need to precisely re-recruit ex-TRM for the formation of hepatic immune memory because total blood volume circulates through the liver more than twenty times per hour. Additionally, secondary liver-resident memory T cell development depends on primary liver TRM (407,423). Other cells may play intermediate roles in the reactivation and re-seeding of TRM. MAIT cells play a non-redundant role in bridging the innate

and adaptive systems, and can orchestrate early events in T cell-mediated immunity (425). Thus, the suggested model is likely a simplification of the actual cycle of events.

Tissue residency is regulated by transcriptional factors promoting the induction of adhesion molecules and the suppression of tissue exit, though the molecular determinants of precursor TRM are less known. The work in this chapter focussed on the importance of CD69 as a marker of increased T cell retention in the liver in the short term. Walsh *et al.* suggest that the role of CD69 in CD8+ T cell residency likely manifests very early in the immune response as deficiency of the C-type lectin did not have an appreciable effect when comparing mid-effector versus memory time point T cell responses in tissues (426). Consistent with this, the data herein suggest that the molecule is likely to mediate initial recruitment and seeding of the liver. CXCR6 and CD11a were also analysed. CD11a is critical to the hepatic homing of CD8+ T cells as *Itgal* (encoding CD11a) knockout cells show approximately ten-fold lower accumulation in the liver compared to wild type cells 24 hours after transfer (236). Furthermore, CD11a, when combined with integrin β-2 to form LFA-1, is required for efficient CD8+ patrolling and killing of *Plasmodium* and HBV in the liver (236,427). In contrast to CD69, CXCR6 has been shown to be necessary for the long term maintenance of TRM, and specifically in the liver following *Plasmodium* sporozoite administration (182,428). There are also examples of metabolic (424,429), transcriptional (208,401), and functional (217) markers of TRM that may help to further dissect and map the heterogeneity of TRM-like cell identities and potential outcomes. This is further investigated in Chapter 5.

Many studies examine TRM after adoptive transfer and short-term antigen exposure by way of protein vaccination or limited infection, but Ad persistence is likely to uniquely affect the liver TRM response to prime-target vaccination. Ad are hepatotropic, even when given IM (405,430), and IV Ad primarily infects the liver. IV Ad is rapidly and almost entirely taken up by LSECs (90%) and

KCs (~10%) (414,415). Cognate antigen recognition and persistence are likely to play a critical role in TRM-like cell recruitment back into the liver. Fernandez-Ruiz *et al.* were the first to show that antigen encounter in the liver enhances TRM formation in the context of malaria vaccination (201), and since then several reports have reflected this finding (237,241). Similarly, TRM in the brain require local antigen recognition for their maintenance (228). Ad triggers robust pro-inflammatory cytokine responses in the liver. The finding that Ad-TIP resulted in at least partial recruitment of OVA-specific transferred TRM-like cells, suggests that inflammation may be significant in TRM-like cell recruitment to the liver. This finding is consistent with work by Mackay *et al.*, wherein long-lived skin CD8+ TRM could be generated using a sensitising inflammatory agent, in the absence of *in situ* antigen (210). Therefore, TRM-like cell recruitment into the liver is likely a function of both cell- and Ad-mediated factors.

The discovery of transcriptional and functional profiles relating to lymphocyte residency allows gene-based identification of TRM. Mackay *et al.* showed the instrumental roles of the transcription factors Hobit and Blimp (208), and others have identified molecules such as Runx3 (206), and Notch (221), in the orchestration of tissue residency. The Mackay *et al.* signature of lymphocyte tissue residency was able to robustly identify TRM, as these samples showed upregulation of genes such as *Dusp6* and *Xcl1*. This gene signature is based on bulk RNA-seq comparisons between putatively resident gut and skin TRM identified by protein expression of CD103+, and their splenic TEM/TCM counterparts (208). To date there are a limited number of publicly available murine hepatic T cell signatures based on unbiased or unsupervised transcriptome classification (431,432), and these do not focus on defining T cell subset immunology. Despite, and potentially because of these constraints, the universal transcriptional program was not able to differentiate TRM from TRM-like cells, indicating that these cells co-express genes related to tissue residency. This suggests TRM-like cells and TRM may share specific residency characteristics.

This is the first direct transcriptomic comparison between TRM, sampled in the memory phase, and T cells sampled early after IV Ad vaccination. There were expected differences, such as enrichment of Wnt signalling in TRM, known to promote the development of memory (433), and enrichment of innate process regulation and enhanced cytolytic capacity in TRM-like cells. Interestingly, however, TRM-like cells showed enrichment of IFN-β response. IFN-β is a crucial regulator of TRM differentiation in inflammatory microenvironments; once in tissues, absence of signalling by this cytokine prevents differentiation into and persistence of CD103− CD69+ TRM (434). Thus, increased type 1 IFN responsiveness may allow TRM-like cells to take up residence and re-differentiate into TRM. TRM-like cells did not uniformly upregulate genes related to T cell activation, for example, *Slfn1*, upregulated in TRM-like cells, inhibits cell proliferation (435). *Itgad* expression was almost completely absent in TRM-like cells, compared to TRM; CD11d (encoded by *Itgad*) deficiency results in a diminished T cell response to SEB and its expression plays a role in response to inflammation (432,436). *Eomes*, encoding a master regulator of effector CD8+ T cell development (437), was upregulated in TRM and almost entirely absent in TRM-like cells, indicating that TRM-like cells may have similar transcriptional regulation as liver CD8+ TRM, as previously shown (174,201,223). *Eomes* was also shown to be downregulated in ex-TRM effector cells by Behr and colleagues (401). Importantly, TRM and TRM-like cells did not differentially express *Zfp683* nor *Prdm1*, which are universal regulators of tissue residency in lymphocytes (208). Finally, a large proportion of the genes differentially expressed between liver TRM and circulating ex-TRM in a recent report (401), were also concordantly differentially expressed in this analysis of TRM and TRM-like cells. These findings indicate that TRM-like cells, while more activated than TRM, have a degree of inhibition and indeed share characteristics with liver TRM, suggesting that they could be the circulating effector counterparts of TRM.

Using multimers to identify and characterise AgSp CD8+ T cells has advanced knowledge of T cell development, except there are situations where these reagents may be unavailable or not broadly

applicable, such as in T cell-mediated malaria vaccines (150). This work set out to discover biomarkers of AgSp TRM-like cells shortly after prime-target and, importantly, a set of genes that were congruently upregulated in OVA-prime-target cells was identified. Upregulation of these genes was related to the prime-target transgene antigen (i.e. not to the Ad vector) and cell antigen-specificity. Recent work has demonstrated impaired MHC class I-multimer identification of T cells following recent activation with their cognate antigen (438), thus the gene panel may be of particular use. The panel includes genes such as *Il2ra*, which is upregulated by CD69+ CD8+ TRM shortly after pulmonary influenza infection and is thought to enhance Blimp-1 expression (226), and *Tnfrsf9* (encoding CD137), shown to be the most distinct transcriptomic marker of virus-specific cells at a single-cell level (438). Validation of the gene panel was not presented in this chapter. I planned to validate the panel using reverse transcriptase qPCR, and I obtained OVA-specific and non-OVA-specific CD69+ T cells from the blood, spleen and liver at several time points between the day of and 28 days after IV boost with Ad-OVA and Ad-TIP. These experiments, however, were put on hold due to the COVID-19 pandemic. Regardless, the gene panel represents an output from this chapter that requires further investigation.

3.4.2 Limitations

The work presented in this chapter is limited by a few factors. I have exclusively focused on the T cell responses after IV boosting, and it is possible that the examination of T cells after IM prime provides further insights into the prime-target-induced liver TRM population. Van Braeckel-Budimir *et al.* showed that repeated antigen exposure extends the durability of lung TRM and lung-homing of circulating memory T cells, suggesting that post-IV boost responses may most adequately represent prolonged TRM-mediated immunity (439). TRM measured in these experiments were almost exclusively sampled during the early-mid effector phase (440), and thus may not truly represent tissue-resident *memory* T cells. TRM, however, can very rapidly adjust to their microenvironment, with the functional and metabolic adaptations of residency being found

as early as seven days after tissue positioning (424). Indeed, Fernandez-Ruiz *et al.* showed that vaccine-specific liver TRM increase as a proportion of total vaccine-specific T cells, and decay by less than ten-fold in number, when sampling between 7 and >100 days after vaccination (201). Similarly, no decay of TRM was shown between days 8 and 30 post-infection with LCMV (401).

CD69 is an early marker of T cell activation, so it is possible that TRM-like cells were activated effector or effector memory T cells. TRM-like cells were defined using CD69 (which was shown here to be important for the early recruitment and retention of cells in the liver) together with other markers such as CD11a (required for TRM persistence and function in the liver (236)) and CD44 (a marker of antigen-experienced T cells (441)). This allows for sensitive, albeit potentially not specific, identification of a subset of cells that are prepared for tissue residency. Indeed, a large proportion of TRM-like cells may be effector memory cells. This does not exclude the utility of TRM-like cells as a CoP. Akondy *et al.* (205) and Youngblood *et al.* (204) indicate that effector CD8+ T cells can dedifferentiate into memory T cells, which suggests that if TRM-like cells are effector cells, the size of their expansion could be advantageous for subsequent memory generation.

3.4.3 Further questions

Knowledge of TRM maintenance is of paramount importance for designing vaccines that intend to induce long-lasting protection. Are TRM following vaccination maintained by circulating T cells and/or are they autonomously long-lived? What signals are required for either method of maintenance? If they are replenished by circulating T cells, are TRM derived from a distinct precursor? Some of these questions have been addressed in the context of model infections in mice, but answers to these questions must be sought, specifically, following vaccination and in humans. This knowledge could assist in the development of vaccines that aim to induce TRM.

It remains unclear precisely whether TRM-like cells were TRM precursors emanating from effector T cells or ex-TRM that had been dislodged from the liver. Further examination of these two alternatives could be performed using chromatin accessibility mapping, exemplified in work by Akondy *et al.* (205), and lineage tracing tools, such as those used by Behr *et al.* (401). Indeed, it is probable that TRM-like cells are a heterogeneous T cell population, including non-conventional T cells such as MAIT, NKT and γδ T cells. These cells are rapidly activated by recognition of conserved, stress-induced, and microbial ligands, and thus may be part of the initial post-IV Ad-OVA proliferation of T cells. Using single-cell technologies and TCR tracking could allow this heterogeneity to be parsed. Furthermore, I evaluated AgSp CD8+ T cell responses following IV Ad-OVA and did not investigate other antigens or other vectors to be used in prime-target strategies.

These data revealed associations worthy of further investigation. The correlations between early TRM-like cells and later stage TRM in the liver should be investigated to determine if TRM-like cells do indeed correlate with both long term liver TRM presence and protection against rodent malaria challenge. If they do correlate, establishing numerical thresholds of TRM-like cells that reliably protect against challenge may be useful in comparing different antigens using the prime-target approach.

3.4.4 Conclusion

The work presented in this chapter indicated that prime-target AgSp cells peak very early after IV boost. These AgSp cells were found in several sites and exhibited phenotypic and transcriptomic features of liver TRM. TRM-like cells showed a heightened predilection for tracking to the liver when sampled early after IV boost. A panel of genes that may allow identification of TRM-like cells following prime-target was identified. While validation and further exploration of the findings presented in this chapter will be relevant, the translational significance may only truly be

corroborated in human studies. Given the results of this chapter and the clinical evaluation of prime-target in Oxford at the Jenner Institute, the following chapters are focused on translating insights from these mouse studies into human clinical trials.

Chapter 4

4 Assessing liver-resident memory T cells and their circulating counterparts

4.1 Introduction

It has now been over 30 years since the work of Ruth and Victor Nussenzweig that identified CD8+ T cells as critical mediators of liver-stage malaria protection in mice (163). This accelerated the field of vaccine strategies targeting the induction of liver-stage-specific CD8+ T cells. To this end, substantial effort has been invested in optimising viral vector strategies able to generate high frequencies of AgSp CD8+ T cells (176,300,306,442). As previously mentioned, a prominent approach entails a ChAd63 prime, followed by an MVA boost. This heterologous viral vector regimen, expressing ME-TRAP, can induce high numbers of CD8+ T cells with modest clinical efficacy in both malaria-naïve and pre-exposed individuals (176,237). CD8+ T cell numbers following vaccination correlate with efficacy, suggesting that increased numbers of circulating CD8+ T cells could improve protection. As discussed in the previous chapter, Gola *et al.* and others have shown liver CD8+ TRM to be long-lived and a crucial population to mediate protection against sporozoite challenge in mice (201,237,241). This chapter presents an in-depth examination of liver TRM and blood TRM-like cells following prime-target vaccination in humans, in the VAC066 phase I/IIa sporozoite challenge trial of IV boosting with ChAd63-MVA encoding ME-TRAP.

Relatively little is known about human TRM in health and disease when compared to our understanding of these cells in mice. The necessities for transcriptional regulation of TRM varies

considerably between mice and humans, despite some homology (219,244). Kumar *et al.* showed that CD69+ memory T cells found in human tissues were phenotypically and transcriptionally different from CD69- tissue and blood memory T cells (219). The authors describe a core transcriptional and functional signature. This signature involved upregulation of molecules for adhesion (CD103) and rapid response once activated (IFNγ, IL-2, IL-17), and simultaneous downregulation of molecules associated with tissue egress (CD62L, S1PR1, CX3CR1). Szabo and colleagues identified, at a single-cell level, a suite of genes that were highly expressed in memory T cells from each tissue compared to blood (443). Notably, a fraction of blood cells also highly expressed the tissue signature (443). FitzPatrick *et al.* examined transplant donor-derived small intestine TRM to show that these cells were not the transcriptionally homogenous population that may be inferred by considering the Kumar *et al.* bulk transcriptional signature (444). In doing so, the authors delineated two CD8+ TRM populations and suggested that β2-integrin expression may be a key differentiator of these subsets. Therefore, human TRM are likely a heterogeneous population within and between tissues that vary from tissue-resident T cells found in mice.

Knowledge regarding human liver TRM, specifically, is increasing. The combination of CD103 and CD69 demarcate a population of intrahepatic CD8+ T cells limited to the memory T cell compartment (246). CD69+ CD103+ are thought to make up approximately 11% of hepatic memory T cells (250,251). While liver CD69+ CD103- CD8+ T cells are weaker effectors than their CD103+ colleagues, they are the principal effectors (250). Like mice, human liver CD8+ TRM express higher levels of CXCR6 than other intrahepatic and peripheral lymphocytes (244,246). In contrast to mice, however, human liver CD69+ CD103+ CD45RA- T cells express lower levels of granzyme B when compared to CD69- hepatic T cells and circulating memory CD8+ T cells (246). Liver TRM express high levels of PD-1 and CD39. These inhibitory molecules allow hepatic CD8+ TRM to maintain themselves in a suppressed state while also performing noncytolytic immunosurveillance (246).

Assessing TRM in humans remains difficult. The challenges associated with mapping human hepatic immune populations, in particular, are threefold: i) access-related, ii) rare populations are thought to be important mediators of immunity (e.g. TRM), and iii) specialised techniques are often required (i.e. in sample collection and preparation, and analyses). The added complexity of trying to understand hepatic immunity in the context of malaria vaccine-induced immunity, at scale, makes for a seemingly insurmountable task. It is, therefore, useful to identify if inferences about the liver can be made by looking at the blood; that is, to identify correlates of hepatic immunity and of vaccine-induced protection. In mice, TRM from various sites can exit tissues in response to stimuli, re-enter the circulation and even contribute to the expansion of memory T cells (213,400,409). A detailed understanding of hepatic TRM and any potential circulating counterparts in humans, as well as an appreciation of their relationship, would likely be critical in identifying correlates of liver-stage malaria protection and further vaccine development.

The aim of the work in this chapter was to investigate liver TRM and blood 'TRM-like' cells. Specifically, the focus was to profile liver TRM using liver FNA in healthy prime-target vaccinated volunteers and consider the differences and similarities between *bona fide* TRM, and TRM-like cells in the blood. This chapter builds on and uses the work of Kumar *et al.* (219), Szabo *et al.* (443), and Zhao *et al.* (445) who describe various transcriptomic signatures of pan-tissue and liver-specific TRM. The objectives of this chapter were to:

1) Identify liver TRM and characterise their phenotype and transcriptome,
2) Assess quantitative and qualitative similarities between liver and blood memory T cell subsets, and
3) Investigate transcriptomic differences between TRM and TRM-like cells at population and single-cell levels.

4.2 Results

4.2.1 Liver fine needle aspirates faithfully represented hepatic immune cell populations

4.2.1.1 Fine needle aspirate yield and composition

Thirteen volunteers consented to hepatic FNA and matched blood sampling between 16 and 24 days after IV ChAd63 or MVA encoding ME-TRAP. The FNA sampling procedure provided modest amounts of lymphocytes (median total $4.8x10^5$ lymphocytes, IQR $3x10^5$; median concentration $4.0x10^5$ lymphocytes/mL, IQR $2.5x10^5$) to perform flow cytometry and *ex vivo* ELISpot from the same sample.

The cellular composition of liver FNA was defined by flow cytometry. The intrahepatic profile of various lymphoid and myeloid lineage cells was similar to that which has previously been reported (Figure 4.1) (245,248). T cell populations expressing CD69 and CD11a were enriched in the liver (Table 4.1). CD103 T cells did not differentially populate the liver or blood. Using an algorithm developed to determine the "liver-like" degree of an FNA sample demonstrated that the median liver-like score of the samples used in these analyses was 78% (IQR 23.6%).

Table 4.1: Populations of CD8+ and CD4+ T cells expressing TRM markers. Wilcoxon matched-pairs signed-rank tests were used to check for the significance of differences between FNA and PBMC samples. An exact p value is reported. Values reported are medians with interquartile ranges. Effective pairing, checked by Spearman correlation coefficient, was present for all samples. NA, not applicable. ND, not detected.

Population	**FNA**	**PBMC**	**p value**
CD8+ TRM (%CD8+ T cells)	*Median (IQR)*	*Median (IQR)*	
CD69+ CD45RA-	13.80 (12.27)	0.380 (0.84)	0.0002
CD69+ CD11a hi CD45RA-	13.70 (12.26)	0.365 (0.83)	0.0002
CD103+ CD45RA-	1.280 (1.00)	1.29 (0.94)	0.4143
CD103+ CD11a hi CD45RA-	1.090 (0.87)	0.950 (0.75)	0.4143
CD69+ CD103+ CD11a hi CD45RA-	0.5200 (0.62)	0.00516 (0.01)	0.0002
CD4+ TRM (%CD4+ T cells)			
CD69+ CD45RA-	4.55 (4.01)	0.15 (0.12)	0.0002
CD69+ CD11a hi CD45RA-	4.31 (4.03)	0.14 (0.12)	0.0002
CD103+ CD45RA-	ND	ND	NA
CD103+ CD11a hi CD45RA-	ND	ND	NA
CD69+ CD103+ CD11a hi CD45RA-	ND	ND	NA

4.2.1.2 Vaccination regimen and time after vaccination did not affect hepatic TRM

FNA were all taken after IV viral vector boost. Groups 1 and 3 received IV ChAd63 ME-TRAP, while groups 2 and 4 received IV MVA ME-TRAP. Ads and MVA are known to be hepatotropic (415), with Ads demonstrating prolonged antigen expression in the liver (237). Despite the differences in vaccination regimen, there were no differences in liver TRM proportions among groups (Figure 4.2). Similarly, there was no trend in liver TRM frequency when considering time after IV boost.

4.2.1.3 Liver FNA identified TRAP-specific T cells

IFNγ ELISpot assays were performed on the samples of four volunteers. The number of cells included in the assay and the number of replicates was minimised to allow for multiple assays to be run from the same samples. FNA samples contained TRAP-specific cells capable of generating IFNγ (Figure 4.3). The AgSp liver:blood T cell ratios were 16.3, 2.04, 1.2 and 2.11 for volunteers 6, 9, 11 and 12, respectively.

4.2.1.4 Intracellular cytokine staining resulted in hepatic lymphocyte death

ICS was performed on three FNA and PBMC samples to assess the TRAP-specific response to vaccination. Fluorescently-labelled multimeric MHC–peptide complexes allow the direct visualisation and phenotypic characterisation of AgSp T cells using flow cytometry and have been used to identify antigen-specific cells in the liver previously (245,446,447). Unfortunately, the exact immunodominant T cell epitopes targeted by liver-stage-*Plasmodium*-specific T cells are yet to be deciphered, and dominant T cell epitopes often do not represent protective epitopes (448,449). ICS advantageously, allows the identification of AgSp cells without the need for an appreciation of an individual's HLA-specific immunodominant epitopes. PBMC TRAP-specific response was consistent with the separately run standard clinical trial ICS procedure (data not shown). The FNA samples had high amounts of cellular debris on flow cytometry size channels and a high rate of cell death (>50%). There were insufficient cells from the FNA samples to sort TRAP-specific CD69+ CD45RA- CD8+ T cells identified by IFNγ or CD107a expression. ELISpot is more sensitive and requires fewer cells

than ICS. Detecting an IFNγ response by ICS requires that cells survive the overnight culture and staining procedure, while ELISpot will detect cytokine at it is being secreted overnight. Therefore ELISpot is less reliant on cells remaining alive after overnight incubation. This may be why no TRAP-specific cells could be sorted after ICS but were seen on ELISpot.

4.2.1.5 Hepatic lymphocytes correlated to matched peripheral blood lymphocytes

Correlations were seen between several intrahepatic and peripherally circulating lymphocyte populations. Cells with a TRM phenotype in the liver significantly correlated to blood memory T cells (Figure 4.4). PBMC CD8+ T cells, as a proportion of total lymphocytes, significantly correlated to matched FNA CD8+ T cells. PBMC CD4+ T cells negatively correlated to matched FNA CD4+ T cells, but this correlation was no longer significant if one volunteer was excluded from the analysis. Total CD3+ T cells did not significantly correlate between the liver and blood. CD69-CD45RA- T cells correlated among liver and blood samples (R^2=0.61, 95%CI slope 0.17-0.54, p=0.0017). The frequencies of TRM and CD8+ T cells were greater in the liver than in the blood, as has been previously reported (245).

4.2.1.6 Hepatic TRM were phenotypically similar to peripheral blood TRM-like cells

The expression characteristic TRM markers was assessed on FNA and PBMC T cells. The CD69 status of CD11a hi CD45RA- CD8+ T cells was a significant contributor to the proportion of cells expressing characteristic TRM markers (Figure 4.5). Both in the liver and blood, CD69+ cells had on average a higher proportion of CD103+, CXCR6+ and PD-1+ cells, compared to CD69- counterparts. This was not evident in the CD103+ CD69+ cell proportion in PBMC, however. The trends in GMFI of PD-1 and CXCR6 when comparing tissues and CD69 status resembled those seen when comparing marker positive frequencies. The GMFI of CD103 was significantly greater in PBMC compared to FNA, and CD69 status did not affect CD103 GMFI.

A tSNE algorithm was used to examine the expression of several markers on 1,068,990 CD45+ single live lymphocytes. These lymphocytes were derived from all 13 volunteers. Of these lymphocytes, each FNA sample contributed on average 32,760 cells (range 6480-50,000), while each PBMC sample contributed 50,000 cells. After manual gating on CD69+ CD45RA- CD8+ cells, five clusters were seen (Figure 4.6), and these cells were identified as non-effector memory and non-naïve CD8+ T cells. CD69+ and CD69- cells were compared to validate whether the clusters were dependent on CD69+ as a marker of their TRM status. There was substantial overlap of CD69+ and CD69- memory T cells, and indeed higher frequencies in the CD69- compartment, of the central clusters in both the FNA and PBMC samples (Figure 4.7). There were three clusters where there was little or no overlap between CD69+ and CD69- CD45RA- cells (Figure 4.8), suggesting relative enrichment of the clusters in the CD69+ T cell compartment.

The three clusters were designated tSNE subsets 1-3 (Figure 4.8) and explored further for their presence in the blood and liver, and expression of TRM markers. All three clusters co-occurred in FNA and PBMC samples; however, Subset 2 appeared less commonly in blood compared to liver. The main drivers of the clusters were CXCR6, PD-1 and CD103, with no substantial differences in the fluorescence intensity of the other markers examined (Figure 4.9). The subsets were classified according to the three parameters; Subset 1 was CXCR6+, PD-1-, CD103-, Subset 2 was CXCR6+, PD-1+, CD103+ and Subset 3 was CXCR6-, PD-1+, CD103+. The presence of circulating cells with markers of tissue residency or 'circulating TRM' goes against the traditional definition of resident cells. The term "TRM-like cells" is used in this chapter, instead of "circulating TRM," to indicate the (PBMC) circulating population of T cells that share phenotypic characteristics with *bona fide* (FNA) liver TRM.

Some parameters were not fed into the clustering algorithm, but these were shown to be equally distributed across the three subsets. Performing tSNE can be computationally intensive, and

reducing the parameters that are fed into it reduces computation time. The parameters not included in the tSNE (i.e. 'metaparameters') comprised the date of acquisition, vaccination group, the number of days following IV boost and sample (volunteer) number (Figure 4.10). Cells from each tSNE subset were equally spread over the various levels of the metaparameters and did not appear to drive differences in the subsets. Group 3 was under-represented due to difficulties in recruiting sufficient volunteers for FNA sampling. This was most likely a random effect.

4.2.2 RNA-seq delineated unique differences between liver TRM and TRM-like cells

Smart-seq2 RNA-seq was performed on 100 cells from matched FNA and PBMC samples (referred to as mini-bulk samples). These cells were sorted with single-cell purity using a live single CD20- CD3+ CD45+ CD8+ CD4- CD45RA- CD69+ or CD69- lymphocytes gating strategy (Figure 4.11A).

PCA was performed on all samples that passed QC. PC1 and PC2 accounted for much of the variability found between CD69+ and CD69- samples (Figure 4.11B); these two PCs represented 28.15% of the variance amongst all samples. The most evident separation of samples in terms of sample type (Figure 4.11C) was present when considering PC2 and PC3. Collection date, flow cells used for sequencing and volunteer identity did not drive variability in any of the first 10 PCs (data not shown). Hierarchical clustering based on Euclidean distances suggested that there were no obvious outlier samples and reiterated the findings of PCA, demonstrating that samples tended to cluster based on CD69 expression status (Figure 4.12). Additionally, clustering showed that several groups were formed by similar sample types. These data suggested there were major biological and experimental components of overall variability and that outliers were not driving this variability.

4.2.2.1 FNA and PBMC memory T cells exhibited previously reported characteristics

DGE analysis was performed on all samples by comparing paired FNA and PBMC samples. Overall, there were 637 and 218 differentially expressed genes with FDR<0.05 and FDR<0.01, respectively.

The 50 most variable genes included *Gzmb*, *Cx3cr1*, *S1pr1*, *Ccr7* and *Sell*, which were all downregulated in FNA cells (Figure 4.13). For nine genes (from *Bcorp1* to *Uty* in Figure 4.13), there was a volunteer effect, where four volunteers downregulated, and four volunteers upregulated the genes in question. These genes were all located on the Y chromosome, suggesting that volunteers with expression of these genes were male. This corresponded with the known clinical data. The genes *Susd2*, *Mtrnr2l8*, *Plp1*, *Snord17* and *Al355297.1* were all strongly upregulated in the CD69+ FNA sample of volunteer 06 and showed uniform expression across all other samples (data not shown). These results corroborated previously reported differences between liver and blood memory T cells (211,244,246).

4.2.2.2 Comparing liver TRM and TEM refined a tissue-resident T cell signature

Comparing FNA CD69+ and CD69- cells provided insights of DGE between TRM and TEM. These analyses revealed 509 and 263 differentially expressed genes between FNA CD69+ and CD69- cells when FDR<0.05 and FDR<0.01, respectively. Of the top 50 upregulated and downregulated genes, those upregulated included *Irf8*, *Tox2* and *Ccl3* and those downregulated included *Ccr4*, *Il23a* and *Tsc2* (Figure 4.14). Clustering based on Spearman's correlation of normalised count values differentiated TRM and TEM by using only the Kumar *et al.* CD8+ signature genes (Figure 4.15) (219). Thirteen of the 25 most downregulated genes and five of the 25 most upregulated genes (Figure 4.14) between FNA CD69+ and CD69- cells were present in the signature proposed by Kumar *et al.* The genes shared between these analyses and the Kumar *et al.* signature formed a 'pan-tissue' signature differentiating CD69+ TRM from CD69- TEM (Table 4.2).

Table 4.2: Pan-tissue core TRM signature. A: Genes that were downregulated in both the CD8+ Kumar et al. core TRM signature (derived by identifying significant DGE between CD69+ and CD69- T cells in the lung and lymph nodes) and the liver TRM signature (CD69+ vs CD69-). B: Genes that were upregulated in both the CD8+ Kumar et al. core TRM signature and the liver TRM signature (219). These genes were differentially expressed when comparing CD69+ to CD69- cells. All genes were differentially expressed with an absolute value of the log(FC)>1 and FDR<0.05. FC, fold change.

A – downregulated genes													
Agpat4	*Vcl*	*Tspan32*	*Rasgrp2*	*Tgfbr3*	*Pxn*	*Npdc1*	*Klf3*	*C11orf21*	*Ripor2*	*Stk38*	*Gnly*	*Klf2*	*Ttyh2*
Prss23	*Ssbp3*	*Adgrg5*	*Lair2*	*Cx3cr1*	*Gk5*	*Ascl2*	*Rasa3*	*Sbk1*	*Sell*	*Flna*	*Fcgr3a*	*Nhsl2*	*Patl2*
B – upregulated genes													
Itgae	*Gzmb*	*Dusp6*	*Arhgap18*	*Adam12*	*Jaml*	*Il23r*	*Il17re*	*Ccr1*	*Spry1*	*Tmigd2*	*Cxcr6*	*Cpne7*	

4.2.2.3 TRM-like cells were not more activated than TRM

Comparing blood and liver CD69+ cells allowed interrogation of gene-level differences between TRM-like cells in the blood and TRM in the liver. There were 614 and 255 differentially expressed genes when FDR<0.05 and FDR<0.01, respectively. The top 25 genes upregulated in TRM-like cells included *Tktl1*, *Slc39a7* and *Agpat4*, whereas those upregulated in TRM were *Cdhr1*, *Fosb*, *Xcl1* and *Trim3* (Figure 4.16). At a sample level, there were two main clusters separated by the most variable genes, wherein both FNA and PBMC samples are present (Figure 4.17, column cluster tree). These clusters were volunteer sex-related as gene-level variability demonstrated a volunteer-specific effect across PBMC and FNA, for nine Y chromosome-associated genes (Figure 4.17, row cluster tree). Using genes in the Kumar *et al.* signature as a basis for clustering showed no clear separation between FNA and PBMC CD69+ samples (Figure 4.17, right). These results suggest that TRM-like cells were indistinguishable from TRM when comparing genes that are known to be functionally and transcriptionally crucial in maintaining T cell residency.

Genes and their products are mostly regulated in concert, so consideration of individual gene-level differences can be limiting; functional analysis allows consideration of gene groups that are regulated in unison. The DGE list of the TRM and TRM-like cells comparison was used as input for two functional analysis methods. ORA and GSEA suggested that DGE between CD69+ FNA and PBMC cells involved biological processes such as T cell differentiation, cell chemotaxis and IFNγ signalling (Figure 4.18A,B). TRM upregulated genes involved in IFNγ response and leucocyte differentiation and activation. Glycosaminoglycan binding and ribosome structural component gene sets were upregulated in PBMC (Figure 4.18B). ORA suggested differences between TRM and TRM-like cells were mostly present at the external surface of the plasma membrane and in MHC class II protein complexes. Similarly, GSEA showed that differentially expressed genes involved those acting at the adherens junctions, membrane protein complex, respiratory chain, and ribosomal subunit (Figure 4.18B). Liver TRM were enriched for genes involved in CD8+ T cell

cytokine signalling, while TRM-like cells showed enrichment of genes necessary for T cell survival, suggesting these cells may not be short-lived effectors (Figure 4.19A). Notably, there were no observed transcriptional differences in genes involved in cytotoxicity or tissue-resident gene signatures between TRM or TRM-like cells (Figure 4.19B). These data suggested that TRM exhibited a differentiated and poised state for rapid effector function, once activated, while simultaneously being capable of producing cytokines and chemokines. TRM-like cells, on the other hand, showed characteristics of increased protein production, adhesion at the cell surface and T cell survival.

4.2.2.4 Distinctions between TRM and TRM-like cells were not dependent on cell location

TRM and TRM-like cells were obtained from the liver and blood, respectively, therefore it would be reasonable to suggest that any differences were due to cell location. DGE between PBMC CD69+ & CD69- cells, and FNA CD69- & PBMC CD69- cells were explored to assess the robustness of the previous contrasts. Comparing across tissues, ten genes co-occurred in the DGE lists generated by comparing FNA and PBMC CD69+, and FNA and PBMC CD69- (not significant, hypergeometric test $p \simeq 1$, Figure 4.20A). GSEA of GO biological process, cellular component or molecular function gene categories demonstrated that there were enriched gene sets shared between both FNA and PBMC CD69+, and FNA and PBMC CD69- contrasts (namely those related to ribosomes and translation). The majority of gene sets, however, were uniquely enriched in each contrast (Figure 4.18B & Figure 4.20B). The gene signature from Kumar *et al.* was able to separate PBMC samples according to CD69 status, by clustering of Pearson correlation dissimilarity structure (Figure 4.20C), though this was mostly due to similarity between CD69- PBMC samples. Considering gene expression differences between PBMC CD69+ and CD69- samples, no terms were enriched with FDR<0.05 on GSEA when using Hallmark MSigDB gene sets or GO sets. Collectively these results suggested that T cell location was not a significant driver of transcriptional differences between TRM and TRM-like cells.

4.2.3 Single-cell RNA-seq revealed subpopulations shared among TRM and TRM-like cells

scRNA-seq was performed on matched PBMC and FNA live single CD20- CD3+ CD45+ CD8+ CD4- CD45RA- CD69+ lymphocytes after FACS-index sorting (Figure 4.11A).

PCA was performed to distinguish between biological and technical variation. PC1 was correlated with the number of features per cell (PC1=1.83% total variation, Figure 4.21A, bottom left). While PC2 had a minor gradient in mitochondrial reads (PC2=1.22% total variation, Figure 4.21A, bottom right), this did not appear to be the primary source of variability. PC3 was associated with cell tissue origin (PC3=0.65% total variation, Figure 4.21B, top left). Six of the top 30 genes contributing to PC2 were HLA-D associated genes (Figure 4.22, middle). There was a clear demarcation of two cell populations in PC2, despite there being no apparent experimental parameter accounting for this variation. *Cxcr6*, *Cd69*, *Runx3*, *S1pr1*, *Klf2* and *Rasgrp2* were significant contributors to heterogeneity in PC3 (Figure 4.22). These results suggested that there were biological and experimental drivers of overall variability.

4.2.3.1 All identified clusters contained TRM and TRM-like cells

Clustering was performed using a shared nearest neighbour approach to identify groups of cells which co-regulated genes. Three main clusters were identified, with TRM and TRM-like cells present in all of them. Cluster (C)0 had a clear demarcation between TRM and TRM-like cells (Figure 4.23) and DGE (69 genes with absolute value $|\ln(FC)|>0.25$ and padj<0.05) included increased expression of *Klf2*, *Runx3* and *S1pr1* in PBMC, and increased expression of *Cxcr6* and *Cd69* in FNA (Table 4.3). The distribution of hepatic and blood cells in C1 was more heterogeneous than in C0, and there were fewer genes that were significantly differentially expressed (32 genes with $|\ln(FC)|>0.25$ and padj<0.05). Comparing the lists of DGE between TRM and TRM-like cells in C1, C0 and the mini-bulk analysis, demonstrated that there was a high degree of agreement between the datasets (40% of C0 differential expression reflected in mini-bulk comparison, 60% of C1

difference reflected in mini-bulk; Figure 4.24), indicating the signature obtained from mini-bulk RNA-seq was an amalgamation of several transcriptomic profiles. C2 had a predominance of cells from volunteer 11 and PBMC samples.

Table 4.3: Differential gene expression between FNA and PBMC clusters. A: DGE between PBMC and FNA in C0. B: DGE between PBMC and FNA in C1. Genes in bold are those which are differentially expressed in both clusters. A positive ln(FC) corresponds to a greater average expression of that gene in PBMC, compared to FNA. A negative ln(FC) corresponds to a greater average expression of that gene in FNA. Cdc25b, Selplg, Ripor2, Klf2, Tsc22d3, S1pr1, Cxcr6 and Litaf *were differentially expressed in both clusters and in the mini-bulk experiment (see Figure 4.24). P values were adjusted using Bonferroni correction. Adj., adjusted. C, cluster.*

A – DGE between PBMC and FNA in C0								
Gene	*ln(FC)*	*Adj. p value*	*Gene*	*ln(FC)*	*Adj. p value*	*Gene*	*ln(FC)*	*Adj. p value*
S1PR1	**1.46**	**8.49E-19**	B4GALT1	0.41	3.22E-02	RHOC	-0.29	1.65E-02
TSC22D3	**1.35**	**2.64E-08**	RPL18A	0.39	9.14E-09	PLXND1	-0.31	1.78E-05
KLF2	**1.16**	**2.50E-32**	RPS2	0.38	1.22E-06	LINC01871	-0.33	3.14E-03
RIPOR2	**0.81**	**2.93E-12**	MT-ND4	0.38	6.10E-04	TRAV1-2	-0.38	2.11E-03
MYC	0.69	8.37E-05	MT-ATP6	0.36	2.73E-06	SESN1	-0.39	1.05E-02
P2RY8	**0.63**	**1.76E-02**	RPL13	0.36	4.82E-07	ID2	-0.40	2.38E-02
EMP3	0.62	5.28E-10	RPS6	0.36	2.00E-04	MAN1A1	-0.41	4.30E-02
UCP2	0.62	2.92E-02	RPS18	0.35	5.67E-06	JAML	-0.42	2.99E-02
PXN	0.59	1.55E-05	RPL5	0.34	1.63E-03	STOM	-0.45	3.73E-02
ADD3	0.57	3.36E-04	RPL32	0.33	9.73E-04	CD2	-0.48	2.57E-05
LITAF	**0.56**	**1.34E-03**	TLE5	0.33	3.06E-02	SLC4A10	-0.49	1.95E-04
SELPLG	**0.55**	**1.67E-02**	RPS19	0.33	4.44E-04	ADGRE5	-0.50	4.13E-03
EFHD2	0.53	1.30E-04	RPS3	0.33	1.53E-04	CD244	-0.53	4.91E-02
TES	0.51	4.56E-03	RPL3	0.33	6.25E-04	IFNGR1	-0.57	1.03E-05
ZFP36L2	**0.50**	**1.87E-03**	RPS27	0.32	1.19E-05	IL23R	-0.58	1.87E-05
CD52	0.49	1.21E-06	C16orf54	0.30	2.04E-02	TSPAN15	-0.60	1.69E-02
RUNX3	**0.48**	**2.16E-02**	**SH3BGRL3**	**0.30**	**1.33E-02**	CASP17P	-0.61	3.53E-05
C12orf75	0.47	1.70E-03	RPL21	0.28	6.86E-04	PRSS35	-0.61	2.73E-03
CDC25B	**0.47**	**2.57E-03**	EEF1A1	0.27	6.99E-06	TNF	-0.63	3.08E-03
MT-CYB	0.46	1.03E-08	MT-CO2	0.27	3.50E-04	LAG3	-0.67	3.65E-05
MT-ATP8	0.43	1.11E-10	RPS14	0.27	1.06E-03	CD69	-0.69	9.65E-05
LYAR	0.43	9.17E-03	MTATP6P1	0.27	1.38E-03	**CXCR6**	**-0.80**	**8.94E-09**
B – DGE between PBMC and FNA in C1								
CX3CR1	1.51	1.71E-05	**LITAF**	**0.88**	**2.17E-07**	RASA3	0.47	1.16E-02
TSC22D3	**1.36**	**1.56E-10**	TIGIT	0.85	5.45E-03	CALM1	0.40	3.10E-03
ADGRG1	1.13	1.06E-04	PLEK	0.74	1.20E-05	**SH3BGRL3**	**0.39**	**5.56E-04**
DUSP2	1.08	2.28E-04	**SELPLG**	**0.73**	**1.51E-02**	PFN1	0.37	1.74E-04
RIPOR2	**1.04**	**7.26E-09**	**RUNX3**	**0.67**	**2.96E-04**	TMSB10	0.30	2.66E-02
KLF2	**0.96**	**6.07E-17**	CLIC3	0.67	1.23E-02	HLA-B	-0.30	2.94E-05
FGFBP2	0.95	2.52E-06	KLF3	0.66	3.74E-03	PLEKHF1	-0.77	1.51E-02
TTC38	0.95	1.20E-02	PRF1	0.62	2.12E-02	PTGDR	-0.82	3.37E-03
P2RY8	**0.92**	**6.47E-03**	PPP2R5C	0.55	4.26E-03	ALOX5AP	-0.87	4.53E-04
S1PR1	**0.92**	**2.99E-06**	**CDC25B**	**0.48**	**1.31E-02**	**CXCR6**	**-0.93**	**4.05E-02**
S1PR5	0.91	2.96E-04	**ZFP36L2**	**0.48**	**2.70E-02**			

4.2.3.2 Heterogeneity among TRM was present

As there was unique DGE between PBMC and FNA in each cluster, transcriptional heterogeneity amongst TRM was examined. There were 142 genes differentially expressed between TRM from C1 and C0 (Figure 4.25). Eight of these were HLA-D-encoding genes, all of which had greater expression in C1. *Ccr1*, *Ccr2* and *Ccr6* had greater expression in C0, whereas chemokine encoding

genes *Ccl5*, *Ccl4l2, Cxcr3*, *Xcl1* and *Xcl2* had greater expression in C1. Other differential expression included upregulation of MAIT cell-associated *Slc4a10*, *Klrb1* and *Trav1-2* in C0. Using signatures that differentiate subsets of TRM, generated by FitzPatrick *et al.*, 28 genes were differentially expressed in at least one signature and the DGE list comparing C1 and C0 (Figure 4.26) (444). The six genes differentially expressed in all datasets were *Il7r*, *Hla-drb1*, *Gzmh*, *Tmigd2*, *Ccl4*, and *Ccl4l2*, with the direction of differential expression concurring across datasets (Figure 4.27). These results suggested that there was heterogeneity among TRM in the clusters and that this pattern of heterogeneity has been seen in TRM from other organs.

The heterogeneity among the clusters was explored in the context of the transcriptional signature discussed in 4.2.2.2. A number of genes upregulated in the Kumar *et al.* signature were differentially expressed between C1 and C0; these included *Adam12*, *Ccr1*, *Il23r* and *Tmigd2*, all of which were upregulated in C0. These genes were also upregulated in the mini-bulk RNA-seq experiment, outlined previously. Only one gene downregulated in the Kumar *et al.* signature was differentially expressed between C0 and C1, *FGR*, which was upregulated in C1. The rest of the genes downregulated in the Kumar *et al.* signature were either not detected, or found at low levels in both clusters (Figure 4.28). C1 did not appear to be a homogenously activated population, however, as they showed upregulation of *Gzmh* and *Ccl5* compared to C0, genes previously shown to be associated with resting CD8+ T cells (443). These data indicated that C0 exhibited characteristics that have classically been associated with tissue residency.

4.2.3.3 There was a shared trajectory among T cells of varying identity

The cells were then examined for enrichment of signatures explicitly related to the liver-residency of T cells. Zhao *et al.* used high-throughput droplet-based scRNA-seq on CD45+ cells from the liver and identified gene signatures unique to liver-resident memory CD8+ T and MAIT cells (445). A qualitative signature enrichment score was calculated for each cell and represented on the UMAP

(Figure 4.29) (390). The liver TRM signature composed of 63 genes (such as *Gzmk*, *Cd160*, *Cxcr6* and *Eomes*) showed high enrichment scores in C1 FNA cells, and to a lesser extent PBMC cells (Figure 4.29). Both FNA and PBMC cells in C0 showed enrichment for the MAIT cell signature, which included chemokine receptors (*Cxcr6*, *Ccr5*, and *Ccr6*) and transcriptional factors (*Ikzf2* and *Zbtb16*) (Figure 4.29). Interestingly, the circulating CD8+ memory T cell signature developed by Zhao *et al.* was highly enriched in C2 and, less so, in C1 (Figure 4.29). In contrast to the analysis related to the Kumar *et al.* signature presented in the previous paragraph, these signatures indicated C1 was comprised of cells resembling a conventional liver-resident T cell population and C0 was likely of MAIT or MAIT-like lineage cells.

The cellular state captured by scRNA-seq occurs at a snapshot in time, and cells are likely sampled along a spectrum of differentiation pathways. Pseudotime analyses can order cells along trajectories and attempt to recapitulate aspects of temporal variation. Pseudotime analysis further suggested that TRM and TRM-like cells were heterogeneous populations and that C2 may have been an intermediate state between C1 and C0 (Figure 4.30). Pseudotemporally upregulated genes in C1 included *Hla-drb1*, *Hla-drb5* and *Hla-dpb1*, in C2 included *Klf2* and *Arid5b* and in C0 included *Klrb1*, *Slc4a10* and *Cebpd* (Figure 4.31). These analyses were performed agnostic to the number and identity of terminal clusters; therefore, these results indicate neither the start nor endpoint of pseudotime. While it is unlikely that conventional C1 T cells (with highly heterogeneous expression of TCRα/β) differentiated into C0 MAIT cells (with semi-invariant TCR), these results suggested that the profiled CD69+ memory T cells may have had the potential to transition into or from an innate-like state. This corroborated previous reports (450,451).

4.2.3.4 TCR analysis revealed clonal relationships between TRM and TRM-like cells

TCR and CDR of the sequenced single cells (Figure 4.11A) were reconstructed using *in silico* techniques. These allowed the TCR recombinants of cells to be identified, permitting the

assessment of clonal identity and TCR chain usage. Out of the 690 cells analysed, productive TCR α and β loci were reconstructed in 634 (91.9%) and 639 (92.6%) cells, respectively. There was productive reconstruction of both α and β loci from 603 (87.4%) cells. Most cells had one productive α or β locus identified (Table 4.4). Relatively few cells had two productive α or β loci (Table 4.4), and this frequency was in keeping with previous literature on dual TCR T cells (452).

Table 4.4: Frequency of α and β TCR recombinants in 690 single T cells from FNA and PBMC samples.

	0 recombinants	**1 recombinant**	**2 recombinants**
All α loci	37	265 (41%)	388 (59%)
All β loci	46	538 (84%)	106 (16%)
Productive α loci	56	520 (82%)	114 (18%)
Productive β loci	51	612 (96%)	27 (4%)

T cell clonality and clone size were assessed. T cell clones were defined as any number of cells sharing TCR α or β chain variable region, joining region and CDR3. There were several T cell clones that had frequencies of over 1% of reconstructed TCRs when defined by either TCR α or TCR β chain (Figure 4.32A). Across sample types, clonality did not vary much within volunteers (Figure 4.32B). Across volunteers, the frequency of unique clones was more similar in FNA when compared to PBMC (differences not tested) (Figure 4.32B), but both FNA and PBMC exhibited substantial amounts of clonal and expanded clone T cells (maximum 65% volunteer 13 PBMC, minimum 22% volunteer 11 PBMC). Volunteer 13 had a higher number of non-unique clones compared to volunteers 11 and 12 (difference not tested), though this was likely influenced by the fact that approximately 150 extra single cells were collected and sequenced for volunteer 13 as the sample yield was high (Figure 4.32C, upper). Random downsampling of volunteer 13 cells to equivalent numbers as volunteers 11 and 12 suggested that clone size and number of clones were likely a function of the extra cells, rather than a bias in the volunteer's TCR repertoire (data not shown). Most expanded clones were present in both tissues. However, there was variability in the proportion of a clone which was present in each tissue within and across volunteers (Figure 4.32C, lower).

MAIT cells were present at considerable frequencies. The proportion of MAIT cell recombinants did not vary greatly across volunteers or sample type (range 43-57%; Figure 4.33A). Relating this information back to the gene expression UMAP confirmed that most of C0 was composed of MAIT cells, with sparse contributions by MAIT cells to other clusters (Figure 4.33B). Importantly, MAIT cells were present in both sample types (Figure 4.33B, lower left) and in all volunteers (Figure 4.33A, lower right). Relating MAIT cell identity back to protein expression measured by flow cytometry at the time of cell sorting, MAIT cells expressed higher quantities of CD69 and CD56, and lower CD11a and CD16 molecules, compared to non-MAIT cells (Figure 4.33C). These analyses confirmed the findings using the qualitative gene signature enrichment score for MAIT cells, presented above, suggesting that MAIT cells were identified with high fidelity using gene expression alone.

TCR chain usage bias between individuals could suggest similar antigen specificity of T cells and overlap of TCR repertoires. Therefore, variable and junction region pairing and chain usage of TCR recombinants in clonal (n=2 T cells) and clonally expanded T cells (n>2 T cells) was assessed. No TCR α pairings were shared among any volunteers (Figure 4.34, comparison across columns), but almost all TCR α pairings in FNA samples were present in PBMC samples for each volunteer (Figure 4.34, comparison between two rows). It was rare for the same TCR α variable regions to be shared between different junctional regions. When considering TCR β pairings, none were shared between volunteers (Figure *4.35*). There were a small number of unique pairings in most FNA samples that were not present in PBMC samples (Figure *4.35*). Therefore, while there was no bias towards shared TCR α or β pairings between volunteers, there was shared usage between tissue samples. Almost all MAIT cells shared the same variable and junctional regions of the TCR α locus regardless of sample type (Figure 4.36). There was more diversity in TCR β recombinant usage, but all β chains present in FNA were present in PBMC.

Most clones shared more than one TCR recombinant. The number of TCR recombinants shared between cells was examined among MAIT and non-MAIT cells. MAIT cells demonstrated marked recombinant sharing between individuals and sample types (Figure 4.37, left). Almost all expanded MAIT cell clones were present in more than one volunteer and in both sample types. Volunteer 12 exhibited four unique clones, compared to one and zero in volunteer 11 and 13 samples, respectively. Non-MAIT cell clones exhibited similar distribution between tissues as MAIT cell clones, but no clones were shared between individuals when considering non-MAIT cell clones (Figure 4.37, right). The TCR analyses suggested that there was shared clonality, TCR α and β chain usage, and MAIT cell frequencies between PBMC and FNA samples.

4.3 Figures

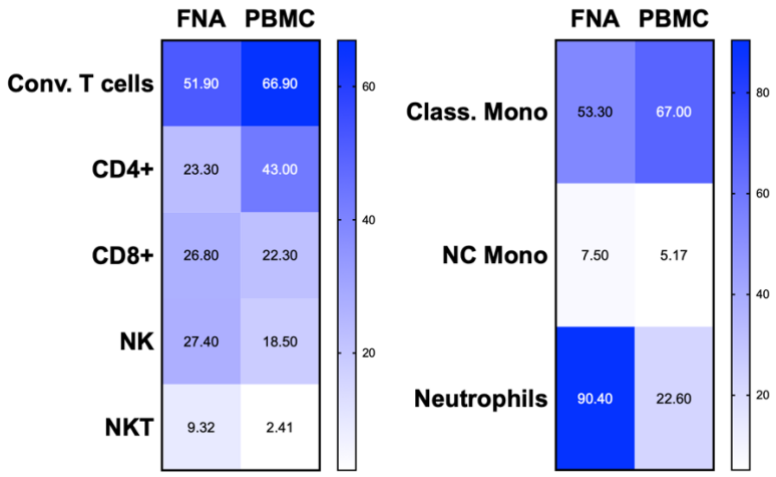


Figure 4.1: Liver and blood leucocyte populations. Median cell fractions expressed as a percentage of live CD45+ lymphocytes (left) and live CD45+ monocytes/granulocytes (right). Conventional T cells identified by CD3+ CD56-. CD4+ T cells identified by CD4+ CD3+ CD8-. CD8+ T cells identified by CD8+ CD3+ CD4-. NK cells identified by CD56+ CD16+ CD3- cells. NKT cells identified by CD56+ CD16+ CD3+. Classical monocytes identified by CD14+ CD16- CD3- monocytes. Non-classical monocytes identified by CD16+ CD14- CD3- monocytes. Neutrophils identified by CD16+ granulocytes. Conv., conventional. Class., classical. Mono, monocyte. NC, non-classical.

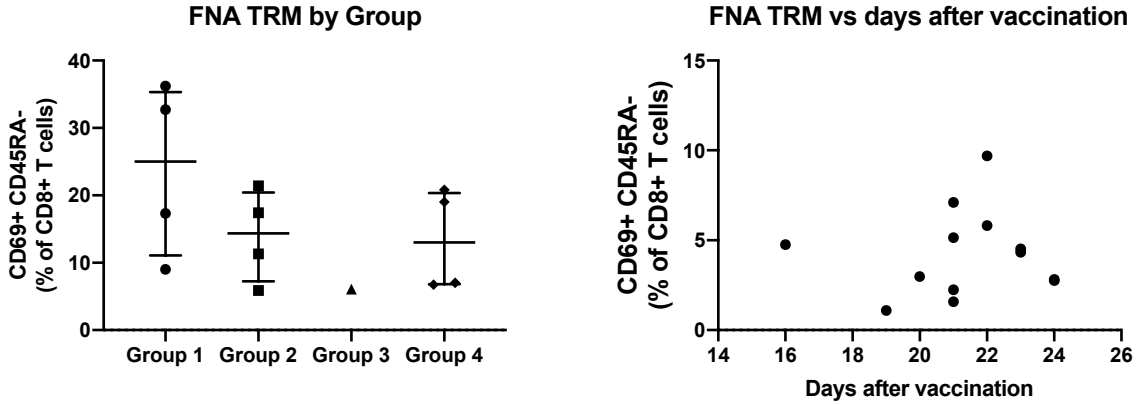


Figure 4.2: Liver TRM by group and time after vaccination. Left, Non-AgSp liver TRM split according to group. Groups differed in terms of viral vector vaccination regimen. Each vaccination was delivered four weeks apart, with the final vaccination being delivered intravenously. Group 1 received CMC, group 2 CMM, group 3 CC and group 4 CM. Bars show median with interquartile range. Right, Non-AgSp liver TRM according to time after IV boost. C, ChAd63 ME-TRAP. M, MVA ME-TRAP.

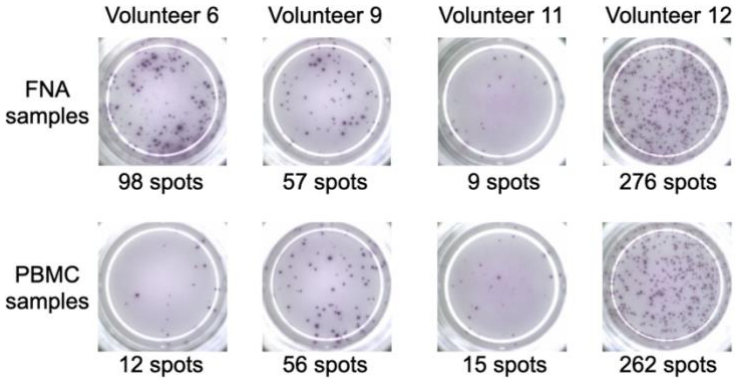


Figure 4.3: ELISpot assays from hepatic and blood samples. Enzyme-Linked Immunospot assays of four volunteer PBMC and FNA samples. PBMC ELISpots were plated with 100,000 lymphocytes, in triplicate. FNA ELISpots were plated with 50,000 lymphocytes, in duplicate. All samples were stimulated with a pool of thrombospondin-related adhesive protein peptides from two species of P. falciparum *or with R10 medium (as a negative control). Images shown here are taken of a representative well, and the numbers are the mean of the technical replicates.*

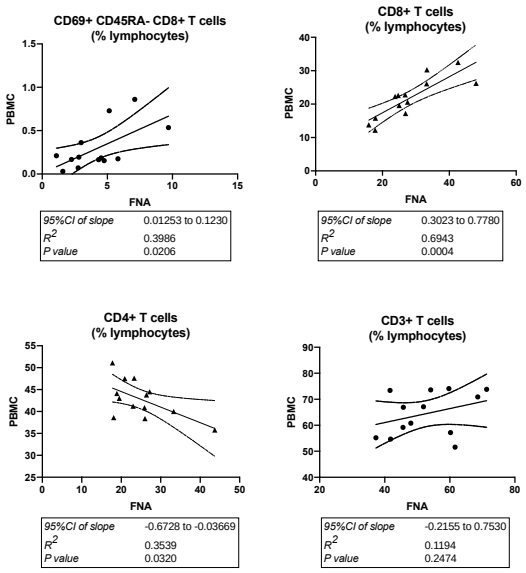
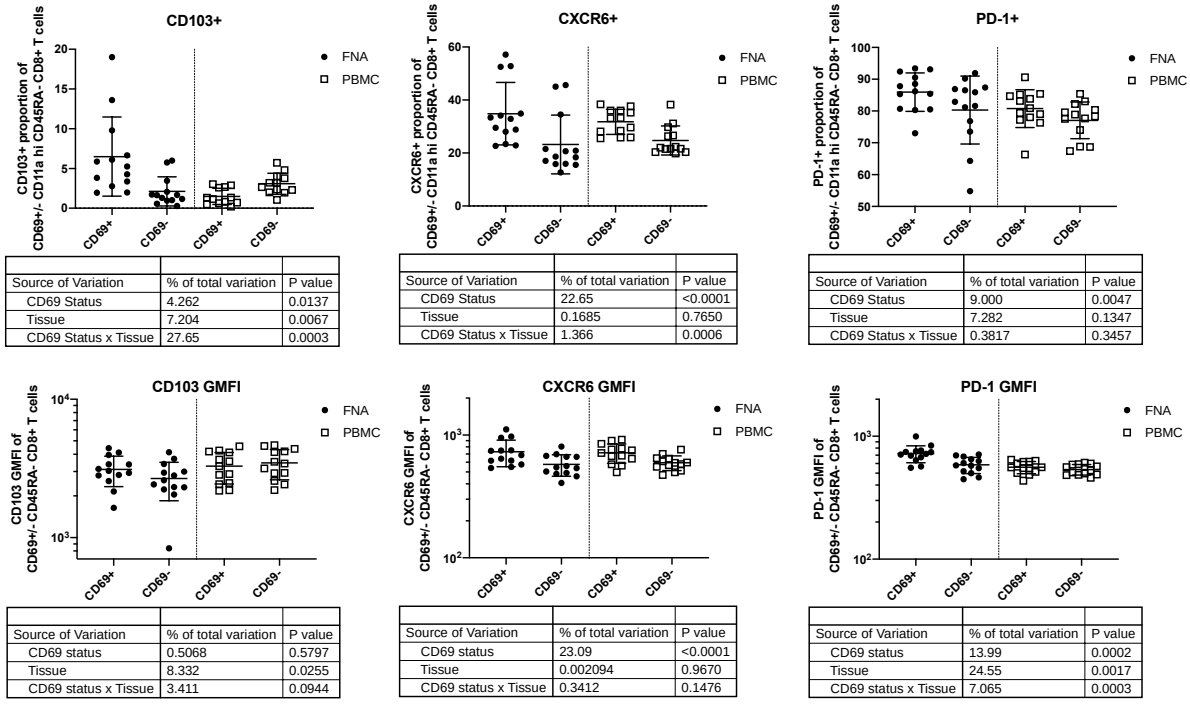


Figure 4.4: Quantitative correlations between liver (FNA) and blood (PBMC) samples. The 95%CI of linear regression slope, R^2 value of goodness of fit and the p value that the slope was significantly non-zero were presented below the respective plots. All plots were derived from 13 matched FNA and PBMC samples. All values were as a proportion of single CD45+ lymphocytes in each sample.



Source of Variation	% of total variation	P value
CD69 Status	4.262	0.0137
Tissue	7.204	0.0067
CD69 Status x Tissue	27.65	0.0003

Source of Variation	% of total variation	P value
CD69 Status	22.65	<0.0001
Tissue	0.1685	0.7650
CD69 Status x Tissue	1.366	0.0006

Source of Variation	% of total variation	P value
CD69 Status	9.000	0.0047
Tissue	7.282	0.1347
CD69 Status x Tissue	0.3817	0.3457

Source of Variation	% of total variation	P value
CD69 status	0.5068	0.5797
Tissue	8.332	0.0255
CD69 status x Tissue	3.411	0.0944

Source of Variation	% of total variation	P value
CD69 status	23.09	<0.0001
Tissue	0.002094	0.9670
CD69 status x Tissue	0.3412	0.1476

Source of Variation	% of total variation	P value
CD69 status	13.99	0.0002
Tissue	24.55	0.0017
CD69 status x Tissue	7.065	0.0003

Figure 4.5: Expression of TRM markers on FNA TRM and PBMC TRM-like cells. TRM/TRM-like (CD69+) cell expression of CD103 (left), CXCR6 (middle) and PD-1 (right) was compared to paired (within-volunteer and within-sample) TEM (CD69-) expression of each marker. Both the positive fraction of cells (top) and the GMFI of the selected markers is presented (bottom). Matching by tissue and CD69 status was performed. A two-way ANOVA was performed to assess the effect of CD69 status and cell tissue origin. Equal variability of differences was assumed when performing the two-way ANOVA (based on a GLM). No multiple comparison corrections were made.

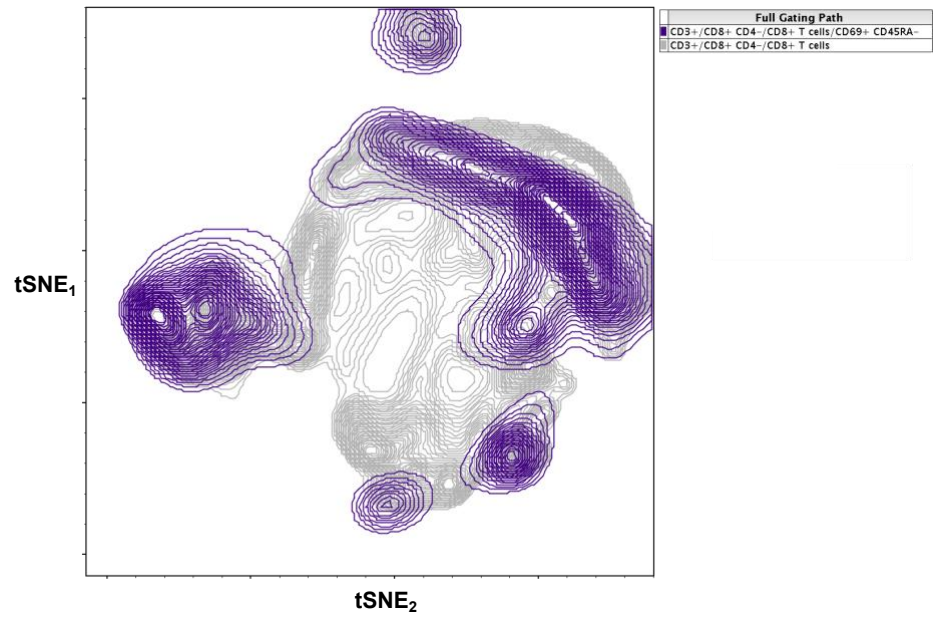


Figure 4.6: Contour tSNE plot of FNA and PBMC CD8+ and CD8+ TRM. Five distinct clusters of CD69+ CD45RA- T cells could be seen. The tSNE algorithm was run using single-cell expression values of 13 markers on 1,068,990 cells pre-gated on CD45+ single live lymphocyte-sized cells. These lymphocytes were derived from all 13 volunteers. Each FNA sample contributed on average 32,760 cells (range 6480-50,000), while each PBMC sample contributed 50,000 cells.

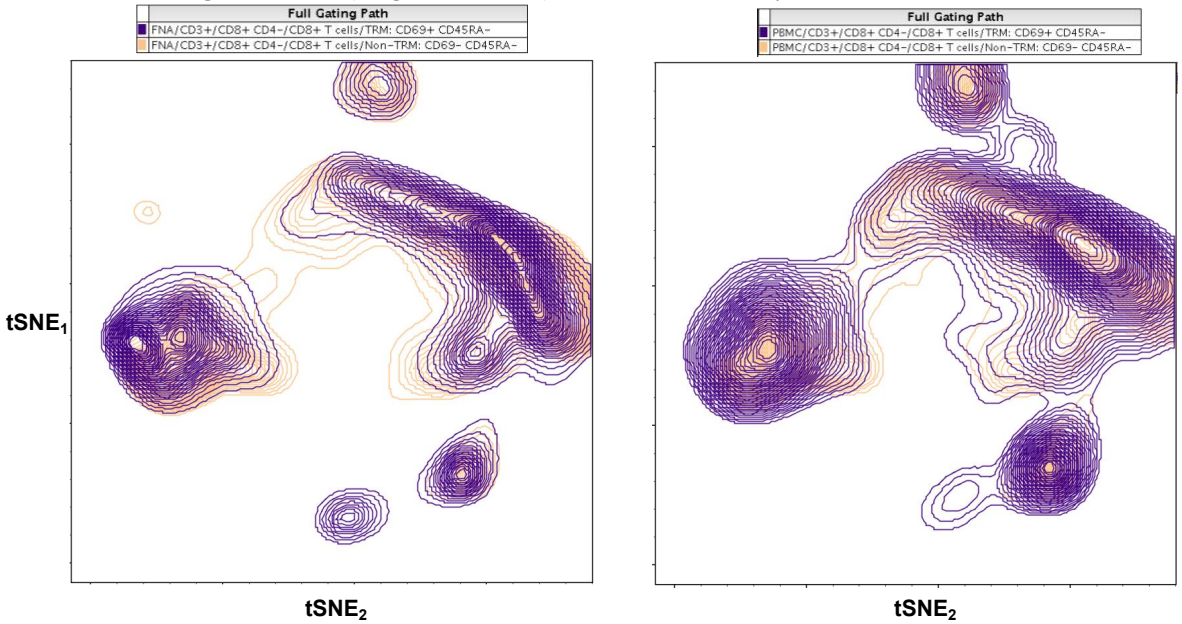


Figure 4.7: Contour tSNE plot of TRM/TRM-like cells compared to TEM (non-TRM) from both tissues. The left plot shows only those cells derived from the liver (FNA), while the right shows those from the blood (PBMC).

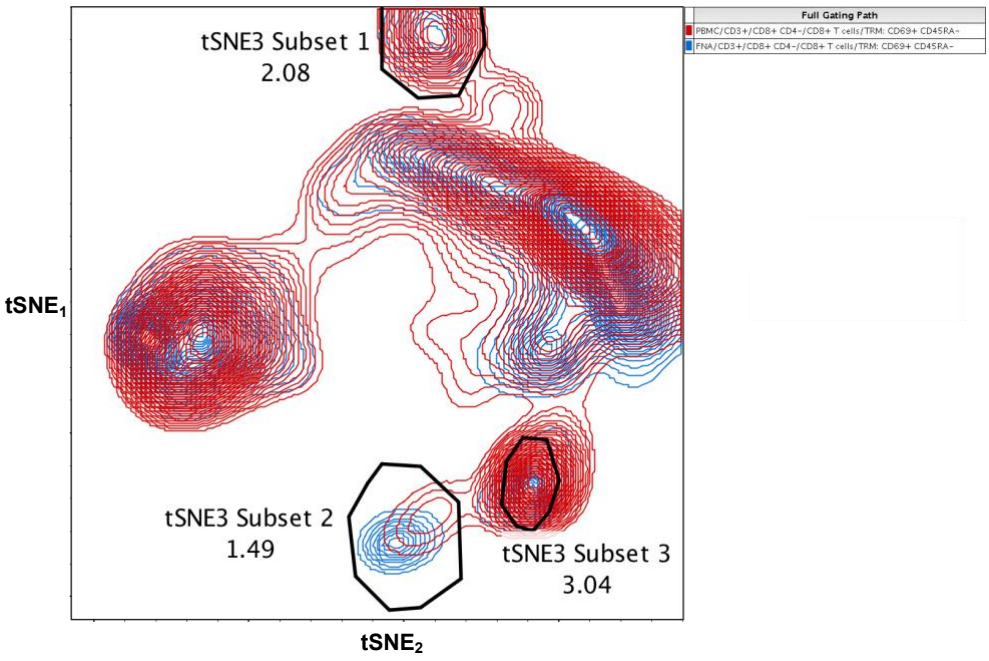


Figure 4.8: Contour tSNE plot of TRM and TRM-like cells. TRM are derived from liver (FNA) samples, and TRM-like cells are from blood (PBMC) samples. Three subsets are presented with the corresponding percentage of total cells. The three subsets have been selected due to their over-representation in CD69+ memory T cells compared to CD69- memory T cells, as shown in the above figures, and their presence in both PBMC and FNA samples.

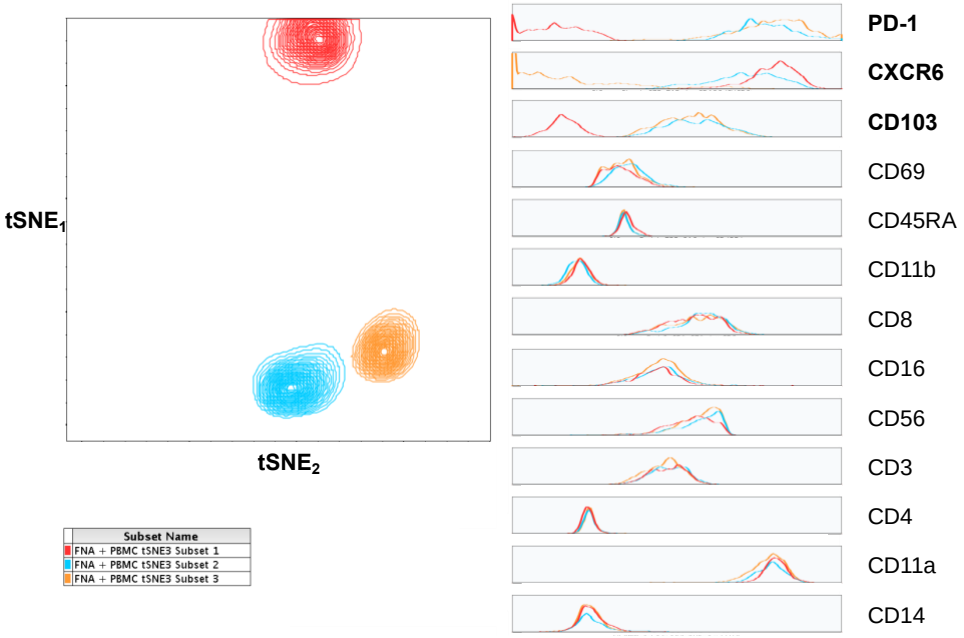


Figure 4.9: Phenotype characterisation of the three tSNE subsets. The three subsets can be differentiated by PD-1, CXCR6 and CD103 expression. The tSNE plot shows the positions of the three subsets and the histograms show the GMFI of the listed markers for the three subsets. The three subsets have been selected due to their over-representation in CD69+ memory T cells compared to CD69- memory T cells.

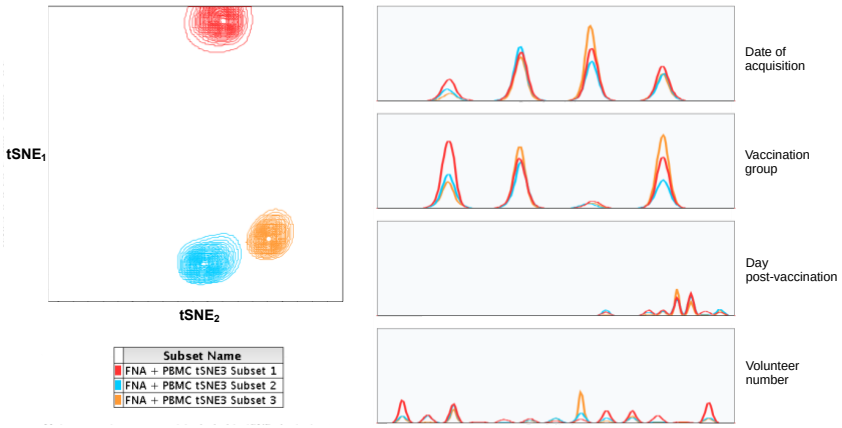


Figure 4.10: Metaparameter characterisation of the three tSNE subsets. tSNE subsets are relatively equally spread across each of the metaparameters. The tSNE plot shows the positions of the three subsets and the histograms show the relative distribution of cells into discrete experimental and technical categories. Metaparameters were not included in the tSNE algorithm. The tSNE algorithm was run using single-cell expression values of 13 markers on 1,068,990 cells pre-gated on CD45+ single live lymphocyte-size. These lymphocytes were derived from all 13 volunteers. Each FNA sample contributed on average 32,760 cells (range 6480-50,000), while each PBMC sample contributed 50,000 cells.

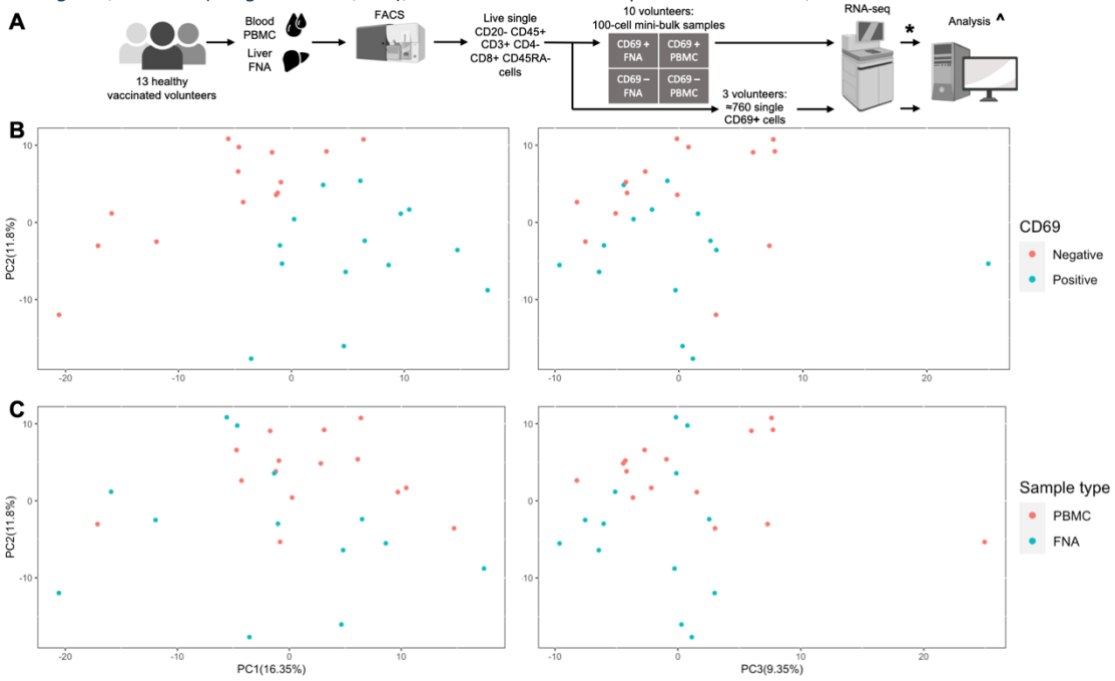


*Figure 4.11: Sequencing experiments overview and bi-plots comparing eigenvectors (PC) 1, 2 and 3. **A**: Sequencing experiments workflow. Fifteen volunteers across all vaccination groups were recruited. Two volunteers were unable to provide samples, due to logistical reasons, and withdrew on the sampling days. Hepatic fine needle aspirate and peripheral venesection were performed within one hour. Lymphocytes were isolated, stained for cell sorting and sorted within three hours of sampling. FNA and PBMC samples from ten volunteers were two-way sorted for 100-cell mini-bulk RNA-seq, and three volunteer samples were sorted for single-cell RNA-seq. Mini-bulk and single-cell RNA-seq results were analysed separately. * represents the mini-bulk QC process, wherein samples from two volunteers were excluded prior to analysis due to low read counts (not included in B, N=8 volunteers). ^ represents QC after analysis, wherein samples from two further volunteers were excluded, one due to excessive variability and the other due to a lack of a sample pair (included in B, but not in differential expression analyses, N=6 volunteers). **B**: Plots of the first three PC, coloured according to CD69 status of the sequenced cells. Separation of CD69+ and CD69- cells was a composite of PC1 and PC2. PC3 did not distinguish CD69 status. **C**: Plots of the first three PC, coloured according to the type of the sample. None of the first three PC separated sample type. Axes are labelled according to the principal component number, and proportion of total variability accounted for by the principal component. Each point represents one sample, composed of 100 single live CD20- CD3+ CD45+ CD8+ CD4- CD45RA- CD69+ or CD69- lymphocytes (from the blood or liver) FACS sorted and sequenced in bulk by the SmartSeq2 protocol. Twenty-eight samples were analysed.*

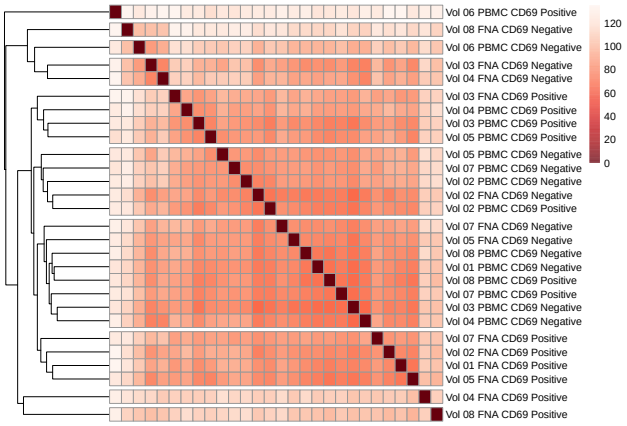


Figure 4.12: Heatmap of sample distances. White corresponds to the maximum distance between samples, that is, that they are least alike. Conversely, more intense reds correspond to the fact that they are more alike. Distances were calculated by measuring the Euclidean distances between samples by using the rlog normalised count number for all detected genes in the sample. The hierarchical clustering tree represents the Euclidean distances. N=8 volunteers.

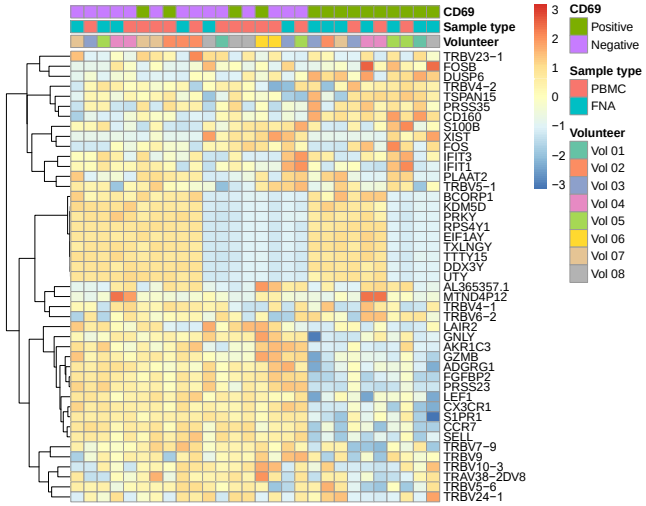


Figure 4.13: Heatmap of the 50 most variable genes between all samples. Yellow/red corresponds to increased counts compared to other samples, and blue corresponds to decreased counts. Genes were selected according to those with the highest variance across samples. All samples that passed primary and secondary QC are presented here (derived from eight volunteers). Rows are clustered according to Pearson correlation of the rlog normalised gene counts. Gene count values are centred and scaled across rows. Five genes showed greatly increased expression in the Vol 06 CD69+ PBMC sample; these were excluded from the heatmap to improve visualisation. The excluded genes were Susd2, Mtrnr2l8, Snord17, Plp1 *and* Al355297.1. *N=8 volunteers.*

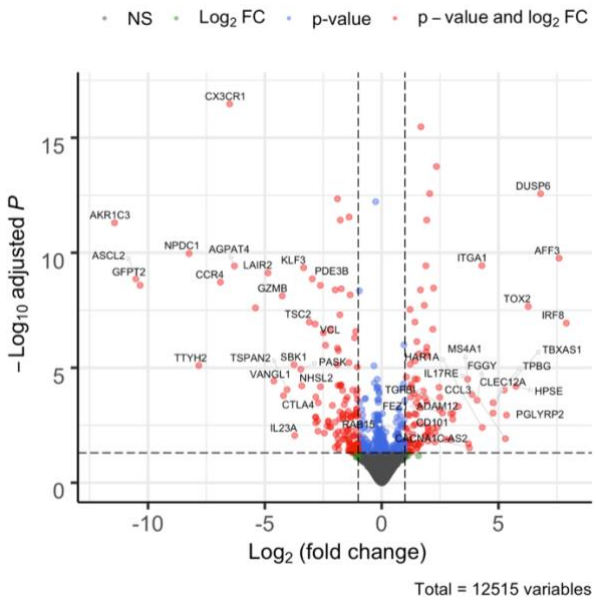


Figure 4.14: Volcano plot of upregulated and downregulated genes between paired FNA CD69+ samples and CD69- samples. The top 50 upregulated and downregulated genes have been annotated. Positive log(FC) values indicate greater gene expression in CD69+ samples, compared to CD69- samples. Negative log(FC) values indicate greater gene expression in CD69- samples. DGE of 12,515 genes was tested for significance using the Wald test. P values were adjusted using the Benjamini-Hochberg correction (FDR). N=6 volunteers.

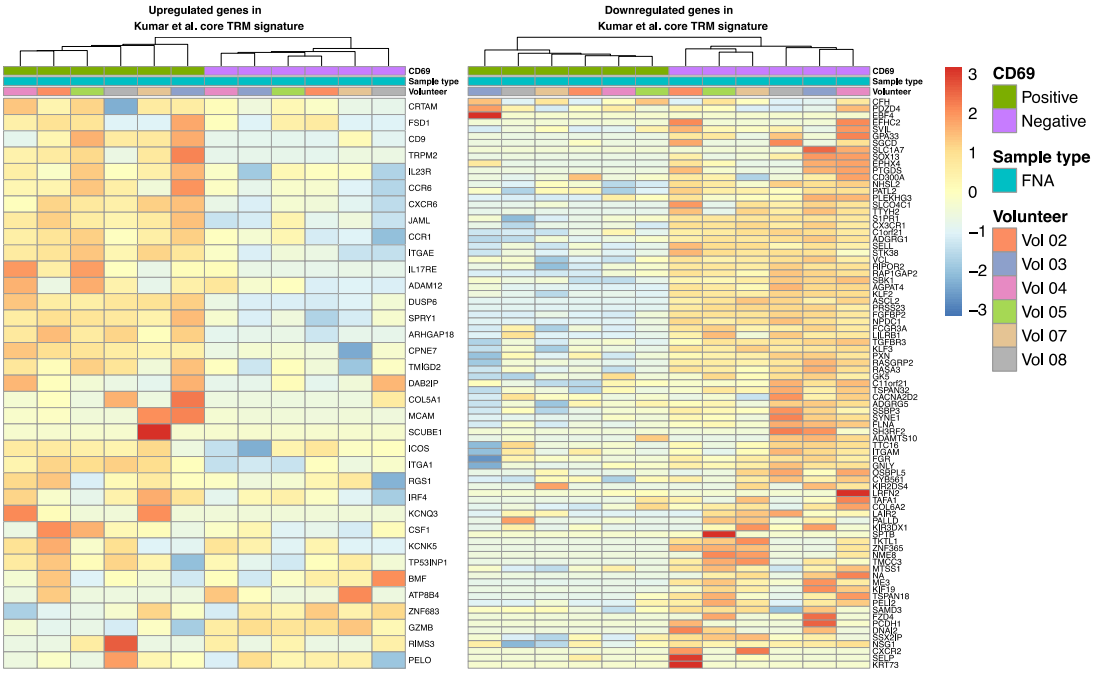


Figure 4.15: Gene heatmap of FNA samples using the core TRM transcriptional signature. Left, heatmap of genes that are upregulated in the CD8+ Kumar et al. core transcriptional signature. Right, heatmap of genes that are downregulated in the CD8+ Kumar et al. core transcriptional signature. Columns are clustered based on Spearman's correlation of sample rlog normalised count values. The clustering tree is not shown. Rows are clustered according to Pearson correlation of the rlog normalised gene counts. Gene count values are centred and scaled across rows. N=6 volunteers.

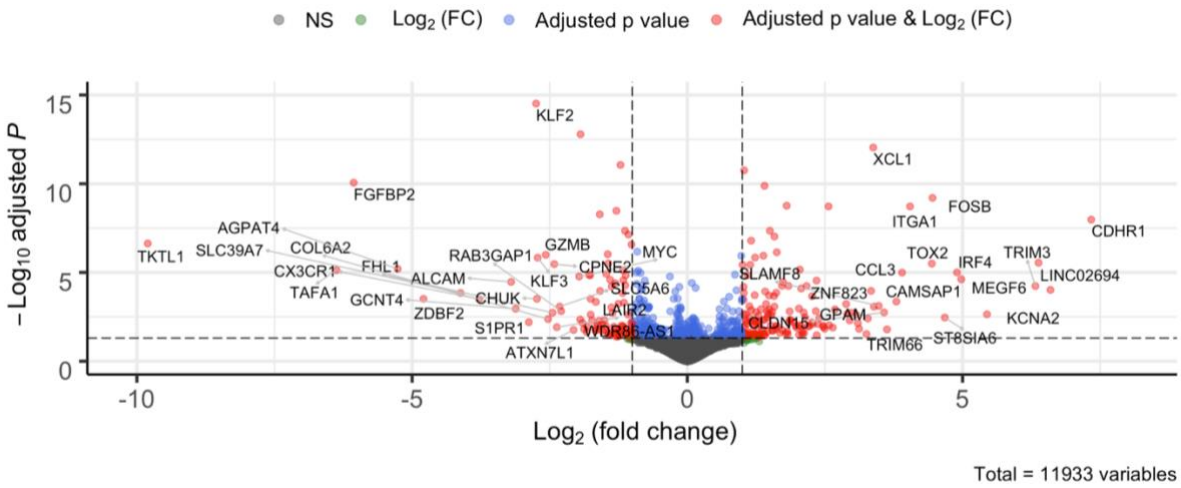


Figure 4.16: Volcano plot of upregulated and downregulated genes between paired FNA CD69+ samples and PBMC CD69+ samples. The top 50 upregulated and downregulated genes have been annotated. Positive log(FC) values indicate greater gene expression in FNA CD69+ samples, compared to PBMC CD69+ samples. Negative log(FC) values indicate greater gene expression in PBMC CD69+ samples. DGE of 11,933 genes was tested for significance using the Wald test. P values were adjusted using the Benjamini-Hochberg correction (FDR). N=6 volunteers.

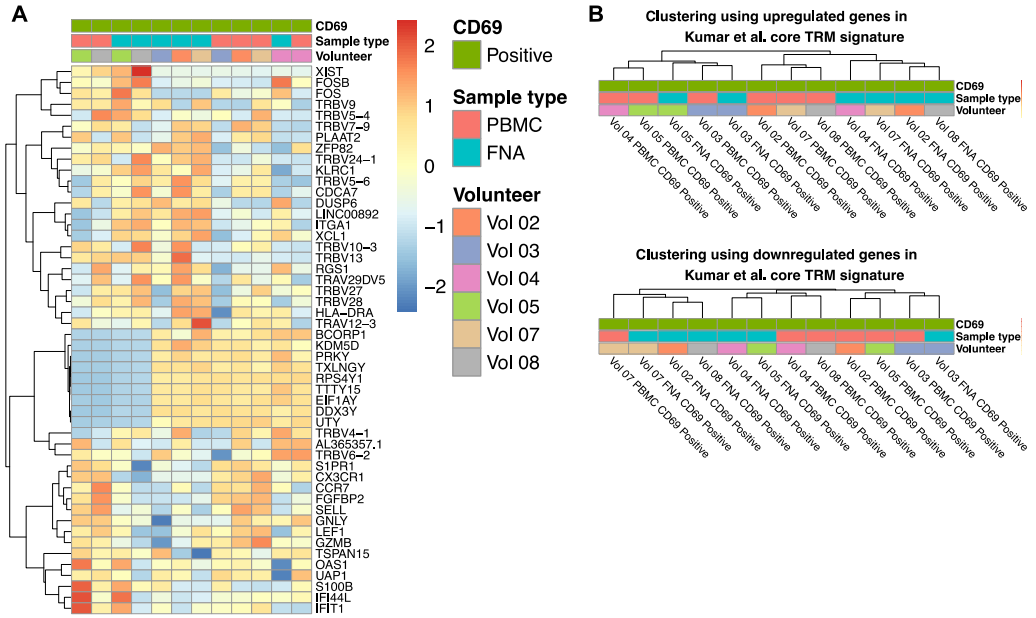


*Figure 4.17: Heatmap and clustering of the FNA CD69+ vs PBMC CD69+ comparison. **A**: 50 most variable genes between FNA CD69+ and PBMC CD69+ samples. Yellow/red corresponds to increased counts compared to other samples, and blue corresponds to decreased counts. Genes were selected according to those with the greatest variance across samples. Columns are clustered based on Spearman's correlation of rlog normalised count values. Rows are clustered according to Pearson correlation of the rlog normalised gene counts. Gene count values are centred and scaled across rows. **B**: hierarchical clustering trees based on Spearman's correlation of sample rlog normalised count values considering upregulated and downregulated genes in CD8+ Kumar et al. core TRM transcriptional signature. N=6 volunteers.*

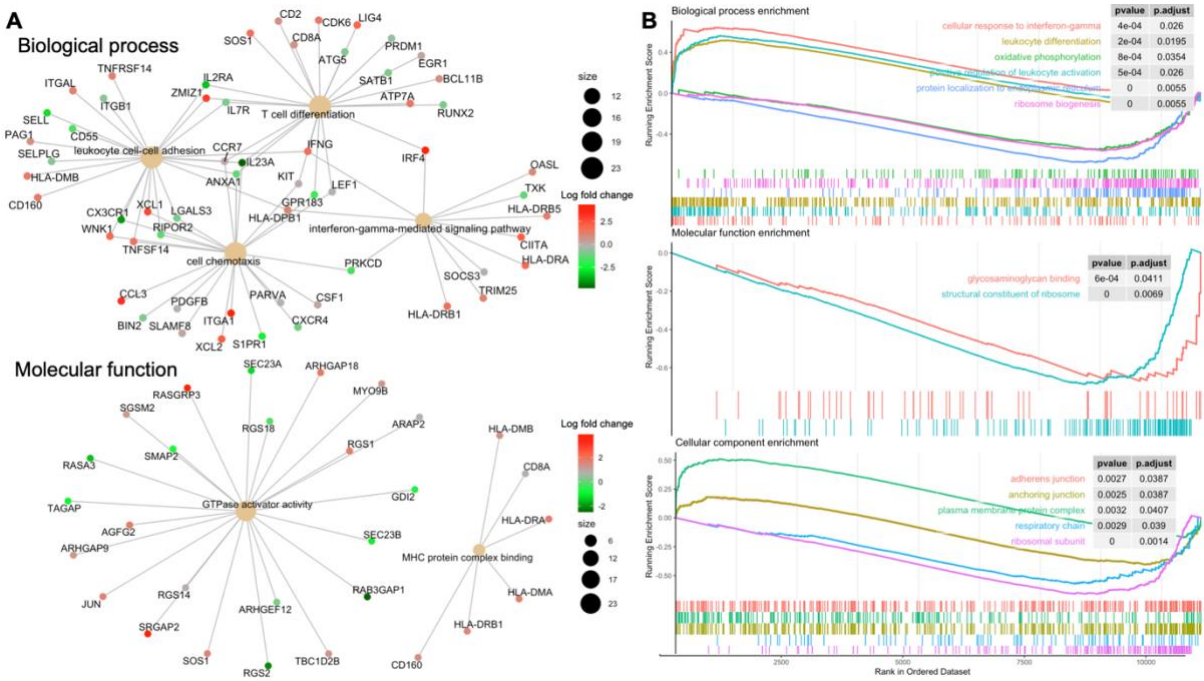


Figure 4.18: ORA and GSEA plots for gene ontology categories of the FNA CD69+ vs PBMC CD69+ comparison. ***A****: Over-representation analysis gene-concept network plots for enriched Gene Ontology biological process and molecular function categories. A hypergeometric test was used to test for significance of gene category over-representation. Gene categories presented had an FDR<0.05. Size refers to the number of genes involved in the category.* ***B****: Gene set enrichment analyses visualised by category running enrichment score among the pre-ranked list of all 11,933 differentially expressed genes. A category's enrichment score is the maximum deviation from zero encountered in the running score. If the normalised enrichment score is positive, this suggests enrichment of the category in FNA CD69+ samples. A negative normalised enrichment score suggests enrichment of the category in PBMC CD69+. GTPase, guanosine triphosphate hydrolase. p.adjust, Benjamini-Hochberg adjusted p value.*

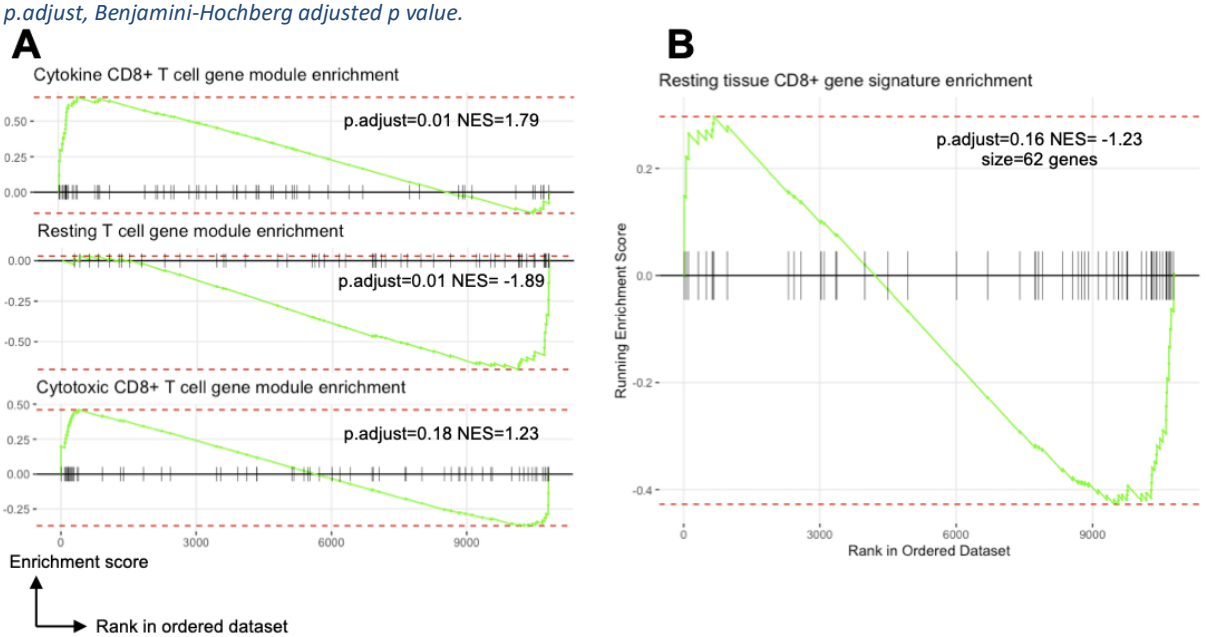


Figure 4.19: GSEA plots for Szabo et al. gene sets in the FNA CD69+ vs PBMC CD69+ comparison. Gene set enrichment analyses visualised by category running enrichment score among the pre-ranked list of all 11,933 differentially expressed genes. A category's enrichment score is the maximum deviation from zero encountered in the running score. If the normalised enrichment score is positive, this suggests enrichment of the category in FNA CD69+ samples. A negative normalised enrichment score suggests enrichment of the category in PBMC CD69+. The ranked list metric is the binary logarithm of the fold change of gene expression between FNA CD69+ and PBMC CD69+ cells. ***A****: Enrichment plots of gene expression modules related to T cell transcriptional states identified by Szabo and colleagues. The CD8+ cytokine module includes genes encoding chemokines and cytokines (*Ccl3, Ccl4, Ccl20*) and inhibitory molecules (*Lag3, Cd226, Havcr2*). The resting T cell module involves genes necessary for CD4+ and CD8+ T cell survival in blood and in tissues. The CD8+ cytotoxic module includes genes associated with cytotoxicity (*Gnly, Gzmk*) and transcription factors associated with*

*effector/memory differentiation (*Zeb2, Eomes, Znf683*). NES is the enrichment score normalised to the mean enrichment of random samples of the same size.* ***B****: Enrichment plot of a tissue CD8+ T cell signature identified by Szabo and colleagues. The complement of genes is derived by differential expression analyses between resting CCL5++ CD8+ memory T cells from several tissues compared to blood.*

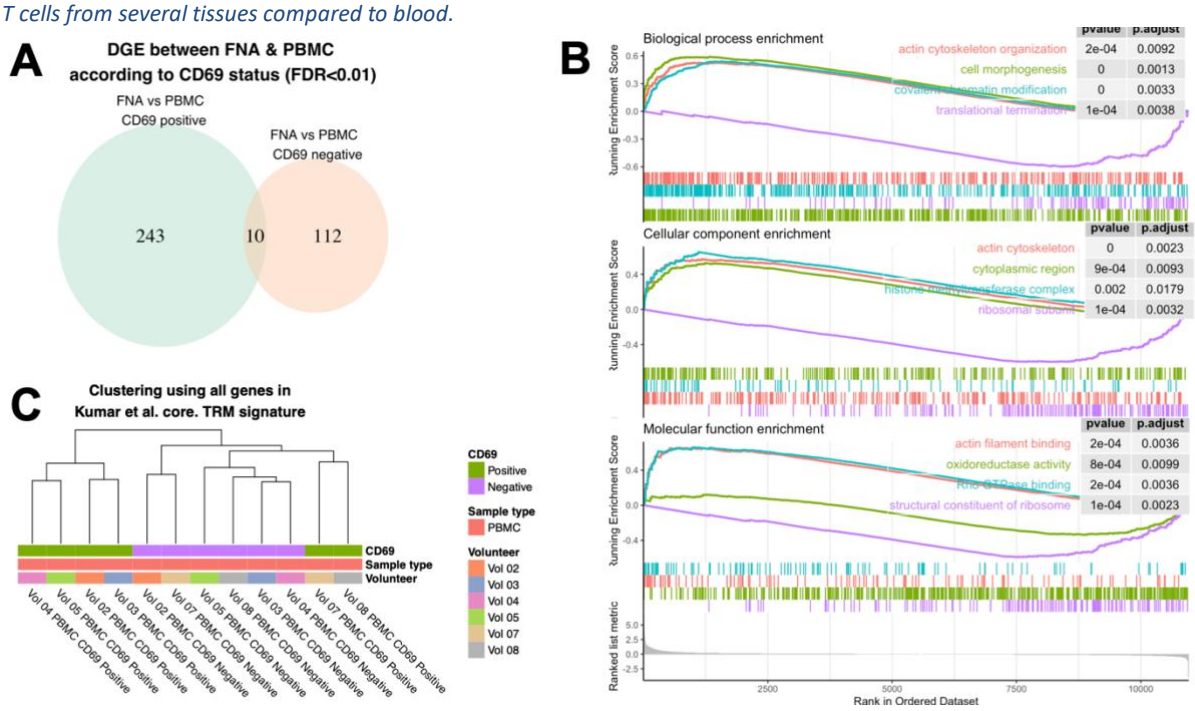


Figure 4.20: FNA CD69- vs PBMC CD69-, and PBMC CD69+ vs CD69- comparisons. ***A****: Venn diagram demonstrating the overlap of genes that are in both FNA vs PBMC comparisons (where CD69+ cells are compared, left blue circle, and CD69- cells, right orange circle). All genes had an FDR<0.01.* ***B****: Pathway analysis for FNA CD69- vs PBMC CD69- comparison. Gene set enrichment analyses visualised by category running enrichment score among the pre-ranked list of all 12,062 differentially expressed genes. A category's enrichment score is the maximum deviation, from zero, encountered in the running score. If the normalised enrichment score is positive, this suggests enrichment of the category in FNA CD69- samples. A negative normalised enrichment score suggests enrichment of the category in PBMC CD69-. All the categories presented had an FDR<0.05. See Chapter 2 for a full description of the enriched gene signatures.* ***C****: Hierarchical clustering tree based on Spearman's correlation of sample rlog normalised count values considering all genes in CD8+ Kumar et al. core TRM transcriptional signature. N=6 volunteers.*

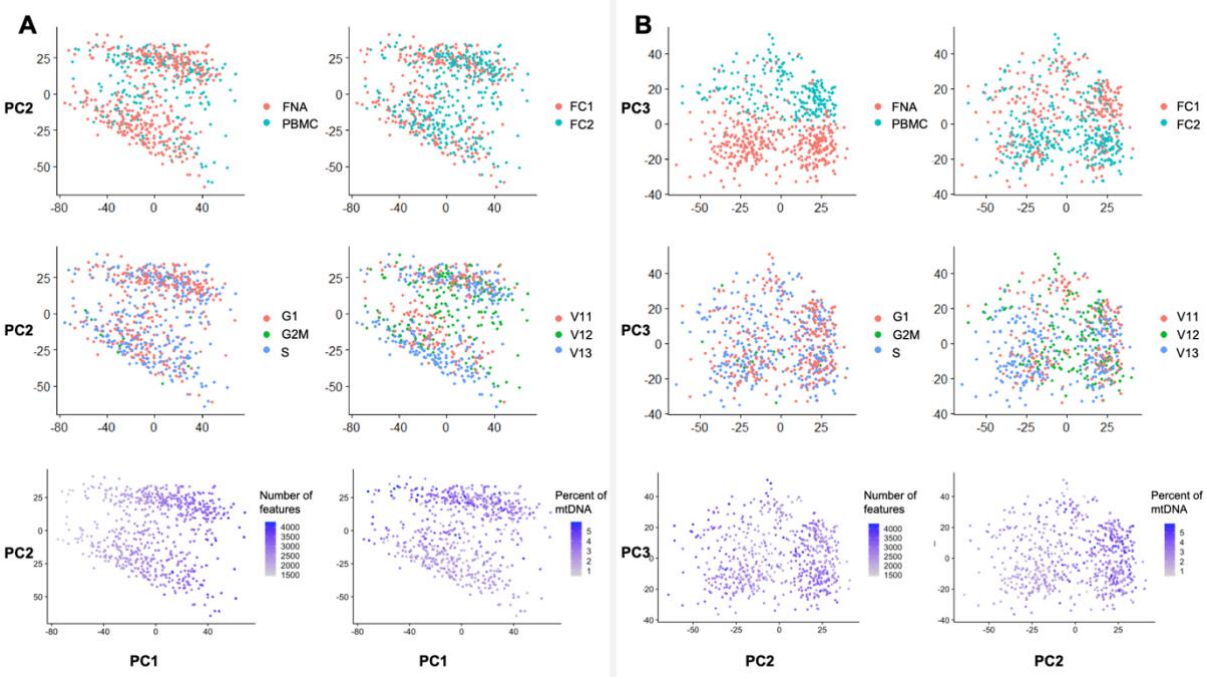


Figure 4.21: Bi-plots comparing eigenvectors (PC) 1, 2 and 3 in scRNA-seq samples. PCA was based on the 500 most variable genes amongst all samples. ***A****: Plots of the first two PC, according to various technical and biological parameters. PC1 is associated with the number of features per cell. PC2 does not appear to be substantially separated by the presented*

*parameters. **B**: Plots of the PC2 and PC3, according to various technical and biological parameters. PC3 appears to separate PBMC and FNA cells. Each point represents one cell, either a PBMC or FNA live single CD20- CD3+ CD45+ CD8+ CD4- CD45RA- CD69+ lymphocyte FACS sorted and sequenced in plates by the SmartSeq2 protocol. Six hundred and twenty-nine cells are presented in this PCA. FACS, fluorescence-assisted cell sorting. FC, flow cell. G1, gap 1 cell cycle phase. G2, gap 2 cell cycle phase. mtDNA, mitochondrial DNA. S, synthesis cell cycle phase. V, volunteer.*

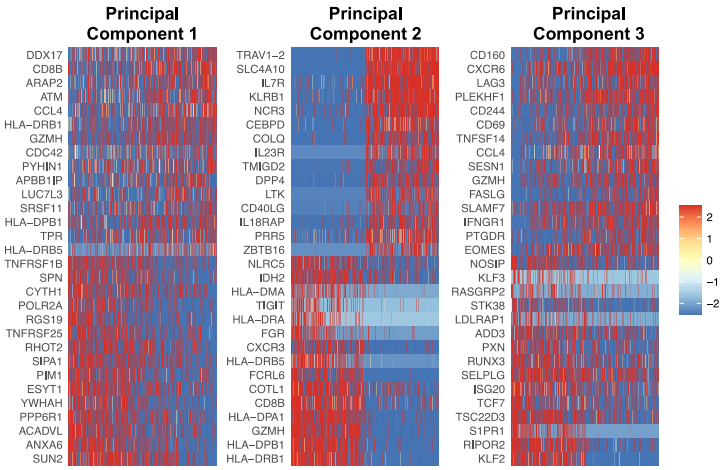


Figure 4.22: Top 30 most variable genes in PC1-3. Dimensional reduction heatmap visualising the sources of heterogeneity in PC1, 2 and 3. Fifteen genes with the most negative or positive contribution to PCA loadings (scores), respectively, were selected to demonstrate maximum heterogeneity. Colour corresponded to row (gene) scaled variance.

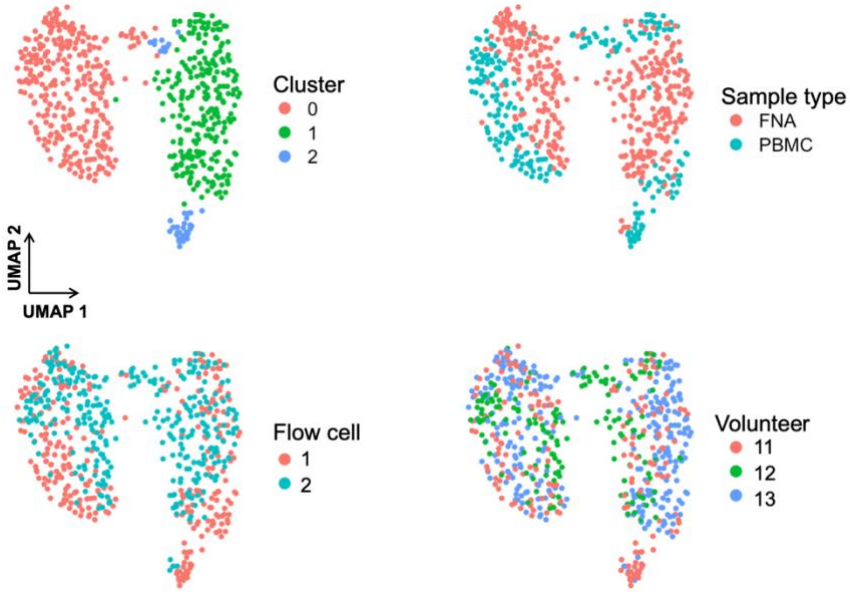


Figure 4.23: UMAP of 629 single cells. Plots according to cluster, sample type, flow cell and volunteer. Seurat FindClusters was run at 0.4 resolution, using a shared nearest neighbour clustering method. Each point represents one cell, either a PBMC or FNA live single CD20- CD3+ CD45+ CD8+ CD4- CD45RA- CD69+ lymphocyte FACS sorted and sequenced by using the SmartSeq2 protocol. Six hundred and twenty-nine cells are presented in these plots.

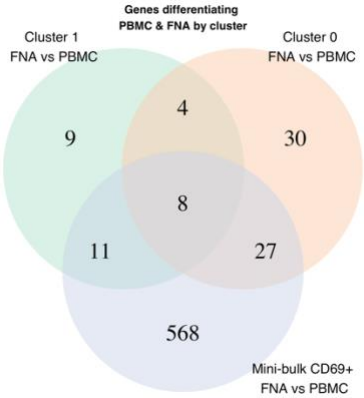


Figure 4.24: Venn diagram of genes differentiating FNA and PBMC cells. Venn diagram demonstrating the degree of convergence of cluster-level DGE and mini-bulk-level DGE. All included genes from single-cell contrasts had a |ln(FC)|>0.25 and an adjusted p value (Bonferroni correction)<0.05 and the genes from mini-bulk contrasts had $|log_2(FC)|>1$ and an FDR<0.05.

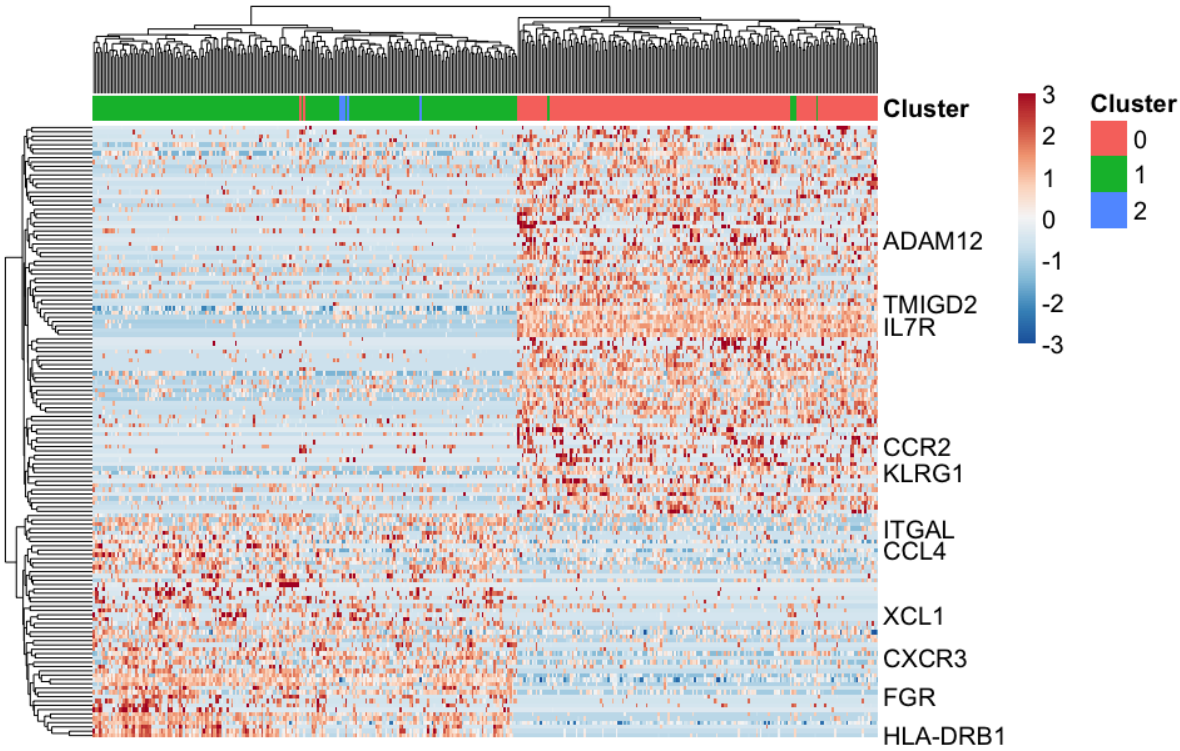


Figure 4.25: Heatmap of the C1 FNA vs C0 FNA cell comparison. There were 142 differentially expressed genes, with a selection shown here. Clusters derived from Seurat clustering shown in Figure 4.23. Cell gene counts centred and scaled across all row values. All genes shown here were present in at least 50% of cells in each cluster, had |ln(FC)|>0.5 and an adjusted p value (Bonferroni correction)<0.05. The row hierarchical clustering dendrogram is based on Euclidean distances of cell gene count values considering all genes.

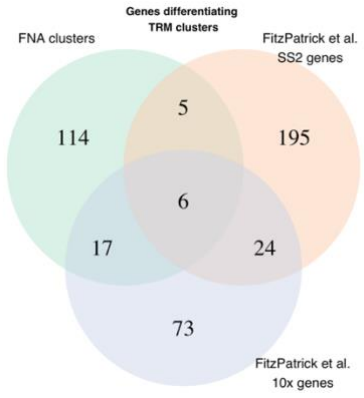


Figure 4.26: Venn diagram of genes differentiating TRM clusters. Venn diagram demonstrating the degree of convergence of C1 vs C0 DGE, of an SS2 experiment detailed in FitzPatrick et al. and of a 10x (droplet-based scRNA-seq platform)

experiment detailed in FitzPatrick et al. (444). All genes in FNA cluster (C1 vs C0) DGE were present in at least 50% of cells in each cluster, had |ln(FC)|>1 and an adjusted p value (Bonferroni correction)<0.05. Genes in the SS2 list were identified using DEsingle (453) and were significantly differentially expressed at an adjusted p value (Bonferroni correction)<0.05. Genes in the 10x list were generated using Wilcoxon rank-sum test and were present in at least 50% of cells in each cluster, had |ln(FC)|>1 and an adjusted p value (Bonferroni correction)<0.05. SS2, Smart-Seq2.

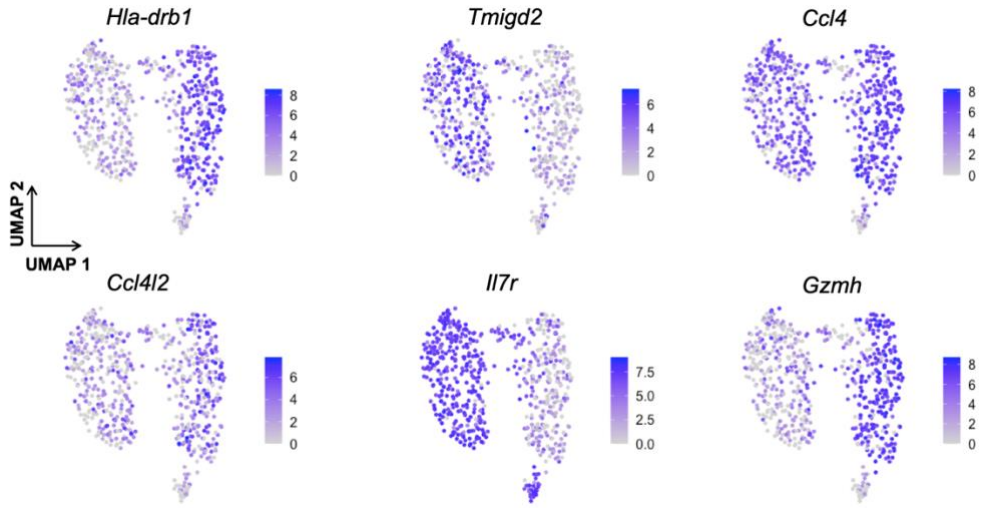


Figure 4.27: Gene expression in genes differentiating TRM clusters. All genes were present in at least 50% of cells in each cluster, had |ln(FC)|>0.5 and an adjusted p value (Bonferroni correction)<0.05. These genes were differentially expressed by all experiments referred to in Figure 4.26.

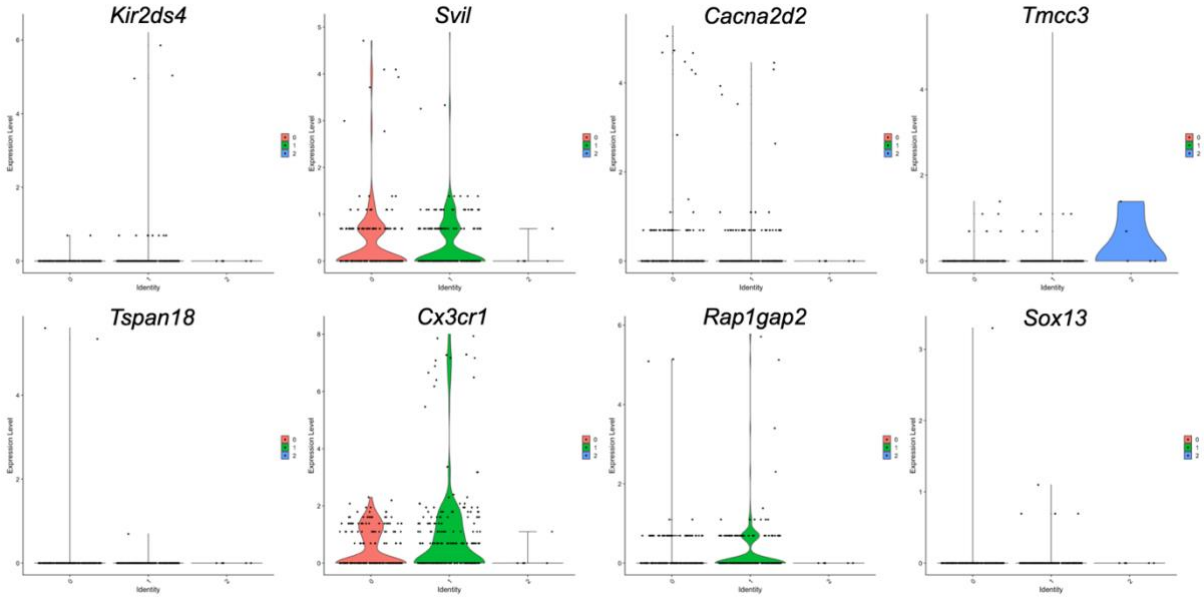


Figure 4.28: Violin plots of genes downregulated in Kumar et al. core TRM signature. Plots show the uniformly low or absent expression of genes in all three clusters.

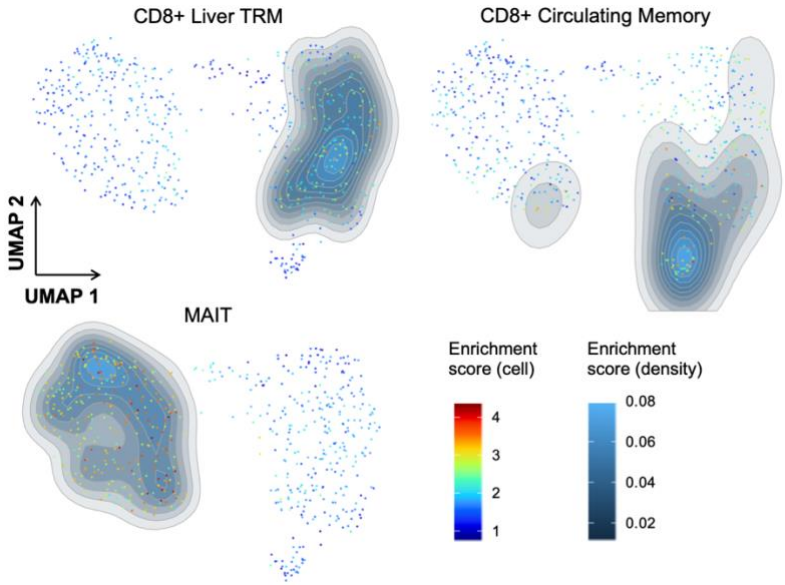


Figure 4.29: UMAP plots with signature enrichment scores. The enrichment of three signatures was assessed for each of the 629 cells and visualised in the UMAP by Single-Cell Signature Explorer (390). The per-cell signature enrichment was plotted, and density distribution of scores was overlaid. The signature scores represent a qualitative measure for visualisation. The signatures were obtained from Zhao et al. (445).

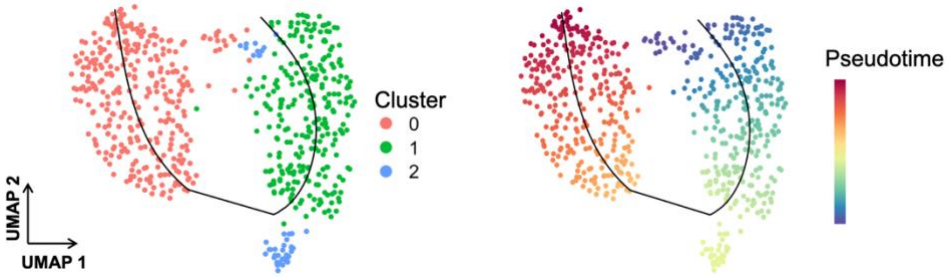


Figure 4.30: Pseudotime trajectory superimposed on clusters and cells coloured by pseudotime. Left, Slingshot was used to determine pseudotime trajectory, and Seurat FindClusters was run at 0.4 resolution to define clusters. Right, pseudotime value represented by cell colour. Maroon represents one extreme of pseudotime, blue the other.

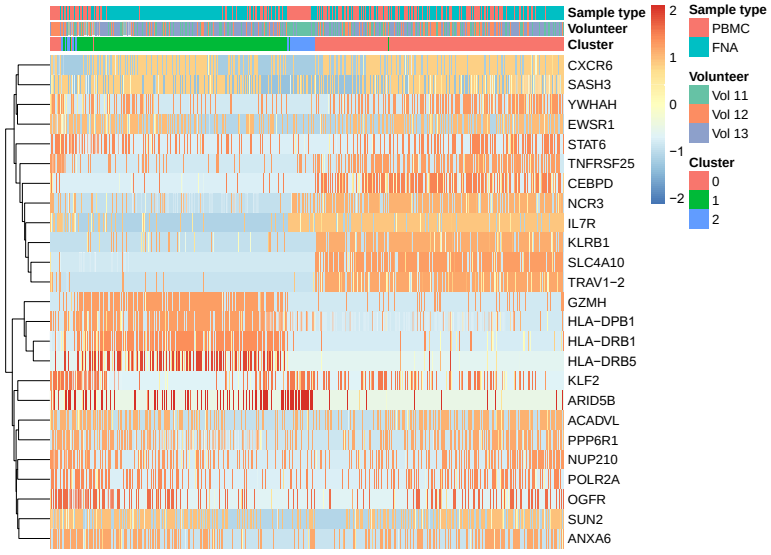


Figure 4.31: Pseudotemporally associated genes. The top 25 genes with the greatest variance across pseudotime. The expression of these genes changes in a continuous manner over pseudotime. Cell gene count is centred and scaled across all row values. The row hierarchical clustering dendrogram is based on Euclidean distances of cell gene count values considering all genes.

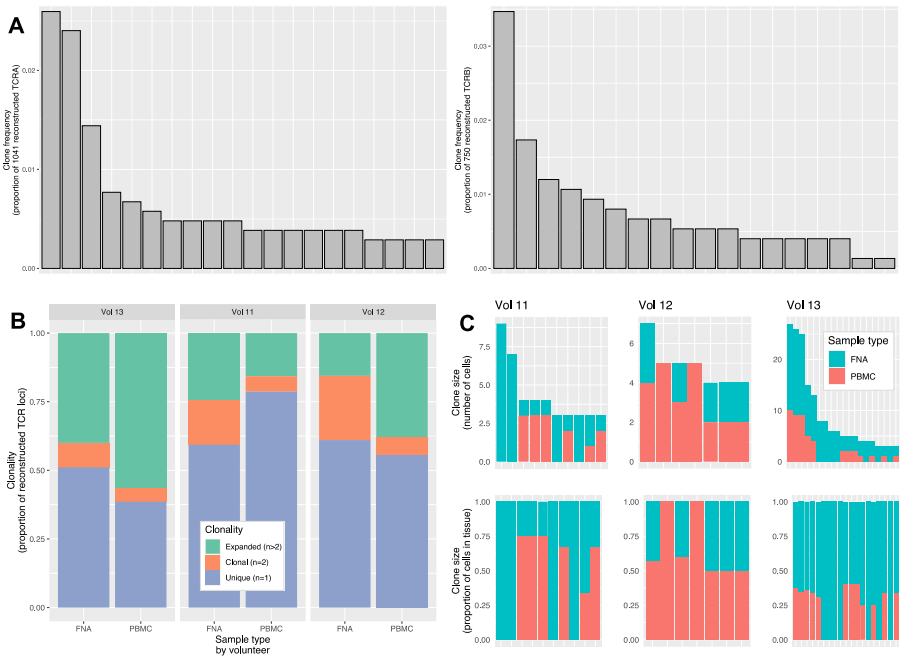


*Figure 4.32: T cell clonality and clone size. **A**: TCR α (left) and β (right) loci clone frequency. Bars represent individual clones, and bar height represents clone frequency. A clone was defined as any number of cells that had the exact same (α or β) TCR loci and CDR3 nucleotide sequence. Clones with more than two cells are displayed here. Non-productive recombinants and recombinants derived from MAIT cells were excluded from these analyses. Clone sizes are reported as a frequency, in relation to the total number of reconstructed TCR recombinants. **B**: Clonality by volunteer and sample type. Alpha and β TCR loci recombinants categorised according to whether they were expanded (shared by more than two cells), clonal (present in two cells) or unique (present in one cell). **C**: Clone size by volunteer and sample type. Bars represent individual clones. Total clone size (top) expressed as the number of cells sharing α or β locus TCR recombinants, and the proportion of the clone (bottom) present in each sample type. Clones with more than two cells are displayed here. TCRA, T cell receptor α locus. TCRB, T cell receptor β locus.*

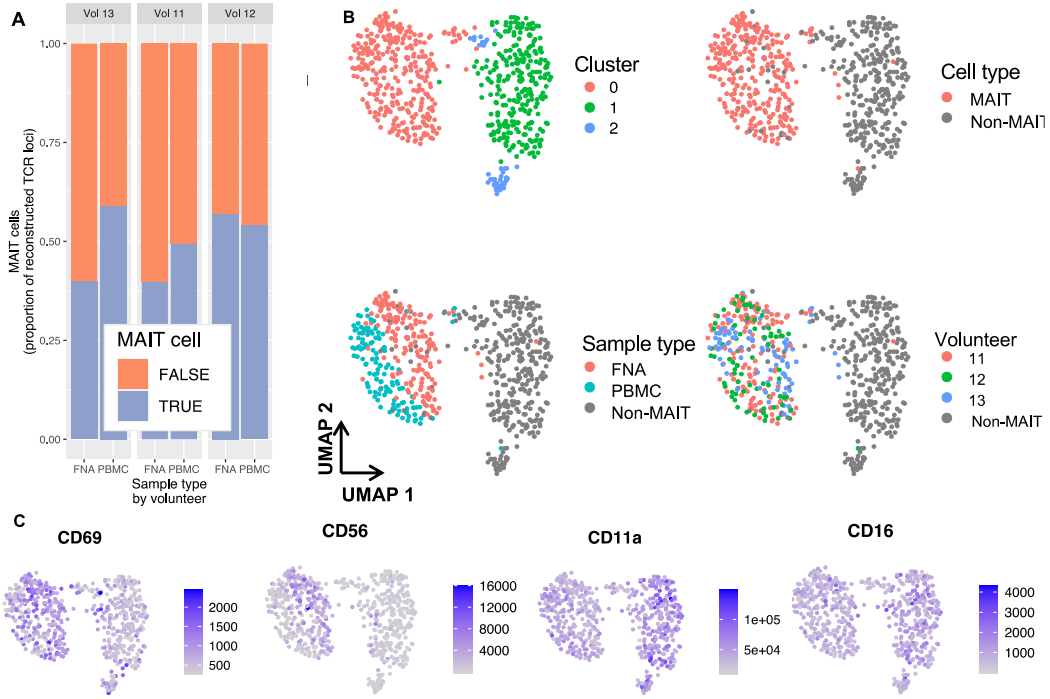


*Figure 4.33: MAIT clones and cells. **A**: Proportion of recombinants that were derived from MAIT cells. MAIT cells were defined based on TCR α locus: any cell that expressed TRAV1-2 paired with TRAJ33, TRAJ12 or TRAJ20 was defined as a MAIT cell, regardless of the TCR β locus recombinant, if present. Any recombinant derived from a MAIT cell was labelled as such and excluded from non-MAIT cell analyses. **B**: UMAP of 629 single cells with plots according to cluster, MAIT cell TCR, sample type and volunteer. In all plots, grey points ("non-MAIT") represent cells that were either not classified as MAIT cells or cells for which TCR reconstruction could not be performed. Seurat FindClusters was run at 0.4 resolution,*

using a shared nearest neighbour clustering method. Each point represents one cell, either a PBMC or FNA live single CD20- CD3+ CD45+ CD8+ CD4- CD45RA- CD69+ lymphocyte FACS sorted and sequenced by using the SmartSeq2 protocol. Six hundred and twenty-nine cells are presented in these plots. ***C****: Index sort information obtained at the time of single-cell isolation for CD69, CD56, CD11a and CD16 molecules. Values represent fluorochrome GMFI that has been compensated, but not transformed.*

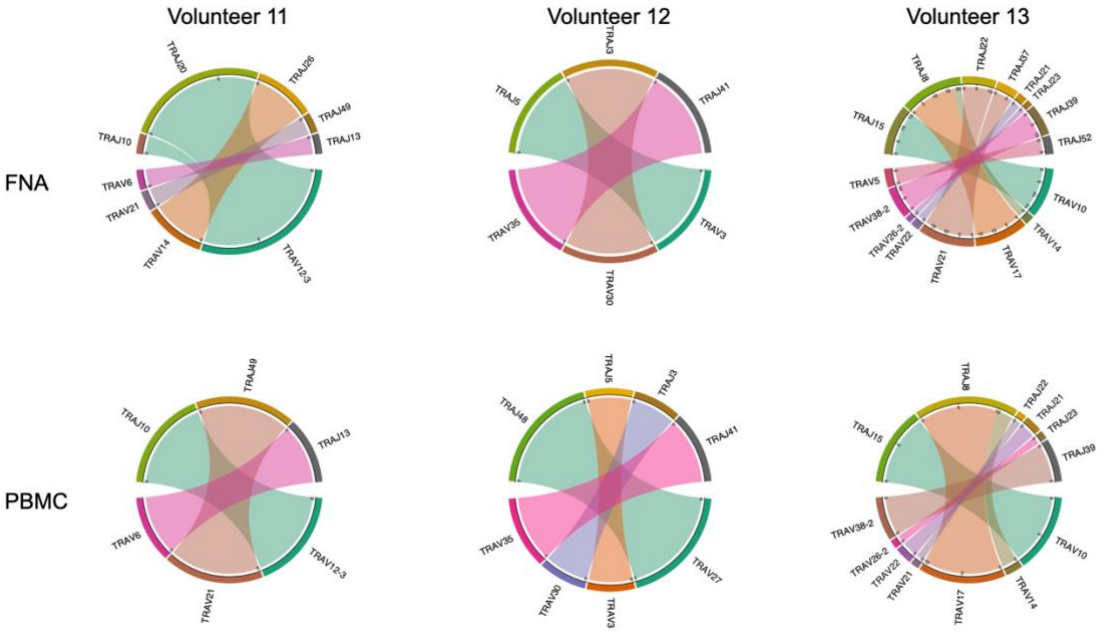


Figure 4.34: TCR α chain usage of clonal T cells by sample and volunteer. Chain pairing of TRAV and TRAJ are displayed as chord diagrams where ribbons connecting arcs indicate the frequency of chain pairing. Only clones of greater than two cells with productive recombinants were included in these analyses. MAIT cells were excluded from these analyses. Ticks on the inside of the arcs are present for every five cells that shared the recombinant. Recombinant totals: volunteer 11 FNA n=13, PBMC n=8; volunteer 12 FNA n=6, PBMC n=12; and volunteer 13 FNA n=75, PBMC n=30. TRAV, TCR α chain variable region. TRAJ, TCR α chain joining region.

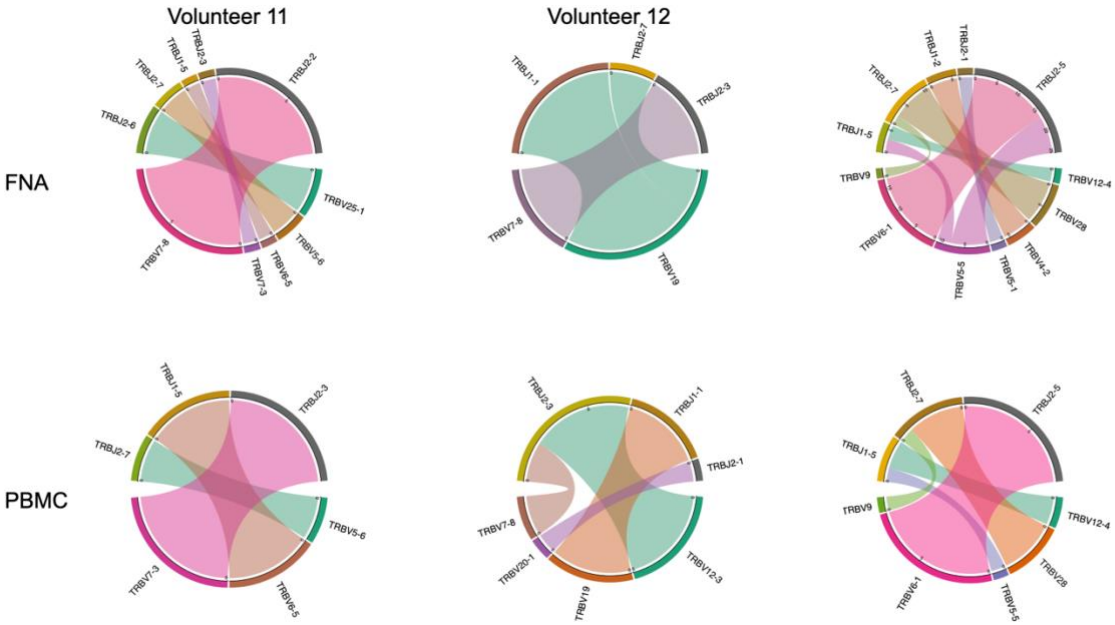


Figure 4.35: TCR β chain usage of clonal T cells by sample and volunteer. Chain pairing of TRBV and TRBJ are displayed as chord diagrams where ribbons connecting arcs indicate the frequency of chain pairing. Only clones of greater than two cells and productive recombinants were included in these analyses. MAIT cells were excluded from these analyses. Ticks on the inside of the arcs are present for every five cells that shared the recombinant. Recombinant totals: volunteer 11

FNA n=16, PBMC n=6; volunteer 12 FNA n=6, PBMC n=12; and volunteer 13 FNA n=51, PBMC n=17. FNA, fine needle aspirate. TRBV, TCR β chain variable region. TRBJ, TCR β chain joining region.

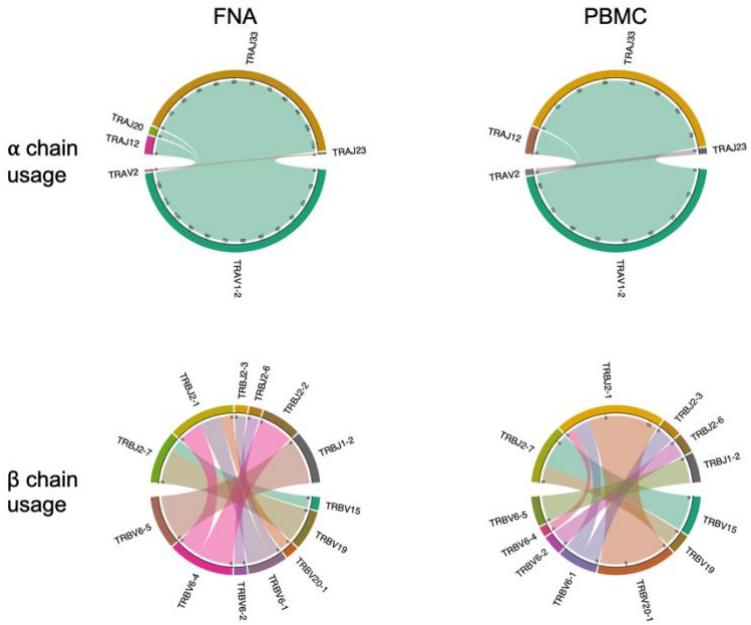


Figure 4.36: TCR α and β chain usage of MAIT cells by sample. Chain pairing of MAIT TRAV and TRAJ, and TRBV and TRBJ are displayed as chord diagrams where ribbons connecting arcs indicate the frequency of chain pairing. Only clones of greater than two cells and productive recombinants were included in these analyses. Ticks on the inside of the arcs are present for every five cells that shared the recombinant. MAIT cells were defined based on TCR α locus: any cell that expressed TRAV1-2 paired with TRAJ33, TRAJ12 or TRAJ20 was defined as a MAIT cell, regardless of the TCR β locus recombinant, if present. Any recombinant derived from a MAIT cell was labelled as such and included in these analyses. Recombinant totals: TCR α FNA n=128, PBMC n=86; and TCR β FNA n=18, PBMC n=24.

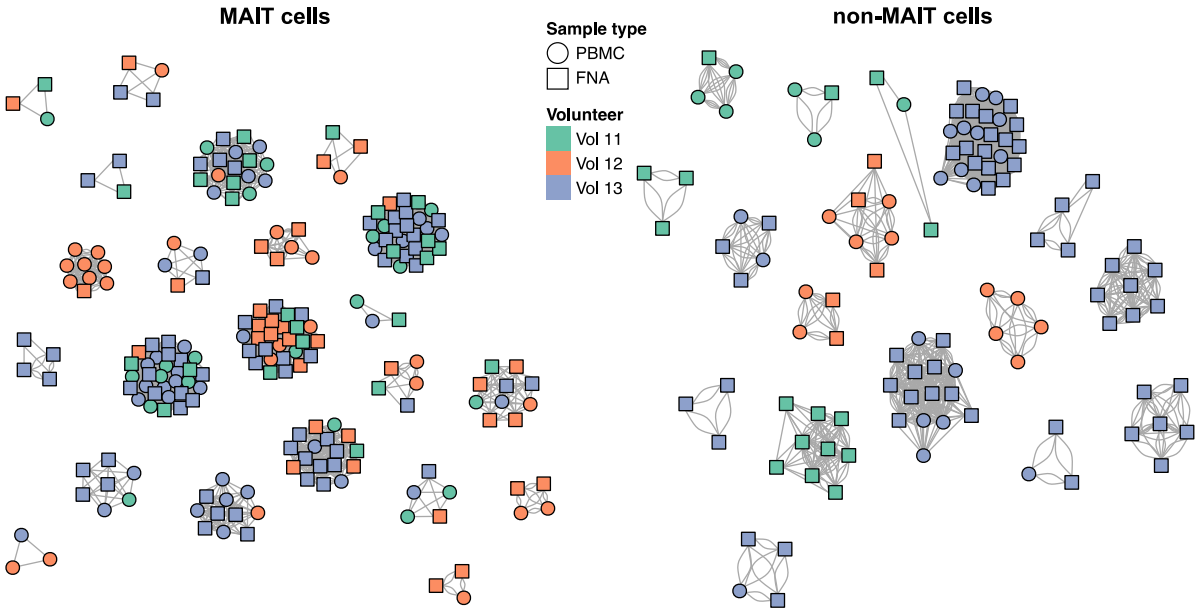


Figure 4.37: Clonal relationships between MAIT and non-MAIT cells. The number of recombinants shared between MAIT (left) and non-MAIT (right) cells. Nodes (vertices) represent individual cells and links (edges) represent a unique recombinant shared between the connected cells. Cells could share up to a maximum of four recombinants (two TCR α and two TCR β). Cells are distributed using a force-directed layout algorithm whereby cells have a simulated 'charge', repelling them from other cells, and links have attractive forces for connected cells. For a given number of cells, more links resulted in tighter clusters. A clone was defined as any number of cells that had the exact same (α or β) TCR loci and CDR3 nucleotide sequence. Clones with more than two cells are displayed here. MAIT cells were defined based on TCR α locus: any cell that expressed TRAV1-2 paired with TRAJ33, TRAJ12 or TRAJ20 was defined as a MAIT cell, regardless of the TCR β locus recombinant.

4.4 Discussion

4.4.1 Novel findings

Given the critical roles CD8+ T cells and TRM have been shown to play in protection from rodent malaria (201,237,241), an assay to measure TRM-like cells in human peripheral blood could be a means of measuring liver TRM and, potentially, liver-stage malaria vaccine performance. Such a biomarker would require interrogation of the biology of TRM. The data presented in this chapter showed the identification of a population of TRM-like cells in the circulation that correlated quantitatively and qualitatively to TRM isolated by liver FNA. Mini-bulk RNA-seq showed that although both cell populations displayed unique transcriptional differences, the differences were not a function of organ-level differences and were substantively distinct to a core TRM signature seen by contrasting CD69+ TRM to CD69- TEM (219). scRNA-seq profiled liver TRM further, identified several subpopulations and shared clonality, and indicated a potential developmental trajectory of these cells. While these findings are consistent with earlier studies, indicating comparable frequencies of lymphocytes and that T cell subsets positively correlate between PBMC and FNA samples (245,246,248), this study is the first to demonstrate that *bona fide* TRM and TRM-like cells are related both quantitatively and qualitatively.

As previous reports have shown that AgSp liver TRM correlate with protection from rodent malaria (201,237,241), the quantitative similarities between liver TRM and blood TRM-like cells were examined by multiparameter flow cytometry. The Maini group has shown the utility of FNA sampling in monitoring intrahepatic immunity as well as hepatitis B virus pathogenesis (246,248). This chapter's work was consistent with these reports, indicating comparable frequencies of lymphocytes and that total CD3+ and CD8+ T cells positively correlated between blood and FNA samples. Liver TRM and blood 'TRM-like' cells correlated, a finding which has not been shown in the literature previously. The Maini group developed a liver-like scoring algorithm to judge the quality of an FNA (245). The scores of the FNA samples in the present study were comparable with,

and indeed slightly better than, those presented in recent studies (245). Therefore, FNA sampling faithfully represented the liver immune environment and quantitative trends in the samples are consistent with what has been demonstrated previously.

Short of showing long-term residence in tissues or lack of recirculation, TRM can be identified by using several markers found on their cell surface. Flow cytometry indicated that memory T cells expressing CD69+ as well as PD-1, CXCR6 and CD103, co-existed in both the liver and blood. The three tSNE subsets defined herein may have represented TRM with varying location within the liver and TRM-like cells that home to these different areas of the liver. The function of liver-resident TRM and NKT cells, both cells that patrol the sinusoids, relies on interactions between CXCR6 and its ligand CXCL16 (181,201). Therefore, Subset 1 may have preferentially homed to the liver sinusoids, given its CXCR6+ status. There is widespread E-cadherin surface expression by human hepatocytes (454), suggesting that CD103+ TRM (Subsets 2 and 3) may be tethered to E-cadherin-expressing hepatocytes within the space of Disse. By contrast, CD69+ CD103- TRM have been shown to be present in portal fields, central veins, and parenchymal zones 1–3 of the liver (244). Therefore, the identified subsets may represent spatial or functional TRM specialisation.

There are several reports of bulk and single-cell transcriptional profiles of human TRM in health and disease (219,221,246,255,443). The widely used CD8+ core TRM transcriptional signature generated by Kumar *et al.* was unified with the DGE list generated herein to create a pan-tissue TRM signature of 41 genes. This signature showed upregulation of genes involved in tissue homing and retention (*Cd103*, *Cxcr6*) inhibition (*Dusp6*) and downregulation of signalling molecules (*Cxc3cr1*, *Tgfbr3*). Recently, He and colleagues generated a cell atlas from 15 organs, encompassing 88,622 single cells (255). They show that TRM exhibit organ-specific transcriptional regulation and developmental trajectories, signifying that tissue milieu can control gene expression. In contrast to other work, He and colleagues did not identify a common TRM gene expression or transcriptional

program. There was, however, widespread links and intense TCR sharing among TRM across organs. Liver-resident immune populations must be specialised as they need to be tolerant to immunogenic loads while still surveying for pathogens and malignancy. Accordingly, TRM showed upregulation of genes encoding inhibitory molecules such as *IRF8* and *TOX2* (455,456), when compared to TEM. Stelma *et al.* found that there were equivalent levels of cytokine (i.e. IFNγ, TNFα and MIP-1β) mRNA expression between liver TRM and TEM, suggesting similar effector functions among these cells (244). The work presented herein reiterated these findings, showing similar effector potential between TRM and TEM, but a more inhibited phenotype in TRM. Therefore, TRM can be reliably identified and differentiated from TEM in the liver by mini-bulk RNA-seq.

The main distinctions between blood and tissue T cells using population-level techniques, such as bulk RNA-seq, are derived from the existence of TRM in tissues. Zinc finger proteins (e.g. *Prdm1*, *Klf2*, *Klf3*) have been deemed transcriptional regulators of TRM (208,443). Likewise, the need to continually re-organise the phospholipid membrane and cytoskeleton during T cell migration within tissues, by Rho-GTPases for example, is critical to T cell differentiation and residency (457). Individual genes upregulated in TRM-like cells were involved in glucose metabolism, zinc transport and *de novo* phospholipid synthesis, suggesting that they may be ready for differentiation and uptake into tissues. It has been shown that TRM are metabolically quiescent and ready for rapid effector function upon activation (208,221). Genes upregulated in TRM comprised those of intercellular communication and IFN-induced proteins, corroborating previously described profiles of TRM.

Blood-derived CD69+ T cells have typically been considered as activated cells. Tissue-residing CD69+ CD8+ T cells are, however, not activated compared to CD69- or blood counterparts (244). Contrasting these findings, TRM were shown to be enriched for gene sets relating to IFNγ response and leucocyte differentiation and activation compared to TRM-like cells. Szabo *et al.* identified

conserved functional states for human blood and tissue-derived T cells (443). Examining these T cell functional modules, TRM-like cells maintained a resting profile, when compared to TRM and the two populations did not differ in terms of a resting tissue CD8+ gene module. TRM-like cells were enriched for terms suggesting they were metabolically active, transcriptionally inhibited and prepared for leucocyte migration and binding to cell surfaces. Therefore, these data suggested that blood CD69+ memory T cells were not merely activated T cells.

Significant transcriptional differences between blood and tissue-derived T cells include apoptosis, cytoskeletal and cell-matrix interaction genes (443). The data presented in this chapter recapitulate some of these differences (for example those of cytoskeleton genes), but TRM and TRM-like cell differences were unique from the differences between CD69- cells compared across liver and blood. This suggested that variations between TRM and TRM-like cells were not simply a function of tissue location. For example, glycosaminoglycan binding genes were enriched in TRM-like cells compared to TRM but not in the liver-blood CD69- comparison. Glycosaminoglycans mediate binding of chemokines and other proteins (458), and potentially facilitate T cell co-stimulation (459), supporting the idea that TRM-like cells may be more able to follow a chemotactic gradient, compared to TRM.

CD69 serves as a signal for retention in tissues by binding to and sequestering S1PR1. Many have shown the importance of CD69, a type II C-lectin receptor, as a canonical TRM marker based on both functional and transcriptional evidence in mice and humans (199,208,219,426,460). There is, however, evidence by deletion of CD69 in mice that demonstrates a reduction, but not abrogation, of CD8+ TRM in the skin and lung suggesting that it may not be necessary for the establishment of TRM in tissues (207,461). The presented data suggest CD69 expression in blood memory T cells, as well as in tissues, coincides with the transcription of genes that are known to be important in tissue residency. The TRM core signature proposed by Kumar *et al.* co-clustered TRM and TRM-like cell

samples, showing that they were less transcriptionally different than liver TEM and TRM, which were clearly separated by the signature. Recent work has shown that a subset of circulating memory T cells expressed a proportion (40%) of tissue signature genes at levels comparable to those in tissues (443). Therefore, TRM-like cells may circulate with a heightened predilection for recruitment into tissues and ability to follow chemotactic gradients. It remains to be seen whether these cells are precursors to TRM or are in fact TRM that have become temporarily dislodged from tissues and are recirculating prior to being taken up again in tissues.

The scRNA-seq gene expression data demonstrated that there were subpopulations of TRM in the liver and that related subpopulations were also present in circulating TRM-like cells. Previous work by FitzPatrick and colleagues showed that intestinal CD8+ TRM comprise two transcriptionally distinct subsets, delineated by *Itgae* and *Itgab2* regulation (444). C0 and C1 resembled the two subsets described by FitzPatrick *et al.*, despite the current study being performed with liver samples. Previous analyses, including almost all solid and hollow organs, identified that CD8+ TRM from the small intestine and liver demonstrated markedly different clustering patterns and developmental trajectories (255). *Itgae* and *Itgab2* were not differentially expressed between C0 and C1. *Itgae* (CD103) expression by TRM has been shown to be more limited in tissue location compared with CD69, which is particularly true of liver TRM (199,201,219,236,462). Ninety-five per cent of CD69+ CD8+ T cells in the liver are CD103- (250). Indeed, C0 demonstrated increased gene expression of MAIT-associated TCRs encoded by *TRAJ33* and *TRAV1-2* and was enriched for a MAIT cell signature. Many HLA-D genes were upregulated in C1, which have been shown to be upregulated in resting TRM populations, and not in activated TRM (especially at loci DM, DP, DQ and DR) (443). Given that all cells were sorted according to surface expression of CD69, CD45RA and CD8, these results suggest that C1 cells resembled classically described resting TRM, the majority of which were likely to have been αβ T cells. Considering gene expression, C0 was likely composed of MAIT cells, capable of both tissue residency and circulation (450,451). Interestingly,

this cluster saw increased expression of *Il-7r* (encoding IL-7Rα) and *Tmigd2*, suggesting these cells share characteristics with inhibited memory precursors T cells (463,464). While C2 was perhaps made up of short-lived effector memory CD8+ T cells, a circulating memory T cell signature was enriched in both C2 and parts of C1. Strikingly, all three clusters included both PBMC- and FNA-derived cells.

In silico reconstruction of single-cell TCRs confirmed the identity of MAIT cells and showed substantial clonal relationships between PBMC and FNA samples. MAIT cells are known to be highly abundant in the liver, and this has been demonstrated using scRNA-seq gene expression (445) and TCR sequencing (465). MAIT cell oligoclonality among the tissues and the circulation, and inter-individual homology have both been shown previously (465,466). These TCR data were therefore in agreement with established literature regarding MAIT cells. Previous work has shown hepatic disease-associated clonotypes in several liver disorders with signs of antigen-driven clonal selection (467). Given that all volunteers received viral vector vaccines containing an ME-TRAP insert, it was hypothesised that some degree of clonotype sharing between individuals might be present; however, this was not seen. While the three volunteers shared some HLA-A,B,C alleles, it was likely that the degree of histocompatibility was not sufficiently high enough for T cell clonotype sharing to be present. Furthermore, TCR response is highly personalized, even among twins, in response to vaccination (468). So far, the breadth and specificity of the *P. falciparum*-specific CD8+ T cell responses have only been poorly described. Indeed only 28 CD8+ T cell epitopes have been described for TRAP (150), therefore TCR specificity to ME-TRAP remains elusive. The finding that clones coexisted and TCR chain sharing occurred between liver and blood was important, as it suggested that TRM-like cells were reflective of liver TRM antigen-specificity or vice versa.

It was over 20 years ago that Sallusto and colleagues proposed that T cells follow a linear differentiation model in which naïve cells differentiate first to TCM and then to TEM (197). Recently,

this 'effectorness' gradient has been recapitulated using scRNA-seq of CD4+ T cells, and pseudotime and multi-omic analyses (469). This study demonstrated that a T cell's position along the gradient determines their response to TCR activation and cytokine and, conversely, that the gradient is detectable even after activation. The pseudotime analyses presented above showed a gradient between C1 and C0, through C2, though the analyses do not provide directional information. On the one hand, C0 may have been the gradient start point and cells differentiated further into the 'most-resident' TRM to C1. Fergusson *et al.* demonstrated that expression of CD161 delineates human T cells with a unique phenotype, independent of lineage, and that it identifies a subset of related lymphocytes including MAIT and CD8+ TCRαβ+ cells, capable of innate-like responses to cytokine stimulation (450). Further work in the same lab showed that CD8+ T cells expressing intermediate levels of CD161 have potent polyclonal, polyfunctional tissue-homing capabilities (451). While CD161+ cells express both CD103 and CD69, and are enriched within tissues, they are also found in the circulation (451). On the other hand, therefore, C1 cells may have been stem-like and have had the capability to spring or re-differentiate into effector cells, suggesting the opposite direction for the gradient. Recent work showed that TRM could de-differentiate and re-join the circulating pool of T cells. Fonseca and colleagues used epigenetic analyses to show that recall immune responses can be initiated from tissues, rather than secondary lymphoid tissue, and that recirculating TRM are advantaged in the re-establishment of residency (400). Therefore, pseudotime analyses suggested a shared differentiation trajectory between subpopulations of TRM and TRM-like cells.

4.4.2 Limitations

This work has limitations. It is likely that only a fraction of the TRM-like cells identified in human peripheral blood and hepatic sampling i) were specific to the vaccine transgene antigen, and ii) established and maintained themselves in the liver long term. TRM are known to undergo bystander, non-cognate activation (470). While bystander T cells lack specificity for the

heterologous pathogen, they can however influence the immune response to infection, highlighting the importance of non-AgSp T cells. Indeed, TRM can orchestrate near sterilising immunity to antigenically unrelated viral infection (262). Liver TRAP-specific TRM were not profiled by ICS, due to >50% cell death after peptide stimulation and a limited sample number, yet ELISpots suggested that there was the enrichment of TRAP-specific IFNγ secreting T cells in the liver compared to blood. Serial FNA after vaccination could address ii), although there were logistical limitations to the present study that prevented this.

4.4.3 Further questions

These data exhibit characteristics of liver TRM that are worthy of further investigation. The association between TRM-like cells and TRM in the liver should be investigated to determine if this was specific to TRM in the liver or if TRM-like cells represent a reliable index of TRM frequencies in many other tissues. The latter is unlikely to be entirely the case as Thome *et al.* showed localisation-dependent heterogeneity in T cell maintenance, suggesting that there are distinct pathways for differentiation CD8+ T cell subsets (212). Indeed, TRM-like cells were present in the blood at low frequencies, and the functional significance of such a rare population remains to be seen. TRM were defined here in the absence of CD103 and while only a small proportion of intrahepatic TRM expressed this marker, understanding the quantitative and qualitative relationship between CD69+ CD103- and CD69+ CD103+ TRM in response to vaccination may elucidate desirable vaccine responses. Kim *et al.* found that both subsets are functionally distinct and contribute to hepatotropic pathogen responses (250).

Tissue residency has been most extensively characterised for CD8+ TRM, but various other lymphocytes have demonstrated similar characteristics in the liver (including CD4+ T, MAIT, Foxp3+ T regulatory, NKT, γδ T and innate lymphoid cells) (202,208,445). What role, if any, do other liver-resident populations play in viral vector-induced hepatic immunity? This is pertinent given

that MAIT and MAIT-like cells formed a major component of the examined single-cell data. These cells are likely to potentiate AgSp CD4+, and CD8+ T cells instead of having vaccine-induced memory properties themselves (471), so synthetic MAIT cell ligands may be effective biological adjuvants for new vaccines. Liver-resident MAIT cells have not previously been studied as targets of malaria vaccination (472). Therefore, it may be possible that other, non-CD8+ TRM liver-resident lymphocyte populations have an underappreciated role in vaccine-induced liver-stage malarial immunity.

It might seem reasonable to suggest that, in isolation, TRM primarily function in antimicrobial immunity, and have minimal tissue-supportive roles such as those of 'non-immune' cells. However, it may be more accurate to view liver TRM as yet another part of a diverse hepatic ecosystem that provides complex protection of tissue function following a myriad of inflammatory insults. For example, LSECs are the most numerous of non-parenchymal hepatic cells and are involved in lymphocyte interactions and adaptive immunity. LSECs are unlike those of other organs and they can allow cognate T cell interactions without extravasation. How do LSECs and CD8+ TRM interact to support direct and indirect hepatic immunity? Clearly TRM do not act in isolation. Work by the Maini group has shown that the liver microenvironment influences the transcriptional profile of tissue-resident lymphocytes (217,246). Suffice it to say that the cross-talk and web of communication between TRM and parenchymal, immune, and accessory cells in the context of liver-stage malaria remains poorly understood.

4.4.4 Conclusion

The work presented in this chapter used FNAs to compare liver CD8+ TRM to circulating TRM-like counterparts and highlighted these peripheral cells as a potential correlate marker of hepatic immunity. While these TRM-like cells differed to TRM in terms of significant pathways, such as leucocyte adhesion and T cell differentiation, they are phenotypically similar and indistinguishable

in terms of T cell residency signatures. Single-cell analyses demonstrated that TRM and TRM-like cells share subpopulation heterogeneity and, potentially, differentiation trajectories. A simple and accessible correlate of hepatic immunity that predicts protection would be particularly helpful in trials of liver-stage malaria vaccines as they progress to phase III, large-scale testing in African infants. This work provides a blueprint for understanding human liver TRM and TRM-like cells following prime-target vaccination. The following chapter builds on this understanding by correlating these and other immunological markers to protection from clinical malaria.

Chapter 5

5 Investigating TRM-like cells as correlates of vaccine-induced protection

5.1 Introduction

Maurice Hilleman, virologist, iconoclastic translational scientist and arguably the most influential vaccinologist of the 20th century is credited with saying "the only correlate of protection is protection." Sceptical at first consideration, but also a maxim of the high bar which vaccine candidates will eventually have to reach for licensure. The sentence, however, is particularly severe in the development of malaria vaccines, where over 30 years of incrementalism has realised a first-generation vaccine, RTS,S/AS01, with a seven-year efficacy of 4.4% (271,473). The development of a multi-stage multi-component malaria vaccine (106) will clearly require further efforts in understanding the immune response induced by each component, at each stage. Liver-stage malaria presents an exceptionally difficult challenge; for reasons incompletely understood, enduring CD8+ T cell-mediated immunity is difficult to engender in humans. Pre-clinical results of prime-target vaccination are promising (237), but there have thus far been no successful human efficacy studies of a prime-target/prime-trap/prime and pull-type vaccination strategy explicitly designed to induce TRM-mediated protection. In the malaria context, no studies have looked at the association between liver TRM and liver-stage malaria protection in humans. This chapter explores TRM-like cells, given their relationship with liver TRM, in humans and assesses their use as a correlate of protection (CoP).

The immune system has supernumerary mechanisms and lymphocytes cooperate. Nevertheless, nearly all licensed vaccines work by inducing antibodies that prevent infection or interfere with microbial vascular entry (474). Cell-mediated immune responses can function as correlates or co-existing correlates of vaccine-induced protection against disease and infection (475). There have been numerous attempts to define vocabulary that differentiates i) an immune function biologically responsible for protection from ii) an immune function that is statistically related to protection but not biologically responsible. Stanley Plotkin suggested the biological function (i) be named a mechanistic CoP (mCoP); and that non-mechanistic, statistical correlates (ii) be named nCoPs (476). When the true mCoP is unknown or difficult to measure, substitute tests must suffice as predictors of protection by vaccines. Irrespective of terminology, CD8+ T cells have many ways of effecting host protection, both by responses that are microbe specific or non-specific (477).

There are several challenges in the identification of CD8+ T cell mCoP and nCoP against liver-stage malaria: parasite and antigen diversity, varying clinical and parasitological endpoints of infection, localisation of the immune response, diversity of vaccine target populations and complementarity of immunological pathways. Earlier efforts were mostly focussed numerically and on generating exceptionally high frequencies of T cells against liver-stage *P. falciparum* antigens (59,306). There was success in human studies of ChAd63-MVA ME-TRAP at inducing insert-specific CD8+ T cells in non-endemic settings (304,306), and these cells were associated with various measures of efficacy (176,300). Unfortunately, similar correlations between vaccine-induced AgSp CD8+ T cells and measures of efficacy in field trials were not seen (307,478), and this was in the context of overall low protective efficacy. Any number of the challenges mentioned above may explain these findings. Recent advances highlight the challenge associated with the localisation of immunity and inform us that liver TRM are necessary for sterile immunity to liver-stage malaria (168,201,237,241,242). Given the objective of prime-target (237), and other related methods (201,241), is to induce liver-stage malaria protection primarily through liver-resident immunity, rather than circulating cells,

reconsideration of circulating T cells as mCoPs of these novel strategies is warranted. Thus TRM-like cells may play a role, in which they are directly associated with TRM and – as a result, or independently – protection.

The search for liver-stage malaria CoPs is facilitated by CHMI, whereby volunteers are deliberately infected with malaria parasites (e.g. sporozoites by mosquito bite) and then followed up closely until they are diagnosed with malaria. The CHMI model has primarily been used to test anti-malarial therapy and vaccine candidates (479). The development of RTS,S (473) provides an example of CHMI effectively predicting vaccine protection under natural exposure. On the other hand, approaches with low protective efficacy in CHMI (300) have also been unsuccessful under natural conditions (480). Sub-studies undertaken within the framework of vaccine CHMI studies allow evaluation of *Plasmodium*-specific human immune responses (481-484) and the identification of potential CoP (176,482-484). The CoP analyses presented herein represent secondary immunological analyses of a phase I/IIa sporozoite challenge study to assess prime-target.

Heterogeneity in endpoints complicates the issue of predicting protection as a function of vaccine-induced immunological measures in CHMI trials. Liver-stage malaria vaccine candidates function by reducing hepatocyte parasite yield in an all-or-nothing fashion, rather than by quantitatively affecting the parasite yield, altering growth patterns or the time-to-emergence of individual parasitised hepatocytes (485). Therefore, in addition to sterile immunity liver-stage vaccines may produce non-sterile, partial protection, reflected by a reduction in the liver-to-blood inoculum (LBI), particularly when measured by qPCR, in vaccinees relative to controls and an increased survival time (300,485,486). Indeed, this is an essential endpoint of phase IIa vaccine trials (176,300) and complements data obtained by the traditional blood-film microscopy endpoint (486-488). So far, however, improvements in liver-stage vaccine immunogenicity (as measured by circulating AgSp CD8+ T cells) and associated reductions in partial protective efficacy have not translated to

substantial increases in vaccine-induced sterile protection, suggesting that the relationship between partial and sterile efficacy, modelled by circulating AgSp CD8+ T cells, is not a simple one. Therefore, for TRM-like cells to be a useful liver-stage malaria CoP specific to TRM, they would ideally be associated with both partial and sterile immunity, independently of other co-correlates.

Given that a direct relationship between vaccine-induced liver TRM and liver-stage malaria protection is problematic to validate in humans and the unique relationship between liver TRM and TRM-like cells shown in the previous two chapters, the focus of this chapter was to characterise TRM-like cells in humans further. Specifically, to profile their kinetic after various routes of immunisation, describe their heterogeneity and measure associations between TRM-like cells, and vaccine-induced AgSp responses and protective efficacy. This chapter uses methods from previous work at the Jenner Institute by Ewer *et al.* (176), Bejon *et al.* (485), and Bliss *et al.* (306) which examined the immunogenicity and efficacy of several ChAd63-MVA ME-TRAP vaccine regimens.

The aim of the work in this chapter was to translate and integrate insights from the previous two chapters – knowledge gained from mice and from in-depth characterisation of T cell populations – to assess blood TRM-like cells as CoPs against malaria in humans. The specific objectives were to:

1) Survey and describe the induction of TRM-like cells following viral vectors,
2) Evaluate TRM-like cells as a correlate of liver-stage malaria vaccine-induced immunity, and
3) Measure TRM-like cells as a correlate of liver-stage malaria vaccine-induced protection.

5.2 Results

5.2.1 TRM-like cells were induced in the short and medium-term after IV viral vector administration in humans

5.2.1.1 TRM-like cells were identified in the blood after IV boost

As part of the phase I/IIa sporozoite challenge study to assess IV boosting (prime-target) with malaria vaccine candidates ChAd63 and MVA encoding ME-TRAP (VAC066, Figure 5.1), T cells from the blood were analysed. Reasoning that precursor or ex-TRM cells may be present in the blood, particularly early after IV boost, assays were performed at several time points, including at the time of IV boost (IV), three days after IV boost (IV+3) and one day before challenge (C-1), approximately 28 days after IV boost. In this chapter, TRM-like cells were defined as CD69+ CD11a hi CD45RA CD8+ CD3+ T cells and, notably, this included all cells, not just ME-TRAP-specific cells as the frequency of AgSp cells was too low to enable meaningful analysis.

The data showed an early peak in the frequency of TRM-like cells in the blood following IV boosting. The frequency of CD69+ CD11a hi cells as a percentage of CD45RA- CD8+ (memory) T cells showed a rapid increase at IV+1, compared to IV, and began to decrease by IV+3 (Figure 5.2A). Similarly, the IV+1 and IV+3 frequency of CD69+ CD11a hi (% total CD8+ cells) were increased compared to pre-vaccination levels (Figure 5.2B). Each blood collection time point (except IV+1) had a visit window (e.g. ±1 day) in which volunteers could attend the clinic appointment. Therefore the time after IV boost at each time point slightly differed across volunteers, particularly at IV+3 and IV+7 time points. Time point data adequately reflected the time after vaccination data as the CD69+ CD11a hi frequency (% CD45RA-) peaked one day after IV boost and was not significantly different from pre-vaccination by four days after IV boost (Figure 5.2C). Clinical haematology measurements were available for each volunteer, allowing estimation of the concentration of TRM-like cells in the blood at each time point. The concentration of TRM-like cells peaked at IV+3 and remained elevated until IV+7 when compared to the pre-IV boost concentration (Figure 5.2D).

TRM-like cell frequencies measured at all time points after IV boost were positively correlated. All Spearman's rank correlation coefficients between pairs of TRM-like cell measurements were greater than zero, albeit not all these associations were statistically significant and true discoveries after multiple comparisons (Figure 5.2E). Pairs of TRM-like cell measurements flagged as true discoveries included IV+1 & C-1, IV+3 & C-1, and IV+7 & C+7. The strongest correlations were seen between IV+3 & C-1 and IV+1 & C-1 TRM-like cell frequencies (r=0.70 and 0.74, respectively). TRM-like cells peaked early after IV boost and peak responses correlated to TRM-like cell frequency immediately prior to CHMI.

The expression of TRM functional proteins showed that TRM-like cells resembled true TRM. TRM-like cell expression of CXCR6 and Ki67 was increased at IV+3 and IV+14 compared to pre-vaccination, and CD69- cell counterparts (Figure 5.3). The CXCR6+ frequency (% CD69+ CD11a hi) peaked at IV+3, while the Ki67+ frequency (% CD69+ CD11a hi) increased until IV+14 (Figure 5.3A, B). The increases in marker positive frequencies were reflected in absolute marker expression. Both CXCR6 and Ki67 had increased GMFI at IV+3 and IV+14, compared to pre-vaccination (Figure 5.3C, D). While these differences were statistically significant, the absolute differences were small. The expression and marker frequency of CXCR6 and Ki67 were also increased, compared to pre-vaccination, at IV+1 and IV+7 (data not shown). Similarly, the expression of both CD103 and PD-1 increased compared to pre-vaccination and remained elevated until IV+14 (data not shown).

5.2.1.2 TRM-like cells were associated with within-assay AgSp T cells

For ease of identification, TRM-like cells were defined in the absence of ME-TRAP-specificity, but most importantly the frequency of total TRM-like cells correlated with the frequency of AgSp T cells when measured within the same assay. The frequency of TRM-like cells was compared to

AgSp CD8+ T cell responses in a subset of volunteers sampled equally from different groups and high/medium/low TRM-like cell responses. IFNγ+ CD107a+ TRM-like cell frequency (% CD8+) correlated significantly to the frequency of TRM-like cells (% CD8+) at IV and IV+3, but not IV+7 (Figure 5.4A). TRM-like cell frequency correlated to total IFNγ+ CD107a+ frequency (% CD8+) at IV, but not IV+3 and IV+7 (Figure 5.4B). IFNγ+ CD107a+ TRM-like cell frequency and IFNγ+ CD107a+ CD8+ frequency correlated with TRM-like cell frequency at IV+14, as well (data not shown). Of note, the IV time point TRM-like cell frequency strongly correlated with the CD69+ CD11a hi CD45RA- frequency (% CD8+ CD3+ CD45+) measured in the FNA samples discussed in Chapter 4 (r=0.76, 95%CI=0.32-0.93, p=0.0052). Therefore, when measured in the same assay, TRM-like cell frequencies correlated with AgSp T cell frequencies.

As there were different viral vector regimens in the VAC066 trial, the difference in TRM-like cell frequency between groups was also assessed. Groups 1 & 3 received IV ChAd63 ME-TRAP, while groups 2 & 4 received IV MVA ME-TRAP. There were no significant differences between the IV ChAd63 and IV MVA groups, at any time point after IV boost (Figure 5.5A), in terms of TRM-like cell frequency (% CD45RA-). When comparing individual groups, there were no statistically significant differences between groups at each time point after IV boost (Figure 5.5B). Similarly, there were no statistically significant differences in the TRM-like cell frequency between groups that received an IM boost (groups 1 & 2) and those that did not receive an IM boost (groups 3 & 4) (data not shown). Therefore, TRM-like cell frequency differences between individuals did not appear to be driven by differences in vaccine vector.

5.2.1.3 TRM-like cells displayed heterogeneity that was preserved over time after IV boost

Given that T cell subsets are often heterogeneous and TRM-like cells may have exhibited lineage, functional and receptor heterogeneity, the TRM-like cell expression of several candidate markers was assessed. In a subsequent experiment, the CD69+ CD11a hi CD45RA- CD8+ CD3+ subset was

further examined for markers of unconventional T cells, such as MAIT (TCR Vα7.2, CD161) (396), TRM (CD103), γδ T (TCR αβ vs TCR γδ) and NKT/NK cells (CD56, CD16, CD11c) (489,490).

These experiments corroborated the findings from Chapter 4, that demonstrated a significant proportion of cells identified as TRM-like cells were either MAIT cells or shared similar transcriptional profiles. The TCR Vα7.2+ frequency (% CD69+ CD11a hi) was not significantly different to the pre-vaccination frequency at any time point, except for IV+7 when it decreased to less than 5% (p=0.0011, Figure 5.6A, left). A similar trend was seen in the CD161++ frequency (% CD69+ CD11a hi), with an almost 3-fold reduction from its peak at IV+7 (Figure 5.6A, middle). Both CD161 and TCR Vα7.2 were expressed in a large proportion of TRM-like cells at all time points (greater than 30%, except IV+7, data not shown). The frequency of TCR Vα7.2+ and CD161++ in the CD69+ CD11a hi subset was significantly higher than their frequencies in paired CD69- CD11a lo populations (Figure 5.6A, middle, analysis not shown). There were no significant differences between CD103+ frequencies (% CD69+ CD11a hi) measured at post-IV time points (Figure 5.6A, right). The expression of TCR Vα7.2 on TCR Vα7.2+ cells was increased at IV+1 but not significantly different at any other time points when compared to IV (Figure 5.6B, left). CD161 expression on CD161++ cells decreased at IV+3 and IV+7, compared to pre-vaccination (Figure 5.6B, middle). The CD103 GMFI did not change in a statistically significant manner over time after IV boost (Figure 5.6B, right). When gating solely on CD69+ CD45RA- CD8+ T cells, in the absence of CD11a hi, the frequency of TCR Vα7.2+ and CD161++ cells (% CD45RA-) decreased at IV+1, IV+3 and IV+7 (data not shown), suggesting that CD11a hi may be a non-redundant identifier of the TRM-like cell subset. These results endorsed the notion that MAIT cells were a significant subset of TRM-like cells, enriched when compared to their frequency of total CD8+ T cells.

Other markers of unconventional T cells did not show heterogeneity in the CD69+ CD11a hi T cell subset. Of the TRM-like cell subset, approximately 98% of cells were TCR αβ+

and the remainder were TCR γδ+, and these proportions were unchanged from IV to IV+14 time points (data not shown). There was very low (<1%) or absent expression of CD11c, CD16 and CD56 in the TRM-like cell population (data not shown).

5.2.1.4 Clinical markers of inflammation were elevated after IV boost

An aim of IV viral vector boosting, as in VAC066, was that the vector would specifically target the immune and inflammatory response to the liver (237). Having looked, in mice, at the ability of IV viral vector vaccination to induce an inflammatory response in the liver and in the blood, here, clinical biochemistry values were assessed to identify whether IV viral vector specifically induced inflammation in the liver. Alanine transaminase (ALT) is commonly measured as part of liver function tests and is a non-specific marker of hepatic injury and inflammation. D-dimer is a fibrin degradation product that is a highly sensitive but non-specific biomarker of coagulation, as well as an acute phase reactant. Its production induces and is induced by IL-6, as part of systemic pro-inflammatory processes.

Both hepatic and systemic inflammation were induced after IV boost. Log-transformed ALT was increased at all time points measured after IV boost, peaking at IV+7, when compared to pre-IV boost levels (Figure 5.7A, left). IM prime or IM boost vaccination did not significantly alter log-transformed ALT (one-way ANOVA p=0.304). Given these results, groups receiving different IV viral vectors were compared in terms of log-transformed ALT after IV boost, but no significant differences between groups were identified (Figure 5.7A, right). D-dimer levels were only measured after IV boost. Log-transformed D-dimer peaked at IV+3 and remained elevated until IV+7 (Figure 5.7B, left), but did not vary according to the IV viral vector administered (Figure 5.7B, right). Albumin, which can be measured as a proxy of the synthetic function of the liver, was not significantly different at any time point throughout VAC066 (data not shown). ALT and D-dimer were not significantly correlated at any post-IV boost time point. Similarly, there were no significant

correlations identified between TRM-like cell frequencies (% CD45RA-), and ALT or D-dimer (analyses not shown). This suggested that there was not an observed dose-response relationship between systemic or hepatic inflammation and the generation of TRM-like cells after IV boost.

Clinical haematology parameters were also assessed for an IV boost effect. Lymphocyte concentration was not significantly different across any time point between IM prime and IV boost (one-way ANOVA p=0.18; Figure 5.7C, left). There were statistically significant decreases in lymphocyte concentration at IV+1 and IV+3 and increases at IV+7 and IV+14, compared to IV (Figure 5.7C, left). In volunteers who underwent FNA (performed 16-24 days after IV boost), there was no statistically significant difference between lymphocyte count measured at that time and at IV boost (data not shown). Given the profound effect of IV viral vector on lymphocyte concentration, lymphocyte concentration was compared between the IV viral vectors administered. Lymphocyte concentration was significantly higher in IV MVA groups (2 & 4), compared to IV ChAd63 groups (1 & 3), at IV+7 and IV+14 (Figure 5.7C, right). Platelets, which are an acute phase reactant, were not significantly different at any time point during VAC066. Therefore, IV viral vector resulted in significant biochemical and haematological changes that did not occur when administering viral vectors as an IM prime or IM boost.

5.2.2 IV viral vector induced a greater TRM-like cell response compared to IM viral vector

IV, but not IM, administration of malaria vaccines, particularly as a boost vaccination, generates high frequencies of hepatic T cells resulting in protection from sporozoite challenge in NHP and murine models (168,201,237,241). Given this, in a further experiment, the TRM-like cell response was compared between IM boost and IV boost time points, after reasoning that TRM-like cells would be a proxy for greater generation of liver TRM in IV, compared to IM vaccination. Samples

were selected to enable comparison between IM boost and IV boost in individuals that received only one prior IM vaccination (i.e. the IM ChAd63 prime).

When aligning time points by IV boost, maximal responses were found at post-IV boost time points. Three T cell subsets were examined: TRM-like cell frequency (% CD45RA-), IFNγ+ or CD107a+ TRM-like cell frequency (% IFNγ+ or CD107a+ CD8+) and CD103+ frequency (% CD69+ CD11a hi CD45RA-) (Figure 5.8A, B, C). The highest median TRM-like cell frequency was at IV+1 (median=11.1%, IQR=10.2-14.5%; Figure 5.8A) and, similarly, the maximal IFNγ+ or CD107a+ TRM-like cell frequency was also at IV+1 (median=6.04%, IQR=3.44-12.9%; Figure 5.8B). The maximum CD103+ frequency occurred at IV+7 (median=2.18; IQR=0.443-3.14%; Figure 5.8C). Given the different vaccination regimens, differences between time points were not assessed. Like previous experiments, there were no differences in any of the three T cell subset frequencies when comparing groups that received a prime and an IM boost prior to IV boost, and groups that received only a prime, at IV, IV+1, IV+3 or IV+7 (data not shown). There were also no differences in the three parameters when comparing groups that received IV ChAd63 compared to IV MVA, at IV, IV+1, IV+3 or IV+7 (data not shown).

In VAC066, two groups received IM MVA boost vaccinations and one received an IV MVA boost, allowing direct comparison of IV and IM boosting. Notably, the dose of the IV boost was ten-fold lower than the dose of the IM boost. TRM-like cell frequency was higher at all time points after IV boost, except only the comparison of frequencies measured one day after vaccination was statistically significant (B+1 vs IV+1, p=0.0476; Figure 5.8D). Post-IV boost time points had higher IFNγ+ or CD107a+ TRM-like cell frequencies, compared to post-IM boost, although there were no statistically significant differences between them (Figure 5.8E). Similarly, none of the differences between IV and IM time points reached statistical significance when comparing CD103+ frequencies (Figure 5.8F).

IV vaccination is likely to have unique effects on the immune system; effects not shared by other routes of vaccination. The hypothesis that this was the case for TRM-like cell frequencies after IV and IM boost was tested by considering within-volunteer associations. All TRM-like cell frequencies (% CD8+) measured at post-IV boost time points positively correlated with pre-IV boost time points. All correlation coefficients between pairs of TRM-like cell parameters were more than zero, except at the time of IV boost (Figure 5.8G); however, none of these associations were true discoveries (Benjamini, Krieger and Yekutieli false discovery approach (491), Q=0.01). The tied strongest correlation was between IV+1 and B+1 TRM-like cell frequency (r=0.886, p=0.03, q=0.27, false discovery; Figure 5.8G). While there was a moderate likelihood that these results occurred due to chance alone, these results suggested that an individual's post-IV boost TRM-like cell response was associated with their boost and prime vaccination response, rather than there being an effect unique to IV boost.

5.2.3 TRM-like cells correlated with established and validated markers of protection

Previous studies have shown that a higher magnitude of T cell immunogenicity induced by ChAd63-MVA regimens correlated with greater protective efficacy against malaria (176,300). Despite TRM-like cells not being defined in a vaccine-antigen-specific manner, it was hypothesised that the magnitude of the response would be commensurate to the magnitude, and potentially breadth of functionality, of the AgSp response. Both ICS and IFNγ ELISpot assays were performed independently, in parallel and on freshly isolated PBMC. These measurements have previously been demonstrated to correlate with vaccine-induced efficacy (176,492).

5.2.3.1 TRM-like cells correlated with a range of TRAP-specific CD8+ T cell subsets

First, each correlate was assessed for differences between vaccinated and unvaccinated group differences. The three T cell frequencies examined were measures of TRAP-specificity: IFNγ+,

CD107a+, and either IFNγ+, TNFα+ or IL-2+ (γ/α/2) frequencies (% CD8+ CD3+ T cells). There were no significant differences between groups 1-4 at IV+7, in any of the three parameters (Figure 5.9A, B, C, left). At C-1, individuals in the four vaccinated groups did not have statistically significant differences of IFNγ+ frequency, compared to controls (Figure 5.9A, middle), whereas at C+7, only group 3 was not significantly different to the control group (Figure 5.9A, right). When considering the CD107a+ frequency, all groups had statistically significant increases compared to controls at C-1 (Figure 5.9B, middle), and again group 3 did not have a significantly different frequency compared to controls (Figure 5.9B, right). All groups had significantly higher γ/α/2 frequencies compared to controls at both C-1 and C+7, except group 3 at C+7 (Figure 5.9C, middle, right). When merging, and comparing vaccinated to unvaccinated groups, all three parameters were significantly different (MW tests, all $p<0.0057$) at C-1 and C+7, except for the IFNγ+ frequency at C-1 ($p=0.16$) values shown in Figure 5.9A, middle). These results indicated that viral vector regimens including an IV boost vaccination effectively induced TRAP-specific T cell responses, compared to unvaccinated controls.

TRM-like cells were generated in response to IV boost but may not have been directly involved in the putative causal pathway resulting in vaccine-induced protection from malaria. Therefore, it was important to assess correlations between TRM-like cells and well-established markers of vaccine-induced protection, such as AgSp CD8+ T cell subsets. The coefficients of association between post-IV boost TRM-like cells and IFNγ+, CD107a+, or γ/α/2 frequencies all indicated a positive correlation, except when considering C+7 TRM-like cells (Figure 5.9D), which were mostly negative, albeit not statistically significant. Of note, IV+3 TRM-like cell frequency was positively correlated with the frequency of the three AgSp T cell subsets, measured at IV+7, C-1, and C+7 (6/9 correlation p values were below the false discovery threshold of 0.00596; Figure 5.9D). These results suggested that irrespective of whether TRM-like cells led to vaccine-induced protection from malaria, they were correlated to AgSp responses.

5.2.3.2 TRM-like cells correlated with IFNγ-secreting T cells more than a month post-CHMI

A predictor of long-lived immune responses that is measured soon after vaccination could reduce the need for intensive immunological follow up of volunteers for extended periods. This would be particularly helpful in large endemic-setting phase III clinical trials. Therefore, associations between TRM-like cells measured shortly after vaccination were examined for their correlation to long-lived T cell responses, as measured by IFNγ ELISpots. The maximum ELISpot response in group 1 was at study day 35 (D35 median=4284 SFC, IQR=3199-6834 SFC), seven days after IM boost (Figure 5.10A). For group 2 it occurred at C-1 (median=5748 SFC, IQR=1556-6455 SFC), for group 3 at D63, which corresponded with IV+7 (median=1163 SFC, IQR=309-8640 SFC) and for group 4, also at D63 (IV+7 median=7007 SFC, IQR=6892-11060 SFC). Both group 2 and 4 had significantly higher ELISpot responses, compared to controls at C-1, C+35 and C+90 (all adjusted $p<0.001$; group values shown in Figure 5.10B). Group 1 had higher ELISpot responses at C-1 (adjusted $p=0.036$) and C+35 (adjusted $p=0.034$), but not C+90, compared to controls. Group 3 did not have significantly different responses compared to controls at any of the challenge time points. Between-group comparisons showed that group 4 and group 2 volunteers had higher ELISpot responses than group 3 at four and three time points, respectively.

TRM-like cells measured soon after IV boost correlated with enduring ME-TRAP-specific T cell responses. When measured at IV+3, TRM-like cell frequency had strong positive correlations with ELISpot responses measured at IV+7, C-1, C+35 and C+90 (all statistically significant; IV+3–C+90 was a false discovery, p value above the false discovery threshold of 0.0035; Figure 5.10C). C-1 TRM-like cell frequencies were also positively correlated with ELISpot responses, but none of these associations were true discoveries (Figure 5.10C). Control volunteer TRM-like cell frequencies measured at C-1 and C+7 did not correlate to ELISpot responses measured at C-1, C+7, C+35 or C+90 (data not shown). Collectively these results indicated that TRM-like cells numerically

correlated with a broad range of AgSp CD8+ T cell subsets at the time of challenge, as well as IFNγ-secreting T cells measured long after malaria challenge.

5.2.3.3 IV+3 TRM-like cell frequency was a correlate of vaccine-antigen immunity

It was possible that the associations between TRM-like cells and AgSp markers of immunity were unduly influenced by several outlier measurements, such as highly vaccine-responsive volunteers. Focussing on IV+3 TRM-like frequency as a potential CoP, correlations were reassessed by excluding all volunteers that achieved sterile protection and were right-censored from VAC066 CHMI. These volunteers were selected *a priori*, given that protection from malaria is known to correlate with vaccine-induced ME-TRAP-specific response. Additionally, as the sample size decreases, the power to determine whether a correlation coefficient truly differs from zero decreases. Removing six individuals increased the threshold at which a correlation would be deemed significant, if there indeed was a real correlation, resulting in a more statistically conservative analysis (493).

Despite a significant loss in power to detect a correlation, IV+3 TRM-like cell frequency was correlated with AgSp T cell responses. The frequency of TRM-like cells measured at IV+3 positively correlated with ELISpot response measured at C-1 and C+35 (Figure 5.11A). This parameter also correlated with IFNγ+ frequency at C+7, albeit with a correlation coefficient 95%CI approximating zero (Figure 5.11B). Given that volunteers experienced their maximal AgSp T cell response at different time points over the duration of the study, IV+3 TRM-like cell frequency was assessed for its correlation to peak ELISpot and ICS response. Indeed, IV+3 TRM-like cell frequency strongly correlated to both maximal ELISpot and maximal ICS response (Figure 5.11C). These analyses suggested that IV+3 TRM-like cell frequencies robustly correlated with markers previously established as CoPs against liver-stage malaria.

5.2.4 TRM-like cells can be used to estimate protection following CHMI

5.2.4.1 A range of protection outcomes occurred as a result of CHMI

Having demonstrated a relationship between TRM-like cells and several markers of vaccine-induced immunity, associations with protection from malaria were assessed in the context of CHMI. The CHMI component of this trial included thirty vaccinated and five unvaccinated volunteers, who were exposed to five infectious *A. stephensi* mosquito bites in a now well-established procedure (494). The TRAP antigen in the infecting *P. falciparum* strain differed from the vaccine strain, thereby constituting a heterologous challenge (301). Volunteers were followed up until diagnosis of malaria (an event in survival analysis) or were deemed to have achieved sterile protection at 21 days (right-censoring in survival analysis). TRM-like cell frequencies were investigated for their association with measurements of vaccine-induced protection and used in survival analyses, leveraging the time-to-event data resulting from CHMI.

There is a range of outcomes that may occur in CHMI trials of pre-erythrocytic malaria vaccines, ranging from no detectable vaccine-induced effect, to substantial but incomplete clearance (reflected in a delay to frank parasitaemia and diagnosis) and to complete liver clearance (sterile protection) (268,301,305). As expected in malaria-naïve individuals, all unvaccinated controls were diagnosed with malaria. Sterile protection was seen in six vaccinated volunteers. Two of these were in group 2 (n=9), one in group 3 (n=6) and three in group 4 (n=7). Comparing overall survival between vaccinated and unvaccinated controls showed no significant difference in time-to-malaria diagnosis between the two groups (hazard ratio (HR)=0.541, 95%CI=0.162-1.81, p=0.134; vaccinated median=14 days, control median=13; Figure 5.12A). Only group 4 had significantly longer time-to-event than controls (p=0.026; Figure 5.12B). Grouping according to the number of vaccines administered (groups 1 & 2 compared to 3 & 4), and according to IV viral vector also showed no differences in survival (data not shown). Therefore, heterologous IV boosting with MVA

after IM ChAd63, encoding ME-TRAP, resulted in significantly improved sterile protection over controls and may be worthy of further investigation.

5.2.4.2 TRM-like cells independently correlated with vaccine-induced protection

Partial pre-erythrocytic malaria vaccine efficacy, observed when sufficient parasites are cleared to produce a delay in time-to-patency, corresponds to clearance of approximately 95% of parasites (485). Volunteers that were afforded any protection (i.e. sterile or partial) demonstrated increased IV+3 TRM-like cell frequencies, compared to those that were not protected (as previously defined (176); Figure 5.13A). Indeed, comparing those with only partial (and not sterile) protection to volunteers with no protection also indicated higher IV+3 TRM-like cell frequencies in the former (difference=4.0%, p=0.005, data not shown). TRM-like cell frequency also demonstrated a biological gradient (TRM-like cell frequency of sterile > partial > no protection groupings) at the time of IV boost (data not shown). IV+3 TRM-like cell frequency positively correlated with time-to-diagnosis and time-to-1000 blood-stage parasites (Figure 5.13B), suggesting clearance of liver parasites and a lower LBI. The association between time-to-diagnosis and IV+3 TRM-like cell remained statistically significant if sterile protected volunteers were removed (p=0.0127). The mean number of parasites in the first three replication cycles after liver emergence, and during the third cycle, both negatively correlated with TRM-like cell frequencies measured at IV+3 (r=-0.54, p=0.002, r=-0.56, p=0018, respectively; Figure 5.13C left and middle). The emerging parasite burden 7.5d after infection was negatively correlated but did not reach statistical significance (r=-0.34, p=0.067; Figure 5.13C right). TRM-like cell frequencies measured at the point of IV boost also correlated, like IV+3, with all parameters presented in Figure 5.13, in a statistically significant manner (analyses not shown). Strikingly, ME-TRAP-specific T cell responses as measured by ICS or ELISpot at C-1, or at their maximum, did not correlate with the presented markers of protection. Together, these results indicated that IV+3 TRM-like cells independently correlated with biological measures of vaccine-induced protection.

Having shown a relationship between vaccine protection and IV+3 TRM-like cell frequency at a biological level, this relationship was further explored in the context of vaccine efficacy and survival analyses. The analyses presented above were limited by their inclusion of raw event frequencies, exclusion of censored volunteers and the assumption that censoring time was equal to event time (495). Survival analyses allow incorporation of both the time until an event occurs and censored patients. All volunteers were stratified according to whether their individual TRM-like cell frequency was above (high responder) or below (low responder) the median of all 35 volunteers (Figure 5.14A). Using this method significantly separated volunteers according to time-to-malaria diagnosis and sterile protection, when using TRM-like cells measured at three time points. In the IV time point analysis (Figure 5.14A left), the high responder and low responder groups had significantly different median survival (high median=15d, 95%CI=14-NA; low median=13d, 95%CI=12.5-14). This was also the case in the IV+3 analysis (high median=15d, 95%CI=14-NA; low median=12.5, 95%CI=12.5-14). In the IV+1 analysis, the hazards were just significantly different (log-rank p=0.049) between strata, and volunteers in both strata achieved sterile protection, suggesting that IV+1 TRM-like cells were less robustly related with protection compared to IV+3 and IV. Therefore, TRM-like cells measured shortly before and after IV boost were associated with delayed malaria diagnosis.

It was possible that the survival benefit associated with TRM-like cells was due to confounding protection by other T cell subsets. As such, similar analyses were conducted using separate T cell populations. In keeping with the biological relationships described above, dichotomising volunteers by C-1 ELISpot response or TRAP-specific IFNγ+ CD8+ T cells was unable to separate volunteers with different times to diagnosis (Figure 5.14B). This was also the case when performing the same analyses of ICS or ELISpot responses measured at any time point (IV+7, C+7, C+90 tested, data not shown). Several other T cell subsets, including CD69- CD45RA- CD8+, CD45RA- CD8+ and

CD8+ frequencies (% CD3+), were also unable to separate strata with significantly different hazards when the frequencies were measured at IV+1, IV+3, IV+7, IV+14, C-1, or C+7 (analyses not shown). There were two exceptions, both measured at the IV time point: CD69- CD45RA- CD8+ frequencies (high median=13d, 95%CI=12.5-14; low median=15.5d, 95%CI=14-NA; log-rank p=0.00041) and CD8+ frequencies (high median=14d, 95%CI=13.5-NA; low median=13d, 95%CI=12.5-16; log-rank p=0.043). Mutually, these results indicate that TRM-like cells, particularly when measured around the time of IV boost, independently correlated to markers of vaccine protection, and could most effectively stratify volunteers in survival analyses.

5.2.4.3 TRM-like cell frequency could be used to model time-to-malaria diagnosis

Given the relationships between TRM-like cell frequencies and protection, regression was performed. Several univariate and multiple Cox regressions were fit using T cell population frequencies to model the hazard function of malaria diagnosis after CHMI. The association between a diagnosis of malaria and the T cell populations was then assessed.

Univariate Cox models of TRM-like cells, and several other T cell populations, were generated to examine the effect of each predictor on the instantaneous risk of malaria diagnosis after CHMI. Regression models using TRM-like cell frequencies measured at IV time points had HRs less than one – suggesting a protective effect of TRM-like cells – except when the frequency was measured at IV+14. The two time points that were significantly associated with reduced HR were at IV boost (each $\log_{10}$ unit increase in TRM-like cells was associated with an 86% reduction in hazard of malaria diagnosis; Figure 5.15A top) and at IV+3 (each $\log_{10}$ unit increase in TRM-like cells was associated with a 75% reduction in hazard of malaria diagnosis; Figure 5.15A second from top). Surprisingly, but consistent with previous analyses, vaccine AgSp responses measured by ELISpot and ICS were not individually associated with a reduced hazard of malaria diagnosis (all Wald p>0.05; Figure 5.15B). Increased log-transformed CD69- CD45RA- CD8+ T cell frequency (% CD3+), when

measured at any time point, was associated with an increased hazard of malaria diagnosis, though none of the univariate Cox models reached statistical significance (data not shown). CD45RA- CD8+ T cell frequency (% CD3+) showed no consistent relationship with hazards of diagnosis (data not shown).

Multiple regression Cox proportional hazards models were subsequently developed using several TRM-like cell frequency parameters. Initially, three models, composed of log-transformed IV and IV+3 time point parameters, were compared by a step-wise forward selection of variables and Δ_i analysis (370) (Table 5.1). The most parsimonious model was the multivariate regression model composed of both TRM-like cell variables (concordance 0.723, Wald test p=0.007). There was also substantial support for the predictive ability of both univariate Cox models as the Δ_i between the multivariate and the IV+3 and IV models were 0.2 and 0.4, respectively (Table 5.1). Both IV and IV+3 were associated with a decreased hazard of malaria diagnosis (61% and 72% reduction per log unit increase, respectively), although individually in the multivariate analysis these variables were not significant and the hazard ratio 95%CI crossed one (Figure 5.16A). While the model satisfied the proportional hazards assumption (p=0.304 overall) and there were no vastly influential observations (Figure 5.16B, C), IV and IV+3 TRM-like cell parameters were previously shown to be moderately positively correlated ($p=3.433x10^{-4}$, Figure 5.2E). The variance inflation factor, which measures the inflation in variance due to parameter correlation, of both variables was 1.38, suggesting that individual coefficient estimates may be reliable (496). In the case of CHMI, the overall model result was likely of greater importance than the contribution of each individual variable in the multivariable model. Thus, this model demonstrated the utility of TRM-like cells in predicting vaccine-induced protection.

Table 5.1: Cox proportional hazards models using statistically significant TRM-like cells. Stepwise forward selection of TRM-like cell frequencies, deemed statistically significant on univariate analyses, and Δ_i analysis was used to declare the most parsimonious model. TRM-like cell frequencies were expressed as percentages of CD8+ T cells and log-transformed. Only two parameters were fed into forward selection: TRM-like cells measured at IV and IV+3.

Predictors	Akaike information criterion	Model
2	130.4	Log-transformed IV TRM-like cells, log-transformed IV+3 TRM-like cells
1	130.6	Log-transformed IV+3 TRM-like cells
1	130.8	Log-transformed IV TRM-like cells

Given the biological plausibility of TRM-like cells as useful predictors of protection, all parameters after IV boost were fed stepwise into multivariable Cox regression models. These analyses suggested that IV+14 and C+7 time point TRM-like cell parameters were important variables for predicting protection (

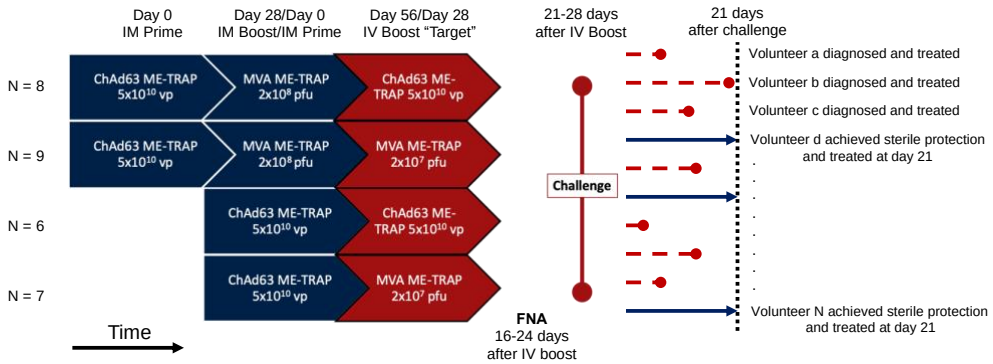
Table 5.2), as well as IV and IV+3. Nine out of the ten most parsimonious models had excessive amounts of predictors (more than three predictors, given 29 total events/malaria diagnoses) (497) (Figure 5.17A), likely resulting in overfitting. Given a Δ_i of 4.4, the three-parameter model of IV+3, IV+14 and C+7 TRM-like cells was explored for its predictive capability. Overall, the model was significant (log-rank p=0.0023, Figure 5.17B); however, the greatly increased hazard ratio resulting from increased C+7 strongly suggested multicollinearity. This was confirmed by the variance inflation factor for C+7, which was 14.5 (as opposed to 6.76 and 6.67 for IV+3 and IV+14, respectively). Therefore, the predictive ability of TRM-like cells is limited by parameter correlation and the small number of total events.

Table 5.2: Multiple regression Cox proportional hazards models using TRM-like cells. Stepwise forward selection of TRM-like cell frequencies and Δ_i analysis was used to declare the most parsimonious model. The ten most parsimonious models are presented here; each row represents a distinct model. TRM-like cell frequencies were expressed as percentages of CD8+ T cells and log-transformed. Seven parameters were fed into forward selection: TRM-like cells measured at IV, IV+1, IV+3, IV+7, IV+14, C-1 and C+1.

Predictors	Akaike information criterion	Log-transformed TRM-like cell parameters in the model
4	28.6	IV, IV+3, IV+14, C+7
5	29.4	IV, IV+1, IV+3, IV+14, C+7
5	30.3	IV, IV+3, IV+14, C+1, C+7
5	30.5	IV, IV+3, IV+7, IV+14, C+7
6	31.0	IV, IV+1, IV+3, IV+7, IV+14, C+7
6	31.2	IV, IV+1, IV+3, IV+14, C-1, C+7
6	32.1	IV, IV+3, IV+7, IV+14, C-1, C+7
7	32.9	IV, IV+1, IV+3, IV+7, IV+14, C-1, C+7
3	33.0	IV+3, IV+14, C+7
4	34.7	IV+3, IV+7, IV+14, C+7

It was plausible that the predictive ability of TRM-like cells may be increased, or even surpassed, by the inclusion of AgSp parameters in a multivariate model. Other established CoP, such as ELISpot and ICS IFNγ+ (% CD8+) responses at several time points, were included in forward stepwise model selection. The most parsimonious model by AIC was composed of six parameters (IV+3 TRM-like cells, IV+14 TRM-like cells, C+7 TRM-like cells, IV ELISpot response, C+7 ELISpot response and IV+7 IFNγ+ (% CD8+), all log-transformed). This model minimised AIC (AIC=19.9, Figure 5.17C) but was composed of covariates that were correlated to varying degrees, resulting in multicollinearity (data not shown). In addition, the parameters were taken from three different assays which, if these correlates were to be further examined in other, larger trials, presents practical difficulties. Lastly, during model selection with less than six predictors, the most parsimonious model for each number of predictors included in the multivariate analysis was composed entirely of TRM-like cell predictors. The same was the case when including CD69- CD45RA- CD8+ T cell frequency or CD45RA- CD8+ T cell frequency predictors (data not shown). These results suggest that the benefits of including AgSp predictors into multivariable analysis did not outweigh the drawbacks of their inclusion. Therefore, TRM-like cells predictors performed as well or better than AgSp predictors in multivariable analysis.

5.3 Figures



ClinicalTrials.gov Identifier: NCT03707353

Figure 5.1: VAC066 trial overview and timeline. The final study cohort included 35 volunteers, across five groups, with group sizes for the first four (intervention) groups as indicated. Not shown in this figure is the infectivity control group (N=5) that did not receive any vaccinations and underwent CHMI with the vaccinated groups. All intervention group volunteers received either two or three vaccines of viral vectors encoding ME-TRAP. Doses were as indicated. Hepatic FNA occurred between 16 and 24 days after IV vaccination/boost. Volunteers underwent CHMI on two separate days (4/2/2019 and 5/2/2019) and participants were equally and randomly divided across these days. Volunteers were followed up twice per day from five days after challenge. Volunteers were treated with 20mg artemether/120mg lumefantrine (Riamet) upon malaria diagnosis or 21 days after challenge. A diagnosis of malaria was made given the following criteria: 1) The presence of symptoms suggestive of malaria in addition to a qPCR result indicating ≥ 1,000 parasites/mL OR 2) Lack of symptoms with a qPCR result indicating ≥ 10,000 parasites/mL. None of the volunteers in the infectivity control group achieved sterile protection. Four volunteers (a-d) are presented above as examples (right, dashed red circles and solid blue arrows).

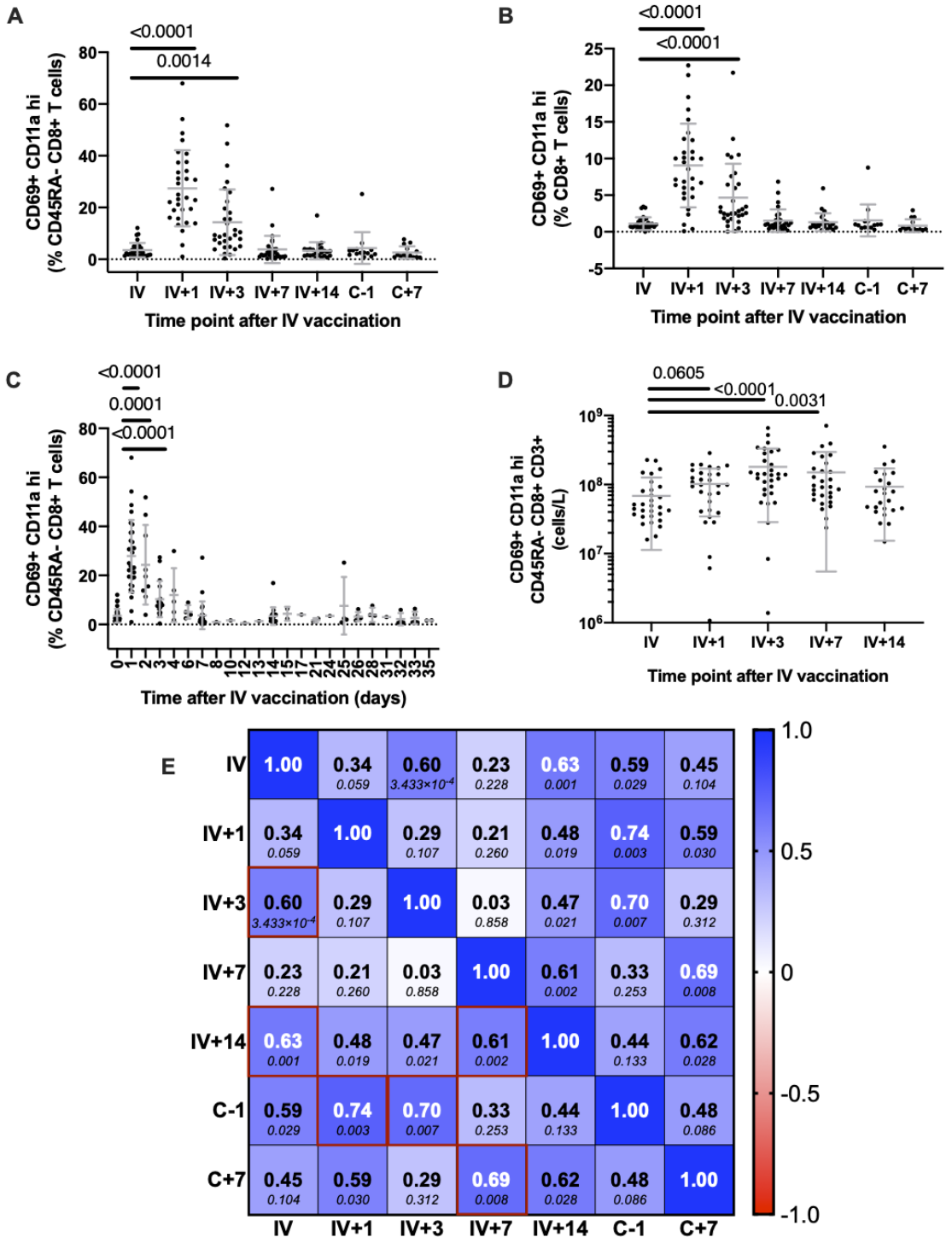


*Figure 5.2: TRM-like cells after IV boost. **A**: CD69+ CD11a hi cells as proportions of CD45RA- CD8+ CD3+ T cells at seven time points after IV boost. **B**: CD69+ CD11a hi cells as proportions of CD8+ CD3+ T cells at six time points after IV boost. **C**: CD69+ CD11a hi cells as proportions of CD45RA- CD8+ CD3+ T cells by time after IV boost. For each time point, there was a window in which volunteers could attend for blood sampling. **D**: CD69+ CD11a hi CD45RA- CD8+ CD3+ T cell concentration calculated using volunteers' clinical haematology value for total lymphocytes. Mean values are presented, and error bars represent the standard deviation. Significance testing of differences between time points was performed using ratio paired t tests and the resultant p values of all tested comparisons are shown (unless specifically mentioned). These analyses were performed by assuming that 30% of lymphocytes were CD8+ CD3+, as has been previously demonstrated in Caucasian UK and US populations (498,499). **E**: Correlation matrix of TRM-like cell values after IV boost. The associations were assessed by comparing CD69+ CD11a hi CD45RA- (% CD8+ CD3+ T cells) cell frequencies. The Spearman's rank correlation coefficient (r) is presented in bold, and the unadjusted p value for the association is presented in italics, for each association. A two-stage linear step-up, Benjamini, Krieger and Yekutieli approach was used to control*

the FDR (Q), which was set at 3%. This suggested that p values less than 0.0117 should be considered true discoveries. True discoveries are highlighted by red boxes.

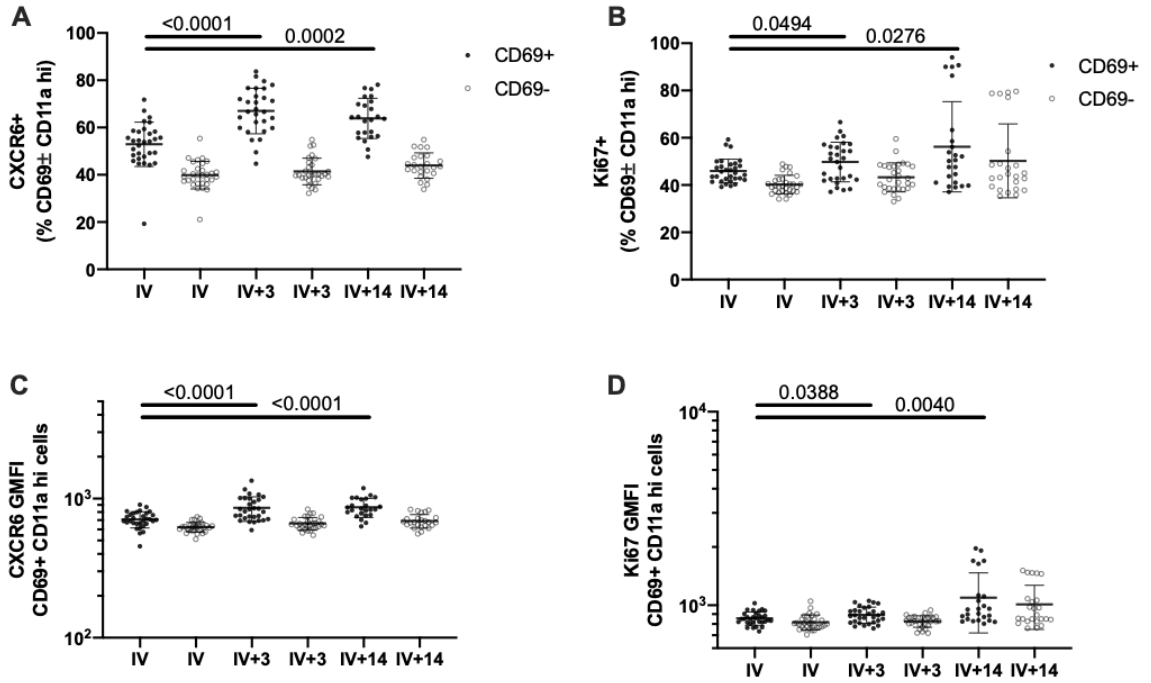


*Figure 5.3: TRM-like cell phenotype after IV boost. Two TRM-associated markers were examined: CXCR6 and Ki67. **A & B**: CXCR6+ (**A**) and Ki67+ (**B**) frequencies of CD69+ and CD69- CD11a hi CD45RA- CD8+ CD3+ T cells. **C & D**: CXCR6 (**C**) and Ki67 (**D**) geometric mean fluorescence intensities of CD69+ and CD69- CD11a hi CD45RA- CD8+ CD3+ T cells. CD69- (effector memory T cell) frequency and expression of the markers are presented as an internal comparator. All comparisons between CD69+ and CD69- cells were significant (p<0.001). Significance testing of differences between individual groups was performed using ratio paired t-tests, and the resultant p values of all tested comparisons are shown (unless specifically mentioned). Statistics were performed on non-transformed data.*

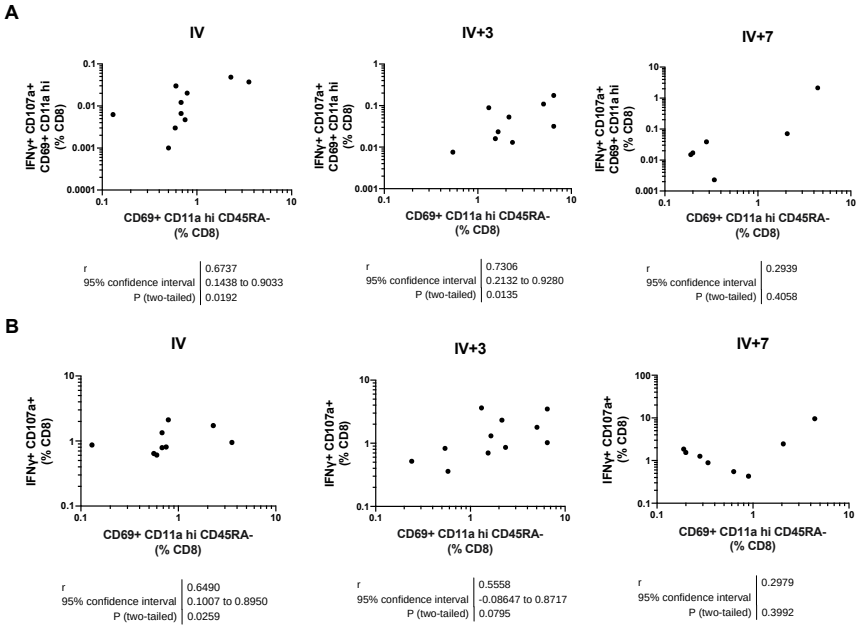


*Figure 5.4: Correlations between AgSp T cells and non-AgSp TRM-like cells. **A**: AgSp TRM-like cells vs non-AgSp TRM-like cells as frequencies of CD8+ T cells on the day of vaccination, and three and seven days after vaccination. **B**: AgSp CD8+ T cells vs non-AgSp TRM-like cells as frequencies of CD8+ T cells on the day of vaccination, and three and seven days after vaccination. Spearman's rank correlation coefficient and an exact p value are reported. Statistics were performed on non-transformed data.*

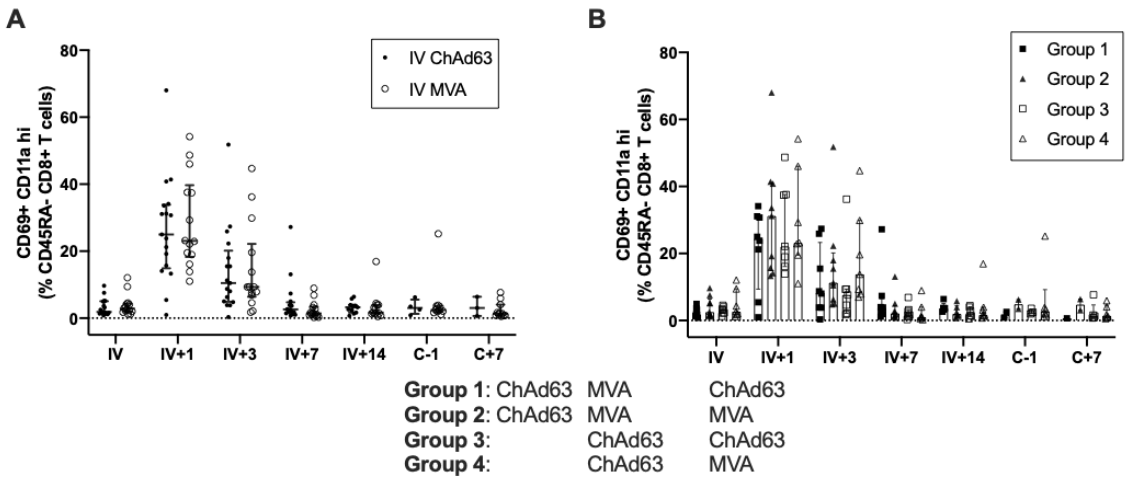


*Figure 5.5: TRM-like cells after IV boost, by IV viral vector and by vaccination regimen. **A**: CD69+ CD11a hi cells as proportions of CD45RA- CD8+ CD3+ T cells at six time points after IV boost, stratified by the IV viral vector. Groups 1 & 3 received ChAd63 ME-TRAP IV and groups 2 & 4 received MVA ME-TRAP IV. There were no significant differences between groups 1 & 3 and 2 & 4 within each time point. **B**: CD69+ CD11a hi cells as proportions of CD45RA- CD8+ CD3+ T cells, stratified by group, which all received differing vaccination regimens. There were no significant differences between groups at any time point (differences tested with an ordinary one-way ANOVA). Within-group differences were significant comparing IV to IV+1 or IV+3 for all groups, except when comparing IV to IV+3 in group 3 (differences tested with paired ratio t tests). Median values are presented, and error bars represent the interquartile range.*

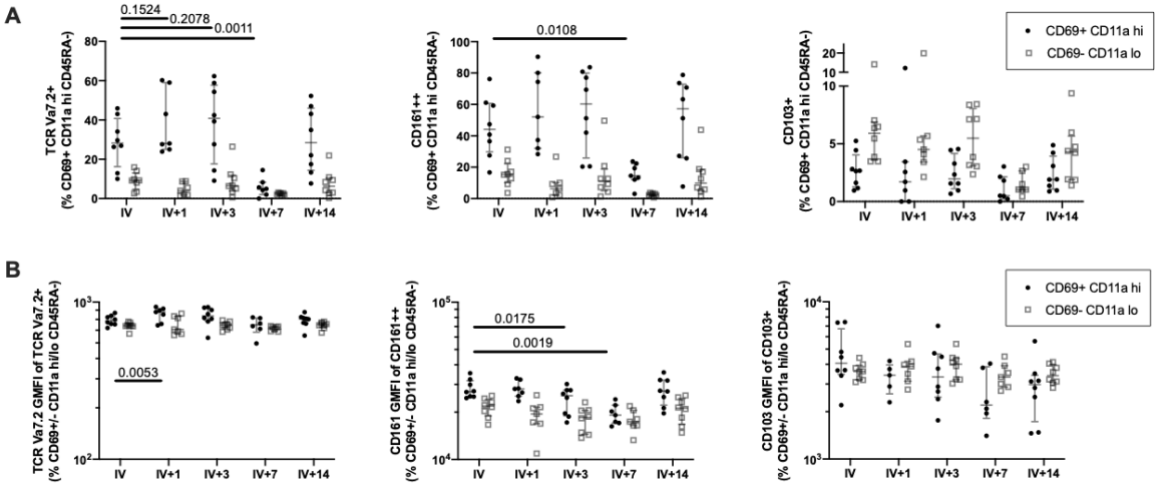


*Figure 5.6: CD69+ CD11a hi subset composition. **A**: TCRVα7.2+ (left), CD161++ (middle) and CD103+ (right) frequencies of CD69+ and CD69- CD11a lo CD45RA- CD8+ CD3+ T cells. **B**: TCRVα7.2 (left), CD161 (middle) and CD103 (right) geometric mean fluorescence intensities of marker positive populations of CD69+ CD11a hi and CD69- CD11a lo CD45RA- CD8+ CD3+ T cells. CD69- CD11a lo frequency and expression of the markers are presented as internal comparators. Significance testing of differences between individual groups was performed using ratio paired t-tests, and the resultant p values of all tested comparisons are shown (unless specifically mentioned). Statistics were performed on non-transformed data.*

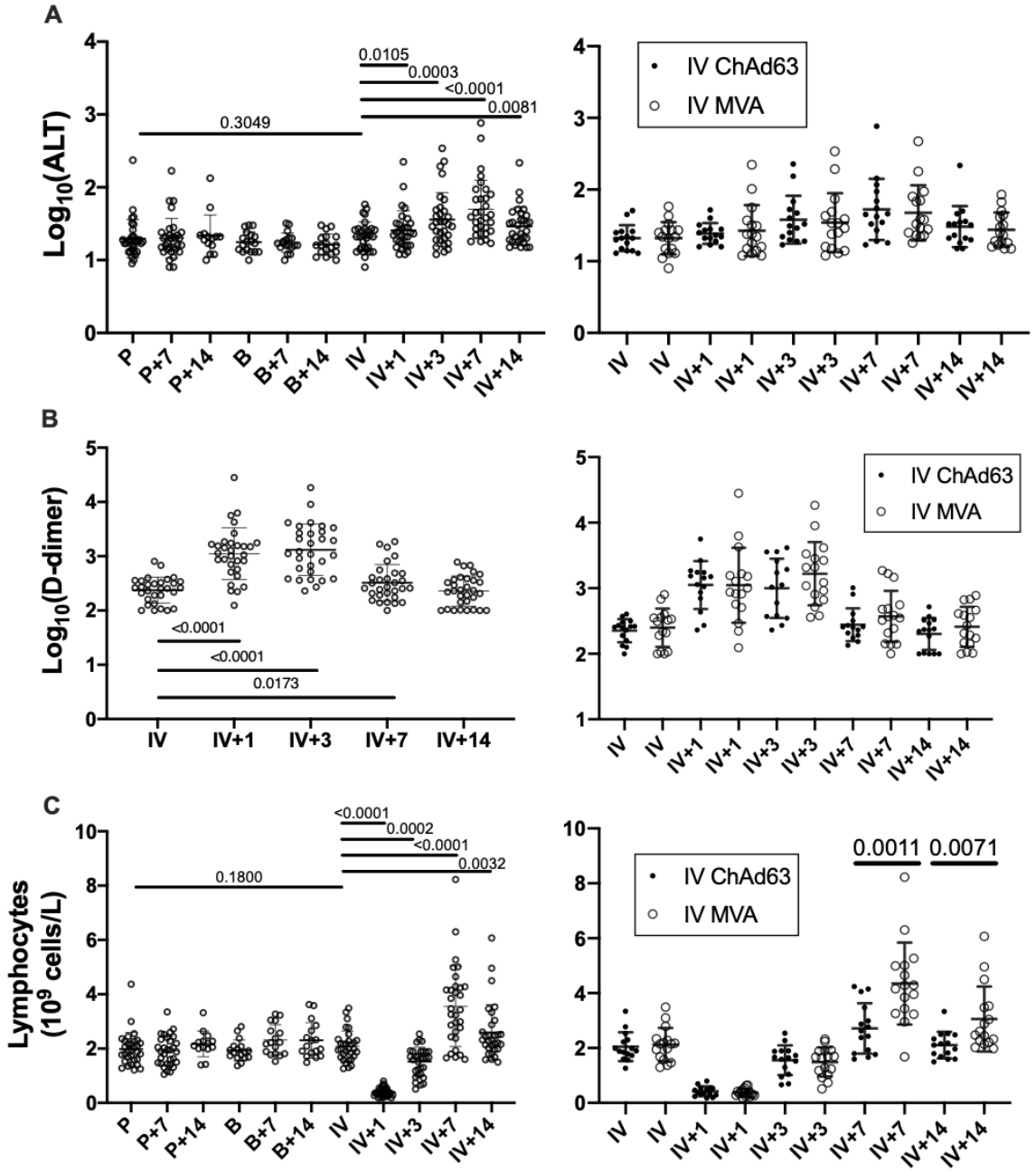


*Figure 5.7: Clinical biochemistry and haematology. **A**: Log-transformed ALT in all volunteers, at eleven time points during the study (left) and stratified by IV viral vector at post-IV time points (right). Groups 1 & 3 received ChAd63 ME-TRAP IV and groups 2 & 4 received MVA ME-TRAP IV. There were no significant differences between groups 1 & 3 and 2 & 4 within each time point. **B**: Log-transformed D-dimer in all volunteers (left) and in all volunteers stratified by IV viral vector (right). D-dimer was only measured at post-IV time points. There were no significant differences between groups 1 & 3 and 2 & 4 within each time point. **C**: Lymphocyte concentrations in all volunteers, at eleven time points during the study (left) and stratified by IV viral vector at post-IV time points (right). Mean values are presented, and error bars represent the standard deviation. B, IM boost. B+n, n days after IM boost vaccination. P, prime. P+n, n days after IM prime vaccination.*

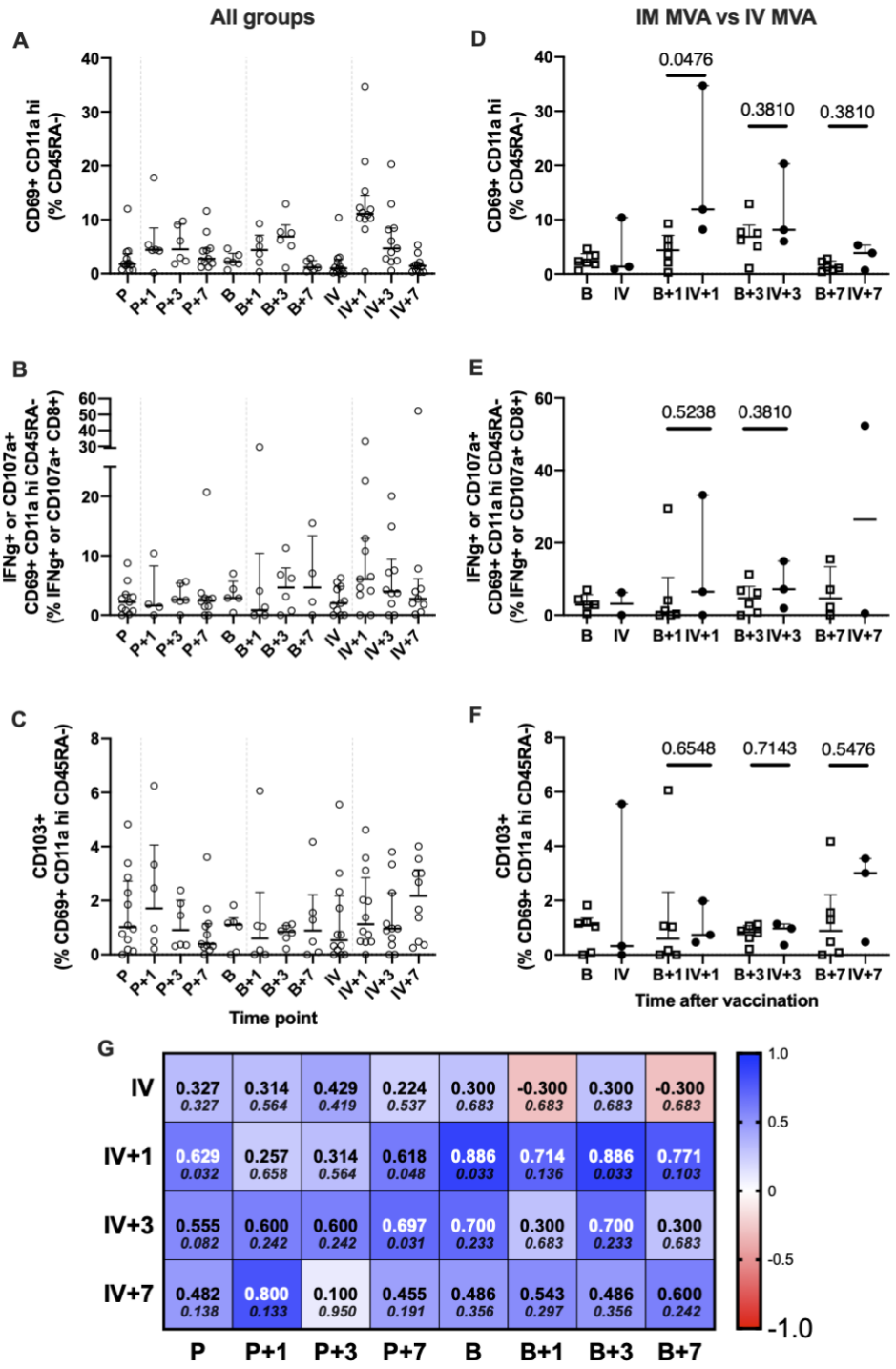


Figure 5.8: T cell subsets over prime, IM boost and IV boost vaccination. ***A, B, C****: CD69+ CD11a hi cells as proportions of CD45RA- CD8+ CD3+ T cells (****A****), IFNγ+ or CD107a+ CD69+ CD11a hi CD45RA- cells as proportions of total IFNγ+ or CD107a+ CD8+ T cells (****B****), and CD103+ cells as proportions of CD69+ CD11a hi CD45RA- CD8+ CD3+ T cells (****C****) at 12 time points during the study. The values are aligned by IV boost and prime vaccination. Groups 1 & 2 received three vaccinations; groups 3 & 4 received two vaccinations. All groups are included for descriptive purposes. Grey lines represent vaccination. Differences were not assessed for statistical significance.* ***D, E, F****: The same three parameters as in A, B and C, respectively, comparing IM boost time points to IV boost time points when volunteers received only one previous vaccination (IM ChAd63). Only values from group 4 (IV MVA, N=3 samples) and groups 1 & 2 (IM MVA, N=6 samples) were compared. Differences were tested with a MW test. Median values are presented, and error bars represent the interquartile range.* ***G****: Correlation matrix of TRM-like cell values after IM prime, IM boost and IV boost vaccinations. The associations were assessed by comparing CD69+ CD11a hi CD45RA- (% CD8+ CD3+ T cells) cell frequencies. The Spearman's rank correlation coefficient (r) is presented in bold, and the unadjusted p value for the association is presented in italics, for each association. A two-stage linear step-up, Benjamini, Krieger and Yekutieli approach was used to control the FDR (Q), which was set at 1%. No p value threshold was set as none of the associations were deemed true discoveries.*

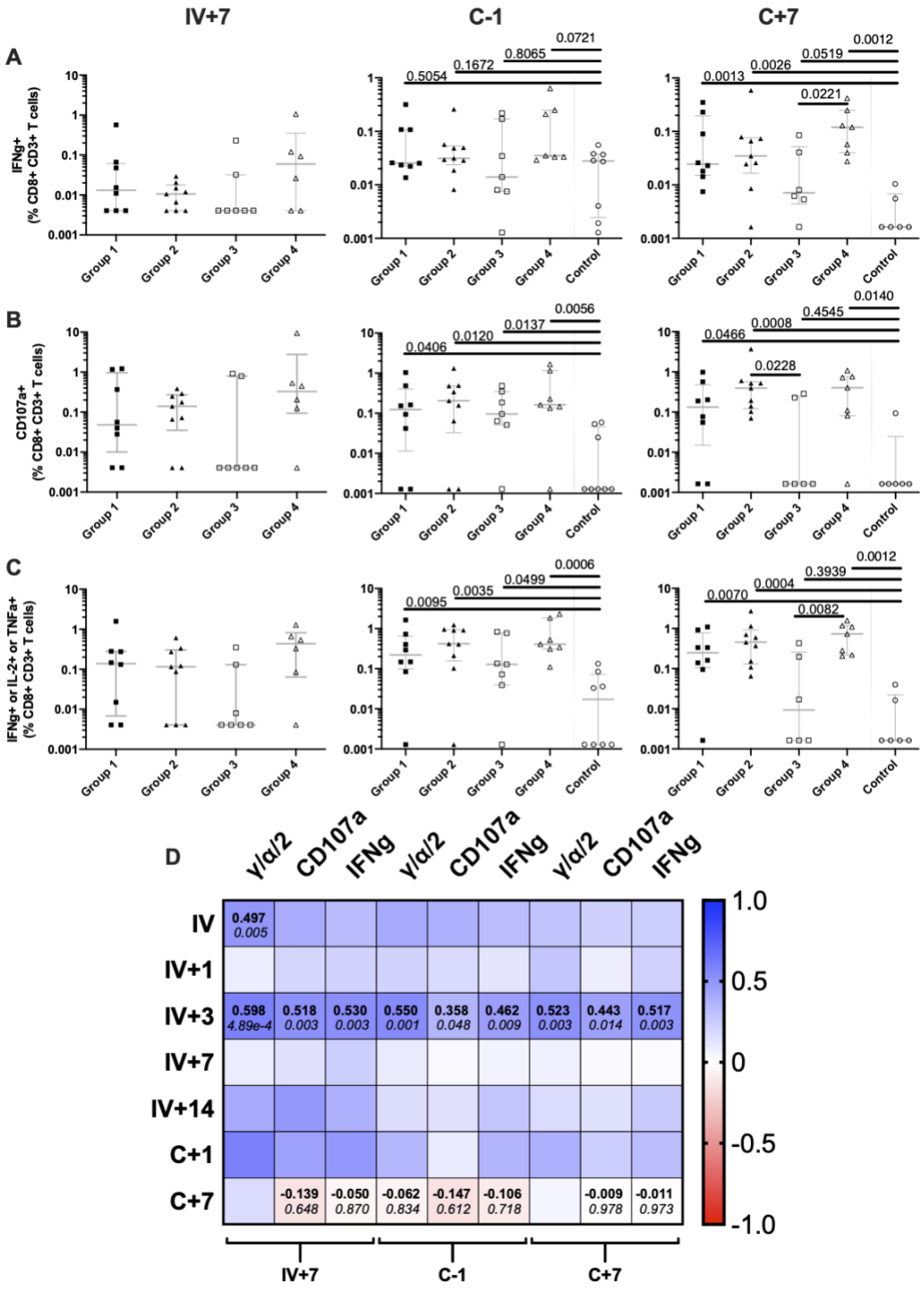


*Figure 5.9: AgSp CD8+ T cell subsets. **A, B, C**: AgSp T cells subsets at three time points in VAC066: IV+7 (left), C-1 (middle) and C+7 (right). **A**: IFNγ+ cells as proportions of CD8+ CD3+ T cells. **B**: CD107a+ cells as proportions of CD8+ CD3+ T cells. **C**: IFNγ+, TNFa+ or IL-2+ cells as proportions of CD8+ CD3+ T cells. The control group was composed of unvaccinated malaria-naïve volunteers. There were no significant differences between groups at the IV+7 time point, in any of the three parameters. Differences were tested with a MW test. Median values are presented, and error bars represent the interquartile range. **D**: Correlation matrix of TRM-like cell frequencies and the AgSp CD8+ T cell subsets. Rows represent TRM-like cell frequencies; CD69+ CD11a hi CD45RA- (% CD8+ CD3+ T cells) cell frequencies, measured at the indicated time point. Columns indicate the three AgSp T cell subsets from A, B, and C, at the indicated time points (bottom). The Spearman's rank correlation coefficient (r) is presented in bold, and the unadjusted p value for the association is presented in italics, for several noteworthy associations. Empty squares indicate associations that were not statistically significant. A two-stage linear step-up, Benjamini, Krieger and Yekutieli approach was used to control the FDR (Q), which was set at 5%. This suggested that p values less than 0.00596 should be considered true discoveries.*

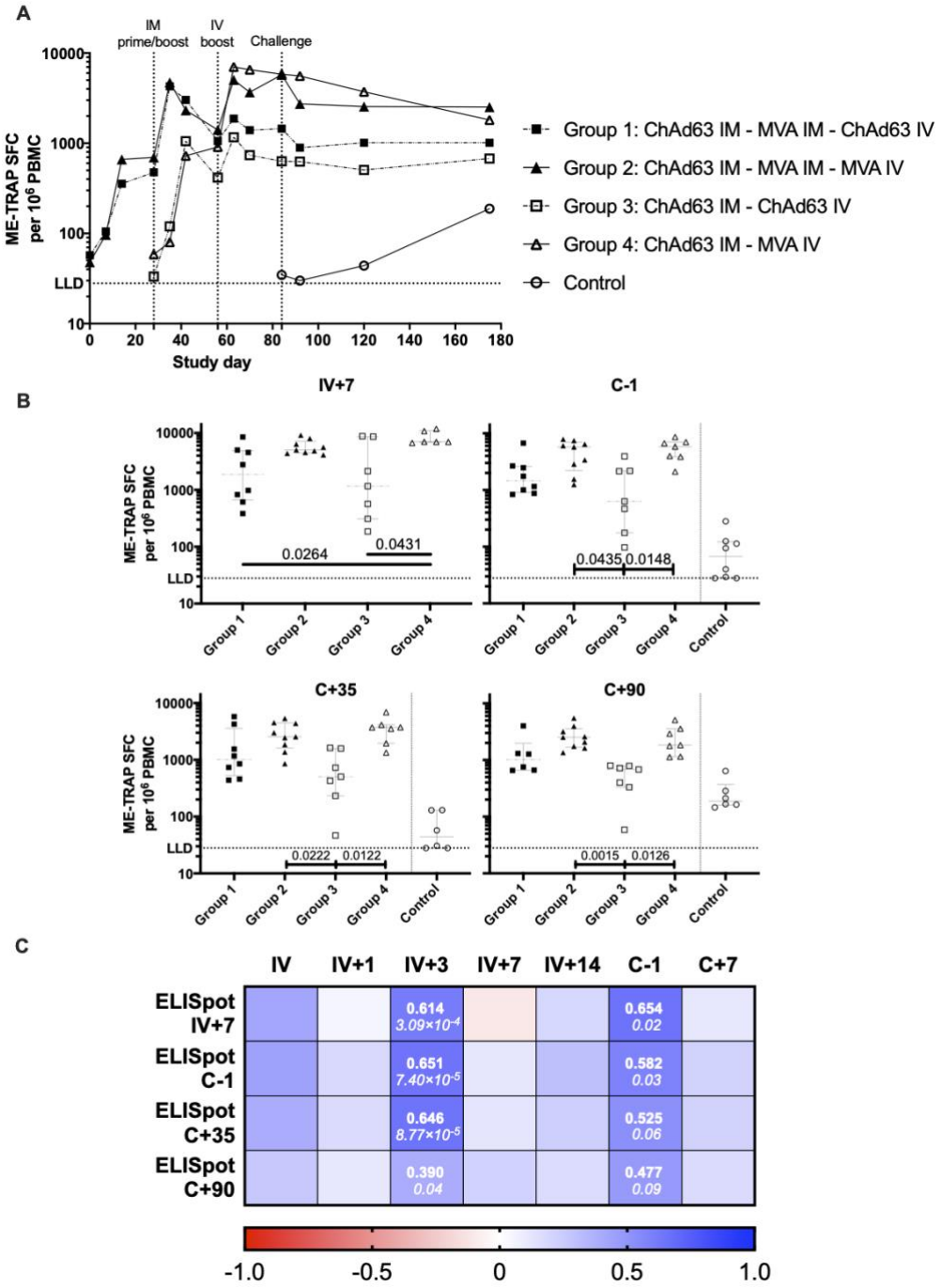


Figure 5.10: AgSp T cell response kinetic by IFNγ ELISpot. ***A****: Time course of ME-TRAP T cell response by ex vivo IFN-γ ELISpot at all time points assessed in VAC066. The values are aligned by IV boost. Groups 1 & 2 received three vaccinations; groups 3 & 4 received two vaccinations (see legend). Dotted lines represent vaccination timings. Median values are presented, and differences were not assessed for statistical significance. The control group was composed of unvaccinated malaria-naïve volunteers. These results are derived from T9/96 strain TRAP and ME peptide pool stimulations.* ***B****: ME-TRAP-responsive T cells at four time points: IV+7 (upper left), C-1 (upper right), C+35 (lower left) and C+90 (lower right). Comparisons between the control group and intervention groups were conducted but are not shown here (see text). Differences were tested using the KW test with Dunn's correction for comparisons between multiple groups (groups 1-4 and control). Significant differences are shown here. Statistics were performed on non-transformed data.* ***C****: Correlation matrix of TRM like cell frequencies and ME-TRAP-responsive T cells by ELISpot. Columns represent TRM-like cell frequencies; CD69+ CD11a hi CD45RA- (% CD8+ CD3+ T cells) cell frequencies, measured at the indicated time point. Rows indicate the IFN-γ ELISpot AgSp T cell response from B, at the indicated time points (left). The Spearman's rank correlation coefficient (r) is presented in bold, and the unadjusted p value for the association is presented in italics, for several associations. Empty squares indicate associations that were not statistically significant. A two-stage linear step-up, Benjamini, Krieger and Yekutieli approach was used to control the FDR (Q), which was set at 3%. This suggested that p values less than 0.0035 should be considered true discoveries. LLD, lower limit of detection.*

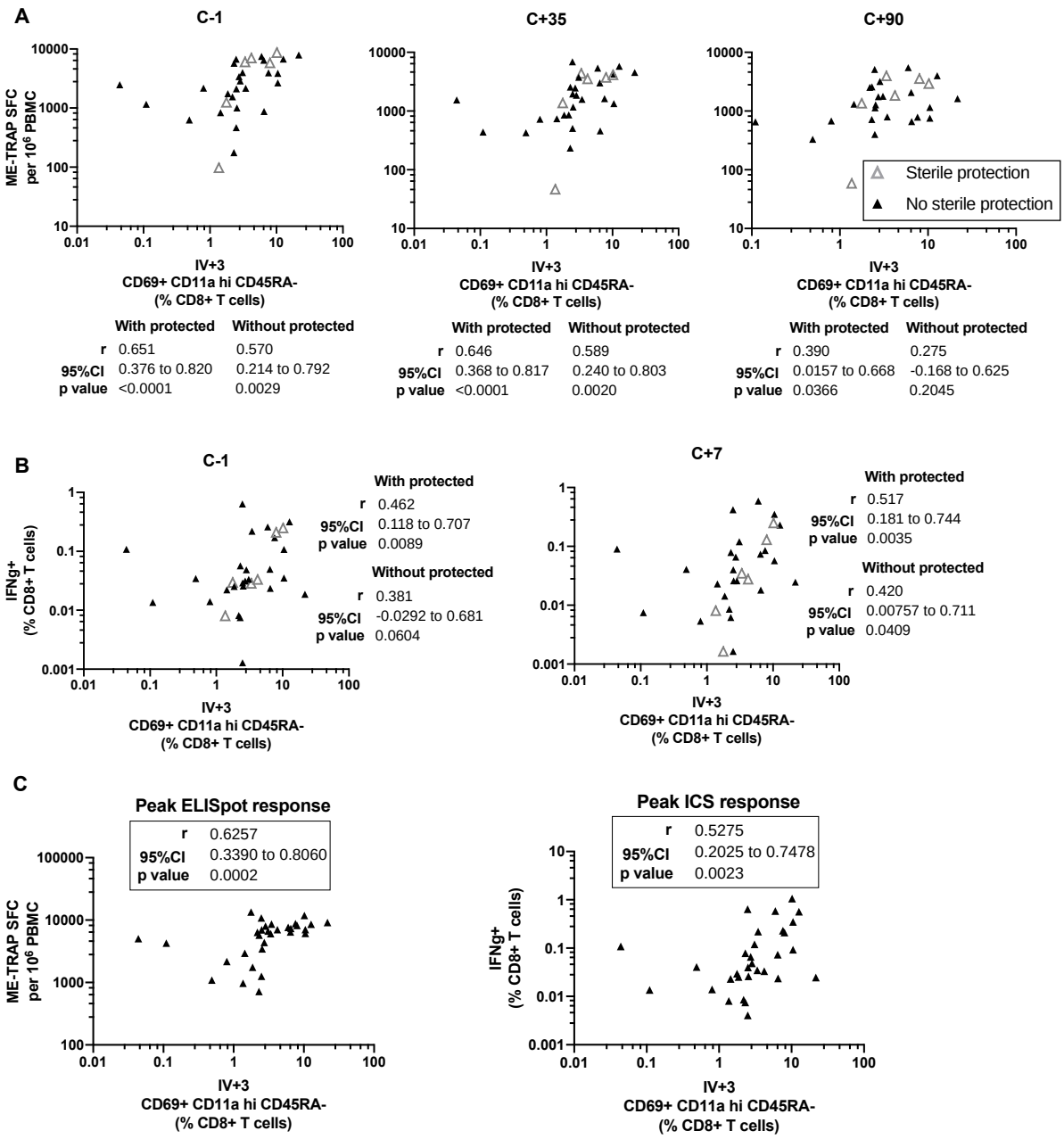
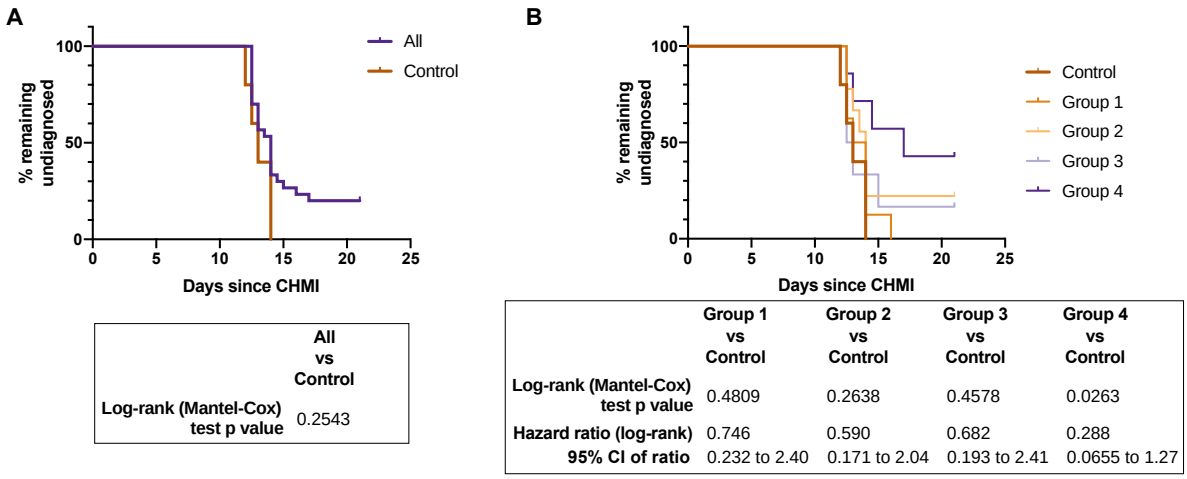


*Figure 5.11: IV+3 TRM-like cells vs ELISpot and ICS responses. X-axes and values are shared between all plots. Empty grey triangles represent volunteers that achieved sterile protection and were removed from the "without protection" analyses. **A**: TRM-like cell frequencies; CD69+ CD11a hi CD45RA- (% CD8+ CD3+ T cells) cell frequencies, at IV+3, compared to IFNγ ELISpot AgSp T cell response at C-1 (left), C+35 (middle) and C+90 (right). **B**: TRM-like cell frequencies at IV+3, compared to IFNγ+ cell (% CD8+ CD3+ T cells) response at C-1 (left) and C+7 (right). **C**: TRM-like cell frequencies at IV+3, compared to the maximum IFN-γ ELISpot AgSp T cell response (left) and the maximum IFNγ+ cell (% CD8+ CD3+ T cells) response as measured by ICS (right). IFN-γ ELISpot was performed at between 10 and 13 time points, and ICS was performed at three time points. Spearman's rank correlation coefficient, the correlation coefficient 95% confidence interval and an approximate, unadjusted p value are reported. Statistics were performed on non-transformed data.*



	All vs Control
Log-rank (Mantel-Cox) test p value	0.2543

	Group 1 vs Control	Group 2 vs Control	Group 3 vs Control	Group 4 vs Control
Log-rank (Mantel-Cox) test p value	0.4809	0.2638	0.4578	0.0263
Hazard ratio (log-rank)	0.746	0.590	0.682	0.288
95% CI of ratio	0.232 to 2.40	0.171 to 2.04	0.193 to 2.41	0.0655 to 1.27

*Figure 5.12: Kaplan-Meier log-rank comparisons of vaccinated compared to control groups. **A**: Kaplan-Meier log-rank comparison of days to diagnosis from CHMI between all vaccinated volunteers (n=30) and controls (n=12). **B**: Kaplan-Meier log-rank comparison of days to diagnosis from CHMI between group 1 (n=8), group 2 (n=9), group 3 (n=6) and group 4 (n=7), and controls (n=12).*

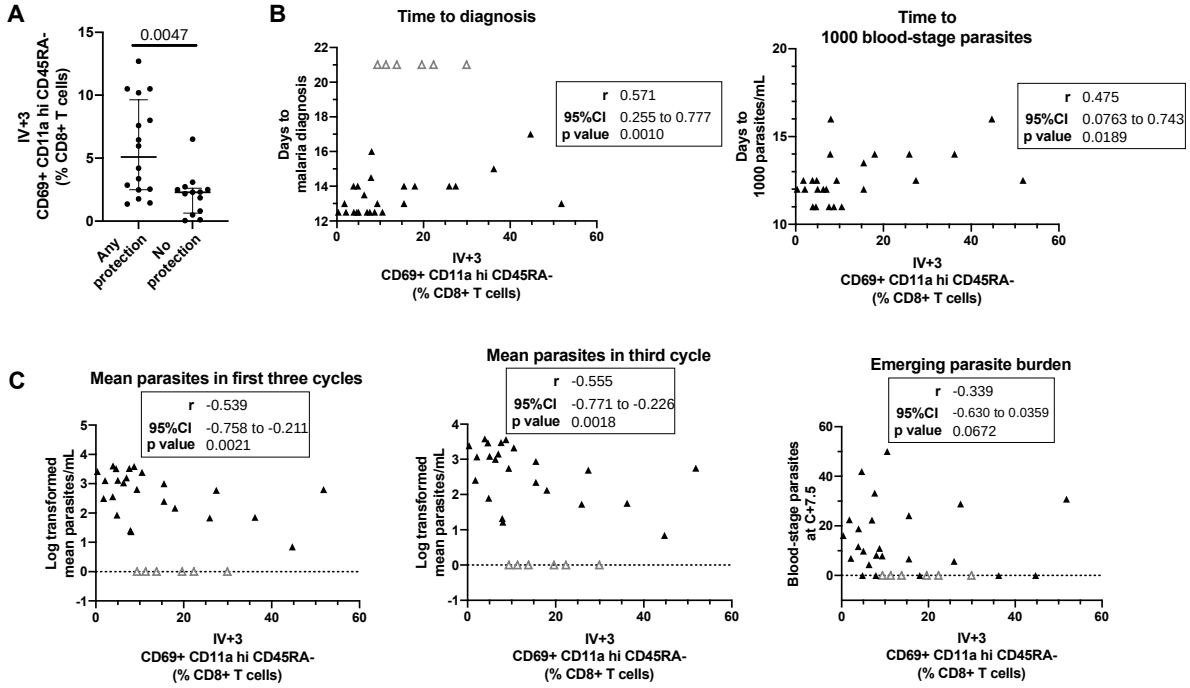


*Figure 5.13: IV+3 TRM-like cells vs indicators of vaccine-induced protection. **A**: TRM-like cell frequencies (CD69+ CD11a hi CD45RA- (% CD8+ CD3+ T cells)) measured at IV+3 compared across volunteers who experienced any (sterile or partial) vaccine-induced protection and those with no protection. Partial protection was defined as volunteers with a diagnosis of malaria 14 days or later, after infectious mosquito bite (176). **B**: Associations of TRM-like cell frequencies at IV+3, and time-to-malaria diagnosis (left) and time-to-1000 blood-stage parasites detected by qPCR (right). Empty grey triangles represent volunteers that were right-censored from the study and deemed to have achieved sterile protection from malaria. These volunteers did not reach 1000 blood-stage parasites, therefore were not included in this analysis. **C**: Associations of TRM-like cells and the mean number of parasites in the first three replication cycles (left), in the third replication cycle (middle) and at day 7.5 (the point of liver parasite emergence) after CHMI (right). Spearman's rank correlation coefficient, the correlation coefficient 95% confidence interval and an approximate, unadjusted p value are reported. Statistics were performed on non-transformed data. For log-transformed PCR data, a pseudocount value of one was added to each qPCR value to allow log transformation of zero values (y=log(1+qPCR)). A two-stage linear step-up, Benjamini, Krieger and Yekutieli approach was used to control the FDR (Q), which was set at 1%. This suggested that p values less than 0.02 should be considered true discoveries.*

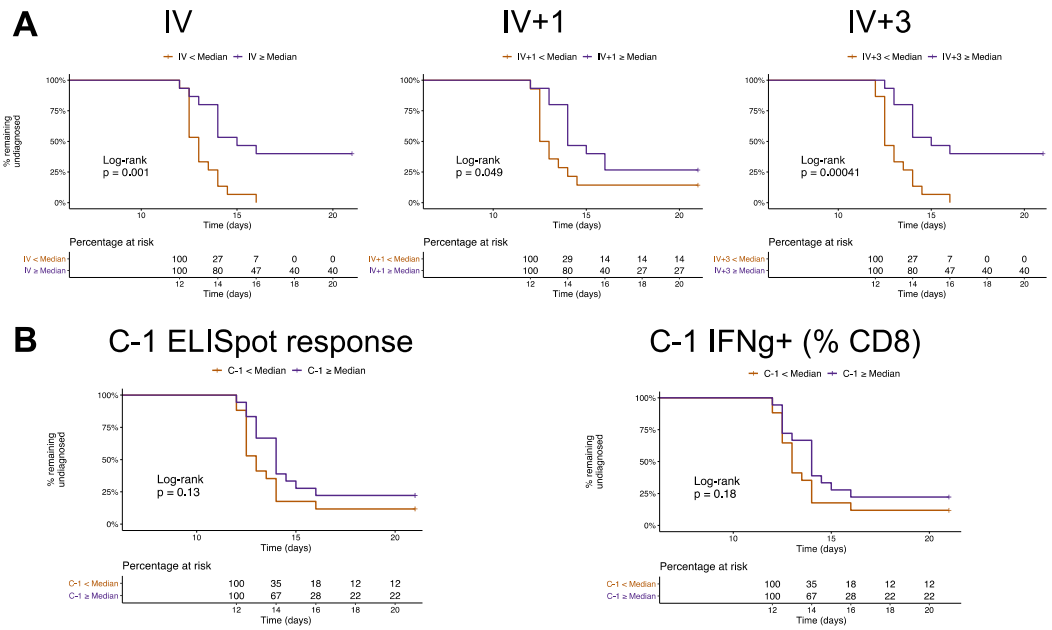


*Figure 5.14: Kaplan-Meier curves of volunteers stratified by various correlates of protective efficacy. **A**: Kaplan-Meier curve comparisons using TRM-like cells measured at several time points to stratify volunteers: TRM-like cells at the day of IV boost (left), TRM-like cells one day after IV boost (middle) and TRM-like cells three days after IV boost (middle). That is, volunteers were stratified according to whether their CD69+ CD11a hi CD45RA- frequency (% CD8+ CD3+ T cells) above or below the median of all values. A log-rank test was performed to test for difference in survival (delay/lack of malaria diagnosis), and the p value is reported in each plot. The risk table shows the percentage of volunteers, in each stratum, at risk of malaria diagnosis at five representative time points. Right censoring occurred at 21 days as all undiagnosed volunteers received antimalarial therapy. Time, on the x-axes, refers to the time after CHMI. **B**: Kaplan Meier curve comparisons using AgSp responses at C-1 to stratify volunteers: IFNγ ELISpot ME-TRAP SFC per million PBMC (left) and IFNγ+ frequency (% CD8+) as measured by ICS (right).*

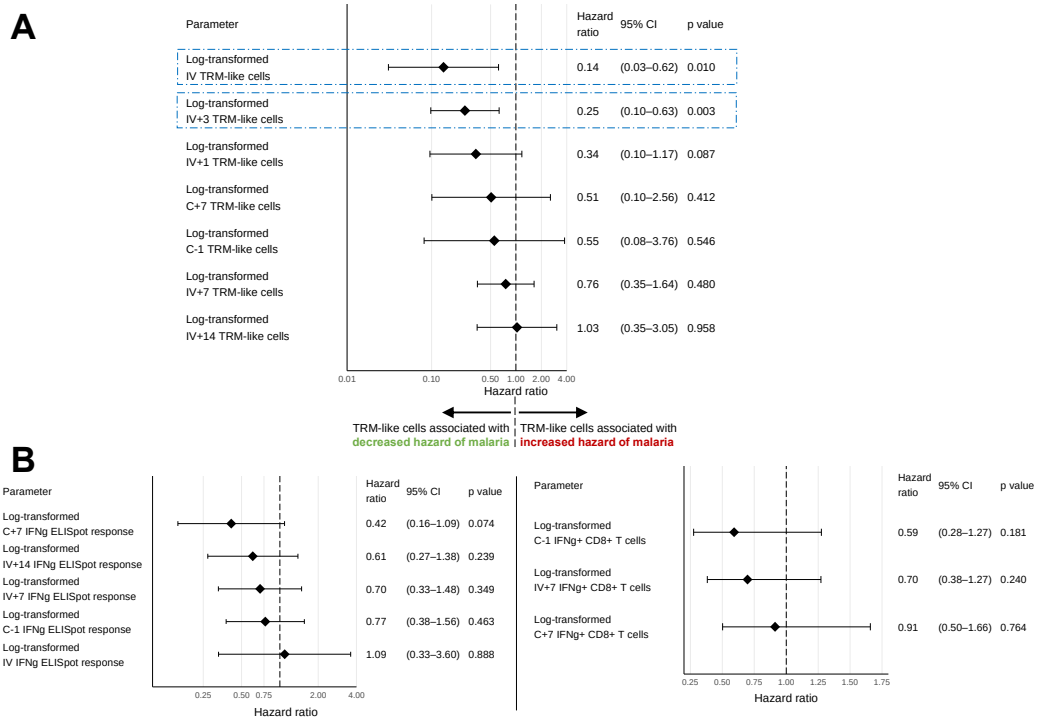


*Figure 5.15: Univariate regression models for protection from malaria after CHMI. **A**: Univariate Cox regression models using TRM-like cells (CD69+ CD11a hi frequency (% CD45RA- CD8+ CD3+ T cells)) measured at seven time points. Each regression model estimated the effect that the variable had on an individual's hazard of being diagnosed with malaria after CHMI. Hazard ratios less than one suggested that an increase in the TRM-like cell frequency decreased the instantaneous risk of malaria diagnosis over the study period. Hazard ratios greater than one suggested that a decrease in TRM-like cell frequency increased the instantaneous risk of malaria diagnosis over the study period. Log transformation*

was applied to the TRM-like cell frequency, and regression was performed on these values. The p value was calculated using a Wald test, with a null hypothesis that the parameter did not alter the hazard of malaria diagnosis after CHMI. Models with a significant p value are indicated by blue boxes. ***B****: Univariate Cox regression models using AgSp responses: IFNγ ELISpot ME-TRAP SFC per million PBMC (left) and IFNγ+ frequency (% CD8+) as measured by ICS (right).*

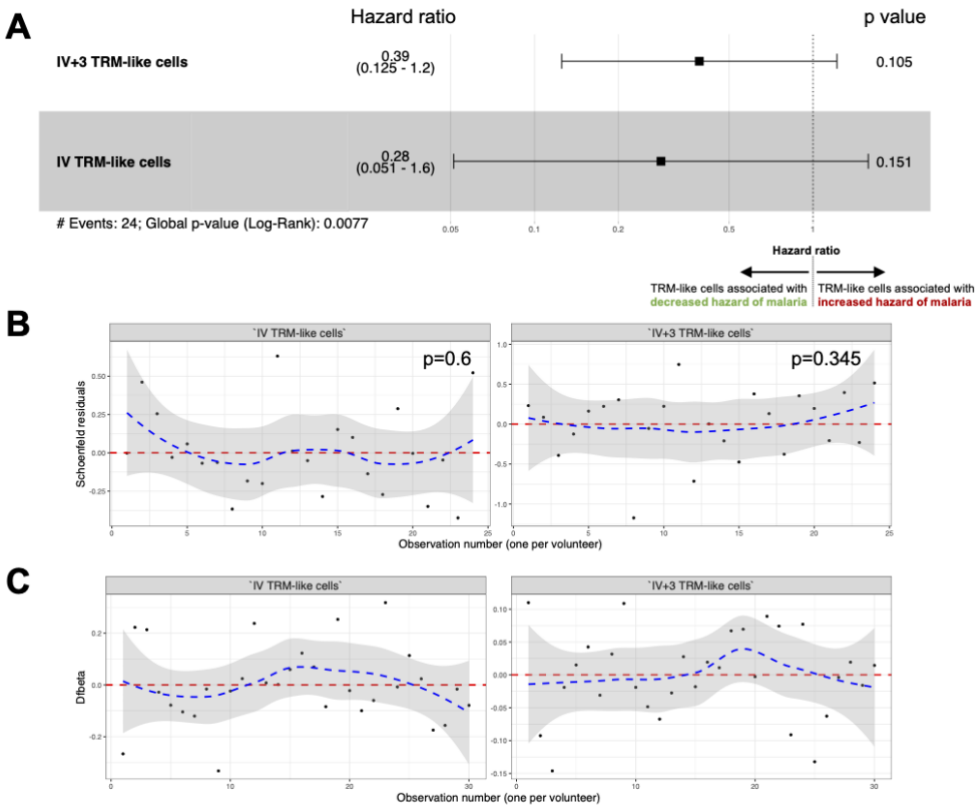


Figure 5.16: Multiple regression model for protection from malaria after CHMI, using significant TRM-like cell variables. ***A****: Multivariate Cox regression model using TRM like cells (CD69+ CD11a hi frequency (% CD45RA- CD8+ CD3+ T cells)) measured at two time points: IV and IV+3. The model estimated the effect that the variables had on an individual's hazard of being diagnosed with malaria after CHMI. Hazard ratios and 95%CI are presented. Log transformation was applied to the TRM-like cell frequency, and regression was performed on these values. The individual variable p values were calculated using a Wald test. The global p value was calculated using a Score (log-rank) test. Events refers to the number of volunteers that were diagnosed with malaria.* ***B****: Schoenfeld residuals plotted to test the proportional hazards assumption. Systematic departures from a horizontal line when plotting Schoenfeld residuals would indicate non-proportional hazards. The assumption of proportional hazards was supported for both covariates and overall, for the model (p=0.304). The blue dashed lines are fit by local linear regression (lowess), to aid in interpretation; the shading represents ± 2-standard-error envelopes around the fit. The red dashed line is at y=0.* ***C****: Dfbetas plotted to assess influential observations. Plotting dfbetas estimated the changes in regression coefficients upon deleting each observation in turn. Comparing the magnitudes of the largest dfbeta values to the regression coefficients suggests that none of the observations were largely influential.*

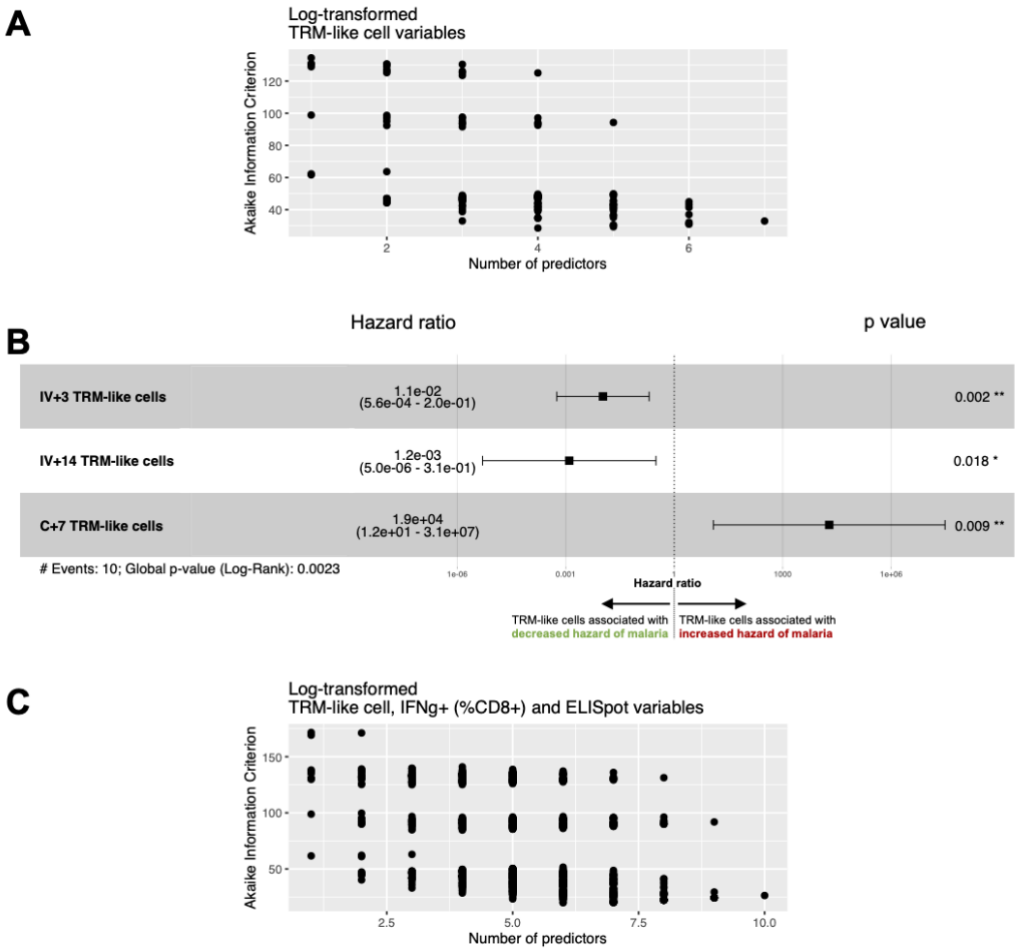


Figure 5.17: Other multiple regression models for protection from malaria after CHMI. ***A****: Akaike information criterion values of models composed of all permutations of log-transformed TRM-like cell parameters. Forward selection of variables to fit a Cox proportional hazards model of time-to-diagnosis after CHMI generated an AIC for each model.* ***B****: Multivariate Cox regression model using TRM like cells (CD69+ CD11a hi frequency (% CD45RA- CD8+ CD3+ T cells)) measured at three time points: IV+3, IV+14 and C+7. The model estimated the effect that the variables had on an individual's hazard of being diagnosed with malaria after CHMI. Hazard ratios and 95%CI are presented. Log transformation was applied to the TRM like cell frequency, and regression was performed on these values. The individual variable p values were calculated using a Wald test. The global p value was calculated using a Score (log-rank) test. Events refers to the number of volunteers that were diagnosed with malaria.* ***C****: Akaike information criterion values of models composed of all permutations of ten log-transformed TRM-like cell, IFNγ+ (%CD8+ as measured by ICS) and IFNγ ELISpot parameters.*

5.4 Discussion

5.4.1 Novel findings

The data described in this chapter provide evidence for using TRM-like cells as measures of vaccine-induced protection in the context of the liver-stage malaria vaccination strategy, prime-target, encoding ME-TRAP. Time course experiments showed that TRM-like cell frequencies reached their maximum at day one post-IV boost and that they were associated with vaccine-induced AgSp cells. While there was heterogeneity within the CD69+ CD11a hi compartment of memory T cells – in which a significant contribution came from MAIT cells – this heterogeneity was mostly unchanged over time after IV boost. TRM-like cells were shown to be consistently associated with established and validated CoP. Most predictive among measurements of TRM-like cells was at IV+3, which was seen to strongly correlate with various markers of vaccine-induced immunity and protection. Survival analysis regression models indicated that TRM-like cell frequencies were at least equivalent to, or better than, vaccine AgSp markers at estimating the hazard of malaria diagnosis after CHMI in vaccinated volunteers. Together, these results provide evidence for using TRM-like cells as vaccine-induced CoPs.

Despite CHMI studies, no single CoP has emerged for vaccine-induced protection against malaria, and it is likely that efficacy is multifactorial and complex (476). To use TRAP-based vaccine responses as an example, in non-endemic CHMI studies, responses exceeding 2000 SFC per million PBMC were induced by IM ChAd-MVA regimens (176,300), and these were variably associated with efficacy (176,300). The evidence from endemic settings presents a fickler picture, as either ME-TRAP-specific T cells did not correlate (308,478), or only a subset of the T cell response correlated with protection (307). Notably, low T cell responses in humans have been associated with an absence of sterile protection in several CHMI and natural infection studies of ME-TRAP vaccines in endemic and non-endemic settings (176,312,480). The data presented in this chapter indicated some of the strongest reported associations between T cell immunogenicity and ME-TRAP vaccine

efficacy, despite TRM-like cells not being defined in terms of ME-TRAP specificity. Many studies only present CoP information if statistically significant (500); given this, it is not altogether surprising that ME-TRAP specific responses in the present study not useful predictors of protection. By presenting TRM-like cell data in combination with that of other T cell subsets suggests the superiority of TRM-like cells as CoPs. It has been shown that assays focussing on antigen-specificity conventionally used in clinical trials are not able to detect the full breadth of T cell responses (501), which may result in difficulties establishing T cell CoPs of liver-stage malaria. Using TRM-like cells in conjunction with other markers of vaccine-induced immunogenicity may provide additional information regarding tissue-specific immunity.

One tacit assumption in the study of liver-stage malaria human T cell CoPs is that a selection of circulating T cells travel to or through the liver, and find and kill infected hepatic cells, while the majority remain in the vasculature. In fact, the exact mechanistic contribution of circulating parasite-specific CD8+ T cells (Tcirc) to the control of liver-stage malaria in humans remains to be seen (448) and data from mice suggest this may be a stochastic contribution as there is not active migration of AgSp CD8+ T cells into the liver (413). Therefore, there is a lack of direct evidence to support the notion that Tcirc are mCoPs in human liver-stage malaria, or indeed if Tcirc can become TRM. Given the strong evidence of TRM-mediated protection from liver-stage malaria in murine and non-human primate models (168,201,237,241,242), there is a need for a TRM-specific CoP. In contrast to Tcirc, a major assumption of TRM-like cells as CoPs is that they are uniquely related to TRM. In the case that this is true, as was suggested by data in Chapter 4, TRM-like cells would be poised for recirculation to, embedding in and surveillance of tissues. In mice, vaccine strategies that maximise liver TRM numbers are of highest efficacy (201); if the same is true in humans, the data presented in this chapter provide indirect evidence linking liver TRM and TRM-like cells by way of enhanced efficacy in volunteers with higher frequencies of TRM-like cells.

Nonetheless, even if TRM-like cells were a perfectly faithful index of the liver TRM niche, it would be difficult to surmise that the level of protective efficacy in the VAC066 study was solely due to the magnitude of the TRM-like cell or TRM response. This is due to the exceptionally overlapping nature of malarial immunity (502). Take, for example, the interplay between liver parasite-specific Tcirc and TRM. Both have been associated with protection against liver-stage malaria (59,168,186,237,241); however, there are presumably thresholds at which each dominates. Without and at very low levels of Tcirc, TRM predominate in protection from liver-stage parasites as they are 'geographically' and functionally more adept at protecting the liver microenvironment (201,237). Sterile protection from liver-stage malaria is possible after adoptive transfer of large quantities of parasite-specific effector T cells into naïve mice (201). Therefore, as levels of Tcirc pass a threshold (59), the level of TRM in the liver is likely of little consequence as the liver is surveyed and infected cells are killed by a large population of Tcirc. Presumably, in the short term after vaccination the quantitative advantage of Tcirc (the latter scenario) predominates but as peripheral effector populations die off and become less numerous, the qualitative advantage of TRM prevails (the former scenario), this remains to be seen in humans though. In this study, TRM-like cells were a relatively rudimentary CoP and these results do not rule out the likely beneficial contribution of Tcirc to protection, but given the finding that Tcirc did not enhance survival models, the current data do not justify their use as CoP of prime-target. Ultimately it is not the case of one (Tcirc) or the other (TRM and TRM-like cells); targeting vaccine responses towards a broad range of both resident and non-resident polyfunctional memory CD8+ T cells will probably engender more protective and longer-lasting immune responses (477).

A novel aspect of this malaria vaccine trial was the administration of a viral vector IV boost. The aim of IV boosting in this trial was to target ME-TRAP-specific T cells to the liver and stimulate TRM development (237). Although not directly compared, IV boosting improved both the immunogenicity and protective efficacy of the ChAd63-MVA heterologous prime-boost regimen,

compared to an equivalent IM-boosted regimen (300,306) (Datoo *et al.*, in prep.). IM immunisation with Ad vectors can result in several modes and locations of Ag presentation, and subsequent expansions of AgSp CD8+ T cells (416). This, and the finding that liver TRM form constitutively from activated T cells (404), suggests that IM viral vectors could potentially produce liver TRM. IV MVA and ChAd63, however, likely resulted in a greater expression of the ME-TRAP transgene and inflammation in the liver, both of which enhance hepatic TRM formation (404). The hepatic tropism of MVA, ChAd63 and other Ad vectors is known (237,503-505), particularly when given IV. The route of vaccine administration profoundly affects the immunological potency and protective efficacy of a given Ad vector (506,507), though this has been less studied using MVA vectors (508).

A long history of using Ad vectors, for example, as oncolytic vaccines and gene therapy tools has allowed considerable study into their interactions with hepatic immune populations (430,509) and hepatocytes (510) when administered IV. It is worth noting that IV delivery does not guarantee improved immunogenicity. For example, interactions with tissue-resident macrophages, such as liver KC, can result in substantial degradation of the vector (503,509), resulting in limited transgene expression and undesirable off-target toxicity (416,511). The unique pathways of viral entry into, innate activation and antigen expression in hepatocytes and KCs in IV, as opposed to IM, viral vector administration are important given the demonstrated potent induction of TRM-like cells by IV, but not IM, viral vector administration despite the ten-fold lower dose of MVA given IV. These results were consistent with NHP studies of PfSPZ vaccination that showed a significantly enhanced AgSp CD8+ T cell response in the livers of animals that received a ten-fold lower dose of IV, compared to IM or intradermal PfSPZ (242). While the widespread implementation of a malaria vaccine requiring an IV vaccination is a clear challenge especially in infants (296,512), the IV boost used in this study was useful for the in-depth examination of CoPs, such as TRM-like cells.

Were TRM-like cells predictors of vaccine-induced protection because they stimulated the development of AgSp TRM or because they performed direct effector functions? This question was not directly answered, though some hypotheses can be made. In trials of PfSPZ vaccination, Vγ9+Vδ2+ T cells measured at the time of vaccination correlated with the outcome of CHMI (242). These, and other innate-like T cells such as MAIT or iNKT cells, can serve as APCs (513-515), produce enhanced priming of CD8+ T cells (515,516), and are capable of very rapid activation (517,518). γδ T cells have been shown to contribute to protection against pre-erythrocytic malaria in mouse models (519), and these T cells expand in humans following sporozoite immunisation (520). Additionally, MAIT and γδ T cells express tissue-homing molecules, enabling recirculation to tissues (472,521). TRM-like cells measured at IV boost correlated with AgSp responses and protection, and they were induced very rapidly after IV boost. This is not the first time that a non-vaccine-AgSp predictor measured before vaccination has correlated to vaccine-induced protection. Warimwe *et al.* showed that individual-level differences in RTS,S efficacy could be attributed to variations in the ratio of monocytes to lymphocytes in peripheral blood when measured before vaccination (522). Therefore, it may have been that TRM-like cells were rapidly produced as a result of IV boost, returned to the liver shortly after and performed innate-like help functions, locally enhancing the production of TRM.

On the other hand, TRM-like cells may have gone on to have direct effector functions. Mouse studies demonstrate that Tcirc have the capacity to i) produce skin TRM after viral infection (523), and ii) convert to mucosal TRM *in situ* upon cognate antigen presentation (213). TRM proliferate vigorously in recall responses in the skin (524) and female reproductive tract (213), suggesting secondary memory TRM can originate from circulating or resident progenitors. Further, TRM-like cells may have simply correlated to an individual's capacity to mount an effector response, and the magnitude of the TRM-like cell response was associated with a greater AgSp effector memory response. This hypothesis was supported by the fact that IV+3 TRM-like cell

frequencies correlated with short- and longer-term AgSp T cell responses, however, it does not account for the association between the IV TRM-like cell frequency and protection. While these scenarios are likely over-simplifications and may even co-occur, the question remains open as to whether TRM-like cells had direct effector functions in the liver. Thus, the generation of diverse CD8+ T cell populations through vaccination is likely to provide the most resilient immunity.

5.4.2 Limitations

There were several limitations to this work. The fundamental feature in defining a T cell response is its magnitude (477), and this is usually denoted as the frequency of AgSp T cells or the proportion of cells exhibiting a specific effector function, such as IFNγ production (176,306,492). Nevertheless, these single parameter measurements are restrictive and do not reflect the full functional potential of a T cell response. In this respect, the frequency of TRM-like cells as a CoP is inadequate at describing the quality of a vaccine-induced response. Moreover, the overlapping contribution of TRM and other T cells resulted in a situation whereby two individuals had almost identical TRM-like cell frequencies, but vastly different protective outcomes. As mentioned though, redundancy is a complicating aspect of malarial immunity and not unique to TRM-like cells (106,448).

Other limitations related to the statistical analyses presented. Prentice presented a set of criteria for hypothesis-testing in the validation of substitute endpoints, which can be applied to CoPs (500). One of the criteria is that the substitute endpoint (in this case, the CoP) is significantly related to vaccination status (525). In this sense, TRM-like cells were not measured at time points such as at IV boost or IV+3 in the non-vaccinated controls. Therefore, this criterion was not met by TRM-like cell frequencies as CoPs. TRM-like cells were measured at C-1 and C+7 in the control group, and these were not correlated with any degree of protection (data not shown). Indeed, non-vaccinated individuals may not have been suitable negative controls for assessing TRM-like cells as

CoPs or vaccine efficacy in this trial of IV boosting. A group vaccinated IV with MVA or ChAd63 without antigenic inserts (or irrelevant antigens), as well as the same IM vaccines given to the intervention groups, would provide an adequate null case to address these limitations. Additionally, this was an open-label non-randomised trial that was subject to the limitations inherent in this design. Age (range 20-45yo), sex (10/35 were female) and ethnicity (25/35 identified as White British, 34/35 identified as White) may have been important influencers of inter-group variability but were not significantly associated with overall protection when assessed in univariate Cox models (data not shown). Histocompatibility and immunogenetics information were available, but the HLA-mediated impact on TRM-like cell (or other T cell) frequency was not assessed given an underpowered study to assess these effects adequately.

TRM-like cells were defined in the absence of specificity for the ME-TRAP antigen. This was performed to reduce the complexity of the flow cytometry assay and allow meaningful analysis. In a sub-analysis, the total TRM-like cell frequency positively correlated with both total AgSp CD8+ frequencies and AgSp TRM-like cell frequencies, when measured in the same assay. Additionally, TRM-like cells measured at IV+3 reliably correlated with short- and longer-term vaccine-specific responses measured by separate ICS and IFNγ ELISpot assays. Indeed, CD11a hi has been used to define a fraction of circulating memory *P. falciparum* liver-stage-specific CD8+ T cells (178); notably though these studies were performed before the recent interest in TRM-mediated liver-stage immunity. Therefore, TRM-like cells were a reliable index of the AgSp response.

It would be plausible to assert that the specificity of TRM-like cells was directed predominantly against MVA or ChAd63 epitopes. Anti-vector T cell responses have the potential to limit vaccine-transgene specific T cell responses by eliminating the vector prior to substantial transgene expression, though the effect of this has been shown to be limited following multiple doses of ChAd63 (306) and similar ChAds (526). Likewise, multiple MVA vaccinations do not induce

detrimental anti-vector immunity (306). Thus, the T cell component of the anti-vector response is likely to have a limited effect on ME-TRAP specific T cell responses. Furthermore, Ad T cell responses and clearance have been shown to follow liver enzyme elevation (527), rise sharply at six days and peak at eight days after IV Ad in mice (528). These studies, however, were performed in the context of primary Ad vaccination. The presented data showed that ALT reached its peak at IV+7. Therefore, it appears unlikely that TRM-like cells were entirely, or indeed chiefly, directed against the vectors.

5.4.3 Further questions

The statistical association between TRM-like cells and protection from malaria is worthy of further investigation. Several potential CD8+ T cell covariates were examined as part of univariate analyses given their necessity and sufficiency for liver-stage protection in most mouse and NHP studies (57,243,448). Not all potential covariates were examined, and the contribution of AgSp CD4+ (166,167), Vδ2+ γδ (166,242,529), NK (530), MAIT (472) and NKT (530) cells to vaccine-induced protection from experimental and clinical malaria should not be overlooked in further studies of prime-target. Still, it was reassuring that despite the relatively small sample size, the modelled effect of TRM-like cell frequency on vaccine efficacy was not strengthened by including the magnitude of AgSp responses or other T cell subsets.

Whether inter-individual variation in efficacy of prime-target strategies encoding other antigens correlate with differences in TRM-like cell frequencies remains an open question. No differences in TRM-like cell frequencies were observed at group (and vaccination regimen) level, as was the case for AgSp responses measured at most time points. While the heterogeneity of TRM-like cells was explored in this and the previous chapter, further assessment is needed and technologies such as cytometry by time-of-flight (531,532) may help to define, at a more granular level, subsets of TRM-like cells. Equally, the proportion of TRM-like cells that are vaccine-antigen-specific may be

assessed by the combination of activation-induced marker assays, FACS and some form of TCR sequencing, as exemplified by Waickman *et al.* (533).

Antibody responses were unlikely to be strong influencers of prime-target-mediated protection. ME-TRAP specific antibodies have previously been shown to be poor predictors of protection of ME-TRAP-directed vectored vaccines (106,176). Anti-ME-TRAP antibodies in all groups, while significantly elevated compared to controls, were equivalent or less than (not statistically significant differences, data not shown) the responses generated by equivalent IM ChAd63-MVA regimens (300,306). Interestingly, single-dose IV ChAd63 or IV MVA induce either very low or undetectable levels of anti-TRAP antibodies (unpublished work, Duncan Bellamy, Jenner Institute). Previous studies have shown a negative correlation between pre-vaccination neutralising ChAd63 antibodies and vaccine-induced T cell responses, but this was not evident after boosting with MVA, suggesting that post-vaccination-induced anti-vector immunity was not associated with inhibition of cellular immunity (534). Anti-vector immunity has not been associated with reduced efficacy in trials of ChAd63 and MVA vectored liver-stage malaria vaccines (176).

5.4.4 Conclusion

These data indicate the utility of using TRM-like cells as correlates of vaccine-induced immunity and protection. TRM-like cell frequency peaked very early after IV boost and exhibited phenotypic features akin to liver TRM. There was limited heterogeneity within the TRM-like cell subset over time after vaccination. Regression models suggested that TRM-like cell frequencies were at least equivalent to ME-TRAP AgSp markers at predicting the risk of malaria diagnosis after CHMI. Many questions remain, however, as to the exact contribution of TRM-like cells in pre-erythrocytic immunity to malaria. To simplify and contextualise this work one may ask 'have immunological CoPs accelerated malaria vaccine development?' To which the somewhat reductive answer, based on previous performance, would be 'no' or 'very little'. Even when iterative development has been

directed by immunological insights (for example with RTS,S or vectored ME-TRAP vaccines), substantial improvements in efficacy have not ensued. Nonetheless, these results provide a valuable contribution to the emerging field of TRM-targeted malaria vaccine strategies. Despite remaining challenges, recent exciting progress and emerging knowledge provide promise for the future. Better insights arising from multi-parameter immunological assays and technologies, advanced statistical methods, and the availability of CHMI in endemic and non-endemic settings, could contribute to the more efficient development of efficacious next-generation malaria vaccines. Ultimately, there is promise that vaccines will complement the suite of interventions required to eliminate and eventually eradicate *P. falciparum* malaria.

Chapter 6

6 Discussion

6.1 Thesis overview

The work described in this thesis set out to investigate two themes - the relationship between liver TRM and a circulating subset of T cells labelled as TRM-like cells, and the association between TRM-like cells and vaccine-induced liver-stage malaria protection. Our understanding of TRM has evolved significantly in the past decade and, yet, relatively little is known about how TRM influence the circulating T cell responses. The work presented here suggested interdependence between liver and blood memory T cell subsets. It also highlighted the use of TRM-like cells as markers of liver-stage immunity and protection.

The key findings of each chapter are emphasised and contextualised below.

6.2 Chapter insights, implications, and inferences

6.2.1 Chapter 3: TRM and prime-target vaccination assessment in mice

Chapter 3 examined the early response, kinetics and transcriptomics of CD8+ T cells in mice and the context of prime-target encoding model antigens. Liver TRM preferentially homed to the liver and AgSp CD8+ T cells peaked shortly after IV boost. These AgSp cells were present in the liver and blood, and expressed several molecules suggestive of tissue residency and liver-homing. Therefore, when sampled in the blood, these cells were named TRM-like cells. TRM-like cells showed heightened partiality for tracking to the liver when transferred early after IV boost. The CD69 molecule was shown to be important in the homing and maintenance of TRM-like cells in the liver in the short term. TRM-like cells could not be distinguished transcriptionally from TRM sampled at a memory time point using a tissue residency transcriptional signature, suggesting similarities between these two cell subsets. Finally, a panel of genes was identified that allowed the recognition of prime-target AgSp TRM-like cells.

The conceptual advance in the field of T cell biology indicating that T lymphocytes do not continuously recirculate and can permanently reside within nonlymphoid tissues occurred in 2009 (198). Since then, a substantial body of evidence regarding the strictly 'resident' nature of TRM has developed (208,219,228,535,536). More recently, studies have emerged suggesting that TRM may exit tissues to form 'ex-TRM' (211,400,401,408,409,411) and 'return' to tissues given their predilection for defence within the tissue microenvironment (400,407,537,538). How do we reconcile the newer findings with the established literature? Many studies emphasising the non-recirculatory nature of TRM were conducted in organisms and tissues at homeostasis, whereas newer studies have typically followed T cells over time and in the context of infection (400), vaccination (539), or another immunological insult (409). Of note, a very recent study by the Maini group performed sampling of hepatic vasculature to assess for ingress and egress of hepatic CD8+ TRM while patients underwent hepatic vein catheterisation or transjugular intrahepatic

portosystemic shunting (211). This study demonstrated no increased presence of TRM phenotype CD8+ T cells in the portal (ingress) or hepatic (egress from the liver) veins, compared to peripheral blood; suggesting the cells were unable to egress into the draining vasculature at 'steady state'. However, there was a significant proportion of CD69+ CD103+ TRM in liver-dLN which the authors proposed may have emigrated from the liver. Critical to the movement of TRM to dLN is antigen exposure (408). TRM retention and survival *in situ* depends on local cytokines and nutrients, creating organ-specific dependencies at steady-state (222,540) which may variably affect TRM egress after immunological challenge. Therefore, what becomes apparent is the notion that residency is likely a dynamic characteristic where there is minimal egress at steady state but following, for example, TCR engagement, TRM may 'leave home' to become TRM-like cells, for example (Figure 6.1).

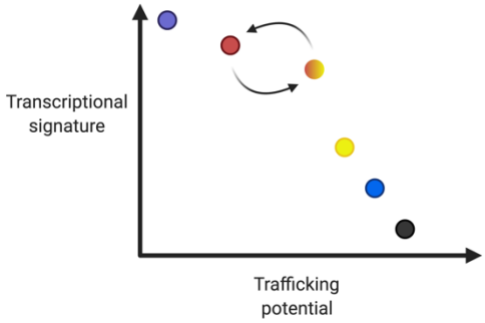


Figure 6.1: Graphical representation of the proposed relationship between TRM and TRM-like cells, as ex-TRM. Arrows indicate potential fates of TRM-like cells (right, yellow-red) and liver TRM (left, red), where liver TRM may egress sinusoids via the hepatic vein and enter the peripheral circulation. A continuous x-axis reflects, for example, a scenario where 'resident' cells have differing propensities to exit tissues, according to their tissue of origin (cf. intestinal TRM and liver TRM), akin to the different trafficking potential of TCM and TEM. The y-axis reflects the information presented in this thesis indicating transcriptional similarities between TRM and TRM-like cells, but distinct axes could equally represent likely epigenetic or proteomic signatures of residency. Figure created with BioRender.com and partially adapted from Rahimi and Luster (254).

In discussing the results of Chapter 3, I applied the evolving understanding of TRM to TRM-like cells and prime-target vaccination and proposed a T cell fate model. Using this model, I suggested that IM prime with an Ad vector generated a small number of liver TRM (Figure 6.2), as was shown herein and by several reports (237,404). IV boost then resulted in vigorous sensing and alarm functions (541) by KC and TRM through TCR-dependent and -independent mechanisms (404). These activation events led to TRM-like cells becoming temporarily present in the circulation. In the short term - between one to three days after IV boost - TRM-like cells would return to the liver (and

potentially other tissues) where they could re-establish residence within hepatic sinusoids (Figure 6.3). After this initial response and the innate-mediated inflammation subsides, prolonged antigen presentation in the liver may have resulted in cognate antigen recognition by TRM and further *in situ* proliferation of these cells (not shown in Figure 6.3). Such a model implies that by TRM-like cells returning to the liver, the frequency of these cells after IV boost could predict the magnitude of the post-IV boost TRM response through contribution to the hepatic resident T cell population. Several questions remain open regarding this model, however.

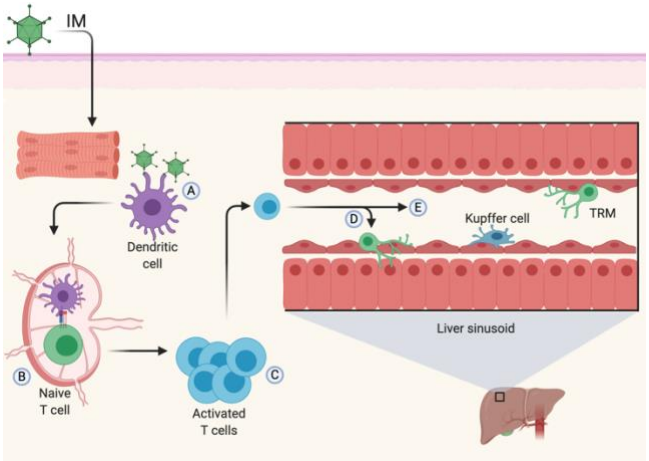


Figure 6.2: Integrating and contextualising the findings of Chapter 3 (I). Summary of events after IM prime. ***A****: IM delivery of Ad results in access to several cell types including skeletal muscle cells, myoblasts, fibroblasts, and endothelial cells, with professional APCs representing a minority of the cellular milieu (542). Direct transduction of APCs (including DCs and macrophages) at the injection site and migration to dLN may occur (416). Alternatively, a variety of other antigen presentation mechanisms may occur, for example, cross-presentation, where Ad transduces muscle cells and debris from these is phagocytosed by APCs (e.g. DCs), which then transfer to the lymph nodes (not shown here). CD8+ T cell responses to Ad and other malaria vaccines are dependent on cross-presentation by CD8α+ DCs (543,544).* ***B****: Once in dLNs, direct presentation of processed vaccine antigen to T cells occurs. Naïve T cells become activated following cognate antigen recognition. DCs imprint specific migratory patterns (545) and tissue-residency fate (546) in the T cells they activate, suggesting the potential for precursor liver TRM clones that home to the liver.* ***C****: Clonal expansion of naïve T cells after DC-T interaction results in vast amounts of circulating activated effector cells with a varying propensity for memory formation.* ***D****: Liver TRM form constitutively from activated T cells following infection and formation is enhanced by hepatic inflammation or antigen presentation (404); this was also shown to occur after IM vaccination. The fenestrated endothelial layer uniquely allows direct interactions of TRM with hepatocytes from within the sinusoid, not requiring vascular exit (223). Not shown here is the small proportion of Ad that travels to the liver and results in small amounts of transgene expression (510), encouraging liver TRM formation after IM vaccination.* ***E****: A majority of clonally expanded T cells will continue through the sinusoids and egress the liver via the hepatic vein (404). Figure created with BioRender.com and partially adapted from Coughlan (416).*

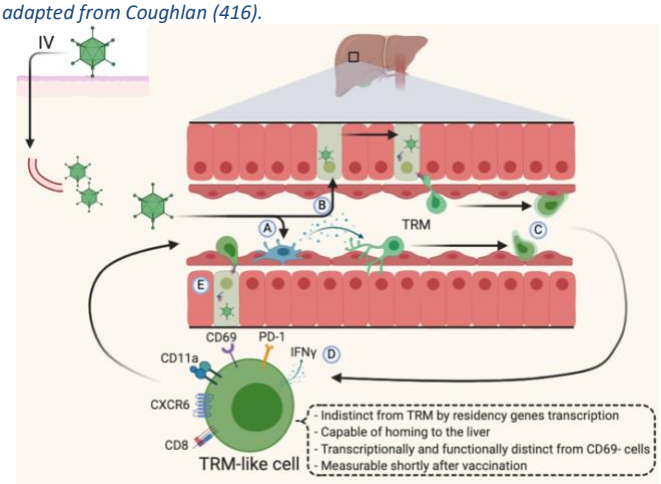


Figure 6.3: Integrating and contextualising the findings of Chapter 3 (II). Summary of Chapter 3 findings and a potential model for the relation between liver TRM and TRM-like cells shortly after IV boost (target) vaccination. ***A****: IV Ad is predominantly taken up by KCs (503). The acute cytokine response is caused by the viral capsid proteins (503) and a pro-inflammatory cytokine cascade occurs as early as 30 minutes after IV Ad (547). The IL-1α-IL-1RI pathway is the primary mediator of this and produces pro-inflammatory cytokines IL-6, IL-12 and TNFα, and chemokines CCL2, CXCL1 and CXCL2 (547,548). Massive KC death ensues within minutes (549). Together, it is postulated, these factors result in potential TCR-independent TRM activation.* ***B****: Hepatocytes are transduced once KCs are relatively depleted. The majority of hepatocyte transgene expression occurs within three days of IV Ad, and it diminishes by 10-14 days after IV Ad (550), though this depends on the dose and the exact Ad used (416). TRM patrol the fenestrated sinusoidal endothelium and recognise transgene peptide presentation on MHC I molecules and become activated.* ***C****: Activated TRM exit the tissues (400,401,407) after TCR engagement (top) or, potentially, TCR-independent activation. These cells egress the liver via the hepatic vein to circulate in the peripheral vasculature.* ***D****: Identification of TRM-like cells in the peripheral blood. They are identified by CD69 and CD11a hi (symbolised here as a subunit of the heterodimer LFA-1), upregulate CXCR6 and PD-1 and are capable of IFNγ production.* ***E****: TRM-like cells may circulate to and re-establish residence within the liver, as it has been shown that ex-TRM prefer homing to their organ of origin (400,401,537,538). Re-establishing residence likely relies on TCR engagement and the cytokine milieu (182,217,222,246,404). The presence of TRM-like cells in the circulation at 'steady state' may reflect a basal level of recirculation by TRM following, for example, innate cell activation by non-self-antigens absorbed in food, transported to the liver by the portal vein. This model omits several innate components that may have played a role in response to IV Ad; these have been discussed in-depth by Atasheva et al. (551). Infection of the spleen occurs to a lesser degree when Ad is administered IV, which is not shown here. Figure created with BioRender.com.*

The evidence that TRM-like cells (as ex-liver TRM) would return to the liver is considerable. TRM-like cells returned to the liver in IV boost adoptive transfer experiments, which was dependent on CD69 expression. Fonseca *et al.* showed that ex-TRM cells remain biased toward relocation back into their parental tissue (400) and Behr *et al.* demonstrated that ex-TRM - from any tissue - have a propensity to traffic and lodge themselves in the liver (401). TRM-like cells in Chapters 3 and 5 were defined using CD11a, among other markers. The notion that CD11a (as part of LFA-1) is necessary for liver homing and establishing TRM populations is well-founded in mice (236,552). There is no direct evidence of this in humans, however. ICAM-1, the ligand of LFA-1, shows tissue-specific expression in the liver and lung (553) and CD11a is an important marker of lung-homing peripheral CD8+ T cells (554). Additionally, Kadoki *et al.* showed that local adaptations strongly influence the TRM transcriptome and function (539), suggesting that T cells may be subject to unprecedented plasticity and propensity for residency once inside an organ.

The proportion of liver TRM endowed by early (before 7 days post-IV boost, corresponding with the peak and ensuing drop in TRM-like cells) compared to later (between 7 and 21 days after IV boost, corresponding with the archetypal anamnestic T cell effector response (555)) remains to be seen. After live attenuated yellow fever virus–17D vaccination, CD8+ T cell lodging in tissues predominantly occurs after recent activation, before 11 days after vaccination (535). Adoptive transfer experiments, in-depth phenotyping of transferred cells at memory time points and further challenge experiments could help clarify the early vs later contribution to the liver TRM niche. The translational relevance of this would be in identifying vaccination strategies that maximise liver TRM induction.

There are other unanswered questions about this model. Do TRM directly exit tissues or do they proliferate before exiting? Are TRM-like cells, as ex-TRM, subject to the same expansion and apoptosis dynamic as classically described, whereby >90% will die after the effector phase? What

are the relative contributions of TCR-dependent and -independent activation mechanisms to egress from tissues? While of initially less translational importance, the answers have implications on the role of TRM-like cells as potential mediators of vaccine-induced protection against liver-stage malaria. These questions are discussed further, below.

The work in Chapter 3, although somewhat preliminary, suggested potential developmental relationships between TRM-like cells and liver TRM in the context of prime-target vaccination. It was speculated that if TRM-like cells were temporarily circulating after IV boost and eventually returning to the liver, they might be useful as potential correlates of liver-stage malaria protection. These observations provided a rationale for in-depth examination of liver TRM and TRM-like cells following prime-target vaccination in humans.

6.2.2 Chapter 4: Assessing liver TRM and their circulating counterparts

This chapter assessed the transcriptional, phenotypic, and clonal similarities and differences between liver TRM and TRM-like cells, in order to use peripheral blood sampling as a proxy for liver sampling. By leveraging mini-bulk and single-cell multi-omic techniques, the data in Chapter 4 showed the identification of a population of TRM-like cells in the circulation that were numerically and characteristically associated to TRM isolated by liver FNA. Despite the two populations displaying unique transcriptional characteristics, the variation was not a function of organ-level differences and was substantively distinct to a core TRM signature seen by contrasting tissue CD69+ TRM to tissue CD69- TEM. Subpopulations existed in TRM and TRM-like cells, and there was a potential developmental trajectory shared by both. While these findings were consistent with earlier reports, indicating comparable frequencies of lymphocytes, and that T cell subsets positively correlate between blood and liver subsets, these results contrasted with the established literature by showing that *bona fide* TRM and TRM-like cells were related both quantitatively and qualitatively.

This is the first reported use of RNA-seq to examine hepatic CD8+ TRM isolated specifically using a stringent FACS criterion. Liver TRM displayed increased expression of adhesion and inhibitory molecules, as well as fine control of migration, and regulatory molecules. The transcriptional and phenotypic profiles of human TRM recapitulated previous findings (219) and demonstrated homology to mouse liver TRM as profiled in Chapter 3 and other studies (208). A significant finding was that TRM could not be differentiated from TRM-like cells when considering the expression of several core transcriptional and functional gene signatures (219,443,445). This suggested that TRM-like cells and TRM were uniquely related in their ability to maintain residency in tissues. Spatial approaches such as spatial transcriptomics and histocytometry could provide fundamental insight into the mentioned residency and functional characteristics. Substantial TCR chain and clone sharing between tissues further advocated for a unique relationship between TRM and TRM-like cells. Further exploration of the TCR repertoire in the i) spleen and lymph nodes, ii) kidneys, and iii) small intestine and skin, would provide insight into whether TCR sharing was unique to liver and blood, and not i) lymphoid, ii) non-epithelial or iii) epithelial organs, respectively. There is potentially a gradient by which a lower threshold is required for T cells to establish residency in non-epithelial tissues (such as the liver and kidneys) compared to epithelial tissues (such as the small intestine or skin) (254,407).

The conclusive identification of MAIT cells in liver 'TRM' and blood TRM-like cells is useful for vaccine design. Several characteristics of MAIT cells suggest an elementary role in the immune response of mammals. MAIT cells have a marked capacity to rapidly secrete and respond to several pro-inflammatory cytokines (450,556). MAIT cells are also abundant in human tissues, comprising 1–4% of all T cells in peripheral blood (557) and up to 20–40% of total liver T cells (556,558). Accordingly, MAIT cells were significant contributors to liver TRM and TRM-like cell populations as defined by CD69+ (± CD11a hi) CD45RA- CD8+. This is important given that previous studies of

human liver TRM have not looked for the presence of MAIT cells nor have they specifically differentiated them from conventional CD8+ TRM (211,217,246), suggesting that MAIT cells may be an under-recognised subset of hepatic T cells in vaccine and TRM studies. Indeed, several reports show that CD161++ T cells share a common transcriptional profile with tissue-homing properties, irrespective of TCR (450,558).

Given that MAIT cells can be activated in a TCR-independent fashion (517,559), they may have contributed to the rapid activation and vigorous induction of TRM-like cells post-IV boost. Assessing the induction of TRM-like cells post-IV boost in MR1 knockout mice would help identify the link between conventional TRM-like cells and MAIT cells. Very recent work has shown that MAIT cell activation, *in vivo* or *in vitro*, augments Ad vector vaccine immunogenicity (425). Provine *et al.* showed several Ad vectors (including ChAd63) could activate human MAIT and Vδ2 T cells, and that MAIT cell-deficient mice had impaired vaccine-induced transgene-specific CD8+ T cell responses. It is tempting to speculate that MAIT cells may be important for the induction of immune responses following other viral vectors, such as MVA, though this remains to be seen. Therefore, MAIT cells were highly abundant in the liver and blood CD69+ memory T cell compartment.

Given the abundance of hepatic MAIT cells and their potential to enhance viral vector vaccine immunogenicity, could synthetic MAIT cell activators be used to expand liver-resident MAIT and conventional memory T cell populations? Two reports using mouse models demonstrated that exogenous delivery of MR1 ligands resulted in the stable expansion of lung resident MR1-restricted T cells (560,561). The latter study showed potential for augmentation of MAIT cell-mediated protection by administering synthetic MAIT ligands as a 'vaccine'. Developing MAIT cell activators has proved difficult due to challenges in molecule stabilisation and minimal understanding of the conditions that facilitate MR1 ligand presentation (561). It has been suggested that ideal MR1 ligands, capable of MAIT activation, should fit into the aromatic cradle in the MR1 binding cleft and

possess a flexible chain capable of interacting with the MAIT TCR Tyr95α (562). Indeed, enhancing TRM formation through hepatic inflammation induced by unconventional T cells has already demonstrated efficacy in liver-stage murine malaria vaccine strategies (324). Complex organic molecules may be difficult to encode for in viral vector inserts, so co-administration of such ligands may be an option to enhance vaccine immunogenicity. Nanoparticles, such as PLGA, could be used to deposit MAIT activation molecules in the liver very rapidly after IV administration (322). In addition, future work utilising nanoparticles conjugated with adjuvants and chemokines (such as CXCL16) to induce MAIT cells and TRM specifically, may be worth further investigation. Suffice it to say that further work is needed to examine the potential for MAIT cells to potentiate vaccine-AgSp liver-resident conventional T cells and investigate the direct effector role that MAIT cells may have in liver-stage malaria, as there are gaps in the literature (472).

Chapter 4 demonstrated the use of FNAs to compare liver CD8+ TRM to TRM-like cells and underscored these circulating cells as a potential correlate marker of hepatic immunity. This work provided a blueprint for understanding human liver TRM and TRM-like cells, particularly given their relevance to a prime-target vaccination clinical trial.

6.2.3 Chapter 5: Investigating TRM-like cells as correlates of vaccine-induced protection

Chapter 5 explored several cellular subsets and particularly TRM-like cells in response to IM and IV viral vectors encoding ME-TRAP as part of a human safety and efficacy trial of prime-target vaccination. TRM-like cell frequencies reached their maximum between one and three days after IV boost, and they were associated with within-assay AgSp cells. The heterogeneity in the TRM-like cell compartment was mostly invariant over time after vaccination, suggesting that these cells expanded quantitatively, but their identity was not inherently altered after IV boost. TRM-like cells were consistently associated with markers of ME-TRAP-specific immunity. Notably,

TRM-like cell frequency measured at IV+3 was strongly correlated with various markers of vaccine-induced immunity and protection (e.g. ME-TRAP-specific ELISpot responses and TRAP-specific IFNγ+ CD8+ T cells). Survival regression models indicated that TRM-like cell frequencies were at least equivalent to vaccine AgSp markers at estimating the hazard of malaria diagnosis after CHMI in vaccinated volunteers. Together, these results provided evidence for using TRM-like cells as vaccine-induced CoPs and implied a robust statistical relationship between protection and TRM-like cells.

The validation and interpretation of immune markers as predictors of malaria vaccine-induced protection depend on their relationship with the vaccine and malaria. For numerous reasons, the assessment of clinical endpoints (such as time-to-parasitaemia or time-to-malaria) in large scale clinical trials is difficult (525). Therefore, there is a rationale to discover and use simpler substitute (i.e. immunological) endpoints to evaluate malaria vaccines. Causal diagrams clarify the relationships between vaccination, immune markers, protection and prevention of clinical endpoints (563). Liver TRM have previously been described as necessary and sufficient for liver-stage malaria protection in mice (201,237) (Figure 6.4), however, this explanation fails to reflect the contribution of co-correlates of protection. Liver TRM cannot be used as substitute endpoints in large scale clinical trials as they are relatively inaccessible. Therefore, TRM-like cells were examined as CoP, given their relationship with liver TRM. TRM-like cells were robustly induced by IV boosting of prime-target and correlated with partial and sterile vaccine-induced efficacy in humans.

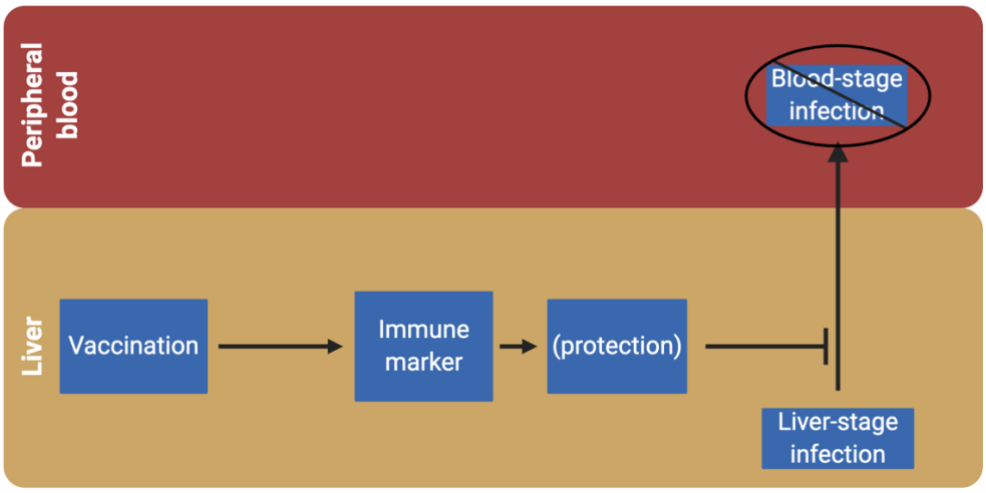


Figure 6.4: TRM as correlates of vaccine protection. Visual representation of the conceptual and causal pathways indicating TRM as necessary and sufficient markers of vaccine-induced liver-stage malaria protection (201,237). The 'immune marker' shown in the centre is malaria AgSp CD8+ TRM in the liver. Protection mediated by TRM prevents blood-stage infection. Arrows imply direct causal relationships. Background colour represents the main site of action/measurement. Figure created with BioRender.com.

The question as to whether TRM-like cells were non-mechanistic, statistical CoP (nCoP) or mechanistic CoP (mCoP) was not directly addressed in this thesis, though hypotheses can be made given the demonstrated relationship between TRM-like cells, TRM and protection. The following scenarios have two main assumptions: 1) TRM-like cells were associated with protection, as shown throughout Chapter 5; and 2) TRM were the predominant mediators of prime-target induced liver-stage malaria protection in humans (TRM were true mCoP if they could be measured) (201,237). Three possible conceptual scenarios given these assumptions include: i) TRM-like cells were functionally and numerically related to TRM, and TRM-like cells contributed to protection (TRM-like cells were mCoP), ii) TRM-like cells were directly related and aided in the induction of TRM, and TRM-like cells made no direct contribution to protection (TRM-like cells were nCoP), and iii) TRM-like cells were not directly related to TRM, and TRM-like cells did not contribute to protection (TRM-like cells were nCoP) (Figure 6.5).

The inherent assumptions, evidence for and evidence against each case are worthy of consideration (Table 6.1, page 237), as they summarise and tie together the work in this thesis. It is worth noting that the exact mechanisms by which circulating vaccine-specific CD8+ T cells exert liver-stage

protection are unknown in humans (e.g. direct evidence of infected hepatocyte killing has not been shown), despite being widely used as correlates of protection. Likewise, models of T cell development and diversification are subject to continuous refinement, notwithstanding terms such as, for example, 'terminal differentiation' being applied to effector T cells (204,205,531). Therefore, the presented models are worthy of further investigation and refinement beyond this thesis.

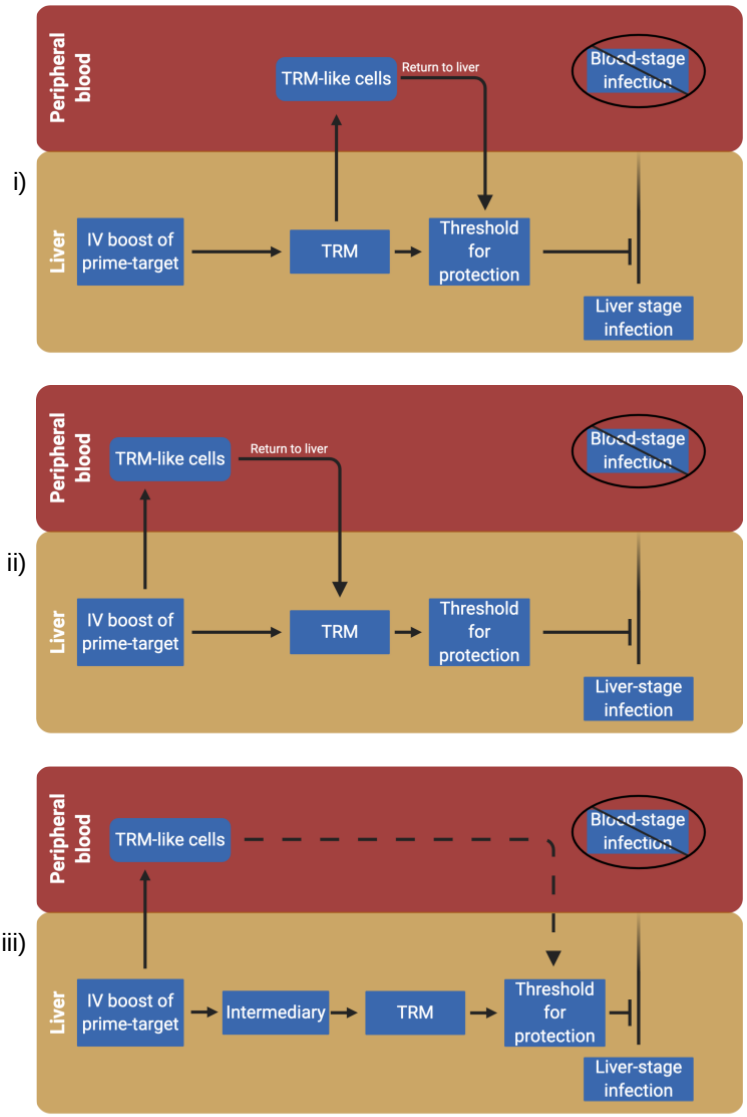


Figure 6.5: TRM-like cells as correlates of vaccine protection. Visual representation of the potential conceptual scenarios and causal pathways relating TRM-like cells to vaccine-induced liver-stage malaria protection. ***Scenario i****: TRM-like cells develop from TRM and help mediate protection upon returning to the liver.* ***Scenario ii****: TRM-like cells exit the liver after vaccination and enhance TRM production after recirculation.* ***Scenario iii****: IV boost results in the production of an unspecified intermediary (e.g. effector CD8+ T cells) and TRM-like cells. The production of an individual's TRM-like cell response is proportional to the induction of the intermediary. Therefore, TRM-like cells are statistically related to protection.* ***All scenarios****: Blood-stage infection is prevented by protection predominantly mediated by TRM. Arrows imply direct causal relationships; the dashed arrow represents a solely statistical relationship, with an unclear mechanistic basis. Background colour represents the main site of action/measurement. Figure created with BioRender.com.*

The three scenarios are excessively simplified versions of the true events that mediated protection in the clinical trial. A potential more complex scenario is a combination of the first two. For example, TRM-like cells as defined herein, contained a substantial amount of MAIT cells. Therefore it is possible that the MAIT cell component of TRM-like cells performed functions such as those described in scenario ii), while the conventional T cells of TRM-like cells exerted direct effector functions such as in scenario i). These conceptual relationships, however, do assist in crystalising ongoing questions. Further inquiry, into the relative contribution of each scenario will help to elucidate the statistical and mechanistic relationship between TRM-like cells and vaccine-mediated protection. Hobit is specifically expressed by TRM, and not by circulating memory T cells (207). The use of Hobit reporter mice (401) to fate map TRM and ex-TRM cells would be an invaluable asset to the study of prime-target memory recall responses. Serial analyses using organism-wide approaches (539) would allow further investigation of the notion that TRM can be seeded far from the tissue of origin. The nature of the vaccine, the dose, and the administration route are likely to be key drivers for the establishment of TRM. As more vaccine candidates are used via non-IM routes to induce TRM (237,242,313,316,318), the described investigative approaches would be well-suited to allow systematic analyses of immune responses that should provide wide-reaching insights and implications.

This CHMI study was performed in malaria-naïve individuals. A range of protective outcomes was seen, including partial and complete (sterile) protection. Group 4 (ChAd63 IM, MVA IV) had increased AgSp responses and significant efficacy over controls. While TRM-like cells did not vary across groups, they were correlated with partial and complete protective outcomes across volunteers. This was demonstrated using simple correlations, dichotomising volunteers according to a TRM-like cell frequency threshold and using Cox regression models of hazard functions. TRM-like cell frequencies consistently outperformed or performed equivalently to vaccine insert-specific T cell subsets as measured by ICS or ELISpot. A challenge in translating these results will be

that CHMI in malaria-naïve individuals may not be reflective of CHMI in malaria exposed or immune individuals (or indeed natural infection). Only a handful of vaccine candidates have been evaluated in both settings (302,308,564,565), so insufficient evidence exists to conclude whether there is a consistent relationship between vaccine CHMI studies in either setting. Several centres in endemic settings can perform CHMI at significant scale (566-568), and it has been argued there should be a lower threshold for CHMI studies of vaccine candidates in malarious areas (569). Advantages of endemic-setting CHMI include study participants with a more similar genetic background to the eventual target population and the possibility of examining the effect of prior malaria exposure and immunity on vaccine efficacy. While useful, the CHMI model is imperfect and limited by minimal standardisation across centres – despite significant efforts (488) – and a lack of diverse parasite strains available to investigate heterologous protection (479). Additionally, issues related to trust, ethics and control of scientific knowledge must not be ignored when transitioning to 'field' evaluation of vaccine candidates (570,571).

The results presented in Chapter 5 contribute to the field of malaria vaccine correlates of protection. Several mechanisms and immune subsets likely contribute to the pathologic and parasite growth outcomes following CHMI. The immune response to malaria should be viewed holistically. The work presented in Chapter 5 is part of a larger body of inquiry considering other aspects of immunity to infection, including antibody, B cell and innate immune responses to viral vector vaccines. These data and the work in this thesis should be appraised together to build a unified evidence base to determine which immune phenotypes are protective and non-protective.

Table 6.1: Evidence relating to scenarios represented in Figure 6.5. Assumptions, supporting evidence and negating evidence is presented for each scenario.

Scenario	Assumptions	Supporting evidence	Negating evidence
i) TRM-like cells were functionally and numerically related to TRM, and TRM-like cells contributed to protection (TRM-like cells were mCoP)	- TRM-like cells developed from TRM. - TRM-like cells return to the liver, survive, and exert effector functions.	- Sharing of TCR α/β chains and clonality between TRM and TRM-like cells (Chapter 4). - Correlation between protection and IV+3 TRM-like cell frequency (Chapter 5). - TRM-like cells and liver TRM DGE had a high degree of overlap (Chapters 3 and 5) with the DGE between ex-TRM and liver TRM in mice (401). - TRM-like cells produced IFNγ upon peptide stimulation (Chapters 3 and 5). - Formation of secondary CD8+ TRM and TEM depends on primary TRM (401,407). - CD8+ ex-TRM have a homing bias to their tissue of origin (421,537,538). - Circulating ex-TRM have an enhanced capacity to protect against reinfection compared to other circulator effector populations (401). - Sensitisation of small numbers of TRM results in an amplified signal to more abundant local innate mediators, triggering an organ-wide state of alarm (209). - Cognate Ag recognition by TRM results in rapid accumulation of unstimulated memory CD8+ T cells within tissues as early as 48h after local Ag challenge (541). - Early effector and not memory phase CD8+ T cells migrate to tissues and express integrins required for tissue maintenance (535).	- Only a small proportion of TRM-like cells were *Plasmodium* AgSp (Chapters 3 and 5). Bystander CD8+ T cell killing of *Plasmodium* parasites does not occur: direct recognition of infected hepatocytes by CD8+ T cells is required for killing (188). - TRM-like cell longevity may not have been long enough for significant effector actions. Most TRM-like cells did not survive >7d after adoptive transfer (Chapter 3). - TRM-like cells may not have contributed in a numerically significant manner. Normally, 90-95% of effector T cells undergo programmed cell death, and only a small, diverse pool of memory cells remains after T cell expansion (572).
ii) TRM-like cells aided in the induction of TRM, and TRM-like cells, while on the causal pathway to protection, did not make a direct contribution to protection (TRM-like cells were nCoP)	- TRM-like cells had innate-like abilities to induce TRM. - TRM-like cells were distinct from TRM, and not progeny T cells of TRM. - TRM-like cells were initially within the liver and egressed from the liver after IV boost.	- Significant proportions of TRM-like cells were CD161++ (Chapter 5) and TRM-like cells upregulated IL-12 and IL-18 receptor genes compared to TRM/TEM (Chapter 4). = Irrespective of TCR, CD161++ cells are liver-homing (558). CD161++ CD8+ T cells share a common phenotype and an enhanced ability for TCR-independent responses to IL-12 and IL-18 (450), cytokines driving bystander CD8+ T cell responses (573). - Large fraction of MAIT cells in liver TRM and TRM-like cells (Chapters 4 and 5) = MAIT cells can be activated by cytokines, mount rapid responses (517), exit tissues (521), and activation augments Ad vector vaccine immunogenicity (425). - Very rapid induction of TRM-like cells (Chapters 3 and 5). = MAIT cell expression of CD69 peaks at day five post-secondary influenza infection, earlier than the peak frequencies of conventional CD8+ T cells (574). Rapid activation of and cytokine production by liver resident NKT cells enhances liver TRM formation by liver-stage malaria vaccines (324). - Correlation between protection and pre-IV boost TRM-like cell frequency (Chapter 5), supporting pre-vaccination presence in the liver. = Pre-IV irradiated sporozoite vaccination levels of Vδ2 cells correlate to protection, and it has been proposed that these unconventional T cells return to the liver to mediate liver-stage malaria protection (242).	- TRM-like cells were indistinguishable from TRM in terms of key residency transcriptional signatures, suggesting similar recirculation potential (Chapter 4). - TRM-like cells were clonally related to liver TRM (Chapter 4). - Only a very small proportion of TRM-like cells were γ/δ TCR+ (Chapter 5). - *In vitro* activated T cells that are adoptively transferred can differentiate into TRM and mediate liver-stage malaria protection (404), without TRM-like cells.

		- Ex-TRM cells are transcriptionally and functionally distinct from other effector cells (401).	
iii) TRM-like cells were not directly related to TRM, and TRM-like cells did not contribute to protection (TRM-like cells were nCoP)	- TRM-like cells correlated to differences in inter-individual vaccine-responsiveness. - TRM-like cells did not constitute functionally distinct circulating memory T cells. - Circulating AgSp TEM that were primed extrahepatically seeded the liver. - Circulating AgSp TEM differentiated into liver TRM.	- Increased CD69 and CD11a molecule expression on circulating memory T cells was transient (Chapters 3 and 5). - There was no increase in TRM-like cells throughout liver-stage *Plasmodium* infection, between C-1 and C+7 (Chapter 5). - The frequency of TRM-like cells at IV+3 correlated with polyfunctional and long-lived circulating AgSp T cell responses (Chapter 5). - Liver TRM derived from *in vitro* activated T cells are functionally equivalent to endogenously generated liver TRM, in mice and humans (246,404). - Liver TRM form constitutively after extrahepatic TCR stimulation (404,539). - CD69 upregulation occurs on T cells following TCR/CD3 engagement, activating cytokines and polyclonal, mitogenic stimulation, suggesting that CD69+ cells correlate with T cell activation, rather than residency potential (460).	- TRM-like cells were better predictors of prime-target-mediated protection than AgSp cells (Chapter 5). - TRM-like cells were transcriptionally, phenotypically, and clonally related to liver TRM (Chapters 3 and 4). - TRM-like cells were transcriptionally different from CD69– counterparts (Chapter 4). - Resident, rather than circulating, CD8+ T cells are the dominant memory population that repopulates the TRM compartment after reinfection (401,407). - CD8+ TRM are sufficient for liver-stage malaria protection (237). - Baseline and post-vaccination CD69 expression by T cells is a biomarker of reduced yellow fever live virus vaccine- and RSV protein-in-adjuvant vaccine-responsiveness in humans (575,576).

6.3 Final remarks

The WHO initially called for malaria eradication in 1955; many lessons can be learnt regarding the failure of this global campaign. The disease had been eliminated from significant proportions of the world. In areas where tremendous decreases were accomplished, the last stages of elimination proved to be the hardest and, as progress stalled, there were colossal rebounds (5). This provides a cautionary tale of what could happen over the next decade if the world undertakes incomplete eradication efforts, particularly in regions with natural potential for high transmission.

Licensed malaria vaccines require more than the endpoints of safety, high efficacy and durability of protection as measured by preclinical studies and clinical trials. Vaccine acceptance, thermostability, storage, cost, administration method, supply chain management, and implementation strategies, at the minimum, need to be well thought out to allow vaccines to be effective counterparts to other key interventions such as LLIN and ACT. Similarly, if these vaccines are given to large populations, there will be a requirement for safety in pregnant women and children. Priorities in implementation-focused research should include the use of an acceptable and easy route of vaccine administration, harmonised dose regimens and the effect of altered physiological states such as pregnancy.

Ultimately, no country has ever eliminated malaria without a good health system and, conversely, countries with a good health system have not had significant malaria burdens in recent history. Evidence of this can be seen on the small island of Hispaniola. With a relatively robust health system, the Dominican Republic has 85-fold and 22-fold lower case and death rates, respectively, compared to Haiti where, among other historical and sociodemographic factors, health infrastructure was decimated by the 2010 earthquake. A highly efficacious malaria vaccine could partially circumvent the difficulties of a suboptimal health system, but it is necessary to view vaccines as another tool in the repertoire of evolving anti-malarial interventions. Also central to

the potential success of vaccines will be guaranteeing efficient and cost-effective distribution systems and redirection of health systems from malaria treatment to prevention and transmission interruption (577).

This thesis would be incomplete without mention of the socio-political context of malaria and vaccine research. An absence of a high-income profitable market to financially justify investment into malaria vaccine design and development has led to the heavy reliance on philanthropic and public backing. Worldwide funding for malaria-related activities has stalled in the past three years. Vaccine funding made up 20% of all malaria-directed funding, worldwide (578). Significant reliance on public and benevolent funding is expected to continue in the foreseeable future (332). Until malaria is no longer widely viewed as a disease of the poor with little relevance to high-income countries there will be added difficulties to design and develop malaria vaccines.

Despite it being the most problematic parasitic disease in history, a highly efficacious vaccine against malaria remains elusive. The complexity of the immune response to vaccination and the parasite is a challenge and can frustrate efforts to study it. Some of the lack of progress in vaccine development can be owed to difficulties the field has faced in understanding these multifaceted mechanisms. Nevertheless, research like this is tremendously important and adds to a growing body of knowledge. This thesis provides a novel contribution to the literature. I have tried to combine basic science and clinical knowledge to tackle a challenging translational problem, defining liver-stage malaria correlates of vaccine-mediated protection. I am confident that by continuing with novel and robust bench-to-bedside research and placing emphasis on challenging existing paradigms, a highly effective liver-stage malaria vaccine will be developed. Deployment of such a vaccine could contribute to preventing the hundreds of millions of malaria cases and hundreds of thousands of malaria deaths happening every year.

Chapter 7

7 References

1. Mukherjee S. The emperor of all maladies : a biography of cancer. New York: Scribner; 2010.
2. Russell PF. Man's mastery of malaria. London: Oxford University Press; 1955.
3. Wilson RJ, Williamson DH. Extrachromosomal DNA in the Apicomplexa. Microbiology and molecular biology reviews : MMBR. 1997;61(1):1-16.
4. Garnham PCC. Malaria parasites and other haemosporidia. London: Blackwell; 1966.
5. Cowman AF, Healer J, Marapana D, Marsh K. Malaria: Biology and Disease. Cell. 2016;167(3):610-24.
6. Otto TD, Gilabert A, Crellen T, Bohme U, Arnathau C, Sanders M, et al. Genomes of all known members of a Plasmodium subgenus reveal paths to virulent human malaria. Nat Microbiol. 2018;3(6):687-97.
7. Liu W, Li Y, Learn GH, Rudicell RS, Robertson JD, Keele BF, et al. Origin of the human malaria parasite Plasmodium falciparum in gorillas. Nature. 2010;467(7314):420-5.
8. Volkman SK, Barry AE, Lyons EJ, Nielsen KM, Thomas SM, Choi M, et al. Recent origin of Plasmodium falciparum from a single progenitor. Science. 2001;293(5529):482-4.
9. Sundararaman SA, Plenderleith LJ, Liu W, Loy DE, Learn GH, Li Y, et al. Genomes of cryptic chimpanzee Plasmodium species reveal key evolutionary events leading to human malaria. Nat Commun. 2016;7:11078.
10. Ollomo B, Durand P, Prugnolle F, Douzery E, Arnathau C, Nkoghe D, et al. A new malaria agent in African hominids. PLoS Pathog. 2009;5(5):e1000446.
11. Loy DE, Liu W, Li Y, Learn GH, Plenderleith LJ, Sundararaman SA, et al. Out of Africa: origins and evolution of the human malaria parasites Plasmodium falciparum and Plasmodium vivax. Int J Parasitol. 2017;47(2-3):87-97.
12. Sharp PM, Plenderleith LJ, Hahn BH. Ape Origins of Human Malaria. Annual Review of Microbiology. 2020;74(1):39-63.

13. Kwiatkowski DP. How malaria has affected the human genome and what human genetics can teach us about malaria. Am J Hum Genet. 2005;77(2):171-92.

14. Haldane JBS. The rate of mutation of human genes. Hereditas. 1949;35(S1):267-73.

15. Carter R, Mendis KN. Evolutionary and historical aspects of the burden of malaria. Clin Microbiol Rev. 2002;15(4):564-94.

16. Allison AC. Protection afforded by sickle-cell trait against subtertian malareal infection. Br Med J. 1954;1(4857):290-4.

17. Miller LH, Mason SJ, Clyde DF, McGinniss MH. The resistance factor to Plasmodium vivax in blacks. The Duffy-blood-group genotype, FyFy. N Engl J Med. 1976;295(6):302-4.

18. Genton B, al-Yaman F, Mgone CS, Alexander N, Paniu MM, Alpers MP, et al. Ovalocytosis and cerebral malaria. Nature. 1995;378(6557):564-5.

19. Payne RO, Silk SE, Elias SC, Milne KH, Rawlinson TA, Llewellyn D, et al. Human vaccination against Plasmodium vivax Duffy-binding protein induces strain-transcending antibodies. JCI Insight. 2017;2(12).

20. Williams TN, Weatherall DJ. World distribution, population genetics, and health burden of the hemoglobinopathies. Cold Spring Harb Perspect Med. 2012;2(9):a011692.

21. Hill AV. Evolution, revolution and heresy in the genetics of infectious disease susceptibility. Philos Trans R Soc Lond B Biol Sci. 2012;367(1590):840-9.

22. In: Arrow KJ, Panosian C, Gelband H, editors. Saving Lives, Buying Time: Economics of Malaria Drugs in an Age of Resistance. Washington (DC)2004.

23. Celli-Fraentzel A. The History of Malaria in the Roman Campagna from Ancient Times. London: John Bale, Sons & Danielsson, Ltd.; 1933. viii + 226 pp. p.

24. Snow RW, Sartorius B, Kyalo D, Maina J, Amratia P, Mundia CW, et al. The prevalence of Plasmodium falciparum in sub-Saharan Africa since 1900. Nature. 2017;550(7677):515-8.

25. World Health Organization. World Malaria Report 2020. Geneva: WHO; 2020.

26. Snow RW, Guerra CA, Noor AM, Myint HY, Hay SI. The global distribution of clinical episodes of Plasmodium falciparum malaria. Nature. 2005;434(7030):214-7.

27. Dondorp AM, Nosten F, Yi P, Das D, Phyo AP, Tarning J, et al. Artemisinin resistance in Plasmodium falciparum malaria. N Engl J Med. 2009;361(5):455-67.

28. Ashley EA, Dhorda M, Fairhurst RM, Amaratunga C, Lim P, Suon S, et al. Spread of artemisinin resistance in Plasmodium falciparum malaria. N Engl J Med. 2014;371(5):411-23.

29. Churcher TS, Lissenden N, Griffin JT, Worrall E, Ranson H. The impact of pyrethroid resistance on the efficacy and effectiveness of bednets for malaria control in Africa. Elife. 2016;5.

30. Bharti PK, Chandel HS, Ahmad A, Krishna S, Udhayakumar V, Singh N. Prevalence of pfhrp2 and/or pfhrp3 Gene Deletion in Plasmodium falciparum Population in Eight Highly Endemic States in India. PLoS One. 2016;11(8):e0157949.

31. Koita OA, Doumbo OK, Ouattara A, Tall LK, Konare A, Diakite M, et al. False-negative rapid diagnostic tests for malaria and deletion of the histidine-rich repeat region of the hrp2 gene. Am J Trop Med Hyg. 2012;86(2):194-8.

32. World Health Assembly. Agenda Item 16.2: Global technical strategy and targets for malaria 2016–2030. Geneva: World Health Organisation; 2015.

33. mal E. R. A. Refresh Consultative Panel on Tools for Malaria Elimination. malERA: An updated research agenda for diagnostics, drugs, vaccines, and vector control in malaria elimination and eradication. PLoS Med. 2017;14(11):e1002455.

34. Feachem RGA, Chen I, Akbari O, Bertozzi-Villa A, Bhatt S, Binka F, et al. Malaria eradication within a generation: ambitious, achievable, and necessary. Lancet. 2019;394(10203):1056-112.

35. World Health Organization. Global technical strategy for malaria 2016–2030. Geneva: WHO; 2015.

36. Medica DL, Sinnis P. Quantitative dynamics of Plasmodium yoelii sporozoite transmission by infected anopheline mosquitoes. Infect Immun. 2005;73(7):4363-9.

37. Yamauchi LM, Coppi A, Snounou G, Sinnis P. Plasmodium sporozoites trickle out of the injection site. Cell Microbiol. 2007;9(5):1215-22.

38. Steel RW, Kappe SH, Sack BK. An expanding toolkit for preclinical pre-erythrocytic malaria vaccine development: bridging traditional mouse malaria models and human trials. Future Microbiol. 2016;11:1563-79.

39. Tavares J, Formaglio P, Thiberge S, Mordelet E, Van Rooijen N, Medvinsky A, et al. Role of host cell traversal by the malaria sporozoite during liver infection. J Exp Med. 2013;210(5):905-15.

40. Frevert U, Engelmann S, Zougbede S, Stange J, Ng B, Matuschewski K, et al. Intravital observation of Plasmodium berghei sporozoite infection of the liver. PLoS Biol. 2005;3(6):e192.

41. Baer K, Roosevelt M, Clarkson AB, Jr., van Rooijen N, Schnieder T, Frevert U. Kupffer cells are obligatory for Plasmodium yoelii sporozoite infection of the liver. Cell Microbiol. 2007;9(2):397-412.

42. Kariu T, Ishino T, Yano K, Chinzei Y, Yuda M. CelTOS, a novel malarial protein that mediates transmission to mosquito and vertebrate hosts. Mol Microbiol. 2006;59(5):1369-79.

43. Ishino T, Yano K, Chinzei Y, Yuda M. Cell-passage activity is required for the malarial parasite to cross the liver sinusoidal cell layer. PLoS Biol. 2004;2(1):E4.

44. Risco-Castillo V, Topcu S, Marinach C, Manzoni G, Bigorgne AE, Briquet S, et al. Malaria Sporozoites Traverse Host Cells within Transient Vacuoles. Cell Host Microbe. 2015;18(5):593-603.

45. Bhanot P, Schauer K, Coppens I, Nussenzweig V. A surface phospholipase is involved in the migration of plasmodium sporozoites through cells. J Biol Chem. 2005;280(8):6752-60.

46. Coppi A, Tewari R, Bishop JR, Bennett BL, Lawrence R, Esko JD, et al. Heparan sulfate proteoglycans provide a signal to Plasmodium sporozoites to stop migrating and productively invade host cells. Cell Host Microbe. 2007;2(5):316-27.

47. Rodrigues CD, Hannus M, Prudencio M, Martin C, Goncalves LA, Portugal S, et al. Host scavenger receptor SR-BI plays a dual role in the establishment of malaria parasite liver infection. Cell Host Microbe. 2008;4(3):271-82.

48. Dame JB, Williams JL, McCutchan TF, Weber JL, Wirtz RA, Hockmeyer WT, et al. Structure of the gene encoding the immunodominant surface antigen on the sporozoite of the human malaria parasite Plasmodium falciparum. Science. 1984;225(4662):593-9.

49. Herrera R, Anderson C, Kumar K, Molina-Cruz A, Nguyen V, Burkhardt M, et al. Reversible Conformational Change in the Plasmodium falciparum Circumsporozoite Protein Masks Its Adhesion Domains. Infect Immun. 2015;83(10):3771-80.

50. Frevert U, Sinnis P, Cerami C, Shreffler W, Takacs B, Nussenzweig V. Malaria circumsporozoite protein binds to heparan sulfate proteoglycans associated with the surface membrane of hepatocytes. J Exp Med. 1993;177(5):1287-98.

51. Robson KJ, Hall JR, Jennings MW, Harris TJ, Marsh K, Newbold CI, et al. A highly conserved amino-acid sequence in thrombospondin, properdin and in proteins from sporozoites and blood stages of a human malaria parasite. Nature. 1988;335(6185):79-82.

52. Dundas K, Shears MJ, Sun Y, Hopp CS, Crosnier C, Metcalf T, et al. Alpha-v-containing integrins are host receptors for the Plasmodium falciparum sporozoite surface protein, TRAP. Proc Natl Acad Sci U S A. 2018;115(17):4477-82.

53. Kappe S, Bruderer T, Gantt S, Fujioka H, Nussenzweig V, Menard R. Conservation of a gliding motility and cell invasion machinery in Apicomplexan parasites. J Cell Biol. 1999;147(5):937-44.

54. Mota MM, Pradel G, Vanderberg JP, Hafalla JC, Frevert U, Nussenzweig RS, et al. Migration of Plasmodium sporozoites through cells before infection. Science. 2001;291(5501):141-4.

55. Vaughan AM, Mikolajczak SA, Wilson EM, Grompe M, Kaushansky A, Camargo N, et al. Complete Plasmodium falciparum liver-stage development in liver-chimeric mice. J Clin Invest. 2012;122(10):3618-28.

56. Holz LE, Fernandez-Ruiz D, Heath WR. Protective immunity to liver-stage malaria. Clinical & Translational Immunology. 2016;5(10):e105.

57. Van Braeckel-Budimir N, Harty JT. CD8 T-cell-mediated protection against liver-stage malaria: lessons from a mouse model. Front Microbiol. 2014;5:272.

58. Sturm A, Amino R, van de Sand C, Regen T, Retzlaff S, Rennenberg A, et al. Manipulation of host hepatocytes by the malaria parasite for delivery into liver sinusoids. Science. 2006;313(5791):1287-90.

59. Schmidt NW, Podyminogin RL, Butler NS, Badovinac VP, Tucker BJ, Bahjat KS, et al. Memory CD8 T cell responses exceeding a large but definable threshold provide long-term immunity to malaria. Proc Natl Acad Sci U S A. 2008;105(37):14017-22.

60. Weiss GE, Gilson PR, Taechalertpaisarn T, Tham WH, de Jong NW, Harvey KL, et al. Revealing the sequence and resulting cellular morphology of receptor-ligand interactions during Plasmodium falciparum invasion of erythrocytes. PLoS Pathog. 2015;11(2):e1004670.

61. Holder AA. Proteins on the surface of the malaria parasite and cell invasion. Parasitology. 1994;108 Suppl:S5-18.

62. Lin CS, Uboldi AD, Epp C, Bujard H, Tsuboi T, Czabotar PE, et al. Multiple Plasmodium falciparum Merozoite Surface Protein 1 Complexes Mediate Merozoite Binding to Human Erythrocytes. J Biol Chem. 2016;291(14):7703-15.

63. Tham WH, Healer J, Cowman AF. Erythrocyte and reticulocyte binding-like proteins of Plasmodium falciparum. Trends Parasitol. 2012;28(1):23-30.

64. Chen L, Lopaticki S, Riglar DT, Dekiwadia C, Uboldi AD, Tham WH, et al. An EGF-like protein forms a complex with PfRh5 and is required for invasion of human erythrocytes by Plasmodium falciparum. PLoS Pathog. 2011;7(9):e1002199.

65. Reddy KS, Amlabu E, Pandey AK, Mitra P, Chauhan VS, Gaur D. Multiprotein complex between the GPI-anchored CyRPA with PfRH5 and PfRipr is crucial for Plasmodium falciparum erythrocyte invasion. Proc Natl Acad Sci U S A. 2015;112(4):1179-84.

66. Crosnier C, Bustamante LY, Bartholdson SJ, Bei AK, Theron M, Uchikawa M, et al. Basigin is a receptor essential for erythrocyte invasion by Plasmodium falciparum. Nature. 2011;480(7378):534-7.

67. Volz JC, Yap A, Sisquella X, Thompson JK, Lim NT, Whitehead LW, et al. Essential Role of the PfRh5/PfRipr/CyRPA Complex during Plasmodium falciparum Invasion of Erythrocytes. Cell Host Microbe. 2016;20(1):60-71.

68. Riglar DT, Richard D, Wilson DW, Boyle MJ, Dekiwadia C, Turnbull L, et al. Super-resolution dissection of coordinated events during malaria parasite invasion of the human erythrocyte. Cell Host Microbe. 2011;9(1):9-20.

69. Harvey KL, Gilson PR, Crabb BS. A model for the progression of receptor-ligand interactions during erythrocyte invasion by Plasmodium falciparum. Int J Parasitol. 2012;42(6):567-73.

70. de Koning-Ward TF, Dixon MW, Tilley L, Gilson PR. Plasmodium species: master renovators of their host cells. Nat Rev Microbiol. 2016;14(8):494-507.

71. McMillan PJ, Millet C, Batinovic S, Maiorca M, Hanssen E, Kenny S, et al. Spatial and temporal mapping of the PfEMP1 export pathway in Plasmodium falciparum. Cell Microbiol. 2013;15(8):1401-18.

72. Das S, Hertrich N, Perrin AJ, Withers-Martinez C, Collins CR, Jones ML, et al. Processing of Plasmodium falciparum Merozoite Surface Protein MSP1 Activates a Spectrin-Binding Function Enabling Parasite Egress from RBCs. Cell Host Microbe. 2015;18(4):433-44.

73. Cunnington AJ, Walther M, Riley EM. Piecing together the puzzle of severe malaria. Sci Transl Med. 2013;5(211):211ps18.

74. Marsh K, Forster D, Waruiru C, Mwangi I, Winstanley M, Marsh V, et al. Indicators of life-threatening malaria in African children. N Engl J Med. 1995;332(21):1399-404.

75. Cohen S, Mc GI, Carrington S. Gamma-globulin and acquired immunity to human malaria. Nature. 1961;192:733-7.

76. Langhorne J, Ndungu FM, Sponaas AM, Marsh K. Immunity to malaria: more questions than answers. Nat Immunol. 2008;9(7):725-32.

77. Bull PC, Lowe BS, Kortok M, Molyneux CS, Newbold CI, Marsh K. Parasite antigens on the infected red cell surface are targets for naturally acquired immunity to malaria. Nat Med. 1998;4(3):358-60.

78. Hviid L, Jensen AT. PfEMP1 - A Parasite Protein Family of Key Importance in Plasmodium falciparum Malaria Immunity and Pathogenesis. Adv Parasitol. 2015;88:51-84.

79. Chan JA, Howell KB, Reiling L, Ataide R, Mackintosh CL, Fowkes FJ, et al. Targets of antibodies against Plasmodium falciparum-infected erythrocytes in malaria immunity. J Clin Invest. 2012;122(9):3227-38.

80. Snow RW, Omumbo JA, Lowe B, Molyneux CS, Obiero JO, Palmer A, et al. Relation between severe malaria morbidity in children and level of Plasmodium falciparum transmission in Africa. Lancet. 1997;349(9066):1650-4.

81. Stone W, Goncalves BP, Bousema T, Drakeley C. Assessing the infectious reservoir of falciparum malaria: past and future. Trends Parasitol. 2015;31(7):287-96.

82. Carneiro I, Roca-Feltrer A, Griffin JT, Smith L, Tanner M, Schellenberg JA, et al. Age-patterns of malaria vary with severity, transmission intensity and seasonality in sub-Saharan Africa: a systematic review and pooled analysis. PLoS One. 2010;5(2):e8988.

83. Marsh K, Kinyanjui S. Immune effector mechanisms in malaria. Parasite Immunol. 2006;28(1-2):51-60.

84. McCann RS, Cohee LM, Goupeyou-Youmsi J, Laufer MK. Maximizing Impact: Can Interventions to Prevent Clinical Malaria Reduce Parasite Transmission? Trends Parasitol. 2020;36(11):906-13.

85. Kafsack BF, Rovira-Graells N, Clark TG, Bancells C, Crowley VM, Campino SG, et al. A transcriptional switch underlies commitment to sexual development in malaria parasites. Nature. 2014;507(7491):248-52.

86. Brancucci NMB, Bertschi NL, Zhu L, Niederwieser I, Chin WH, Wampfler R, et al. Heterochromatin protein 1 secures survival and transmission of malaria parasites. Cell Host Microbe. 2014;16(2):165-76.

87. Poran A, Notzel C, Aly O, Mencia-Trinchant N, Harris CT, Guzman ML, et al. Single-cell RNA sequencing reveals a signature of sexual commitment in malaria parasites. Nature. 2017;551(7678):95-9.

88. Usui M, Prajapati SK, Ayanful-Torgby R, Acquah FK, Cudjoe E, Kakaney C, et al. Plasmodium falciparum sexual differentiation in malaria patients is associated with host factors and GDV1-dependent genes. Nat Commun. 2019;10(1):2140.

89. Peatey CL, Skinner-Adams TS, Dixon MW, McCarthy JS, Gardiner DL, Trenholme KR. Effect of antimalarial drugs on Plasmodium falciparum gametocytes. J Infect Dis. 2009;200(10):1518-21.

90. Joice R, Nilsson SK, Montgomery J, Dankwa S, Egan E, Morahan B, et al. Plasmodium falciparum transmission stages accumulate in the human bone marrow. Sci Transl Med. 2014;6(244):244re5.

91. Aguilar R, Magallon-Tejada A, Achtman AH, Moraleda C, Joice R, Cistero P, et al. Molecular evidence for the localization of Plasmodium falciparum immature gametocytes in bone marrow. Blood. 2014;123(7):959-66.

92. Billker O, Lindo V, Panico M, Etienne AE, Paxton T, Dell A, et al. Identification of xanthurenic acid as the putative inducer of malaria development in the mosquito. Nature. 1998;392(6673):289-92.

93. Sologub L, Kuehn A, Kern S, Przyborski J, Schillig R, Pradel G. Malaria proteases mediate inside-out egress of gametocytes from red blood cells following parasite transmission to the mosquito. Cell Microbiol. 2011;13(6):897-912.

94. Sinden RE. Sexual Development of Malarial Parasites. In: Baker JR, Muller R, editors. Advances in Parasitology. 22: Academic Press; 1983. p. 153-216.

95. van Dijk MR, Janse CJ, Thompson J, Waters AP, Braks JA, Dodemont HJ, et al. A central role for P48/45 in malaria parasite male gamete fertility. Cell. 2001;104(1):153-64.

96. Quakyi IA, Carter R, Rener J, Kumar N, Good MF, Miller LH. The 230-kDa gamete surface protein of Plasmodium falciparum is also a target for transmission-blocking antibodies. J Immunol. 1987;139(12):4213-7.

97. Tomas AM, Margos G, Dimopoulos G, van Lin LH, de Koning-Ward TF, Sinha R, et al. P25 and P28 proteins of the malaria ookinete surface have multiple and partially redundant functions. EMBO J. 2001;20(15):3975-83.

98. Bennink S, Kiesow MJ, Pradel G. The development of malaria parasites in the mosquito midgut. Cell Microbiol. 2016;18(7):905-18.

99. Gerald N, Mahajan B, Kumar S. Mitosis in the human malaria parasite Plasmodium falciparum. Eukaryot Cell. 2011;10(4):474-82.

100. Ouedraogo AL, Roeffen W, Luty AJ, de Vlas SJ, Nebie I, Ilboudo-Sanogo E, et al. Naturally acquired immune responses to Plasmodium falciparum sexual stage antigens Pfs48/45 and Pfs230 in an area of seasonal transmission. Infect Immun. 2011;79(12):4957-64.

101. Kim TS, Kim HH, Kim JY, Kong Y, Na BK, Lin K, et al. Comparison of the antibody responses to Plasmodium vivax and Plasmodium falciparum antigens in residents of Mandalay, Myanmar. Malar J. 2011;10:228.

102. Tran TM, Li S, Doumbo S, Doumtabe D, Huang CY, Dia S, et al. An intensive longitudinal cohort study of Malian children and adults reveals no evidence of acquired immunity to Plasmodium falciparum infection. Clin Infect Dis. 2013;57(1):40-7.

103. Sokhna CS, Faye FBK, Spiegel A, Dieng H, Trape JF. Rapid reappearance of Plasmodium falciparum after drug treatment among Senegalese adults exposed to moderate seasonal transmission. Am J Trop Med Hyg. 2001;65(3):167-70.

104. Riley EM, Stewart VA. Immune mechanisms in malaria: new insights in vaccine development. Nat Med. 2013;19(2):168-78.

105. Cockburn IA, Seder RA. Malaria prevention: from immunological concepts to effective vaccines and protective antibodies. Nat Immunol. 2018;19(11):1199-211.

106. Ewer KJ, Sierra-Davidson K, Salman AM, Illingworth JJ, Draper SJ, Biswas S, et al. Progress with viral vectored malaria vaccines: A multi-stage approach involving "unnatural immunity". Vaccine. 2015;33(52):7444-51.

107. Offeddu V, Thathy V, Marsh K, Matuschewski K. Naturally acquired immune responses against Plasmodium falciparum sporozoites and liver infection. Int J Parasitol. 2012;42(6):535-48.

108. Druilhe P, Pradier O, Marc JP, Miltgen F, Mazier D, Parent G. Levels of antibodies to Plasmodium falciparum sporozoite surface antigens reflect malaria transmission rates and are persistent in the absence of reinfection. Infect Immun. 1986;53(2):393-7.

109. Tapchaisri P, Chomcharn Y, Poonthong C, Asavanich A, Limsuwan S, Maleevan O, et al. Anti-sporozoite antibodies induced by natural infection. Am J Trop Med Hyg. 1983;32(6):1203-8.

110. Hoffman SL, Oster CN, Plowe CV, Woollett GR, Beier JC, Chulay JD, et al. Naturally acquired antibodies to sporozoites do not prevent malaria: vaccine development implications. Science. 1987;237(4815):639-42.

111. Dobano C, Sanz H, Sorgho H, Dosoo D, Mpina M, Ubillos I, et al. Concentration and avidity of antibodies to different circumsporozoite epitopes correlate with RTS,S/AS01E malaria vaccine efficacy. Nat Commun. 2019;10(1):2174.

112. Suscovich TJ, Fallon JK, Das J, Demas AR, Crain J, Linde CH, et al. Mapping functional humoral correlates of protection against malaria challenge following RTS,S/AS01 vaccination. Sci Transl Med. 2020;12(553).

113. Doolan DL, Khamboonruang C, Beck HP, Houghten RA, Good MF. Cytotoxic T lymphocyte (CTL) low-responsiveness to the Plasmodium falciparum circumsporozoite protein in naturally-exposed endemic populations: analysis of human CTL response to most known variants. Int Immunol. 1993;5(1):37-46.

114. Good MF, Pombo D, Quakyi IA, Riley EM, Houghten RA, Menon A, et al. Human T-cell recognition of the circumsporozoite protein of Plasmodium falciparum: immunodominant T-cell domains map to the polymorphic regions of the molecule. Proc Natl Acad Sci U S A. 1988;85(4):1199-203.

115. Wahl C, Bochtler P, Chen L, Schirmbeck R, Reimann J. B7-H1 on hepatocytes facilitates priming of specific CD8 T cells but limits the specific recall of primed responses. Gastroenterology. 2008;135(3):980-8.

116. Schildberg FA, Hegenbarth SI, Schumak B, Scholz K, Limmer A, Knolle PA. Liver sinusoidal endothelial cells veto CD8 T cell activation by antigen-presenting dendritic cells. Eur J Immunol. 2008;38(4):957-67.

117. Wunderlich F, Al-Quraishy S, Dkhil MA. Liver-inherent immune system: its role in blood-stage malaria. Front Microbiol. 2014;5:559.

118. McCuskey RS. The hepatic microvascular system in health and its response to toxicants. Anat Rec (Hoboken). 2008;291(6):661-71.

119. Ficht X, Iannacone M. Immune surveillance of the liver by T cells. Sci Immunol. 2020;5(51).

120. Jenne CN, Kubes P. Immune surveillance by the liver. Nat Immunol. 2013;14(10):996-1006.

121. Wisse E, De Zanger RB, Charels K, Van Der Smissen P, McCuskey RS. The liver sieve: considerations concerning the structure and function of endothelial fenestrae, the sinusoidal wall and the space of Disse. Hepatology. 1985;5(4):683-92.

122. Bertolino P, Bowen DG, McCaughan GW, Fazekas de St Groth B. Antigen-specific primary activation of CD8+ T cells within the liver. J Immunol. 2001;166(9):5430-8.

123. Guidotti LG, Inverso D, Sironi L, Di Lucia P, Fioravanti J, Ganzer L, et al. Immunosurveillance of the liver by intravascular effector CD8(+) T cells. Cell. 2015;161(3):486-500.

124. Parker GA, Picut CA. Immune functioning in non lymphoid organs: the liver. Toxicol Pathol. 2012;40(2):237-47.

125. Kopydlowski KM, Salkowski CA, Cody MJ, van Rooijen N, Major J, Hamilton TA, et al. Regulation of macrophage chemokine expression by lipopolysaccharide in vitro and in vivo. J Immunol. 1999;163(3):1537-44.

126. Hsu W, Shu SA, Gershwin E, Lian ZX. The current immune function of hepatic dendritic cells. Cell Mol Immunol. 2007;4(5):321-8.

127. Crispe IN. The liver as a lymphoid organ. Annu Rev Immunol. 2009;27:147-63.

128. Selmi C, Mackay IR, Gershwin ME. The immunological milieu of the liver. Semin Liver Dis. 2007;27(2):129-39.

129. Surh CD, Sprent J. Homeostasis of naive and memory T cells. Immunity. 2008;29(6):848-62.

130. Amino R, Thiberge S, Martin B, Celli S, Shorte S, Frischknecht F, et al. Quantitative imaging of Plasmodium transmission from mosquito to mammal. Nat Med. 2006;12(2):220-4.

131. Chakravarty S, Cockburn IA, Kuk S, Overstreet MG, Sacci JB, Zavala F. CD8+ T lymphocytes protective against malaria liver stages are primed in skin-draining lymph nodes. Nat Med. 2007;13(9):1035-41.

132. Torgler R, Bongfen SE, Romero JC, Tardivel A, Thome M, Corradin G. Sporozoite-mediated hepatocyte wounding limits Plasmodium parasite development via MyD88-mediated NF-kappa B activation and inducible NO synthase expression. J Immunol. 2008;180(6):3990-9.

133. Seguin MC, Klotz FW, Schneider I, Weir JP, Goodbary M, Slayter M, et al. Induction of nitric oxide synthase protects against malaria in mice exposed to irradiated Plasmodium berghei infected mosquitoes: involvement of interferon gamma and CD8+ T cells. J Exp Med. 1994;180(1):353-8.

134. Grand M, Waqasi M, Demarta-Gatsi C, Wei Y, Peronet R, Commere PH, et al. Hepatic Inflammation Confers Protective Immunity Against Liver Stages of Malaria Parasite. Front Immunol. 2020;11:585502.

135. Roland J, Soulard V, Sellier C, Drapier AM, Di Santo JP, Cazenave PA, et al. NK cell responses to Plasmodium infection and control of intrahepatic parasite development. J Immunol. 2006;177(2):1229-39.

136. Wolf AS, Sherratt S, Riley EM. NK Cells: Uncertain Allies against Malaria. Front Immunol. 2017;8:212.

137. Miller JL, Sack BK, Baldwin M, Vaughan AM, Kappe SHI. Interferon-mediated innate immune responses against malaria parasite liver stages. Cell Rep. 2014;7(2):436-47.

138. Baer K, Klotz C, Kappe SH, Schnieder T, Frevert U. Release of hepatic Plasmodium yoelii merozoites into the pulmonary microvasculature. PLoS Pathog. 2007;3(11):e171.

139. Winau F, Hegasy G, Weiskirchen R, Weber S, Cassan C, Sieling PA, et al. Ito cells are liver-resident antigen-presenting cells for activating T cell responses. Immunity. 2007;26(1):117-29.

140. Benechet AP, De Simone G, Di Lucia P, Cilenti F, Barbiera G, Le Bert N, et al. Dynamics and genomic landscape of CD8(+) T cells undergoing hepatic priming. Nature. 2019;574(7777):200-5.

141. Klein I, Crispe IN. Complete differentiation of CD8+ T cells activated locally within the transplanted liver. J Exp Med. 2006;203(2):437-47.

142. Liehl P, Zuzarte-Luis V, Chan J, Zillinger T, Baptista F, Carapau D, et al. Host-cell sensors for Plasmodium activate innate immunity against liver-stage infection. Nat Med. 2014;20(1):47-53.

143. He X, Xia L, Tumas KC, Wu J, Su XZ. Type I Interferons and Malaria: A Double-Edge Sword Against a Complex Parasitic Disease. Front Cell Infect Microbiol. 2020;10:594621.

144. Liehl P, Meireles P, Albuquerque IS, Pinkevych M, Baptista F, Mota MM, et al. Innate immunity induced by Plasmodium liver infection inhibits malaria reinfections. Infect Immun. 2015;83(3):1172-80.

145. Sano G, Hafalla JC, Morrot A, Abe R, Lafaille JJ, Zavala F. Swift development of protective effector functions in naive CD8(+) T cells against malaria liver stages. J Exp Med. 2001;194(2):173-80.

146. Obeid M, Franetich JF, Lorthiois A, Gego A, Gruner AC, Tefit M, et al. Skin-draining lymph node priming is sufficient to induce sterile immunity against pre-erythrocytic malaria. EMBO Mol Med. 2013;5(2):250-63.

147. Corradin G, Levitskaya J. Priming of CD8(+) T Cell Responses to Liver Stage Malaria Parasite Antigens. Front Immunol. 2014;5:527.

148. Butler NS, Schmidt NW, Vaughan AM, Aly AS, Kappe SH, Harty JT. Superior antimalarial immunity after vaccination with late liver stage-arresting genetically attenuated parasites. Cell Host Microbe. 2011;9(6):451-62.

149. Vaughan AM, Kappe SHI. Genetically attenuated malaria parasites as vaccines. Expert Rev Vaccines. 2017;16(8):765-7.

150. Heide J, Vaughan KC, Sette A, Jacobs T, Schulze Zur Wiesch J. Comprehensive Review of Human Plasmodium falciparum-Specific CD8+ T Cell Epitopes. Front Immunol. 2019;10:397.

151. Doolan DL, Houghten RA, Good MF. Location of human cytotoxic T cell epitopes within a polymorphic domain of the Plasmodium falciparum circumsporozoite protein. Int Immunol. 1991;3(6):511-6.

152. Gonzalez JM, Peter K, Esposito F, Nebie I, Tiercy JM, Bonelo A, et al. HLA-A*0201 restricted CD8+ T-lymphocyte responses to malaria: identification of new Plasmodium falciparum epitopes by IFN-gamma ELISPOT. Parasite Immunol. 2000;22(10):501-14.

153. Sedegah M, Sim BK, Mason C, Nutman T, Malik A, Roberts C, et al. Naturally acquired CD8+ cytotoxic T lymphocytes against the Plasmodium falciparum circumsporozoite protein. J Immunol. 1992;149(3):966-71.

154. Hoffman SL, Oster CN, Mason C, Beier JC, Sherwood JA, Ballou WR, et al. Human lymphocyte proliferative response to a sporozoite T cell epitope correlates with resistance to falciparum malaria. J Immunol. 1989;142(4):1299-303.

155. Fidock DA, Gras-Masse H, Lepers JP, Brahimi K, Benmohamed L, Mellouk S, et al. Plasmodium falciparum liver stage antigen-1 is well conserved and contains potent B and T cell determinants. J Immunol. 1994;153(1):190-204.

156. Luty AJ, Lell B, Schmidt-Ott R, Lehman LG, Luckner D, Greve B, et al. Interferon-gamma responses are associated with resistance to reinfection with Plasmodium falciparum in young African children. J Infect Dis. 1999;179(4):980-8.

157. Flanagan KL, Mwangi T, Plebanski M, Odhiambo K, Ross A, Sheu E, et al. Ex vivo interferon-gamma immune response to thrombospondin-related adhesive protein in coastal Kenyans: longevity and risk of Plasmodium falciparum infection. Am J Trop Med Hyg. 2003;68(4):421-30.

158. Connelly M, King CL, Bucci K, Walters S, Genton B, Alpers MP, et al. T-cell immunity to peptide epitopes of liver-stage antigen 1 in an area of Papua New Guinea in which malaria is holoendemic. Infect Immun. 1997;65(12):5082-7.

159. Migot-Nabias F, Deloron P, Ringwald P, Dubois B, Mayombo J, Minh TN, et al. Immune response to Plasmodium falciparum liver stage antigen-1: geographical variations within

Central Africa and their relationship with protection from clinical malaria. Transactions of The Royal Society of Tropical Medicine and Hygiene. 2000;94(5):557-62.

160. Todryk SM, Bejon P, Mwangi T, Plebanski M, Urban B, Marsh K, et al. Correlation of memory T cell responses against TRAP with protection from clinical malaria, and CD4 CD25 high T cells with susceptibility in Kenyans. PLoS One. 2008;3(4):e2027.

161. Ong'echa JM, Lal AA, Terlouw DJ, Ter Kuile FO, Kariuki SK, Udhayakumar V, et al. Association of interferon-gamma responses to pre-erythrocytic stage vaccine candidate antigens of Plasmodium falciparum in young Kenyan children with improved hemoglobin levels: XV. Asembo Bay Cohort Project. Am J Trop Med Hyg. 2003;68(5):590-7.

162. Weiss WR, Sedegah M, Beaudoin RL, Miller LH, Good MF. CD8+ T cells (cytotoxic/suppressors) are required for protection in mice immunized with malaria sporozoites. Proc Natl Acad Sci U S A. 1988;85(2):573-6.

163. Schofield L, Villaquiran J, Ferreira A, Schellekens H, Nussenzweig R, Nussenzweig V. Gamma interferon, CD8+ T cells and antibodies required for immunity to malaria sporozoites. Nature. 1987;330(6149):664-6.

164. Berenzon D, Schwenk RJ, Letellier L, Guebre-Xabier M, Williams J, Krzych U. Protracted protection to Plasmodium berghei malaria is linked to functionally and phenotypically heterogeneous liver memory CD8+ T cells. J Immunol. 2003;171(4):2024-34.

165. Lyke KE, Ishizuka AS, Berry AA, Chakravarty S, DeZure A, Enama ME, et al. Attenuated PfSPZ Vaccine induces strain-transcending T cells and durable protection against heterologous controlled human malaria infection. Proc Natl Acad Sci U S A. 2017;114(10):2711-6.

166. Seder RA, Chang LJ, Enama ME, Zephir KL, Sarwar UN, Gordon IJ, et al. Protection against malaria by intravenous immunization with a nonreplicating sporozoite vaccine. Science. 2013;341(6152):1359-65.

167. Mordmuller B, Surat G, Lagler H, Chakravarty S, Ishizuka AS, Lalremruata A, et al. Sterile protection against human malaria by chemoattenuated PfSPZ vaccine. Nature. 2017;542(7642):445-9.

168. Epstein JE, Tewari K, Lyke KE, Sim BK, Billingsley PF, Laurens MB, et al. Live attenuated malaria vaccine designed to protect through hepatic CD8(+) T cell immunity. Science. 2011;334(6055):475-80.

169. Douradinha B, van Dijk M, van Gemert GJ, Khan SM, Janse CJ, Waters AP, et al. Immunization with genetically attenuated P52-deficient Plasmodium berghei sporozoites induces a long-lasting effector memory CD8+ T cell response in the liver. J Immune Based Ther Vaccines. 2011;9(1):6.

170. Mikolajczak SA, Lakshmanan V, Fishbaugher M, Camargo N, Harupa A, Kaushansky A, et al. A next-generation genetically attenuated Plasmodium falciparum parasite created by triple gene deletion. Mol Ther. 2014;22(9):1707-15.

171. Romero P, Maryanski JL, Corradin G, Nussenzweig RS, Nussenzweig V, Zavala F. Cloned cytotoxic T cells recognize an epitope in the circumsporozoite protein and protect against malaria. Nature. 1989;341(6240):323-6.

172. Franke ED, Corradin G, Hoffman SL. Induction of protective CTL responses against the Plasmodium yoelii circumsporozoite protein by immunization with peptides. J Immunol. 1997;159(7):3424-33.

173. Kimura K, Kimura D, Matsushima Y, Miyakoda M, Honma K, Yuda M, et al. CD8+ T cells specific for a malaria cytoplasmic antigen form clusters around infected hepatocytes and are protective at the liver stage of infection. Infect Immun. 2013;81(10):3825-34.

174. Cockburn IA, Amino R, Kelemen RK, Kuo SC, Tse SW, Radtke A, et al. In vivo imaging of CD8+ T cell-mediated elimination of malaria liver stages. Proc Natl Acad Sci U S A. 2013;110(22):9090-5.

175. Reyes-Sandoval A, Wyllie DH, Bauza K, Milicic A, Forbes EK, Rollier CS, et al. CD8+ T effector memory cells protect against liver-stage malaria. J Immunol. 2011;187(3):1347-57.

176. Ewer KJ, O'Hara GA, Duncan CJ, Collins KA, Sheehy SH, Reyes-Sandoval A, et al. Protective CD8+ T-cell immunity to human malaria induced by chimpanzee adenovirus-MVA immunisation. Nat Commun. 2013;4:2836.

177. Schmidt NW, Butler NS, Harty JT. Plasmodium-host interactions directly influence the threshold of memory CD8 T cells required for protective immunity. J Immunol. 2011;186(10):5873-84.

178. Schmidt NW, Butler NS, Badovinac VP, Harty JT. Extreme CD8 T cell requirements for anti-malarial liver-stage immunity following immunization with radiation attenuated sporozoites. PLoS Pathog. 2010;6(7):e1000998.

179. Cockburn IA, Tse SW, Radtke AJ, Srinivasan P, Chen YC, Sinnis P, et al. Dendritic cells and hepatocytes use distinct pathways to process protective antigen from plasmodium in vivo. PLoS Pathog. 2011;7(3):e1001318.

180. Radtke AJ, Kastenmuller W, Espinosa DA, Gerner MY, Tse SW, Sinnis P, et al. Lymph-node resident CD8alpha+ dendritic cells capture antigens from migratory malaria sporozoites and induce CD8+ T cell responses. PLoS Pathog. 2015;11(2):e1004637.

181. Geissmann F, Cameron TO, Sidobre S, Manlongat N, Kronenberg M, Briskin MJ, et al. Intravascular immune surveillance by CXCR6+ NKT cells patrolling liver sinusoids. PLoS Biol. 2005;3(4):e113.

182. Tse SW, Radtke AJ, Espinosa DA, Cockburn IA, Zavala F. The chemokine receptor CXCR6 is required for the maintenance of liver memory CD8(+) T cells specific for infectious pathogens. J Infect Dis. 2014;210(9):1508-16.

183. Morrot A, Hafalla JC, Cockburn IA, Carvalho LH, Zavala F. IL-4 receptor expression on CD8+ T cells is required for the development of protective memory responses against liver stages of malaria parasites. J Exp Med. 2005;202(4):551-60.

184. Chen DH, Tigelaar RE, Weinbaum FI. Immunity to sporozoite-induced malaria infeciton in mice. I. The effect of immunization of T and B cell-deficient mice. J Immunol. 1977;118(4):1322-7.

185. Butler NS, Schmidt NW, Harty JT. Differential effector pathways regulate memory CD8 T cell immunity against Plasmodium berghei versus P. yoelii sporozoites. J Immunol. 2010;184(5):2528-38.

186. Doll KL, Pewe LL, Kurup SP, Harty JT. Discriminating Protective from Nonprotective Plasmodium-Specific CD8+ T Cell Responses. J Immunol. 2016;196(10):4253-62.

187. Frevert U, Krzych U. Plasmodium cellular effector mechanisms and the hepatic microenvironment. Front Microbiol. 2015;6:482.

188. Cockburn IA, Tse SW, Zavala F. CD8+ T cells eliminate liver-stage Plasmodium berghei parasites without detectable bystander effect. Infect Immun. 2014;82(4):1460-4.

189. John CC, Moormann AM, Sumba PO, Ofulla AV, Pregibon DC, Kazura JW. Gamma interferon responses to Plasmodium falciparum liver-stage antigen 1 and thrombospondin-related adhesive protein and their relationship to age, transmission intensity, and protection against malaria. Infect Immun. 2004;72(9):5135-42.

190. Bucci K, Kastens W, Hollingdale MR, Shankar A, Alpers MP, King CL, et al. Influence of age and HLA type on interferon-gamma (IFN-gamma) responses to a naturally occurring polymorphic epitope of Plasmodium falciparum liver stage antigen-1 (LSA-1). Clin Exp Immunol. 2000;122(1):94-100.

191. Chelimo K, Sumba PO, Kazura JW, Ofula AV, John CC. Interferon-gamma responses to Plasmodium falciparum liver-stage antigen-1 and merozoite-surface protein-1 increase with age in children in a malaria holoendemic area of western Kenya. Malar J. 2003;2(1):37.

192. King T, Lamb T. Interferon-gamma: The Jekyll and Hyde of Malaria. PLoS Pathog. 2015;11(10):e1005118.

193. Nussler A, Pied S, Goma J, Renia L, Miltgen F, Grau GE, et al. TNF inhibits malaria hepatic stages in vitro via synthesis of IL-6. Int Immunol. 1991;3(4):317-21.

194. Mordmuller BG, Metzger WG, Juillard P, Brinkman BM, Verweij CL, Grau GE, et al. Tumor necrosis factor in Plasmodium falciparum malaria: high plasma level is associated with fever, but high production capacity is associated with rapid fever clearance. Eur Cytokine Netw. 1997;8(1):29-35.

195. Shear HL, Marino MW, Wanidworanun C, Berman JW, Nagel RL. Correlation of increased expression of intercellular adhesion molecule-1, but not high levels of tumor necrosis factor-alpha, with lethality of Plasmodium yoelii 17XL, a rodent model of cerebral malaria. Am J Trop Med Hyg. 1998;59(6):852-8.

196. Welten SPM, Sandu I, Baumann NS, Oxenius A. Memory CD8 T cell inflation vs tissue-resident memory T cells: Same patrollers, same controllers? Immunol Rev. 2018;283(1):161-75.

197. Sallusto F, Lenig D, Förster R, Lipp M, Lanzavecchia A. Two subsets of memory T lymphocytes with distinct homing potentials and effector functions. Nature. 1999;401(6754):708-12.

198. Gebhardt T, Wakim LM, Eidsmo L, Reading PC, Heath WR, Carbone FR. Memory T cells in nonlymphoid tissue that provide enhanced local immunity during infection with herpes simplex virus. Nat Immunol. 2009;10(5):524-30.

199. Steinert EM, Schenkel JM, Fraser KA, Beura LK, Manlove LS, Igyarto BZ, et al. Quantifying Memory CD8 T Cells Reveals Regionalization of Immunosurveillance. Cell. 2015;161(4):737-49.

200. Fan X, Rudensky AY. Hallmarks of Tissue-Resident Lymphocytes. Cell. 2016;164(6):1198-211.

201. Fernandez-Ruiz D, Ng WY, Holz LE, Ma JZ, Zaid A, Wong YC, et al. Liver-Resident Memory CD8(+) T Cells Form a Front-Line Defense against Malaria Liver-Stage Infection. Immunity. 2016;45(4):889-902.

202. Mackay LK, Kallies A. Transcriptional Regulation of Tissue-Resident Lymphocytes. Trends Immunol. 2017;38(2):94-103.

203. Sasson SC, Gordon CL, Christo SN, Klenerman P, Mackay LK. Local heroes or villains: tissue-resident memory T cells in human health and disease. Cell Mol Immunol. 2020;17(2):113-22.

204. Youngblood B, Hale JS, Kissick HT, Ahn E, Xu X, Wieland A, et al. Effector CD8 T cells dedifferentiate into long-lived memory cells. Nature. 2017;552(7685):404-9.

205. Akondy RS, Fitch M, Edupuganti S, Yang S, Kissick HT, Li KW, et al. Origin and differentiation of human memory CD8 T cells after vaccination. Nature. 2017;552(7685):362-7.

206. Milner JJ, Toma C, Yu B, Zhang K, Omilusik K, Phan AT, et al. Runx3 programs CD8(+) T cell residency in non-lymphoid tissues and tumours. Nature. 2017;552(7684):253-7.

207. Mackay LK, Rahimpour A, Ma JZ, Collins N, Stock AT, Hafon ML, et al. The developmental pathway for CD103(+)CD8+ tissue-resident memory T cells of skin. Nat Immunol. 2013;14(12):1294-301.

208. Mackay LK, Minnich M, Kragten NA, Liao Y, Nota B, Seillet C, et al. Hobit and Blimp1 instruct a universal transcriptional program of tissue residency in lymphocytes. Science. 2016;352(6284):459-63.

209. Schenkel JM, Fraser KA, Beura LK, Pauken KE, Vezys V, Masopust D. T cell memory. Resident memory CD8 T cells trigger protective innate and adaptive immune responses. Science. 2014;346(6205):98-101.

210. Mackay LK, Stock AT, Ma JZ, Jones CM, Kent SJ, Mueller SN, et al. Long-lived epithelial immunity by tissue-resident memory T (TRM) cells in the absence of persisting local antigen presentation. Proc Natl Acad Sci U S A. 2012;109(18):7037-42.

211. Pallett LJ, Burton AR, Amin OE, Rodriguez-Tajes S, Patel AA, Zakeri N, et al. Longevity and replenishment of human liver-resident memory T cells and mononuclear phagocytes. J Exp Med. 2020;217(9).

212. Thome JJ, Yudanin N, Ohmura Y, Kubota M, Grinshpun B, Sathaliyawala T, et al. Spatial map of human T cell compartmentalization and maintenance over decades of life. Cell. 2014;159(4):814-28.

213. Beura LK, Mitchell JS, Thompson EA, Schenkel JM, Mohammed J, Wijeyesinghe S, et al. Intravital mucosal imaging of CD8(+) resident memory T cells shows tissue-autonomous recall responses that amplify secondary memory. Nat Immunol. 2018;19(2):173-82.

214. Schenkel JM, Fraser KA, Casey KA, Beura LK, Pauken KE, Vezys V, et al. IL-15-Independent Maintenance of Tissue-Resident and Boosted Effector Memory CD8 T Cells. J Immunol. 2016;196(9):3920-6.

215. Steinbach K, Vincenti I, Kreutzfeldt M, Page N, Muschaweckh A, Wagner I, et al. Brain-resident memory T cells represent an autonomous cytotoxic barrier to viral infection. J Exp Med. 2016;213(8):1571-87.

216. Zhou AC, Wagar LE, Wortzman ME, Watts TH. Intrinsic 4-1BB signals are indispensable for the establishment of an influenza-specific tissue-resident memory CD8 T-cell population in the lung. Mucosal Immunol. 2017;10(5):1294-309.

217. Swadling L, Pallett LJ, Diniz MO, Baker JM, Amin OE, Stegmann KA, et al. Human Liver Memory CD8(+) T Cells Use Autophagy for Tissue Residence. Cell Rep. 2020;30(3):687-98 e6.

218. Slutter B, Van Braeckel-Budimir N, Abboud G, Varga SM, Salek-Ardakani S, Harty JT. Dynamics of influenza-induced lung-resident memory T cells underlie waning heterosubtypic immunity. Sci Immunol. 2017;2(7).

219. Kumar BV, Ma W, Miron M, Granot T, Guyer RS, Carpenter DJ, et al. Human Tissue-Resident Memory T Cells Are Defined by Core Transcriptional and Functional Signatures in Lymphoid and Mucosal Sites. Cell Rep. 2017;20(12):2921-34.

220. Topham DJ, Reilly EC. Tissue-Resident Memory CD8(+) T Cells: From Phenotype to Function. Front Immunol. 2018;9:515.

221. Hombrink P, Helbig C, Backer RA, Piet B, Oja AE, Stark R, et al. Programs for the persistence, vigilance and control of human CD8(+) lung-resident memory T cells. Nat Immunol. 2016;17(12):1467-78.

222. Mackay LK, Wynne-Jones E, Freestone D, Pellicci DG, Mielke LA, Newman DM, et al. T-box Transcription Factors Combine with the Cytokines TGF-beta and IL-15 to Control Tissue-Resident Memory T Cell Fate. Immunity. 2015;43(6):1101-11.

223. Tse SW, Cockburn IA, Zhang H, Scott AL, Zavala F. Unique transcriptional profile of liver-resident memory CD8+ T cells induced by immunization with malaria sporozoites. Genes Immun. 2013;14(5):302-9.

224. Skon CN, Lee JY, Anderson KG, Masopust D, Hogquist KA, Jameson SC. Transcriptional downregulation of S1pr1 is required for the establishment of resident memory CD8+ T cells. Nat Immunol. 2013;14(12):1285-93.

225. Kallies A, Xin A, Belz GT, Nutt SL. Blimp-1 transcription factor is required for the differentiation of effector CD8(+) T cells and memory responses. Immunity. 2009;31(2):283-95.

226. Behr FM, Kragten NAM, Wesselink TH, Nota B, van Lier RAW, Amsen D, et al. Blimp-1 Rather Than Hobit Drives the Formation of Tissue-Resident Memory CD8(+) T Cells in the Lungs. Front Immunol. 2019;10:400.

227. Sowell RT, Rogozinska M, Nelson CE, Vezys V, Marzo AL. Cutting edge: generation of effector cells that localize to mucosal tissues and form resident memory CD8 T cells is controlled by mTOR. J Immunol. 2014;193(5):2067-71.

228. Wakim LM, Woodward-Davis A, Bevan MJ. Memory T cells persisting within the brain after local infection show functional adaptations to their tissue of residence. Proc Natl Acad Sci U S A. 2010;107(42):17872-9.

229. Jameson SC, Masopust D. Understanding Subset Diversity in T Cell Memory. Immunity. 2018;48(2):214-26.

230. Guebre-Xabier M, Schwenk R, Krzych U. Memory phenotype CD8(+) T cells persist in livers of mice protected against malaria by immunization with attenuated Plasmodium berghei sporozoites. Eur J Immunol. 1999;29(12):3978-86.

231. Krzych U, Schwenk R, Guebre-Xabier M, Sun P, Palmer D, White K, et al. The role of intrahepatic lymphocytes in mediating protective immunity induced by attenuated Plasmodium berghei sporozoites. Immunol Rev. 2000;174:123-34.

232. Rissiek B, Lukowiak M, Raczkowski F, Magnus T, Mittrucker HW, Koch-Nolte F. In Vivo Blockade of Murine ARTC2.2 During Cell Preparation Preserves the Vitality and Function of Liver Tissue-Resident Memory T Cells. Front Immunol. 2018;9:1580.

233. Iijima N, Iwasaki A. T cell memory. A local macrophage chemokine network sustains protective tissue-resident memory CD4 T cells. Science. 2014;346(6205):93-8.

234. Thomas SY, Scanlon ST, Griewank KG, Constantinides MG, Savage AK, Barr KA, et al. PLZF induces an intravascular surveillance program mediated by long-lived LFA-1-ICAM-1 interactions. J Exp Med. 2011;208(6):1179-88.

235. Pichyangkul S, Spring MD, Yongvanitchit K, Kum-Arb U, Limsalakpetch A, Im-Erbsin R, et al. Chemoprophylaxis with sporozoite immunization in P. knowlesi rhesus monkeys confers protection and elicits sporozoite-specific memory T cells in the liver. PLoS One. 2017;12(2):e0171826.

236. McNamara HA, Cai Y, Wagle MV, Sontani Y, Roots CM, Miosge LA, et al. Up-regulation of LFA-1 allows liver-resident memory T cells to patrol and remain in the hepatic sinusoids. Sci Immunol. 2017;2(9).

237. Gola A, Silman D, Walters AA, Sridhar S, Uderhardt S, Salman AM, et al. Prime and target immunization protects against liver-stage malaria in mice. Sci Transl Med. 2018;10(460).

238. Zarling S, Berenzon D, Dalai S, Liepinsh D, Steers N, Krzych U. The survival of memory CD8 T cells that is mediated by IL-15 correlates with sustained protection against malaria. J Immunol. 2013;190(10):5128-41.

239. Walk J, Stok JE, Sauerwein RW. Can Patrolling Liver-Resident T Cells Control Human Malaria Parasite Development? Trends Immunol. 2019;40(3):186-96.

240. Nganou-Makamdop K, van Gemert GJ, Arens T, Hermsen CC, Sauerwein RW. Long term protection after immunization with P. berghei sporozoites correlates with sustained IFNgamma responses of hepatic CD8+ memory T cells. PLoS One. 2012;7(5):e36508.

241. Olsen TM, Stone BC, Chuenchob V, Murphy SC. Prime-and-Trap Malaria Vaccination To Generate Protective CD8(+) Liver-Resident Memory T Cells. J Immunol. 2018;201(7):1984-93.

242. Ishizuka AS, Lyke KE, DeZure A, Berry AA, Richie TL, Mendoza FH, et al. Protection against malaria at 1 year and immune correlates following PfSPZ vaccination. Nat Med. 2016;22(6):614-23.

243. Weiss WR, Jiang CG. Protective CD8+ T lymphocytes in primates immunized with malaria sporozoites. PLoS One. 2012;7(2):e31247.

244. Stelma F, de Niet A, Sinnige MJ, van Dort KA, van Gisbergen K, Verheij J, et al. Human intrahepatic CD69 + CD8+ T cells have a tissue resident memory T cell phenotype with reduced cytolytic capacity. Sci Rep. 2017;7(1):6172.

245. Gill US, Pallett LJ, Thomas N, Burton AR, Patel AA, Yona S, et al. Fine needle aspirates comprehensively sample intrahepatic immunity. Gut. 2019;68(8):1493-503.

246. Pallett LJ, Davies J, Colbeck EJ, Robertson F, Hansi N, Easom NJW, et al. IL-2(high) tissue-resident T cells in the human liver: Sentinels for hepatotropic infection. J Exp Med. 2017;214(6):1567-80.

247. Swadling L, Pallett LJ, Maini MK. Liver-resident CD8+ T cells: Learning lessons from the local experts. J Hepatol. 2020;72(6):1049-51.

248. Gill US, Pallett LJ, Kennedy PTF, Maini MK. Liver sampling: a vital window into HBV pathogenesis on the path to functional cure. Gut. 2018;67(4):767-75.

249. Masopust D, Soerens AG. Tissue-Resident T Cells and Other Resident Leukocytes. Annu Rev Immunol. 2019;37:521-46.

250. Kim JH, Han JW, Choi YJ, Rha MS, Koh JY, Kim KH, et al. Functions of human liver CD69(+)CD103(-)CD8(+) T cells depend on HIF-2alpha activity in healthy and pathologic livers. J Hepatol. 2020;72(6):1170-81.

251. Hill AV, Reyes-Sandoval A, O'Hara G, Ewer K, Lawrie A, Goodman A, et al. Prime-boost vectored malaria vaccines: progress and prospects. Hum Vaccin. 2010;6(1):78-83.

252. Golden-Mason L, Kelly AM, Doherty DG, Traynor O, McEntee G, Kelly J, et al. Hepatic interleuklin 15 (IL-15) expression: implications for local NK/NKT cell homeostasis and development. Clin Exp Immunol. 2004;138(1):94-101.

253. Alves NL, Hooibrink B, Arosa FA, van Lier RA. IL-15 induces antigen-independent expansion and differentiation of human naive CD8+ T cells in vitro. Blood. 2003;102(7):2541-6.

254. Rahimi RA, Luster AD. Redefining Memory T Cell Subsets. Trends Immunol. 2020;41(8):645-8.

255. He S, Wang LH, Liu Y, Li YQ, Chen HT, Xu JH, et al. Single-cell transcriptome profiling of an adult human cell atlas of 15 major organs. Genome Biol. 2020;21(1):294.

256. Hunter S, Willcox CR, Davey MS, Kasatskaya SA, Jeffery HC, Chudakov DM, et al. Human liver infiltrating gammadelta T cells are composed of clonally expanded circulating and tissue-resident populations. J Hepatol. 2018;69(3):654-65.

257. Song G, Shi Y, Zhang M, Goswami S, Afridi S, Meng L, et al. Global immune characterization of HBV/HCV-related hepatocellular carcinoma identifies macrophage and T-cell subsets associated with disease progression. Cell Discov. 2020;6(1):90.

258. Maini MK, Boni C, Lee CK, Larrubia JR, Reignat S, Ogg GS, et al. The role of virus-specific CD8(+) cells in liver damage and viral control during persistent hepatitis B virus infection. J Exp Med. 2000;191(8):1269-80.

259. Ando K, Moriyama T, Guidotti LG, Wirth S, Schreiber RD, Schlicht HJ, et al. Mechanisms of class I restricted immunopathology. A transgenic mouse model of fulminant hepatitis. J Exp Med. 1993;178(5):1541-54.

260. Ariotti S, Hogenbirk MA, Dijkgraaf FE, Visser LL, Hoekstra ME, Song JY, et al. T cell memory. Skin-resident memory CD8(+) T cells trigger a state of tissue-wide pathogen alert. Science. 2014;346(6205):101-5.

261. Kim J, Chang DY, Lee HW, Lee H, Kim JH, Sung PS, et al. Innate-like Cytotoxic Function of Bystander-Activated CD8(+) T Cells Is Associated with Liver Injury in Acute Hepatitis A. Immunity. 2018;48(1):161-73 e5.

262. Kim TS, Shin EC. The activation of bystander CD8(+) T cells and their roles in viral infection. Exp Mol Med. 2019;51(12):1-9.

263. Plotkin S. History of vaccination. Proc Natl Acad Sci U S A. 2014;111(34):12283-7.

264. Mueller I, Galinski MR, Tsuboi T, Arevalo-Herrera M, Collins WE, King CL. Chapter Three - Natural Acquisition of Immunity to Plasmodium vivax: Epidemiological Observations and Potential Targets. In: Hay SI, Price R, Baird JK, editors. Advances in Parasitology. 81: Academic Press; 2013. p. 77-131.

265. Nikolaeva D, Draper SJ, Biswas S. Toward the development of effective transmission-blocking vaccines for malaria. Expert Rev Vaccines. 2015;14(5):653-80.

266. Gordon DM, McGovern TW, Krzych U, Cohen JC, Schneider I, LaChance R, et al. Safety, immunogenicity, and efficacy of a recombinantly produced Plasmodium falciparum circumsporozoite protein-hepatitis B surface antigen subunit vaccine. J Infect Dis. 1995;171(6):1576-85.

267. Stoute JA, Slaoui M, Heppner DG, Momin P, Kester KE, Desmons P, et al. A preliminary evaluation of a recombinant circumsporozoite protein vaccine against Plasmodium falciparum malaria. RTS,S Malaria Vaccine Evaluation Group. N Engl J Med. 1997;336(2):86-91.

268. Kester KE, Cummings JF, Ofori-Anyinam O, Ockenhouse CF, Krzych U, Moris P, et al. Randomized, double-blind, phase 2a trial of falciparum malaria vaccines RTS,S/AS01B and RTS,S/AS02A in malaria-naive adults: safety, efficacy, and immunologic associates of protection. J Infect Dis. 2009;200(3):337-46.

269. Rts SCTP. Efficacy and safety of RTS,S/AS01 malaria vaccine with or without a booster dose in infants and children in Africa: final results of a phase 3, individually randomised, controlled trial. Lancet. 2015;386(9988):31-45.

270. White MT, Verity R, Griffin JT, Asante KP, Owusu-Agyei S, Greenwood B, et al. Immunogenicity of the RTS,S/AS01 malaria vaccine and implications for duration of vaccine efficacy: secondary analysis of data from a phase 3 randomised controlled trial. Lancet Infect Dis. 2015;15(12):1450-8.

271. Olotu A, Fegan G, Wambua J, Nyangweso G, Leach A, Lievens M, et al. Seven-Year Efficacy of RTS,S/AS01 Malaria Vaccine among Young African Children. N Engl J Med. 2016;374(26):2519-29.

272. Tinto H, Otieno W, Gesase S, Sorgho H, Otieno L, Liheluka E, et al. Long-term incidence of severe malaria following RTS,S/AS01 vaccination in children and infants in Africa: an open-label 3-year extension study of a phase 3 randomised controlled trial. Lancet Infect Dis. 2019;19(8):821-32.

273. European Medicines Agency. First malaria vaccine receives positive scientific opinion from EMA London: EMA; 2015 [Accessed October 2018].

274. Malaria Vaccine Implementation Programme. Proposed framework for policy decision on RTS,S/AS01 malaria vaccine. Geneva: World Health Organisation; 2019.

275. Ockenhouse CF, Regules J, Tosh D, Cowden J, Kathcart A, Cummings J, et al. Ad35.CS.01-RTS,S/AS01 Heterologous Prime Boost Vaccine Efficacy against Sporozoite Challenge in Healthy Malaria-Naive Adults. PLoS One. 2015;10(7):e0131571.

276. Dunachie SJ, Walther M, Vuola JM, Webster DP, Keating SM, Berthoud T, et al. A clinical trial of prime-boost immunisation with the candidate malaria vaccines RTS,S/AS02A and MVA-CS. Vaccine. 2006;24(15):2850-9.

277. Heppner DG, Jr., Kester KE, Ockenhouse CF, Tornieporth N, Ofori O, Lyon JA, et al. Towards an RTS,S-based, multi-stage, multi-antigen vaccine against falciparum malaria: progress at the Walter Reed Army Institute of Research. Vaccine. 2005;23(17-18):2243-50.

278. Collins KA, Snaith R, Cottingham MG, Gilbert SC, Hill AVS. Enhancing protective immunity to malaria with a highly immunogenic virus-like particle vaccine. Sci Rep. 2017;7:46621.

279. Venkatraman N, Tiono AB, Bowyer G, Powlson J, Collins KA, Coulibaly S, et al. Phase I assessments of first-in-human administration of a novel malaria anti-sporozoite vaccine candidate, R21 in matrix-M adjuvant, in UK and Burkinabe volunteers. medRxiv. 2019:19009282.

280. Freund J, Thomson KJ, Sommer HE, Walter AW, Schenkein EL. Immunization of Rhesus Monkeys against Malarial Infection (P. Knowlesi) with Killed Parasites and Adjuvants. Science. 1945;102(2643):202-4.

281. Nussenzweig RS, Vanderberg J, Most H, Orton C. Protective immunity produced by the injection of x-irradiated sporozoites of plasmodium berghei. Nature. 1967;216(5111):160-2.

282. Clyde DF, Most H, McCarthy VC, Vanderberg JP. Immunization of man against sporozite-induced falciparum malaria. Am J Med Sci. 1973;266(3):169-77.

283. Mueller AK, Labaied M, Kappe SH, Matuschewski K. Genetically modified Plasmodium parasites as a protective experimental malaria vaccine. Nature. 2005;433(7022):164-7.

284. Hoffman SL, Billingsley PF, James E, Richman A, Loyevsky M, Li T, et al. Development of a metabolically active, non-replicating sporozoite vaccine to prevent Plasmodium falciparum malaria. Hum Vaccin. 2010;6(1):97-106.

285. Richie TL, Billingsley PF, Sim BK, James ER, Chakravarty S, Epstein JE, et al. Progress with Plasmodium falciparum sporozoite (PfSPZ)-based malaria vaccines. Vaccine. 2015;33(52):7452-61.

286. Greenwood B. Progress with the PfSPZ Vaccine for malaria. Lancet Infect Dis. 2017;17(5):463-4.

287. Roestenberg M, McCall M, Hopman J, Wiersma J, Luty AJ, van Gemert GJ, et al. Protection against a malaria challenge by sporozoite inoculation. N Engl J Med. 2009;361(5):468-77.

288. Spring M, Murphy J, Nielsen R, Dowler M, Bennett JW, Zarling S, et al. First-in-human evaluation of genetically attenuated Plasmodium falciparum sporozoites administered by bite of Anopheles mosquitoes to adult volunteers. Vaccine. 2013;31(43):4975-83.

289. Bijker EM, Bastiaens GJ, Teirlinck AC, van Gemert GJ, Graumans W, van de Vegte-Bolmer M, et al. Protection against malaria after immunization by chloroquine prophylaxis and sporozoites is mediated by preerythrocytic immunity. Proc Natl Acad Sci U S A. 2013;110(19):7862-7.

290. Goswami D, Betz W, Locham NK, Parthiban C, Brager C, Schafer C, et al. A replication-competent late liver stage-attenuated human malaria parasite. JCI Insight. 2020;5(13).

291. Zaidi I, Diallo H, Conteh S, Robbins Y, Kolasny J, Orr-Gonzalez S, et al. gammadelta T Cells Are Required for the Induction of Sterile Immunity during Irradiated Sporozoite Vaccinations. J Immunol. 2017;199(11):3781-8.

292. Mo AX, Pesce J, Hall BF. Exploring immunological mechanisms of the whole sporozoite vaccination against P. falciparum malaria. Vaccine. 2015;33(25):2851-7.

293. Jongo SA, Shekalaghe SA, Church LWP, Ruben AJ, Schindler T, Zenklusen I, et al. Safety, Immunogenicity, and Protective Efficacy against Controlled Human Malaria Infection of Plasmodium falciparum Sporozoite Vaccine in Tanzanian Adults. Am J Trop Med Hyg. 2018;99(2):338-49.

294. Epstein JE, Paolino KM, Richie TL, Sedegah M, Singer A, Ruben AJ, et al. Protection against Plasmodium falciparum malaria by PfSPZ Vaccine. JCI Insight. 2017;2(1):e89154.

295. Jongo SA, Church LWP, Mtoro AT, Schindler T, Chakravarty S, Ruben AJ, et al. Increase of Dose Associated With Decrease in Protection Against Controlled Human Malaria Infection by PfSPZ Vaccine in Tanzanian Adults. Clin Infect Dis. 2020;71(11):2849-57.

296. Sissoko MS, Healy SA, Katile A, Omaswa F, Zaidi I, Gabriel EE, et al. Safety and efficacy of PfSPZ Vaccine against Plasmodium falciparum via direct venous inoculation in healthy malaria-exposed adults in Mali: a randomised, double-blind phase 1 trial. Lancet Infect Dis. 2017;17(5):498-509.

297. Duffy PE, Patrick Gorres J. Malaria vaccines since 2000: progress, priorities, products. NPJ Vaccines. 2020;5:48.

298. Roestenberg M, Teirlinck AC, McCall MB, Teelen K, Makamdop KN, Wiersma J, et al. Long-term protection against malaria after experimental sporozoite inoculation: an open-label follow-up study. Lancet. 2011;377(9779):1770-6.

299. Walk J, Reuling IJ, Behet MC, Meerstein-Kessel L, Graumans W, van Gemert GJ, et al. Modest heterologous protection after Plasmodium falciparum sporozoite immunization: a double-blind randomized controlled clinical trial. BMC Med. 2017;15(1):168.

300. Hodgson SH, Ewer KJ, Bliss CM, Edwards NJ, Rampling T, Anagnostou NA, et al. Evaluation of the efficacy of ChAd63-MVA vectored vaccines expressing circumsporozoite protein and ME-TRAP against controlled human malaria infection in malaria-naive individuals. J Infect Dis. 2015;211(7):1076-86.

301. McConkey SJ, Reece WH, Moorthy VS, Webster D, Dunachie S, Butcher G, et al. Enhanced T-cell immunogenicity of plasmid DNA vaccines boosted by recombinant modified vaccinia virus Ankara in humans. Nat Med. 2003;9(6):729-35.

302. Dunachie SJ, Walther M, Epstein JE, Keating S, Berthoud T, Andrews L, et al. A DNA prime-modified vaccinia virus ankara boost vaccine encoding thrombospondin-related adhesion protein but not circumsporozoite protein partially protects healthy malaria-naive adults against Plasmodium falciparum sporozoite challenge. Infect Immun. 2006;74(10):5933-42.

303. Gilbert SC, Plebanski M, Harris SJ, Allsopp CE, Thomas R, Layton GT, et al. A protein particle vaccine containing multiple malaria epitopes. Nat Biotechnol. 1997;15(12):1280-4.

304. O'Hara GA, Duncan CJ, Ewer KJ, Collins KA, Elias SC, Halstead FD, et al. Clinical assessment of a recombinant simian adenovirus ChAd63: a potent new vaccine vector. J Infect Dis. 2012;205(5):772-81.

305. Webster DP, Dunachie S, Vuola JM, Berthoud T, Keating S, Laidlaw SM, et al. Enhanced T cell-mediated protection against malaria in human challenges by using the recombinant poxviruses FP9 and modified vaccinia virus Ankara. Proc Natl Acad Sci U S A. 2005;102(13):4836-41.

306. Bliss CM, Bowyer G, Anagnostou NA, Havelock T, Snudden CM, Davies H, et al. Assessment of novel vaccination regimens using viral vectored liver stage malaria vaccines encoding ME-TRAP. Sci Rep. 2018;8(1):3390.

307. Ogwang C, Kimani D, Edwards NJ, Roberts R, Mwacharo J, Bowyer G, et al. Prime-boost vaccination with chimpanzee adenovirus and modified vaccinia Ankara encoding TRAP

provides partial protection against Plasmodium falciparum infection in Kenyan adults. Sci Transl Med. 2015;7(286):286re5.

308. Moorthy VS, Imoukhuede EB, Milligan P, Bojang K, Keating S, Kaye P, et al. A randomised, double-blind, controlled vaccine efficacy trial of DNA/MVA ME-TRAP against malaria infection in Gambian adults. PLoS Med. 2004;1(2):e33.

309. Bejon P, Mwacharo J, Kai OK, Todryk S, Keating S, Lang T, et al. Immunogenicity of the candidate malaria vaccines FP9 and modified vaccinia virus Ankara encoding the pre-erythrocytic antigen ME-TRAP in 1-6 year old children in a malaria endemic area. Vaccine. 2006;24(22):4709-15.

310. Bliss CM, Drammeh A, Bowyer G, Sanou GS, Jagne YJ, Ouedraogo O, et al. Viral Vector Malaria Vaccines Induce High-Level T Cell and Antibody Responses in West African Children and Infants. Mol Ther. 2017;25(2):547-59.

311. Mensah VA, Roetynck S, Kanteh EK, Bowyer G, Ndaw A, Oko F, et al. Safety and Immunogenicity of Malaria Vectored Vaccines Given with Routine Expanded Program on Immunization Vaccines in Gambian Infants and Neonates: A Randomized Controlled Trial. Front Immunol. 2017;8:1551.

312. Tiono AB, Nebie I, Anagnostou N, Coulibaly AS, Bowyer G, Lam E, et al. First field efficacy trial of the ChAd63 MVA ME-TRAP vectored malaria vaccine candidate in 5-17 months old infants and children. PLoS One. 2018;13(12):e0208328.

313. Darrah PA, Zeppa JJ, Maiello P, Hackney JA, Wadsworth MH, 2nd, Hughes TK, et al. Prevention of tuberculosis in macaques after intravenous BCG immunization. Nature. 2020;577(7788):95-102.

314. Perdomo C, Zedler U, Kuhl AA, Lozza L, Saikali P, Sander LE, et al. Mucosal BCG Vaccination Induces Protective Lung-Resident Memory T Cell Populations against Tuberculosis. MBio. 2016;7(6).

315. Zens KD, Chen JK, Farber DL. Vaccine-generated lung tissue-resident memory T cells provide heterosubtypic protection to influenza infection. JCI Insight. 2016;1(10).

316. Stary G, Olive A, Radovic-Moreno AF, Gondek D, Alvarez D, Basto PA, et al. VACCINES. A mucosal vaccine against Chlamydia trachomatis generates two waves of protective memory T cells. Science. 2015;348(6241):aaa8205.

317. Wakim LM, Smith J, Caminschi I, Lahoud MH, Villadangos JA. Antibody-targeted vaccination to lung dendritic cells generates tissue-resident memory CD8 T cells that are highly protective against influenza virus infection. Mucosal Immunol. 2015;8(5):1060-71.

318. Shin H, Iwasaki A. A vaccine strategy that protects against genital herpes by establishing local memory T cells. Nature. 2012;491(7424):463-7.

319. Granier C, Blanc C, Karaki S, Tran T, Roussel H, Tartour E. Tissue-resident memory T cells play a key role in the efficacy of cancer vaccines. Oncoimmunology. 2017;6(11):e1358841.

320. Nizard M, Roussel H, Diniz MO, Karaki S, Tran T, Voron T, et al. Induction of resident memory T cells enhances the efficacy of cancer vaccine. Nat Commun. 2017;8:15221.

321. van der Gracht ET, Schoonderwoerd MJ, van Duikeren S, Yilmaz AN, Behr FM, Colston JM, et al. Adenoviral vaccines promote protective tissue-resident memory T cell populations against cancer. J Immunother Cancer. 2020;8(2).

322. Mohammad AK, Reineke JJ. Quantitative detection of PLGA nanoparticle degradation in tissues following intravenous administration. Mol Pharm. 2013;10(6):2183-9.

323. Tay SS, Wong YC, Roediger B, Sierro F, Lu B, McDonald DM, et al. Intrahepatic activation of naive CD4+ T cells by liver-resident phagocytic cells. J Immunol. 2014;193(5):2087-95.

324. Holz LE, Chua YC, de Menezes MN, Anderson RJ, Draper SL, Compton BJ, et al. Glycolipid-peptide vaccination induces liver-resident memory CD8(+) T cells that protect against rodent malaria. Sci Immunol. 2020;5(48).

325. Edozien JC, Gilles HM, Udeozo IOK. Adult and cord-blood gamma-globulin and immunity to malaria in Nigerians. The Lancet. 1962;280(7263):951-5.

326. Draper SJ, Sack BK, King CR, Nielsen CM, Rayner JC, Higgins MK, et al. Malaria Vaccines: Recent Advances and New Horizons. Cell Host Microbe. 2018;24(1):43-56.

327. Sheehy SH, Duncan CJ, Elias SC, Choudhary P, Biswas S, Halstead FD, et al. ChAd63-MVA-vectored blood-stage malaria vaccines targeting MSP1 and AMA1: assessment of efficacy against mosquito bite challenge in humans. Mol Ther. 2012;20(12):2355-68.

328. Ragotte RJ, Higgins MK, Draper SJ. The RH5-CyRPA-Ripr Complex as a Malaria Vaccine Target. Trends Parasitol. 2020;36(6):545-59.

329. Steiner-Monard V, Kamaka K, Karoui O, Roethlisberger S, Audran R, Daubenberger C, et al. The Candidate Blood-stage Malaria Vaccine P27A Induces a Robust Humoral Response in a Fast Track to the Field Phase 1 Trial in Exposed and Nonexposed Volunteers. Clin Infect Dis. 2019;68(3):466-74.

330. Fried M, Duffy PE. Designing a VAR2CSA-based vaccine to prevent placental malaria. Vaccine. 2015;33(52):7483-8.

331. Payne RO, Silk SE, Elias SC, Miura K, Diouf A, Galaway F, et al. Human vaccination against RH5 induces neutralizing antimalarial antibodies that inhibit RH5 invasion complex interactions. JCI Insight. 2017;2(21).

332. Birkett AJ. Status of vaccine research and development of vaccines for malaria. Vaccine. 2016;34(26):2915-20.

333. Huff CG, Marchbank DF, Shiroishi T. Changes in infectiousness of malarial gametocytes. II. Analysis of the possible causative factors. Exp Parasitol. 1958;7(4):399-417.

334. Kaslow DC, Quakyi IA, Syin C, Raum MG, Keister DB, Coligan JE, et al. A vaccine candidate from the sexual stage of human malaria that contains EGF-like domains. Nature. 1988;333(6168):74-6.

335. Kocken CH, Jansen J, Kaan AM, Beckers PJ, Ponnudurai T, Kaslow DC, et al. Cloning and expression of the gene coding for the transmission blocking target antigen Pfs48/45 of Plasmodium falciparum. Mol Biochem Parasitol. 1993;61(1):59-68.

336. Williamson KC, Criscio MD, Kaslow DC. Cloning and expression of the gene for Plasmodium falciparum transmission-blocking target antigen, Pfs230. Mol Biochem Parasitol. 1993;58(2):355-8.

337. Menon V, Kapulu MC, Taylor I, Jewell K, Li Y, Hill F, et al. Assessment of Antibodies Induced by Multivalent Transmission-Blocking Malaria Vaccines. Front Immunol. 2017;8:1998.

338. Li Y, Leneghan DB, Miura K, Nikolaeva D, Brian IJ, Dicks MD, et al. Enhancing immunogenicity and transmission-blocking activity of malaria vaccines by fusing Pfs25 to IMX313 multimerization technology. Sci Rep. 2016;6:18848.

339. Sauerwein RW, Bousema T. Transmission blocking malaria vaccines: Assays and candidates in clinical development. Vaccine. 2015;33(52):7476-82.

340. Nunes JK, Woods C, Carter T, Raphael T, Morin MJ, Diallo D, et al. Development of a transmission-blocking malaria vaccine: progress, challenges, and the path forward. Vaccine. 2014;32(43):5531-9.

341. Theisen M, Roeffen W, Singh SK, Andersen G, Amoah L, Van De Vegte-Bolmer M, et al. A multi-stage malaria vaccine candidate targeting both transmission and asexual parasite life-cycle stages. Vaccine. 2014;32(22):2623-30.

342. Pichyangkul S, Tongtawe P, Kum-Arb U, Yongvanitchit K, Gettayacamin M, Hollingdale MR, et al. Evaluation of the safety and immunogenicity of Plasmodium falciparum apical membrane antigen 1, merozoite surface protein 1 or RTS,S vaccines with adjuvant system AS02A administered alone or concurrently in rhesus monkeys. Vaccine. 2009;28(2):452-62.

343. Bettencourt P. Current Challenges in the Identification of Pre-Erythrocytic Malaria Vaccine Candidate Antigens. Front Immunol. 2020;11:190.

344. Howick VM, Russell AJC, Andrews T, Heaton H, Reid AJ, Natarajan K, et al. The Malaria Cell Atlas: Single parasite transcriptomes across the complete Plasmodium life cycle. Science. 2019;365(6455).

345. Sherrard-Smith E, Sala KA, Betancourt M, Upton LM, Angrisano F, Morin MJ, et al. Synergy in anti-malarial pre-erythrocytic and transmission-blocking antibodies is achieved by reducing parasite density. Elife. 2018;7.

346. Elias SC, Collins KA, Halstead FD, Choudhary P, Bliss CM, Ewer KJ, et al. Assessment of immune interference, antagonism, and diversion following human immunization with biallelic blood-stage malaria viral-vectored vaccines and controlled malaria infection. J Immunol. 2013;190(3):1135-47.

347. Bowyer G, Grobbelaar A, Rampling T, Venkatraman N, Morelle D, Ballou RW, et al. CXCR3(+) T Follicular Helper Cells Induced by Co-Administration of RTS,S/AS01B and Viral-Vectored Vaccines Are Associated With Reduced Immunogenicity and Efficacy Against Malaria. Front Immunol. 2018;9:1660.

348. Porter DW, Thompson FM, Berthoud TK, Hutchings CL, Andrews L, Biswas S, et al. A human Phase I/IIa malaria challenge trial of a polyprotein malaria vaccine. Vaccine. 2011;29(43):7514-22.

349. Ockenhouse CF, Sun PF, Lanar DE, Wellde BT, Hall BT, Kester K, et al. Phase I/IIa safety, immunogenicity, and efficacy trial of NYVAC-Pf7, a pox-vectored, multiantigen, multistage vaccine candidate for Plasmodium falciparum malaria. J Infect Dis. 1998;177(6):1664-73.

350. Forbes EK, Biswas S, Collins KA, Gilbert SC, Hill AV, Draper SJ. Combining liver- and blood-stage malaria viral-vectored vaccines: investigating mechanisms of CD8+ T cell interference. J Immunol. 2011;187(7):3738-50.

351. Rampling T, Ewer KJ, Bowyer G, Bliss CM, Edwards NJ, Wright D, et al. Safety and High Level Efficacy of the Combination Malaria Vaccine Regimen of RTS,S/AS01B With Chimpanzee Adenovirus 63 and Modified Vaccinia Ankara Vectored Vaccines Expressing ME-TRAP. J Infect Dis. 2016;214(5):772-81.

352. Brod F, Miura K, Taylor I, Li Y, Marini A, Salman AM, et al. Combination of RTS,S and Pfs25-IMX313 Induces a Functional Antibody Response Against Malaria Infection and Transmission in Mice. Front Immunol. 2018;9:2780.

353. Yusuf Y, Yoshii T, Iyori M, Mizukami H, Fukumoto S, Yamamoto DS, et al. A Viral-Vectored Multi-Stage Malaria Vaccine Regimen With Protective and Transmission-Blocking Efficacies. Front Immunol. 2019;10:2412.

354. Florens L, Washburn MP, Raine JD, Anthony RM, Grainger M, Haynes JD, et al. A proteomic view of the Plasmodium falciparum life cycle. Nature. 2002;419(6906):520-6.

355. Gardner MJ, Hall N, Fung E, White O, Berriman M, Hyman RW, et al. Genome sequence of the human malaria parasite Plasmodium falciparum. Nature. 2002;419(6906):498-511.

356. Kyes SA, Kraemer SM, Smith JD. Antigenic variation in Plasmodium falciparum: gene organization and regulation of the var multigene family. Eukaryot Cell. 2007;6(9):1511-20.

357. Singh V, Gupta P, Pande V. Revisiting the multigene families: Plasmodium var and vir genes. J Vector Borne Dis. 2014;51(2):75-81.

358. Kyes S, Christodoulou Z, Pinches R, Kriek N, Horrocks P, Newbold C. Plasmodium falciparum var gene expression is developmentally controlled at the level of RNA polymerase II-mediated transcription initiation. Mol Microbiol. 2007;63(4):1237-47.

359. Preston MD, Assefa SA, Ocholla H, Sutherland CJ, Borrmann S, Nzila A, et al. PlasmoView: a web-based resource to visualise global Plasmodium falciparum genomic variation. J Infect Dis. 2014;209(11):1808-15.

360. Li S, Plebanski M, Smooker P, Gowans EJ. Editorial: Why Vaccines to HIV, HCV, and Malaria Have So Far Failed—Challenges to Developing Vaccines Against Immunoregulating Pathogens. Frontiers in Microbiology. 2015;6:1318.

361. Cunnington AJ, Riley EM. Suppression of vaccine responses by malaria: insignificant or overlooked? Expert Rev Vaccines. 2010;9(4):409-29.

362. Felgner PL, Roestenberg M, Liang L, Hung C, Jain A, Pablo J, et al. Pre-erythrocytic antibody profiles induced by controlled human malaria infections in healthy volunteers under chloroquine prophylaxis. Sci Rep. 2013;3:3549.

363. Cockburn IA, Chen YC, Overstreet MG, Lees JR, van Rooijen N, Farber DL, et al. Prolonged antigen presentation is required for optimal CD8+ T cell responses against malaria liver stage parasites. PLoS Pathog. 2010;6(5):e1000877.

364. Dunachie S, Hill AV, Fletcher HA. Profiling the host response to malaria vaccination and malaria challenge. Vaccine. 2015;33(40):5316-20.

365. Liehl P, Mota MM. Innate recognition of malarial parasites by mammalian hosts. Int J Parasitol. 2012;42(6):557-66.

366. March S, Ng S, Velmurugan S, Galstian A, Shan J, Logan DJ, et al. A microscale human liver platform that supports the hepatic stages of Plasmodium falciparum and vivax. Cell Host Microbe. 2013;14(1):104-15.

367. Cottingham MG, Andersen RF, Spencer AJ, Saurya S, Furze J, Hill AV, et al. Recombination-mediated genetic engineering of a bacterial artificial chromosome clone of modified vaccinia virus Ankara (MVA). PLoS One. 2008;3(2):e1638.

368. Lee JM, Lee HS, Hyun JJ, Lee JM, Yoo IK, Kim SH, et al. Slow-Pull Using a Fanning Technique Is More Useful Than the Standard Suction Technique in EUS-Guided Fine Needle Aspiration in Pancreatic Masses. Gut Liver. 2018;12(3):360-6.

369. Picelli S, Faridani OR, Bjorklund AK, Winberg G, Sagasser S, Sandberg R. Full-length RNA-seq from single cells using Smart-seq2. Nat Protoc. 2014;9(1):171-81.

370. Burnham KP, Anderson DR. Multimodel Inference:Understanding AIC and BIC in Model Selection. Sociological Methods & Research. 2004;33(2):261-304.

371. Ewels P, Magnusson M, Lundin S, Kaller M. MultiQC: summarize analysis results for multiple tools and samples in a single report. Bioinformatics. 2016;32(19):3047-8.

372. Dobin A, Davis CA, Schlesinger F, Drenkow J, Zaleski C, Jha S, et al. STAR: ultrafast universal RNA-seq aligner. Bioinformatics. 2013;29(1):15-21.

373. Liao Y, Smyth GK, Shi W. featureCounts: an efficient general purpose program for assigning sequence reads to genomic features. Bioinformatics. 2014;30(7):923-30.

374. Love MI, Huber W, Anders S. Moderated estimation of fold change and dispersion for RNA-seq data with DESeq2. Genome Biol. 2014;15(12):550.

375. Benjamini Y, Hochberg Y. Controlling the False Discovery Rate: A Practical and Powerful Approach to Multiple Testing. Journal of the Royal Statistical Society Series B (Methodological). 1995;57(1):289-300.

376. Zhu A, Ibrahim JG, Love MI. Heavy-tailed prior distributions for sequence count data: removing the noise and preserving large differences. Bioinformatics. 2019;35(12):2084-92.

377. Ashburner M, Ball CA, Blake JA, Botstein D, Butler H, Cherry JM, et al. Gene ontology: tool for the unification of biology. The Gene Ontology Consortium. Nat Genet. 2000;25(1):25-9.

378. Liberzon A, Birger C, Thorvaldsdottir H, Ghandi M, Mesirov JP, Tamayo P. The Molecular Signatures Database (MSigDB) hallmark gene set collection. Cell Syst. 2015;1(6):417-25.

379. Mootha VK, Lindgren CM, Eriksson KF, Subramanian A, Sihag S, Lehar J, et al. PGC-1alpha-responsive genes involved in oxidative phosphorylation are coordinately downregulated in human diabetes. Nat Genet. 2003;34(3):267-73.

380. Yu G, Wang L-G, Han Y, He Q-Y. clusterProfiler: an R Package for Comparing Biological Themes Among Gene Clusters. OMICS: A Journal of Integrative Biology. 2012;16(5):284-7.

381. Korotkevich G, Sukhov V, Sergushichev A. Fast gene set enrichment analysis. bioRxiv. 2019:060012.

382. Luo W, Brouwer C. Pathview: an R/Bioconductor package for pathway-based data integration and visualization. Bioinformatics. 2013;29(14):1830-1.

383. Amezquita RA, Lun ATL, Becht E, Carey VJ, Carpp LN, Geistlinger L, et al. Orchestrating single-cell analysis with Bioconductor. Nat Methods. 2020;17(2):137-45.

384. Lun AT, McCarthy DJ, Marioni JC. A step-by-step workflow for low-level analysis of single-cell RNA-seq data with Bioconductor. F1000Res. 2016;5:2122.

385. Butler A, Hoffman P, Smibert P, Papalexi E, Satija R. Integrating single-cell transcriptomic data across different conditions, technologies, and species. Nat Biotechnol. 2018;36(5):411-20.

386. Hafemeister C, Satija R. Normalization and variance stabilization of single-cell RNA-seq data using regularized negative binomial regression. Genome Biol. 2019;20(1):296.

387. Waltman L, van Eck NJ. A smart local moving algorithm for large-scale modularity-based community detection. The European Physical Journal B. 2013;86(11):471.

388. McInnes et al., (2018). UMAP: Uniform Manifold Approximation and Projection. Journal of Open Source Software, 3(29), 861.

389. Street K, Risso D, Fletcher RB, Das D, Ngai J, Yosef N, et al. Slingshot: cell lineage and pseudotime inference for single-cell transcriptomics. BMC Genomics. 2018;19(1):477.

390. Pont F, Tosolini M, Fournie JJ. Single-Cell Signature Explorer for comprehensive visualization of single cell signatures across scRNA-seq datasets. Nucleic Acids Res. 2019;47(21):e133.

391. Stubbington MJT, Lonnberg T, Proserpio V, Clare S, Speak AO, Dougan G, et al. T cell fate and clonality inference from single-cell transcriptomes. Nat Methods. 2016;13(4):329-32.

392. Langmead B, Salzberg SL. Fast gapped-read alignment with Bowtie 2. Nat Methods. 2012;9(4):357-9.

393. Grabherr MG, Haas BJ, Yassour M, Levin JZ, Thompson DA, Amit I, et al. Full-length transcriptome assembly from RNA-Seq data without a reference genome. Nat Biotechnol. 2011;29(7):644-52.

394. Ye J, Ma N, Madden TL, Ostell JM. IgBLAST: an immunoglobulin variable domain sequence analysis tool. Nucleic Acids Res. 2013;41(Web Server issue):W34-40.

395. Bray NL, Pimentel H, Melsted P, Pachter L. Near-optimal probabilistic RNA-seq quantification. Nat Biotechnol. 2016;34(5):525-7.

396. Garner LC, Klenerman P, Provine NM. Insights Into Mucosal-Associated Invariant T Cell Biology From Studies of Invariant Natural Killer T Cells. Front Immunol. 2018;9:1478.

397. Kim D, Langmead B, Salzberg SL. HISAT: a fast spliced aligner with low memory requirements. Nat Methods. 2015;12(4):357-60.

398. Li H, Handsaker B, Wysoker A, Fennell T, Ruan J, Homer N, et al. The Sequence Alignment/Map format and SAMtools. Bioinformatics. 2009;25(16):2078-9.

399. Szabo PA, Miron M, Farber DL. Location, location, location: Tissue resident memory T cells in mice and humans. Sci Immunol. 2019;4(34).

400. Fonseca R, Beura LK, Quarnstrom CF, Ghoneim HE, Fan Y, Zebley CC, et al. Developmental plasticity allows outside-in immune responses by resident memory T cells. Nat Immunol. 2020;21(4):412-21.

401. Behr FM, Parga-Vidal L, Kragten NAM, van Dam TJP, Wesselink TH, Sheridan BS, et al. Tissue-resident memory CD8(+) T cells shape local and systemic secondary T cell responses. Nat Immunol. 2020.

402. Low JS, Farsakoglu Y, Amezcua Vesely MC, Sefik E, Kelly JB, Harman CCD, et al. Tissue-resident memory T cell reactivation by diverse antigen-presenting cells imparts distinct functional responses. J Exp Med. 2020;217(8).

403. Epstein JE, Tewari K, Lyke KE, Sim BKL, Billingsley PF, Laurens MB, et al. Live Attenuated Malaria Vaccine Designed to Protect Through Hepatic CD8⁺ T Cell Immunity. Science. 2011;334(6055):475-80.

404. Holz LE, Prier JE, Freestone D, Steiner TM, English K, Johnson DN, et al. CD8(+) T Cell Activation Leads to Constitutive Formation of Liver Tissue-Resident Memory T Cells that Seed a Large and Flexible Niche in the Liver. Cell Rep. 2018;25(1):68-79 e4.

405. Tatsis N, Fitzgerald JC, Reyes-Sandoval A, Harris-McCoy KC, Hensley SE, Zhou D, et al. Adenoviral vectors persist in vivo and maintain activated CD8+ T cells: implications for their use as vaccines. Blood. 2007;110(6):1916-23.

406. Finn JD, Bassett J, Millar JB, Grinshtein N, Yang TC, Parsons R, et al. Persistence of transgene expression influences CD8+ T-cell expansion and maintenance following immunization with recombinant adenovirus. J Virol. 2009;83(23):12027-36.

407. Behr FM, Beumer-Chuwonpad A, Kragten NAM, Wesselink TH, Stark R, van Gisbergen K. Circulating memory CD8(+) T cells are limited in forming CD103(+) tissue-resident memory T cells at mucosal sites after reinfection. Eur J Immunol. 2020.

408. Beura LK, Wijeyesinghe S, Thompson EA, Macchietto MG, Rosato PC, Pierson MJ, et al. T Cells in Nonlymphoid Tissues Give Rise to Lymph-Node-Resident Memory T Cells. Immunity. 2018;48(2):327-38 e5.

409. Klicznik MM, Morawski PA, Hollbacher B, Varkhande SR, Motley SJ, Kuri-Cervantes L, et al. Human CD4(+)CD103(+) cutaneous resident memory T cells are found in the circulation of healthy individuals. Sci Immunol. 2019;4(37).

410. Milner JJ, Toma C, He Z, Kurd NS, Nguyen QP, McDonald B, et al. Heterogenous Populations of Tissue-Resident CD8(+) T Cells Are Generated in Response to Infection and Malignancy. Immunity. 2020;52(5):808-24 e7.

411. Kurd NS, He Z, Louis TL, Milner JJ, Omilusik KD, Jin W, et al. Early precursors and molecular determinants of tissue-resident memory CD8(+) T lymphocytes revealed by single-cell RNA sequencing. Sci Immunol. 2020;5(47).

412. Kok L, Dijkgraaf FE, Urbanus J, Bresser K, Vredevoogd DW, Cardoso RF, et al. A committed tissue-resident memory T cell precursor within the circulating CD8+ effector T cell pool. J Exp Med. 2020;217(10).

413. Spencer AJ, Longley RJ, Gola A, Ulaszewska M, Lambe T, Hill AV. The Threshold of Protection from Liver-Stage Malaria Relies on a Fine Balance between the Number of Infected Hepatocytes and Effector CD8(+) T Cells Present in the Liver. J Immunol. 2017;198(5):2006-16.

414. Ganesan LP, Mohanty S, Kim J, Clark KR, Robinson JM, Anderson CL. Rapid and efficient clearance of blood-borne virus by liver sinusoidal endothelium. PLoS Pathog. 2011;7(9):e1002281.

415. Krueger PD, Kim TS, Sung SS, Braciale TJ, Hahn YS. Liver-resident CD103+ dendritic cells prime antiviral CD8+ T cells in situ. J Immunol. 2015;194(7):3213-22.

416. Coughlan L. Factors Which Contribute to the Immunogenicity of Non-replicating Adenoviral Vectored Vaccines. Front Immunol. 2020;11:909.

417. Morris MA, Gibb DR, Picard F, Brinkmann V, Straume M, Ley K. Transient T cell accumulation in lymph nodes and sustained lymphopenia in mice treated with FTY720. Eur J Immunol. 2005;35(12):3570-80.

418. Hofmann M, Brinkmann V, Zerwes HG. FTY720 preferentially depletes naive T cells from peripheral and lymphoid organs. Int Immunopharmacol. 2006;6(13-14):1902-10.

419. Obar JJ, Lefrancois L. Early events governing memory CD8+ T-cell differentiation. Int Immunol. 2010;22(8):619-25.

420. Parga-Vidal L, van Gisbergen K. Area under Immunosurveillance: Dedicated Roles of Memory CD8 T-Cell Subsets. Cold Spring Harb Perspect Biol. 2020.

421. Behr FM, Chuwonpad A, Stark R, van Gisbergen KPJM. Armed and Ready: Transcriptional Regulation of Tissue-Resident Memory CD8 T Cells. Frontiers in immunology. 2018;9:1770-.

422. Mueller SN, Mackay LK. Tissue-resident memory T cells: local specialists in immune defence. Nature Reviews Immunology. 2016;16(2):79-89.

423. Frank R, Gabel M, Heiss K, Mueller A-K, Graw F. Varying Immunizations With Plasmodium Radiation-Attenuated Sporozoites Alter Tissue-Specific CD8(+) T Cell Dynamics. Frontiers in immunology. 2018;9:1137-.

424. Frizzell H, Fonseca R, Christo SN, Evrard M, Cruz-Gomez S, Zanluqui NG, et al. Organ-specific isoform selection of fatty acid-binding proteins in tissue-resident lymphocytes. Sci Immunol. 2020;5(46).

425. Provine NM, Amini A, Garner LC, Spencer AJ, Dold C, Hutchings C, et al. MAIT cell activation augments adenovirus vector vaccine immunogenicity. Science. 2021;371(6528):521-6.

426. Walsh DA, Borges da Silva H, Beura LK, Peng C, Hamilton SE, Masopust D, et al. The Functional Requirement for CD69 in Establishment of Resident Memory CD8(+) T Cells Varies with Tissue Location. J Immunol. 2019;203(4):946-55.

427. Sung CC, Horng JH, Siao SH, Chyuan IT, Tsai HF, Chen PJ, et al. Asialo GM1-positive liver-resident CD8 T cells that express CD44 and LFA-1 are essential for immune clearance of hepatitis B virus. Cell Mol Immunol. 2020.

428. Wein AN, McMaster SR, Takamura S, Dunbar PR, Cartwright EK, Hayward SL, et al. CXCR6 regulates localization of tissue-resident memory CD8 T cells to the airways. J Exp Med. 2019;216(12):2748-62.

429. Pan Y, Tian T, Park CO, Lofftus SY, Mei S, Liu X, et al. Survival of tissue-resident memory T cells requires exogenous lipid uptake and metabolism. Nature. 2017;543(7644):252-6.

430. Lieber A, He CY, Meuse L, Schowalter D, Kirillova I, Winther B, et al. The role of Kupffer cell activation and viral gene expression in early liver toxicity after infusion of recombinant adenovirus vectors. J Virol. 1997;71(11):8798-807.

431. Halpern KB, Shenhav R, Massalha H, Toth B, Egozi A, Massasa EE, et al. Paired-cell sequencing enables spatial gene expression mapping of liver endothelial cells. Nature biotechnology. 2018;36(10):962-70.

432. Xiong X, Kuang H, Ansari S, Liu T, Gong J, Wang S, et al. Landscape of Intercellular Crosstalk in Healthy and NASH Liver Revealed by Single-Cell Secretome Gene Analysis. Molecular cell. 2019;75(3):644-60.e5.

433. van Loosdregt J, Coffer PJ. The Role of WNT Signaling in Mature T Cells: T Cell Factor Is Coming Home. J Immunol. 2018;201(8):2193-200.

434. Bergsbaken T, Bevan MJ, Fink PJ. Local Inflammatory Cues Regulate Differentiation and Persistence of CD8(+) Tissue-Resident Memory T Cells. Cell reports. 2017;19(1):114-24.

435. Mavrommatis E, Fish EN, Platanias LC. The schlafen family of proteins and their regulation by interferons. J Interferon Cytokine Res. 2013;33(4):206-10.

436. Wu H, Rodgers JR, Perrard X-YD, Perrard JL, Prince JE, Abe Y, et al. Deficiency of CD11b or CD11d Results in Reduced Staphylococcal Enterotoxin-Induced T Cell Response and T Cell Phenotypic Changes. The Journal of Immunology. 2004;173(1):297-306.

437. Pearce EL, Mullen AC, Martins GA, Krawczyk CM, Hutchins AS, Zediak VP, et al. Control of effector CD8+ T cell function by the transcription factor Eomesodermin. Science. 2003;302(5647):1041-3.

438. Fuchs YF, Sharma V, Eugster A, Kraus G, Morgenstern R, Dahl A, et al. Gene Expression-Based Identification of Antigen-Responsive CD8+ T Cells on a Single-Cell Level. Frontiers in Immunology. 2019;10(2568).

439. Van Braeckel-Budimir N, Varga SM, Badovinac VP, Harty JT. Repeated Antigen Exposure Extends the Durability of Influenza-Specific Lung-Resident Memory CD8(+) T Cells and Heterosubtypic Immunity. Cell Rep. 2018;24(13):3374-82 e3.

440. Abbas AK, Lichtman AH, Pillai S. Cellular and molecular immunology. 2018.

441. Baaten B, Tinoco R, Chen A, Bradley L. Regulation of Antigen-Experienced T Cells: Lessons from the Quintessential Memory Marker CD44. Frontiers in Immunology. 2012;3(23).

442. Ewer KJ, Lambe T, Rollier CS, Spencer AJ, Hill AV, Dorrell L. Viral vectors as vaccine platforms: from immunogenicity to impact. Curr Opin Immunol. 2016;41:47-54.

443. Szabo PA, Levitin HM, Miron M, Snyder ME, Senda T, Yuan J, et al. Single-cell transcriptomics of human T cells reveals tissue and activation signatures in health and disease. Nat Commun. 2019;10(1):4706.

444. FitzPatrick MEB, Provine NM, Garner LC, Powell K, Amini A, Irwin SL, et al. Human intestinal tissue-resident memory T cells comprise transcriptionally and functionally distinct subsets. Cell Rep. 2021;34(3):108661.

445. Zhao J, Zhang S, Liu Y, He X, Qu M, Xu G, et al. Single-cell RNA sequencing reveals the heterogeneity of liver-resident immune cells in human. Cell Discov. 2020;6:22.

446. Sprengers D, van der Molen RG, Kusters JG, Kwekkeboom J, van der Laan LJ, Niesters HG, et al. Flow cytometry of fine-needle-aspiration biopsies: a new method to monitor the intrahepatic immunological environment in chronic viral hepatitis. J Viral Hepat. 2005;12(5):507-12.

447. Sims S, Willberg C, Klenerman P. MHC-peptide tetramers for the analysis of antigen-specific T cells. Expert Rev Vaccines. 2010;9(7):765-74.

448. Kurup SP, Butler NS, Harty JT. T cell-mediated immunity to malaria. Nat Rev Immunol. 2019;19(7):457-71.

449. Van Braeckel-Budimir N, Gras S, Ladell K, Josephs TM, Pewe L, Urban SL, et al. A T Cell Receptor Locus Harbors a Malaria-Specific Immune Response Gene. Immunity. 2017;47(5):835-47 e4.

450. Fergusson JR, Smith KE, Fleming VM, Rajoriya N, Newell EW, Simmons R, et al. CD161 defines a transcriptional and functional phenotype across distinct human T cell lineages. Cell Rep. 2014;9(3):1075-88.

451. Fergusson JR, Huhn MH, Swadling L, Walker LJ, Kurioka A, Llibre A, et al. CD161(int)CD8+ T cells: a novel population of highly functional, memory CD8+ T cells enriched within the gut. Mucosal Immunol. 2016;9(2):401-13.

452. Schuldt NJ, Binstadt BA. Dual TCR T Cells: Identity Crisis or Multitaskers? J Immunol. 2019;202(3):637-44.

453. Miao Z, Deng K, Wang X, Zhang X. DEsingle for detecting three types of differential expression in single-cell RNA-seq data. Bioinformatics. 2018;34(18):3223-4.

454. Gonzalez-Sanchez E, Vaquero J, Fouassier L, Chignard N. E-cadherin, guardian of liver physiology. Clin Res Hepatol Gastroenterol. 2015;39(1):3-6.

455. Seo H, Chen J, Gonzalez-Avalos E, Samaniego-Castruita D, Das A, Wang YH, et al. TOX and TOX2 transcription factors cooperate with NR4A transcription factors to impose CD8(+) T cell exhaustion. Proc Natl Acad Sci U S A. 2019;116(25):12410-5.

456. Miyagawa F, Zhang H, Terunuma A, Ozato K, Tagaya Y, Katz SI. Interferon regulatory factor 8 integrates T-cell receptor and cytokine-signaling pathways and drives effector differentiation of CD8 T cells. Proc Natl Acad Sci U S A. 2012;109(30):12123-8.

457. Saoudi A, Kassem S, Dejean A, Gaud G. Rho-GTPases as key regulators of T lymphocyte biology. Small GTPases. 2014;5.

458. Kaur S, Kuznetsova SA, Pendrak ML, Sipes JM, Romeo MJ, Li Z, et al. Heparan sulfate modification of the transmembrane receptor CD47 is necessary for inhibition of T cell receptor signaling by thrombospondin-1. J Biol Chem. 2011;286(17):14991-5002.

459. Simon Davis DA, Parish CR. Heparan sulfate: a ubiquitous glycosaminoglycan with multiple roles in immunity. Front Immunol. 2013;4:470.

460. Cibrian D, Sanchez-Madrid F. CD69: from activation marker to metabolic gatekeeper. Eur J Immunol. 2017;47(6):946-53.

461. Takamura S, Yagi H, Hakata Y, Motozono C, McMaster SR, Masumoto T, et al. Specific niches for lung-resident memory CD8+ T cells at the site of tissue regeneration enable CD69-independent maintenance. J Exp Med. 2016;213(13):3057-73.

462. Schenkel JM, Fraser KA, Masopust D. Cutting edge: resident memory CD8 T cells occupy frontline niches in secondary lymphoid organs. J Immunol. 2014;192(7):2961-4.

463. Clarke J, Panwar B, Madrigal A, Singh D, Gujar R, Wood O, et al. Single-cell transcriptomic analysis of tissue-resident memory T cells in human lung cancer. J Exp Med. 2019;216(9):2128-49.

464. Joshi NS, Cui W, Chandele A, Lee HK, Urso DR, Hagman J, et al. Inflammation directs memory precursor and short-lived effector CD8(+) T cell fates via the graded expression of T-bet transcription factor. Immunity. 2007;27(2):281-95.

465. Lepore M, Kalinichenko A, Colone A, Paleja B, Singhal A, Tschumi A, et al. Parallel T-cell cloning and deep sequencing of human MAIT cells reveal stable oligoclonal TCRbeta repertoire. Nat Commun. 2014;5:3866.

466. Carnero Contentti E, Farez MF, Correale J. Mucosal-Associated Invariant T Cell Features and TCR Repertoire Characteristics During the Course of Multiple Sclerosis. Front Immunol. 2019;10:2690.

467. Liaskou E, Klemsdal Henriksen EK, Holm K, Kaveh F, Hamm D, Fear J, et al. High-throughput T-cell receptor sequencing across chronic liver diseases reveals distinct disease-associated repertoires. Hepatology. 2016;63(5):1608-19.

468. Pogorelyy MV, Minervina AA, Touzel MP, Sycheva AL, Komech EA, Kovalenko EI, et al. Precise tracking of vaccine-responding T cell clones reveals convergent and personalized response in identical twins. Proc Natl Acad Sci U S A. 2018;115(50):12704-9.

469. Cano-Gamez E, Soskic B, Roumeliotis TI, So E, Smyth DJ, Baldrighi M, et al. Single-cell transcriptomics identifies an effectorness gradient shaping the response of CD4(+) T cells to cytokines. Nat Commun. 2020;11(1):1801.

470. Ge C, Monk IR, Pizzolla A, Wang N, Bedford JG, Stinear TP, et al. Bystander Activation of Pulmonary Trm Cells Attenuates the Severity of Bacterial Pneumonia by Enhancing Neutrophil Recruitment. Cell Rep. 2019;29(13):4236-44 e3.

471. Suliman S, Murphy M, Musvosvi M, Gela A, Meermeier EW, Geldenhuys H, et al. MR1-Independent Activation of Human Mucosal-Associated Invariant T Cells by Mycobacteria. J Immunol. 2019;203(11):2917-27.

472. Schmaler M, Orlova-Fink N, Rutishauser T, Abdulla S, Daubenberger C. Human unconventional T cells in Plasmodium falciparum infection. Semin Immunopathol. 2020;42(3):265-77.

473. Keating C. The history of the RTS,S/AS01 malaria vaccine trial. Lancet. 2020;395(10233):1336-7.

474. Thakur A, Pedersen LE, Jungersen G. Immune markers and correlates of protection for vaccine induced immune responses. Vaccine. 2012;30(33):4907-20.

475. Plotkin SA. Vaccines: correlates of vaccine-induced immunity. Clin Infect Dis. 2008;47(3):401-9.

476. Plotkin SA. Updates on immunologic correlates of vaccine-induced protection. Vaccine. 2020;38(9):2250-7.

477. Seder RA, Darrah PA, Roederer M. T-cell quality in memory and protection: implications for vaccine design. Nat Rev Immunol. 2008;8(4):247-58.

478. Bejon P, Mwacharo J, Kai O, Mwangi T, Milligan P, Todryk S, et al. A phase 2b randomised trial of the candidate malaria vaccines FP9 ME-TRAP and MVA ME-TRAP among children in Kenya. PLoS Clin Trials. 2006;1(6):e29.

479. Stanisic DI, McCarthy JS, Good MF. Controlled Human Malaria Infection: Applications, Advances, and Challenges. Infect Immun. 2018;86(1).

480. Mensah VA, Gueye A, Ndiaye M, Edwards NJ, Wright D, Anagnostou NA, et al. Safety, Immunogenicity and Efficacy of Prime-Boost Vaccination with ChAd63 and MVA Encoding ME-TRAP against Plasmodium falciparum Infection in Adults in Senegal. PLoS One. 2016;11(12):e0167951.

481. Woodberry T, Minigo G, Piera KA, Amante FH, Pinzon-Charry A, Good MF, et al. Low-level Plasmodium falciparum blood-stage infection causes dendritic cell apoptosis and dysfunction in healthy volunteers. J Infect Dis. 2012;206(3):333-40.

482. Hodgson SH, Llewellyn D, Silk SE, Milne KH, Elias SC, Miura K, et al. Changes in Serological Immunology Measures in UK and Kenyan Adults Post-controlled Human Malaria Infection. Front Microbiol. 2016;7:1604.

483. Duncan CJ, Sheehy SH, Ewer KJ, Douglas AD, Collins KA, Halstead FD, et al. Impact on malaria parasite multiplication rates in infected volunteers of the protein-in-adjuvant vaccine AMA1-C1/Alhydrogel+CPG 7909. PLoS One. 2011;6(7):e22271.

484. Burel JG, Apte SH, Groves PL, Klein K, McCarthy JS, Doolan DL. Reduced Plasmodium Parasite Burden Associates with CD38+ CD4+ T Cells Displaying Cytolytic Potential and Impaired IFN-gamma Production. PLoS Pathog. 2016;12(9):e1005839.

485. Bejon P, Andrews L, Andersen RF, Dunachie S, Webster D, Walther M, et al. Calculation of liver-to-blood inocula, parasite growth rates, and preerythrocytic vaccine efficacy, from serial quantitative polymerase chain reaction studies of volunteers challenged with malaria sporozoites. J Infect Dis. 2005;191(4):619-26.

486. Witney AA, Doolan DL, Anthony RM, Weiss WR, Hoffman SL, Carucci DJ. Determining liver stage parasite burden by real time quantitative PCR as a method for evaluating pre-erythrocytic malaria vaccine efficacy. Molecular and Biochemical Parasitology. 2001;118(2):233-45.

487. Murphy SC, Hermsen CC, Douglas AD, Edwards NJ, Petersen I, Fahle GA, et al. External quality assurance of malaria nucleic acid testing for clinical trials and eradication surveillance. PLoS One. 2014;9(5):e97398.

488. Laurens MB, Duncan CJ, Epstein JE, Hill AV, Komisar JL, Lyke KE, et al. A consultation on the optimization of controlled human malaria infection by mosquito bite for evaluation of candidate malaria vaccines. Vaccine. 2012;30(36):5302-4.

489. Qualai J, Li LX, Cantero J, Tarrats A, Fernandez MA, Sumoy L, et al. Expression of CD11c Is Associated with Unconventional Activated T Cell Subsets with High Migratory Potential. PLoS One. 2016;11(4):e0154253.

490. Saez de Guinoa J, Jimeno R, Gaya M, Kipling D, Garzon MJ, Dunn-Walters D, et al. CD1d-mediated lipid presentation by CD11c(+) cells regulates intestinal homeostasis. EMBO J. 2018;37(5).

491. Benjamini Y, Krieger AM, Yekutieli D. Adaptive linear step-up procedures that control the false discovery rate. Biometrika. 2006;93(3):491-507.

492. Flaxman A, Ewer KJ. Methods for Measuring T-Cell Memory to Vaccination: From Mouse to Man. Vaccines (Basel). 2018;6(3).

493. Jeffrey J. Walline. Designing Clinical Research: an Epidemiologic Approach, 2nd Ed. Optometry and Vision Science. 2001;78(8):560.

494. Sauerwein RW, Roestenberg M, Moorthy VS. Experimental human challenge infections can accelerate clinical malaria vaccine development. Nat Rev Immunol. 2011;11(1):57-64.

495. Zwiener I, Blettner M, Hommel G. Survival analysis: part 15 of a series on evaluation of scientific publications. Dtsch Arztebl Int. 2011;108(10):163-9.

496. Vatcheva KP, Lee M, McCormick JB, Rahbar MH. Multicollinearity in Regression Analyses Conducted in Epidemiologic Studies. Epidemiology (Sunnyvale, Calif). 2016;6(2):227.

497. Harrell FE, Jr., Lee KL, Mark DB. Multivariable prognostic models: issues in developing models, evaluating assumptions and adequacy, and measuring and reducing errors. Stat Med. 1996;15(4):361-87.

498. Reichert T, DeBruyère M, Deneys V, Tötterman T, Lydyard P, Yuksel F, et al. Lymphocyte subset reference ranges in adult caucasians. Clinical Immunology and Immunopathology. 1991;60(2):190-208.

499. Bofill M, Janossy G, Lee CA, MacDonald-Burns D, Phillips AN, Sabin C, et al. Laboratory control values for CD4 and CD8 T lymphocytes. Implications for HIV-1 diagnosis. Clin Exp Immunol. 1992;88(2):243-52.

500. McCall MBB, Kremsner PG, Mordmuller B. Correlating efficacy and immunogenicity in malaria vaccine trials. Semin Immunol. 2018;39:52-64.

501. Bowyer G, Rampling T, Powlson J, Morter R, Wright D, Hill AVS, et al. Activation-induced Markers Detect Vaccine-Specific CD4(+) T Cell Responses Not Measured by Assays Conventionally Used in Clinical Trials. Vaccines (Basel). 2018;6(3).

502. Lefebvre MN, Harty JT. You Shall Not Pass: Memory CD8 T Cells in Liver-Stage Malaria. Trends Parasitol. 2020;36(2):147-57.

503. Tao N, Gao GP, Parr M, Johnston J, Baradet T, Wilson JM, et al. Sequestration of adenoviral vector by Kupffer cells leads to a nonlinear dose response of transduction in liver. Mol Ther. 2001;3(1):28-35.

504. Jaffe HA, Danel C, Longenecker G, Metzger M, Setoguchi Y, Rosenfeld MA, et al. Adenovirus-mediated in vivo gene transfer and expression in normal rat liver. Nat Genet. 1992;1(5):372-8.

505. Kalyuzhniy O, Di Paolo NC, Silvestry M, Hofherr SE, Barry MA, Stewart PL, et al. Adenovirus serotype 5 hexon is critical for virus infection of hepatocytes in vivo. Proc Natl Acad Sci U S A. 2008;105(14):5483-8.

506. Holst PJ, Orskov C, Thomsen AR, Christensen JP. Quality of the transgene-specific CD8+ T cell response induced by adenoviral vector immunization is critically influenced by virus dose and route of vaccination. J Immunol. 2010;184(8):4431-9.

507. Kaufman DR, Bivas-Benita M, Simmons NL, Miller D, Barouch DH. Route of adenovirus-based HIV-1 vaccine delivery impacts the phenotype and trafficking of vaccine-elicited CD8+ T lymphocytes. J Virol. 2010;84(12):5986-96.

508. Wilck MB, Seaman MS, Baden LR, Walsh SR, Grandpre LE, Devoy C, et al. Safety and immunogenicity of modified vaccinia Ankara (ACAM3000): effect of dose and route of administration. J Infect Dis. 2010;201(9):1361-70.

509. Worgall S, Wolff G, Falck-Pedersen E, Crystal RG. Innate immune mechanisms dominate elimination of adenoviral vectors following in vivo administration. Hum Gene Ther. 1997;8(1):37-44.

510. Waddington SN, McVey JH, Bhella D, Parker AL, Barker K, Atoda H, et al. Adenovirus serotype 5 hexon mediates liver gene transfer. Cell. 2008;132(3):397-409.

511. Schiedner G, Bloch W, Hertel S, Johnston M, Molojavyi A, Dries V, et al. A hemodynamic response to intravenous adenovirus vector particles is caused by systemic Kupffer cell-mediated activation of endothelial cells. Hum Gene Ther. 2003;14(17):1631-41.

512. Steinhardt LC, Richie TL, Yego R, Akach D, Hamel MJ, Gutman JR, et al. Safety, Tolerability, and Immunogenicity of Plasmodium falciparum Sporozoite Vaccine Administered by Direct Venous Inoculation to Infants and Young Children: Findings From an Age De-escalation, Dose-Escalation, Double-blind, Randomized Controlled Study in Western Kenya. Clin Infect Dis. 2020;71(4):1063-71.

513. Brandes M, Willimann K, Moser B. Professional antigen-presentation function by human gammadelta T Cells. Science. 2005;309(5732):264-8.

514. Vomhof-DeKrey EE, Yates J, Leadbetter EA. Invariant NKT cells provide innate and adaptive help for B cells. Curr Opin Immunol. 2014;28:12-7.

515. Gottschalk C, Mettke E, Kurts C. The Role of Invariant Natural Killer T Cells in Dendritic Cell Licensing, Cross-Priming, and Memory CD8(+) T Cell Generation. Front Immunol. 2015;6:379.

516. Brandes M, Willimann K, Bioley G, Levy N, Eberl M, Luo M, et al. Cross-presenting human gammadelta T cells induce robust CD8+ alphabeta T cell responses. Proc Natl Acad Sci U S A. 2009;106(7):2307-12.

517. Hinks TSC, Zhang XW. MAIT Cell Activation and Functions. Front Immunol. 2020;11:1014.

518. Brigl M, Brenner MB. How invariant natural killer T cells respond to infection by recognizing microbial or endogenous lipid antigens. Semin Immunol. 2010;22(2):79-86.

519. Tsuji M, Mombaerts P, Lefrancois L, Nussenzweig RS, Zavala F, Tonegawa S. Gamma delta T cells contribute to immunity against the liver stages of malaria in alpha beta T-cell-deficient mice. Proc Natl Acad Sci U S A. 1994;91(1):345-9.

520. Teirlinck AC, McCall MB, Roestenberg M, Scholzen A, Woestenenk R, de Mast Q, et al. Longevity and composition of cellular immune responses following experimental Plasmodium falciparum malaria infection in humans. PLoS Pathog. 2011;7(12):e1002389.

521. Voillet V, Buggert M, Slichter CK, Berkson JD, Mair F, Addison MM, et al. Human MAIT cells exit peripheral tissues and recirculate via lymph in steady state conditions. JCI Insight. 2018;3(7).

522. Warimwe GM, Fletcher HA, Olotu A, Agnandji ST, Hill AV, Marsh K, et al. Peripheral blood monocyte-to-lymphocyte ratio at study enrollment predicts efficacy of the RTS,S malaria vaccine: analysis of pooled phase II clinical trial data. BMC Med. 2013;11:184.

523. Osborn JF, Hobbs SJ, Mooster JL, Khan TN, Kilgore AM, Harbour JC, et al. Central memory CD8+ T cells become CD69+ tissue-residents during viral skin infection independent of CD62L-mediated lymph node surveillance. PLoS Pathog. 2019;15(3):e1007633.

524. Park SL, Zaid A, Hor JL, Christo SN, Prier JE, Davies B, et al. Local proliferation maintains a stable pool of tissue-resident memory T cells after antiviral recall responses. Nat Immunol. 2018;19(2):183-91.

525. Nguipdop Djomo P, Thomas SL, Fine PEM, Innitiative for Vaccine Research. Correlates of vaccine-induced protection: methods and implications. Geneva: WHO; 2013. Report No.: WHO/IVB/13.01.

526. Capone S, Brown A, Hartnell F, Sorbo MD, Traboni C, Vassilev V, et al. Optimising T cell (re)boosting strategies for adenoviral and modified vaccinia Ankara vaccine regimens in humans. NPJ Vaccines. 2020;5:94.

527. Wonganan P, Clemens CC, Brasky K, Pastore L, Croyle MA. Species differences in the pharmacology and toxicology of PEGylated helper-dependent adenovirus. Mol Pharm. 2011;8(1):78-92.

528. Chen J, Zajac AJ, McPherson SA, Hsu HC, Yang P, Wu Q, et al. Primary adenovirus-specific cytotoxic T lymphocyte response occurs after viral clearance and liver enzyme elevation. Gene Ther. 2005;12(13):1079-88.

529. Jagannathan P, Lutwama F, Boyle MJ, Nankya F, Farrington LA, McIntyre TI, et al. Vdelta2+ T cell response to malaria correlates with protection from infection but is attenuated with repeated exposure. Sci Rep. 2017;7(1):11487.

530. Moris P, Jongert E, van der Most RG. Characterization of T-cell immune responses in clinical trials of the candidate RTS,S malaria vaccine. Hum Vaccin Immunother. 2018;14(1):17-27.

531. Milner JJ, Nguyen H, Omilusik K, Reina-Campos M, Tsai M, Toma C, et al. Delineation of a molecularly distinct terminally differentiated memory CD8 T cell population. Proc Natl Acad Sci U S A. 2020;117(41):25667-78.

532. Newell EW, Sigal N, Bendall SC, Nolan GP, Davis MM. Cytometry by time-of-flight shows combinatorial cytokine expression and virus-specific cell niches within a continuum of CD8+ T cell phenotypes. Immunity. 2012;36(1):142-52.

533. Waickman AT, Victor K, Li T, Hatch K, Rutvisuttinunt W, Medin C, et al. Dissecting the heterogeneity of DENV vaccine-elicited cellular immunity using single-cell RNA sequencing and metabolic profiling. Nat Commun. 2019;10(1):3666.

534. Kimani D, Jagne YJ, Cox M, Kimani E, Bliss CM, Gitau E, et al. Translating the immunogenicity of prime-boost immunization with ChAd63 and MVA ME-TRAP from malaria naive to malaria-endemic populations. Mol Ther. 2014;22(11):1992-2003.

535. Masopust D, Choo D, Vezys V, Wherry EJ, Duraiswamy J, Akondy R, et al. Dynamic T cell migration program provides resident memory within intestinal epithelium. J Exp Med. 2010;207(3):553-64.

536. Woodland DL, Kohlmeier JE. Migration, maintenance and recall of memory T cells in peripheral tissues. Nat Rev Immunol. 2009;9(3):153-61.

537. Hofmann M, Pircher H. E-cadherin promotes accumulation of a unique memory CD8 T-cell population in murine salivary glands. Proc Natl Acad Sci U S A. 2011;108(40):16741-6.

538. Masopust D, Vezys V, Usherwood EJ, Cauley LS, Olson S, Marzo AL, et al. Activated primary and memory CD8 T cells migrate to nonlymphoid tissues regardless of site of activation or tissue of origin. J Immunol. 2004;172(8):4875-82.

539. Kadoki M, Patil A, Thaiss CC, Brooks DJ, Pandey S, Deep D, et al. Organism-Level Analysis of Vaccination Reveals Networks of Protection across Tissues. Cell. 2017;171(2):398-413 e21.

540. Nath AP, Braun A, Ritchie SC, Carbone FR, Mackay LK, Gebhardt T, et al. Comparative analysis reveals a role for TGF-beta in shaping the residency-related transcriptional signature in tissue-resident memory CD8+ T cells. PLoS One. 2019;14(2):e0210495.

541. Schenkel JM, Fraser KA, Vezys V, Masopust D. Sensing and alarm function of resident memory CD8(+) T cells. Nat Immunol. 2013;14(5):509-13.

542. Mercier S, Gahery-Segard H, Monteil M, Lengagne R, Guillet JG, Eloit M, et al. Distinct roles of adenovirus vector-transduced dendritic cells, myoblasts, and endothelial cells in mediating an immune response against a transgene product. J Virol. 2002;76(6):2899-911.

543. Quinn KM, Zak DE, Costa A, Yamamoto A, Kastenmuller K, Hill BJ, et al. Antigen expression determines adenoviral vaccine potency independent of IFN and STING signaling. J Clin Invest. 2015;125(3):1129-46.

544. Lau LS, Fernandez-Ruiz D, Mollard V, Sturm A, Neller MA, Cozijnsen A, et al. CD8+ T cells from a novel T cell receptor transgenic mouse induce liver-stage immunity that can be boosted by blood-stage infection in rodent malaria. PLoS Pathog. 2014;10(5):e1004135.

545. Dudda JC, Simon JC, Martin S. Dendritic cell immunization route determines CD8+ T cell trafficking to inflamed skin: role for tissue microenvironment and dendritic cells in establishment of T cell-homing subsets. J Immunol. 2004;172(2):857-63.

546. Mani V, Bromley SK, Aijo T, Mora-Buch R, Carrizosa E, Warner RD, et al. Migratory DCs activate TGF-beta to precondition naive CD8(+) T cells for tissue-resident memory fate. Science. 2019;366(6462).

547. Di Paolo NC, Miao EA, Iwakura Y, Murali-Krishna K, Aderem A, Flavell RA, et al. Virus binding to a plasma membrane receptor triggers interleukin-1 alpha-mediated proinflammatory macrophage response in vivo. Immunity. 2009;31(1):110-21.

548. Anders HJ. Of Inflammasomes and Alarmins: IL-1beta and IL-1alpha in Kidney Disease. J Am Soc Nephrol. 2016;27(9):2564-75.

549. Smith JS, Xu Z, Tian J, Stevenson SC, Byrnes AP. Interaction of systemically delivered adenovirus vectors with Kupffer cells in mouse liver. Hum Gene Ther. 2008;19(5):547-54.

550. Yang Y, Ertl HCJ, Wilson JM. MHC class I-cestricted cytotoxic T lymphocytes to viral antigens destroy hepatocytes in mice infected with E1-deleted recombinant adenoviruses. Immunity. 1994;1(5):433-42.

551. Atasheva S, Yao J, Shayakhmetov DM. Innate immunity to adenovirus: lessons from mice. FEBS Lett. 2019;593(24):3461-83.

552. McNamara HA, Cockburn IA. The three Rs: Recruitment, Retention and Residence of leukocytes in the liver. Clin Transl Immunology. 2016;5(12):e123.

553. Uhlen M, Fagerberg L, Hallstrom BM, Lindskog C, Oksvold P, Mardinoglu A, et al. Proteomics. Tissue-based map of the human proteome. Science. 2015;347(6220):1260419.

554. Ogongo P, Porterfield JZ, Leslie A. Lung Tissue Resident Memory T-Cells in the Immune Response to Mycobacterium tuberculosis. Front Immunol. 2019;10:992.

555. Kaech SM, Cui W. Transcriptional control of effector and memory CD8+ T cell differentiation. Nat Rev Immunol. 2012;12(11):749-61.

556. Dusseaux M, Martin E, Serriari N, Peguillet I, Premel V, Louis D, et al. Human MAIT cells are xenobiotic-resistant, tissue-targeted, CD161hi IL-17-secreting T cells. Blood. 2011;117(4):1250-9.

557. Gherardin NA, Souter MN, Koay HF, Mangas KM, Seemann T, Stinear TP, et al. Human blood MAIT cell subsets defined using MR1 tetramers. Immunol Cell Biol. 2018;96(5):507-25.

558. Billerbeck E, Kang YH, Walker L, Lockstone H, Grafmueller S, Fleming V, et al. Analysis of CD161 expression on human CD8+ T cells defines a distinct functional subset with tissue-homing properties. Proc Natl Acad Sci U S A. 2010;107(7):3006-11.

559. Rha MS, Han JW, Kim JH, Koh JY, Park HJ, Kim SI, et al. Human liver CD8(+) MAIT cells exert TCR/MR1-independent innate-like cytotoxicity in response to IL-15. J Hepatol. 2020;73(3):640-50.

560. Chen Z, Wang H, D'Souza C, Sun S, Kostenko L, Eckle SB, et al. Mucosal-associated invariant T-cell activation and accumulation after in vivo infection depends on microbial riboflavin synthesis and co-stimulatory signals. Mucosal Immunol. 2017;10(1):58-68.

561. Wang H, D'Souza C, Lim XY, Kostenko L, Pediongco TJ, Eckle SBG, et al. MAIT cells protect against pulmonary Legionella longbeachae infection. Nat Commun. 2018;9(1):3350.

562. Veerapen N, Hobrath J, Besra AK, Besra GS. Chemical insights into the search for MAIT cells activators. Mol Immunol. 2020.

563. Joffe M, Gambhir M, Chadeau-Hyam M, Vineis P. Causal diagrams in systems epidemiology. Emerg Themes Epidemiol. 2012;9(1):1.

564. Kester KE, McKinney DA, Tornieporth N, Ockenhouse CF, Heppner DG, Hall T, et al. Efficacy of recombinant circumsporozoite protein vaccine regimens against experimental Plasmodium falciparum malaria. J Infect Dis. 2001;183(4):640-7.

565. Bojang KA, Milligan PJ, Pinder M, Vigneron L, Alloueche A, Kester KE, et al. Efficacy of RTS,S/AS02 malaria vaccine against Plasmodium falciparum infection in semi-immune adult men in The Gambia: a randomised trial. Lancet. 2001;358(9297):1927-34.

566. Shekalaghe S, Rutaihwa M, Billingsley PF, Chemba M, Daubenberger CA, James ER, et al. Controlled human malaria infection of Tanzanians by intradermal injection of aseptic, purified, cryopreserved Plasmodium falciparum sporozoites. Am J Trop Med Hyg. 2014;91(3):471-80.

567. Kapulu MC, Njuguna P, Hamaluba MM, Team C-SS. Controlled Human Malaria Infection in Semi-Immune Kenyan Adults (CHMI-SIKA): a study protocol to investigate in vivo Plasmodium falciparum malaria parasite growth in the context of pre-existing immunity. Wellcome Open Res. 2018;3:155.

568. Hodgson SH, Juma E, Salim A, Magiri C, Njenga D, Molyneux S, et al. Lessons learnt from the first controlled human malaria infection study conducted in Nairobi, Kenya. Malar J. 2015;14:182.

569. Chilengi R. Clinical development of malaria vaccines: should earlier trials be done in malaria endemic countries? Hum Vaccin. 2009;5(9):627-36.

570. Bijker EM, Sauerwein RW, Bijker WE. Controlled human malaria infection trials: How tandems of trust and control construct scientific knowledge. Soc Stud Sci. 2016;46(1):56-86.

571. Jamrozik E, Selgelid MJ. Human infection challenge studies in endemic settings and/or low-income and middle-income countries: key points of ethical consensus and controversy. J Med Ethics. 2020;46(9):601-9.

572. Gerlach C, van Heijst JW, Schumacher TN. The descent of memory T cells. Ann N Y Acad Sci. 2011;1217:139-53.

573. Martin MD, Shan Q, Xue HH, Badovinac VP. Time and Antigen-Stimulation History Influence Memory CD8 T Cell Bystander Responses. Front Immunol. 2017;8:634.

574. van Wilgenburg B, Loh L, Chen Z, Pediongco TJ, Wang H, Shi M, et al. MAIT cells contribute to protection against lethal influenza infection in vivo. Nat Commun. 2018;9(1):4706.

575. Bovay A, Speiser DE, Fuertes Marraco SA. Early drop of circulating T cells negatively correlates with the protective immune response to Yellow Fever vaccination. Hum Vaccin Immunother. 2020:1-8.

576. Lingblom CMD, Kowli S, Swaminathan N, Maecker HT, Lambert SL. Baseline immune profile by CyTOF can predict response to an investigational adjuvanted vaccine in elderly adults. J Transl Med. 2018;16(1):153.

577. mal E. R. A. Refresh Consultative Panel on Health Systems Policy Research. malERA: An updated research agenda for health systems and policy research in malaria elimination and eradication. PLoS Med. 2017;14(11):e1002454.

578. Chapman N, Doubell A, Oversteegen L, Chowdhary V, Rugarabamu G, Zanetti R, et al. G-Finder 2017 Report - Neglected Disease Research and Development: Reflecting on a decade of global investment. Sydney: Policy Cures Research; 2017.